BIASED AGONISTS AND ALLOSTERIC MODULATORS OF THE TYPE 1 CANNABINOID RECEPTOR: POTENTIAL TREATMENTS FOR HUNTINGTON DISEASE

by

Robert Brad Laprairie

Submitted in partial fulfilment of the requirements
for the degree of Doctor of Philosophy

at

Dalhousie University
Halifax, Nova Scotia
February 2016

TABLE OF CONTENTS

LIST OF TABLES

LIST OF FIGURES

ABSTRACT

Huntington disease (HD) is caused by the inheritance of a single copy of the mutant *huntingtin* gene. HD patients suffer from progressive cognitive decline, psychoses, depression, an inability to gain and maintain weight, and profound motor dysfunction, ultimately leading to death. Although the causal genetic defect was defined more than 20 years ago, treatment of HD is still limited to managing individual symptoms rather than managing disease processes and delaying disease onset and progression. A decrease in type 1 cannabinoid receptor (CB_1) mRNA and protein levels in the caudate and putamen precedes symptoms in HD and is correlated with HD progression and severity. Activation of CB_1 modulates neuronal activity in regions of the brain critical for cognition, mood, metabolism, and motor control. I hypothesized that pharmacological enhancement of CB_1 activity and abundance would reduce the signs and symptoms of HD and, because CB_1 loss precedes other changes, may slow disease progression. Through meta-analysis of the existing literature and several experimental approaches, I confirmed that CB_1 mRNA and protein levels decline in the caudate and putamen of HD patients and in the striatum of a mouse model of HD. Activation of CB_1 with the CB_1 agonist arachidonoyl-2'-chloroethylamide normalized CB_1 mRNA levels in mouse cells modelling medium spiny projection neurons and expressing mutant *huntingtin* (ST*Hdh*) suggesting CB_1 agonism could increase CB_1 levels in models of HD. I determined that CB_1 mRNA and protein levels were increased by CB_1 agonists (*e.g.* the endocannabinoid anandamide) that were functionally-selective toward $G\alpha_{i/o}$- and $G\beta\gamma$-dependent signaling. In contrast, CB_1 agonists that were functionally-selective for arrestin (*e.g.* the plant-derived cannabinoid Δ^9-tetrahydrocannabinol) reduced CB_1 protein levels. In ST*Hdh* cells, $G\alpha_{i/o}$/$G\beta\gamma$-selective CB_1 agonists improved cell viability and function, whereas arrestin-selective CB_1 agonists reduced cell viability and function. The potency and efficacy of cannabinoid agonists can be fine-tuned *via* positive (PAM) or negative (NAM) allosteric modulators that increase or decrease CB_1-dependent signaling, respectively, without directly activating CB_1. The CB_1 allosteric modulators GAT228 (*R*-enantiomer), GAT229 (*S*-enantiomer), and GAT211 (equimolar racemic mixture of GAT228 and GAT229) were tested to determine if they increased CB_1 activity in HD. GAT228 was a CB_1 allosteric partial agonist that produced neutral or negative effects in cell culture and animal models of HD. GAT229 had no direct agonist activity but was a PAM that enhanced $G\alpha_{i/o}$-dependent signaling and improved cell viability in a cell culture model of HD, delayed disease progression, and normalized gene expression in an animal model of HD. GAT211 displayed effects that were intermediate between its enantiomers. Therefore, the signs of HD can be managed *via* CB_1 so long as signaling is selectively enhanced without supraphysiological activation or receptor downregulation. My research provides a strong first proof-of-principle for the use of $G\alpha_{i/o}$-selective CB_1 PAMs to manage the signs and symptoms of HD.

LIST OF ABREVIATIONS USED

2-AG	2-arachidonylglycerol
AEA	Anandamide
ACEA	2'-arachidonyl ethanolamine
ANOVA	Analysis of variance
BRET	Bioluminescence resonance energy transfer
Cal-AM	Calcein-AM
CB_1	Type 1 cannabinoid receptor
CB_2	Type 2 cannabinoid receptor
CCL	Chemokine (C-C) motif ligand
CBD	Cannabidiol
CHO	Chinese hamster ovary cells
CI	Confidence interval
CP	CP55,940; (-)-*cis*-3-[2-Hydroxy-4-(1,1-dimethylheptyl)phenyl]-*trans*-4-(3-hydroxypropyl)cyclohexanol
CPu	Caudate and putamen
CRC	Concentration-response curve
CREB	cAMP response element binding protein
CTx	*Cholera* toxin
DARPP-32	Dopamine- and cAMP-regulated phosphoprotein 32 kDa
DSE	Depolarization-induced suppression of excitation
EthD-1	Ethidium homodimer-1
FAAH	Fatty acid amide hydrolase
FRET	Fluorescence resonance energy transfer
GABA	γ-amino butyric acid
GFP^2	Green fluorescent protein^2
GM-CSF	Granulocyte macrophage colony-stimulating factor
GPCR	G protein-coupled receptor
HEK293A	Human embryonic kidney 293A cells
HEK-CRE	HEK-Cignal Lenti cAMP response element cells
HERG	Human ether-a-go-go related gene

HD	Huntington disease
IL	Interleukin
MAGL	Monoacyl glycerol lipase
mHtt	Mutant huntingtin protein
MIP	Macrophage inflammatory protein
NAM	Negative allosteric modulator
NF-κB	Nuclear factor kappa B
O-2050	6aR,10aR)-3-(1-methanesulfonylamino-4-hexyn-6-yl)-6a,7,10,10a-tetrahydro-6,6,9-trimethyl-6H-dibenzo[b,d]pyran
OD	Optical density
PAM	Positive allosteric modulator
PPARγ	Peroxisome proliferator-activated receptor γ
PTx	*Pertussis* toxin
qRT-PCR	Quantitative reverse transcriptase PCR
RFP	Red fluorescent protein
Rluc	*Renilla* luciferase
RT	Reverse transcriptase
SEM	Standard error of the mean
THC	Δ^9-tetrahydrocannabinol
TNFα	Tumor necrosis factor alpha
TRPV1	Transient receptor potential cation channel subfamily V 1;
UHDRS	Universal Huntington's disease rating scale
WIN	WIN55,212-2; (R)-(+)-[2,3-Dihydro-5-methyl-3-(4-morpholinylmethyl)pyrrolo[1,2,3-de]-1,4-benzoxazin-6-yl]-1-napthalenylmethanone

ACKNOWLEDGEMENTS

I am extremely grateful for the love and encouragement of my wife, Kimberly. Without her constant support and hard work this thesis, and indeed my career, would not be possible. To my sons, Ezra, Silas, and Philip: you are my joy and driving force on the good days and, more importantly, the bad days. Thank you to my mom, Mari, and my dad, Patrick, who worked so hard to help my family and I get where we are now.

To Dr. Eileen Denovan-Wright: thank you so very much for being my mentor, guide, critic, and friend. I am proud to have been your student and grown under your supervision. I already exceeded my colon and semi-colon limit for this thesis in these Acknowledgements; please forgive me. I would also like to extend my gratitude to Dr. Melanie Kelly, Kathleen Murphy, Amina Bagher, and the many past and present students of the Denovan-Wright lab. Thanks to my advisory committee: Drs. Kishore Pasumarthi and James Fawcett for their knowledge and assistance. I have relied on the entire Department of Pharmacology for support during my tenure as a student here, and for this I thank you all.

Foremost, I am grateful to God because He has given me the strength to run this race.

Finally, I would like to acknowledge financial support from Dalhousie University, the Canadian Institutes of Health Research (CIHR), the Huntingtin Society of Canada (HSC), Killam Trusts, Nova Scotia Health Research Foundation (NSHRF), the Molly Appeal for Neuroscience Research, the International Cannabinoids Research Society (ICRS) and the American Society for Pharmacology and Experimental Therapeutics (ASPET) without which I could not have completed this work.

CHAPTER 1

INTRODUCTION

Copyright statement

Contribution statement

The manuscript used as the basis for this chapter was written in equal partnership with Dr. Amina Bagher with guidance from Dr. Eileen Denovan-Wright. Data were collected by myself with assistance from Drs. Amina Bagher and Sophie Precious.

1.1. HUNTINGTON DISEASE

Huntington disease (HD) is caused by the expansion of a polymorphic CAG trinucleotide repeat in the first exon of the gene encoding *huntingtin* [Huntington's Disease Collaborative Research Group (HDCRG), 1993]. Expression of mutant huntingtin protein (mHtt) leads to highly disabling psychiatric, cognitive, metabolic, and motor symptoms that progress over several decades leading to death (Newcombe, 1981; Adams *et al*., 1988; Roos *et al*., 1993; Foroud *et al.,* 1999; Carroll *et al.*, 2015; Gil Polo *et al*., 2015). Psychiatric and cognitive symptoms often appear prior to other symptoms and include depression, anxiety, compulsive behaviours, increased likelihood of addiction, blunted emotion, working memory deficits, impaired executive function, and eventual dementia (Adams *et al*., 1988; Roos *et al*., 1993; Carroll *et al.*, 2015). Metabolic dysfunctions include inability to gain weight, malnutrition, reduced lean muscle mass, and increased body fat content (Ross *et al*., 2014; Süssmuth *et al*., 2015). Motor symptoms are typically present by the third or fourth decade (Ross *et al*., 2014). Motor symptoms begin as uncontrollable, jerky, choreiform movements and progressively worsen until chewing and swallowing become difficult (Ross *et al*., 2014). Death often occurs by choking or aspiration of food (Ross *et al*., 2014).

There is no cure for HD. Current treatment of HD is limited to reducing the severity of psychiatric, cognitive, and motor symptoms (Warby *et al*., 2014). Current pharmacotherapy for HD patients is limited to the management of specific symptoms rather than inhibition of the effects of mHtt. Depression and compulsive behaviours are managed using antidepressants (Bonelli *et al*., 2004; Beglinger *et al*., 2014), and atypical antipsychotics (Edlinger *et al.*, 2013; Warby *et al*., 2014), respectively. Chorea is most-often managed with the dopamine-depleting agent tetrabenazine and typical antipsychotics (Ross *et al*., 2014). The hypokinesia that occurs late in HD progression is managed with the same drugs that are used in the treatment of Parkinson disease (Ross *et al.*, 2014). Often, patients undergo long-term treatment with multiple medications to control these different components of their disease (Warby *et al*., 2014). While

each medication effectively manages specific symptoms (Begliner *et al.*, 2014), these treatments do not affect disease progression caused by mHtt expression (Koppel *et al*., 2014; Carroll *et al*., 2015; Young, 2016) and, in the case of antidopaminergic agents, may exacerbate the progression and severity of bradykinesia and hypokinesia (Tedroff *et al*., 2015). In addition, patient compliance is often low because of the multiple prescriptions required to control symptoms and the high caloric diet required to maintain weight (Gil Polo *et al*., 2015). HD could be cured by elimination of the mHtt gene (Ramsingh *et al.*, 2015; McBride and Clark, 2016; Young, 2016). However, effective gene-based therapies directed at elimination of mHtt expression have yet to be developed (Young, 2016). Other pharmacological strategies that reduce the signs and symptoms of HD, but do not target the mHtt gene, may be developed (Ramsingh *et al*., 2015). Current treatments of HD have been developed for the management of other disorders and do not, therefore, address the fundamentally different underlying pathophysiological effects of mHtt in HD (Carroll *et al*., 2015).

1.1.1. PATHOLOGICAL EFFECTS OF MUTANT HUNTINGTIN PROTEIN

Cellular dysfunction is prominent in the medium spiny projection neurons (MSN) of the caudate and putamen (CPu) and cell death occurs earlier in MSNs than other neuronal populations in HD (Vonsattel *et al*., 1985). Therefore, there has been an intense effort to define changes in cellular function in the basal ganglia and particularly in the CPu, which is functionally equivalent to the striatum in rodents (Fig. 1-1) (Vonsattel *et al*., 1985; Luthi-Cart *et al*., 2002). The chorea that occurs early in HD progression suggests dysfunction of the MSNs, specifically those of the indirect motor pathway expressing D_2 and enkephalin (Fig. 1-1) (Delorme *et al*., 2015; Tedroff *et al*., 2015). The hypokinesia that occurs late in HD progression suggests that MSNs of the direct motor pathway also degenerate in HD (Fig. 1-1) (Tedroff *et al*., 2015). Deficits in cognition, working memory, emotion, addiction, and metabolism, as well as wide-spread neuronal atrophy indicate that neuronal dysfunction is not limited to the CPu, but occurs in structures such as the cortex and hypothalamus as well (Carroll *et al*., 2015; Klöppel *et al*., 2015).

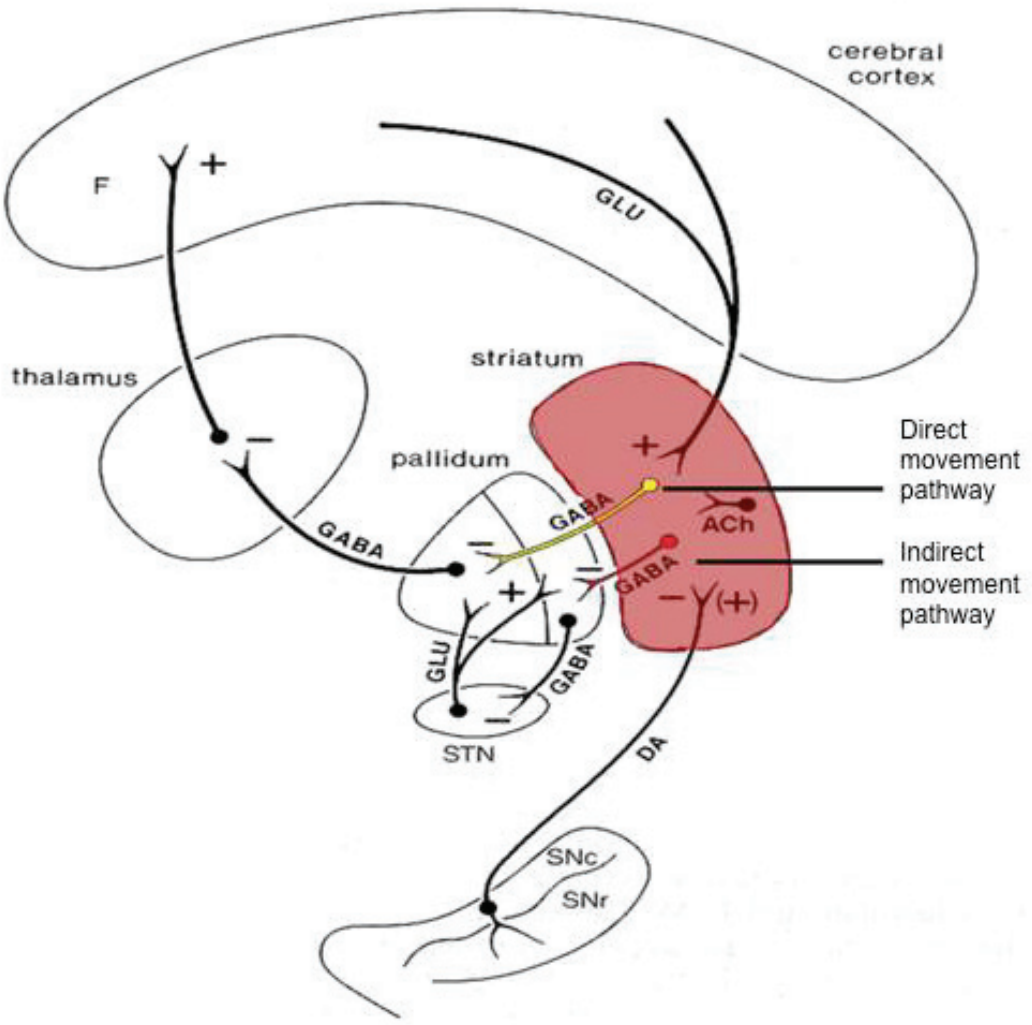

Figure 1-1. Neurodegeneration during HD progression is cell-specific. HD pathophysiology is associated with a cell-specific degeneration of MSN of the indirect movement pathway that express D_2 receptors and, later in disease progression, MSN of the direct movement pathway that express D_1 receptors. Here, a schematic of the direct and indirect pathways is illustrated. The CPu (striatum) is highlighted red, the MSN of the direct pathway are yellow, and the MSN of the indirect pathway are red. SNc, substantia nigra pars compacta; SNr, substantia nigra pars reticulata; DA, dopaminergic neuron; F, frontal cortex; STN, subthalamic neuron; ACh, acetylcholine; GABA, γ-aminobutyric acid; GLU, glutamate; "+", excitatory; "- ", inhibitory (adapted from Nestler *et al*., 2001).

The soluble, amino (*N*)-terminal fragment of mHtt is considered a toxic gain-of-function protein that produces cellular pathology in HD (Atwal *et al.,* 2007; Hogel *et al.*, 2012). Cellular changes precede the striatal atrophy and death of MSNs that occurs late in HD pathogenesis (Zuccato and Cattaneo, 2014). Expression of *N*-mHtt leads to a variety of changes in cellular function including inhibition of proteasomal and autophagic processes, excitotoxic stress, reduced mitochondrial respiration and ATP production, reduced expression of neurotrophic factors, a dampened inflammatory response in the CNS, and the transcriptional dysregulation of a subset of genes (reviewed in Zuccato and Cattaneo, 2014; Martin *et al.*, 2015; Sharma and Taliyan, 2015). *N*-terminal mHtt has been shown to interfere with the transcription of critical regulatory genes, including the NR2B subunit of the NMDA receptor, peroxisome proliferator-activated receptor γ co-factor 1α (PGC1α), brain-derived neurotrophic factor (BDNF), and NF-κB p65/RelA (Ghose *et al*., 2011; Laprairie *et al*., 2013, 2014a). One hypothesis is that *N*-mHtt interferes with transcription at the gene promoter either through sequestration of transcription factors or incorporation into the pre-initiation complex (Hogel *et al.*, 2012). In addition to the effects of *N*-mHtt, loss of normal Htt may contribute to transcriptional dysregulation (Soldati *et al*., 2011). Htt inhibits the transcriptional repressor REST (Ravache *et al*., 2010). Loss of REST inhibition contributes to decreased neurotrophic factor levels (Schiffer *et al*., 2014). Transcriptional dysregulation in HD may lead to a wide array of changes in neuronal function that are the direct result of mHtt, or occur later as compensatory changes to altered cell function (Prasad and Bondy, 2015; Sharma and Taliyan, 2015).

1.1.2. Changes in gene expression in Huntington disease

Early studies that looked at levels of individual mRNAs and proteins demonstrated that the levels of 1.2% of all mRNA transcripts and their associated proteins were altered when mHtt was expressed (Cha *et al*., 1998; Cha, 2000; Denovan-Wright and Robertson, 2000; Glass *et al*., 2000). In addition, multiple microarray studies have reported profound and early changes in gene expression is the basal ganglia of HD patients (Luthi-Carter *et al*., 2002; Desplats *et al*., 2006;

Hodges *et al*., 2006; reviewed in Laprairie *et al*., 2015a). Altered gene expression also occurs in a subset of genes in the cortex, which shows less neurodegeneration than the CPu but whose function is altered in HD, and in peripheral blood and adipose tissue where these changes may be monitored as biomarkers of disease progression (Halliday *et al*., 1998; Borovecki *et al*., 2002; Lovrecic *et al*., 2009). Therefore, transcriptional dysregulation may underlie many of the cellular dysfunctions observed in HD. Given that changes in gene expression occur over decades, early changes in gene expression may influence later changes in gene expression (Li *et al*., 2002; Zhai *et al*., 2004; Hogel *et al*., 2012). Normalization of the expression of genes critical to healthy neuronal function and viability that are dysregulated early in HD may delay or limit the progressive symptoms of HD without directly targeting the mHtt gene (Fernández-Ruiz *et al.*, 2015; Mason and Barker, 2015; Ramsingh *et al*., 2015; Tedroff *et al*., 2015).

1.2. THE TYPE 1 CANNABINOID RECEPTOR

The type 1 cannabinoid receptor (CB_1) is the most abundant G protein-coupled receptor (GPCR) in the central nervous system (CNS) and is expressed at high levels in the basal ganglia (CPu) relative to other brain regions (Mailleux and Vanderhaeghen, 1992). CB_1 regulates neuronal activity in the CPu, limbic system, and other regions of the brain as a key component of the larger endocannabinoid system (ECS) (Gerdeman and Fernandez-Ruiz, 2008).

The ECS regulates neurotransmission and cell excitability throughout the CNS and regulates cellular metabolism and inflammation in neuronal and non-neuronal cells (Howlett *et al*., 2002; Pertwee *et al.,* 2010). In the brain, pre-synaptic CB_1 receptors are activated by endogenous (endo) cannabinoids, which are synthesized and released from the post-synaptic neuron following depolarization (Kreitzer and Regher, 2001; Giuffrida *et al*., 2001). In the CNS, the type 2 cannabinoid receptor (CB_2) is predominantly expressed in glial cells and inhibits pro-inflammatory processes (Atwood and Mackie, 2010; Lopez-Rodriguez *et al*., 2013). In addition to CB_1 and CB_2, the ECS is made up of putative cannabinoid receptors GPR18, GPR55, and GPR119, the cation-permeable transient receptor potential vanilloid 1 (TRPV1), the anabolic

enzymes diacyl glycerol lipase (DAGL) and *N*-acyl phosphatidylethanolamine phospholipase D (NAPE-PLD), the catabolic enzymes abhydrolase domain containing protein 4 (ABHD4), 6 (ABHD6), 12 (ABHD12), fatty acid amide hydrolase (FAAH), monoacyl glycerol lipase (MAGL), and *N*-acylethanolamine acid amidase (NAAA), the phosphatases Protein tyrosine phosphatase, non-receptor type 22 (PTPN22) and Glycerophosphodiester phosphodiesterase 1 (GDE1), and the endocannabinoids (Howlett *et al*., 2002; Pertwee *et al.,* 2010). The most abundant endocannabinoid is 2-arachidonoylglycerol (2-AG), which is approximately 1,0000-fold more abundant than anandamide (AEA) (Martin *et al*., 1999). 2-AG and AEA display similar affinity and efficacy at CB_1 and CB_2 (Pertwee, 2008). In addition to CB_2 limiting pro-inflammatory signaling, the ECS affects inflammatory processes because 2-AG and AEA are synthesized from the pro-inflammatory lipid arachidonic acid (Martin *et al*., 1999; Lopez-Rodriguez *et al*., 2013).

Activation of CB_1 by cannabinoids limits neurotransmitter release from pre-synaptic neurons *via* inhibition of Ca^{2+} and rectifying K^+ currents and activates G protein- (predominantly $G\alpha_{i/o}$) and arrestin-dependent signaling (Nguyen *et al*., 2012; Di Marzo *et al.*, 2015). Because CB_1 regulates neurotransmitter release, and facilitates pro-survival signaling *via* coupling to $G\alpha_{i/o}$, activation of CB_1 is considered neuroprotective (Di Marzo *et al.*, 2015).

1.2.1. Alterations in the endocannabinoid system in Huntington disease

CB_1 mRNA and protein levels decrease by 50% in the MSN of the striatum prior to the onset of cognitive, behavioural and motor symptoms in HD patients, as well as in all cell culture and animal models characterized to-date (Denovan-Wright and Robertson, 2000; Glass *et al*., 2000; reviewed in Sagredo *et al.*, 2012). Although the earliest and most-prominent decline in CB_1 mRNA and protein levels occurs in the D_2- and enkephalin-expressing MSNs of the striatum during HD, decreases in CB_1 abundance are also observed throughout the basal ganglia, cortex, hippocampus, hypothalamus, as well as in white adipose tissue and whole blood (van Laere *et al.*,

2010; reviewed in Sagredo *et al*., 2012; Laprairie *et al*., 2015a). Thus, CB_1 expression is inhibited across multiple tissues in HD (McCaw *et al*., 2004).

In addition to CB_1, levels of CB_2, FAAH, and NAPE-PLD mRNA and protein are dysregulated in the central nervous system and peripheral tissues of HD patients and many animal models of HD (Bari *et al.*, 2013; Laprairie *et al*., 2014a,b; reviewed in Laprairie *et al*., 2015a) (Fig. 1-2). Whereas lower CB_1 levels appear to be the direct and early result of mHtt (McCaw *et al*., 2004; Bari *et al*., 2013; Laprairie *et al*., 2013, 2014b), changes in CB_2, FAAH, and NAPE-PLD abundance occur later in HD progression and may be compensatory, secondary changes in response to HD pathogenesis (Dowie *et al*., 2010; Naydenov *et al*., 2014a,b; reviewed in Laprairie *et al*., 2015a).

Declining levels of CB_1 mRNA and protein contributes to HD pathophysiology (Mievis *et al*., 2011; Chiarlone *et al.*, 2014; Naydenov *et al*., 2014a; Blázquez *et al*., 2011, 2015). Similar to mouse models of HD, CB_1 knockout mice display performance deficits in the rotarod, hypolocomotion, heightened anxiety, and increased mortality (Zimmer *et al*.,1999). Performance deficits in the rotarod and accelerated rotarod are exacerbated in mouse models of HD that lack CB_1 (*i.e.* HD *x* $CB_1^{-/-}$) compared to HD mice with a full complement of CB_1 (*i.e.* HD *x* $CB_1^{+/+}$) (Blázquez *et al*., 2011; Mievis *et al*., 2011). HD *x* $CB_1^{-/-}$ mice exhibit reduced locomotor activity, earlier symptom onset, earlier mortality, and greater striatal atrophy compared to HD *x* $CB_1^{+/+}$ mice whether CB_1 is knocked-out globally (Blázquez *et al*., 2011; Mievis *et al*., 2011), within only the striatum (Blázquez *et al*., 2015), or within only cortical glutamatergic neurons that

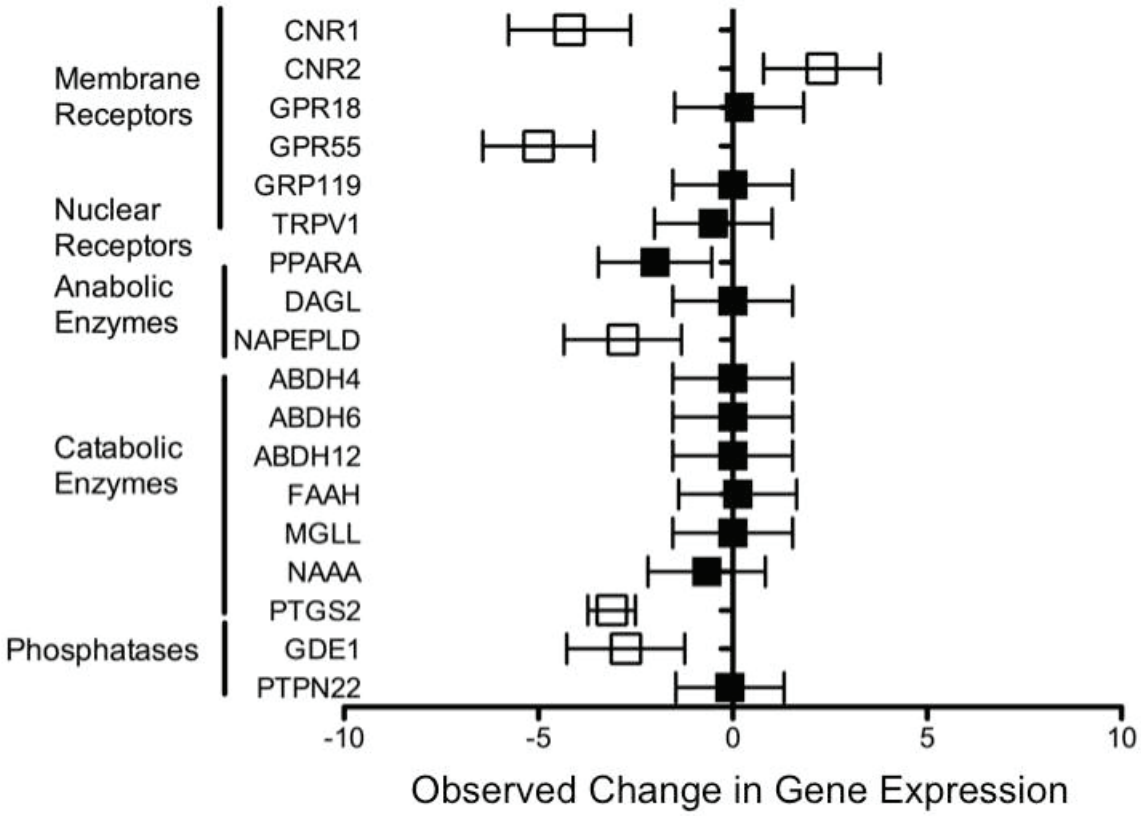

Figure 1-2. Summary of ECS transcriptional dysregulation in microarray studies of HD. Data are represented as the observed change in gene expression (OCGE; sum of changes for each gene in each HD microarray study that reported transcript levels divided by the number of studies reporting transcript levels). Error bars are 95% CI. Open boxes denote an OCGE different from 0 ($P < 0.05$, non-overlapping CI). Data were collected from microarray studies ($n = 39$ studies) available through Gene Expression Omnibus (GEO) datasets for brain tissue in HD according to the methods described in Laprairie *et al*., 2015a. Abbreviations used in this figure are: CNR, cannabinoid receptor; GPR, G protein-coupled receptor; TRPV1, transient receptor potential receptor vanniloid 1; PPARA, peroxisome proliferator-activated receptor α; DAGL, diacylglycerol lipase; NAPEPLD, *N*-acyl phosphatidylethanolamine-specific phospholipase D; ABHD, abhydrolase domain-containing; FAAH, fatty acid amide hydrolase; MGLL, monoacylglycerol lipase; NAAA, *N*-acetylethanolamine-hydrolyzing acid amidase; GDE1, glycerophosphodiester phosphodiesterase; PTPN22, protein tyrosine phosphatase, non-receptor type 22.

project to the striatum (Chiarlone *et al.*, 2014). In human HD patients, age of disease onset is earlier in patients with a CB_1 variant allele [$(AAT)_n$] that reduces the stability of the CB_1 mRNA transcript, and consequently, reduces CB_1 abundance (Kloster *et al*., 2013). Genetic rescue of CB_1 expression in the MSNs of early-stage motor symptomatic HD mice using adeno-associated virus improves MSN dendritic spiny density, normalizes the expression of striatal synaptic markers such as BDNF, and reduces striatal atrophy, but does not affect motor impairment observed in this mouse model (Naydenov *et al*., 2014b; Blázquez *et al*., 2015). At this time, the effects of genetic rescue of CB_1 expression prior to symptom onset are unknown. Thus, restoring CB_1 levels in MSNs reduces the severity of some components of HD pathophysiology.

1.2.2. Cannabinoid-based management of Huntington disease

Given the widespread dysregulation of the ECS in HD, it should come as no surprise that the ECS – especially CB_1 – has been extensively studied as a therapeutic target for managing the signs and symptoms of HD. Presently, there is a need for safe and effective pharmacotherapeutic strategies that reduce the psychiatric, cognitive, metabolic, and motor dysfunctions that are outwardly present in HD by circumventing the cellular, pathological, effects of mHtt.

Pharmacological manipulation of the ECS in HD aims to increase endocannabinoid tone, CB_1 activity, and/or CB_1 abundance in order to reduce the signs and symptoms of HD. Unfortunately, past studies that aimed to reduce the signs and symptoms of HD *via* pharmacological targeting of CB_1 have had limited success in cell culture and animal models of HD and in HD patients. Beyond the endocannabinoids AEA and 2-AG, there exists a wide array of phytocannabinoids (derived from *Cannabis sativa*) and synthetic cannabinoids that differ in their structure and pharmacology (Pertwee, 2008). Treatment of cells expressing mHtt with the phytocannabinoid Δ^9-tetrahydrocannabinol (THC) has been shown to promote neuronal survival in some studies (Blázquez *et* al., 2011, 2015), and reduce survival in other studies (Laprairie *et al.,* 2015b). Treatment of cells expressing mHtt with HU-210 (synthetic CB_1 agonist) was neuroprotective and occurred *via* CB_1, $G\alpha_{i/o}$-, and ERK-dependent signaling (Scotter *et al*., 2010);

however, the authors observed that HU-210 also promoted enhanced coupling of CB_1 to $G\alpha_s$, which may limit the therapeutic potential of HU-210 in more-complicated *in vivo* systems if the neuroprotective benefit was conferred *via* $G\alpha_{i/o}$. Increasing CB_1 activity and/or abundance *via* CB_1 agonism can improve neuronal viability in the presence of mHtt. I have observed that treatment of HD cells with AEA, or its derivatives, induces CB_1 promoter activity, mRNA and protein levels (Laprairie *et al*., 2013). Induction of CB_1 occurs *via* a CB_1-, and $G\alpha_{i/o}$ -dependent pathway (Laprairie *et al*., 2013), which is similar to the neuroprotective signaling pathway described by Scotter *et al*. (2010) for HU-210.

In animal models of HD, the synthetic cannabinoid WIN55,212-2 and inhibitors of endocannabinoid catabolism (*e.g.* URB597 and WWL123) have been shown to normalize CB_1 levels in the striatum (Dowie *et al.*, 2010; Naydenov *et al.*, 2014b; Pietropaolo *et al.*, 2015), reduce motor impairment (WIN55,212-2 only) (Pietropaolo *et al.*, 2015), and reduce seizure frequency (Naydenov *et al.*, 2014b) when administered to symptomatic HD mice over 2 weeks. However, orthosteric agonists such as WIN55,212-2 may produce psychotropic side effects associated with supraphysiological receptor activation, receptor desensitization or downregulation (Chiodi *et al*., 2012), and URB597 and WWL123 were of limited efficacy in HD mice (Dowie *et al.*, 2010; Naydenov *et al.*, 2014b). Nabilone, HU-210, and THC have been shown to exacerbate deficits in motor control, reduce CB_1 binding, and increase seizure frequency when administered chronically to symptomatic HD mice (Müller-Vahl *et al*., 1999; Curtis *et al*., 2009; Dowie *et al*., 2010). There is some evidence that AM404 (a FAAH inhibitor), cannabidiol (CBD), and HU-308 (CB_2 agonist) reduce locomotor impairment and neuronal cell death in rats given striatal lesions with 3-nitropropionic acid or malonate, but this has not been observed in genetic models of HD (Lastres-Becker *et al*., 2003; Sagredo *et al*., 2009). Inhibition of serine hydrolase α/β-hydrolase domain 6 (ABHD6), which leads to increased 2-AG levels, blocks spontaneous seizures in R6/2 mice (Naydenov *et al*., 2014b).

Treatment of HD patients with the phytocannabinoid CBD produces neither beneficial nor detrimental effects (Consroe *et al*., 1993). Treatment of early-symptomatic HD patients with nabilone has been shown to improve motor score and reduce chorea when administered acutely (Curtis *et al*., 2009), but increase the frequency of choreic movement when administered chronically (Müller-Vahl *et al*., 1999). These results suggest that certain cannabinoids, such as THC or nabilone, may be detrimental to HD, whereas increased endocannabinoid tone, achieved through the inhibition of the catabolic enzymes FAAH or ABDH6, may be neutral or beneficial in HD.

Although the aim of all of the studies described above was to increase CB_1 activity in HD, the effects of the cannabinoids used varied widely. What can account for the disparate effects of cannabinoids in HD? The dose used, the duration of treatment, and the model all vary between studies and each of these accounts for some of different results observed in each study. Yet what is fundamentally lacking is an understanding of how the different types of cannabinoid used affect CB_1-dependent signal transduction in both normal and HD states. Many cannabinoids are biased agonists (Fig. 1-3) (Bosier *et al*., 2010; Luttrell *et al*., 2015). Biased agonists bind the orthosteric site of a GPCR in distinct ways in order to selectively facilitate some signaling pathways (*e.g.* $G\alpha_{i/o}$) over others (*e.g.* arrestin). Biased agonism may explain the differing efficacy of cannabinoids in HD and could be exploited to selectively enhance only those CB_1-dependent signaling pathways that ameliorate the signs and symptoms of HD (Fig. 1-3) (Luttrell *et al*., 2015).

Orthosteric agonists, even biased agonists, may produce supraphysiological receptor activation that leads to receptor desensitization or downregulation when administered chronically (Ross, 2007). Allosteric modulators lack intrinsic efficacy and are unable to activate their receptor in the absence of orthosteric agonist (Ross, 2007; Wootten *et al.*, 2013). Allosteric modulation of endogenous ligand-dependent GPCR signaling could avoid supraphysiological receptor activation (Ross, 2007). Allosteric modulators bind to a separate site on a GPCR apart

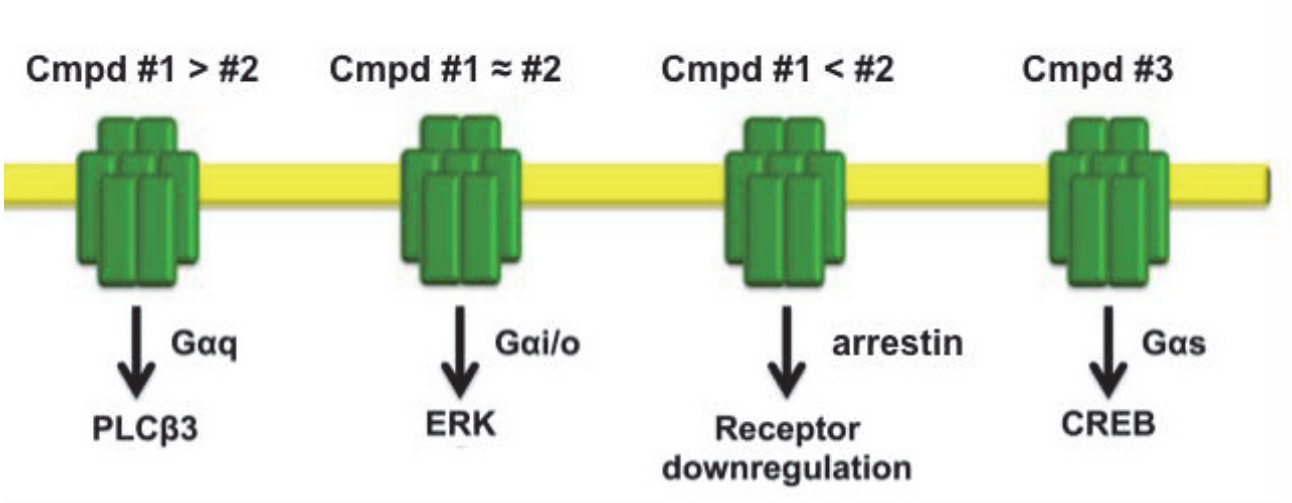

Figure 1-3. **CB_1 agonist bias**. Agonists may bias the signaling of their cognate receptors to favour one or more of the pathways that GPCRs can signal through. Here, compound #1 is biased compared to compound #2 for $G\alpha_q$-dependent PLCβ3 signaling, whereas compounds #1 and #2 are approximately equal for $G\alpha_{i/o}$-dependent ERK signaling, compound #2 is biased compared to compound #1 for arrestin recruitment, and only compound #3 signals *via* $G\alpha_s$ for this GPCR (*e.g.* CB_1, green).

from the orthosteric site in order to enhance [positive allosteric modulator (PAM)] or diminish [negative allosteric modulator (NAM)] the efficacy and potency of orthosteric ligand-dependent signaling through the GPCR (Fig. 1-4) (Ross, 2007; Wootten *et al.*, 2013). In the case of CB_1, allosteric modulators enhance or diminish endocannabinoid-dependent receptor activation (Ross, 2007). Existing characterized allosteric modulators of CB_1 include the functional NAMs Org27569, PSNCBAM-1, and pregnenolone (Price *et al*., 2005; Horswill *et al*., 2007; Vallée *et al*., 2014) and the PAMs lipoxin A_4, ZCZ011, and GAT211 (Pamplona *et al.*, 2012; Ignatowska-Jankowska *et al.*, 2015; Adam *et al.*, 2007; Laprairie *et al.*, 2015c). Therefore, PAMs of CB_1 may be more useful than orthosteric agonists because their use would not be expected to produce psychotropic side effects associated with supraphysiological receptor activation, receptor desensitization or downregulation (Ross, 2007; Wootten *et al.*, 2013).

1.3. OBJECTIVES OF THIS RESEARCH

The overall hypothesis of my research is that pharmacological enhancement of CB_1 abundance and $G\alpha_{i/o}$-dependent activity will reduce the signs and symptoms of HD, whereas enhancement of arrestin-dependent activity at CB_1 will reduce CB_1 abundance and exacerbate the signs and symptoms of HD. The aims of my research were to understand: 1) the regulation of CB_1 expression as part of the ECS within the context HD, 2) the signaling bias of CB_1 ligands and how to exploit specific signaling properties in order to limit cell intrinsic deficits in the presence of mHtt, and 3) to explore allosteric modulation of CB_1 in order to reduce the signs and symptoms of HD.

I have chosen to present each of my published works that pertain to my thesis as separate chapters. Each chapter is introduced separately to provide the reader with the context of the study. Further, although many of the same methods were used for each chapter, I have provided separate methods sections for all chapters so that differences in technique and approach are highlighted. I have only included results that I produced, and removed data that was collected by collaborators for each study. To meet the above aims, I have examined the co-regulation of CB_1 and the ECS

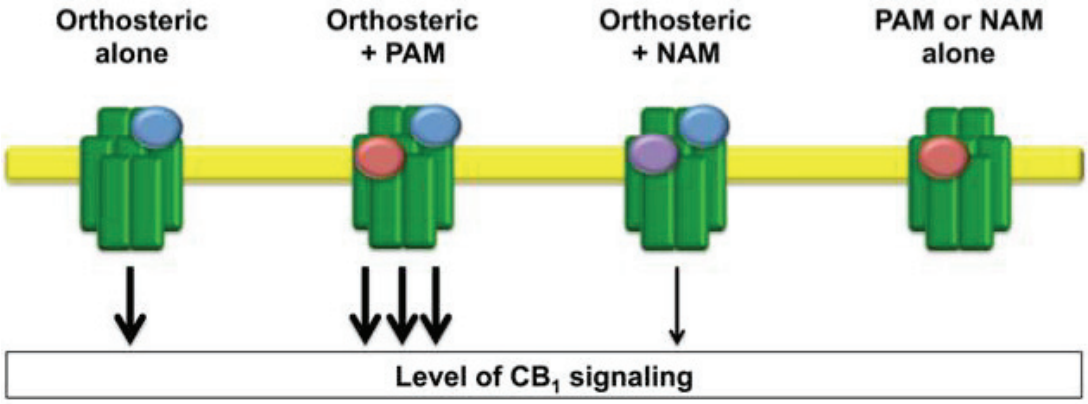

Figure 1-4. **CB_1 allosteric modulators**. Orthosteric ligands bind to the site of a GPCR that is also bound by the endogenous ligand (blue circle). Binding of the orthosteric ligand to its cognate GPCR leads to receptor activation and downstream signaling. Allosteric ligands bind to a distinct receptor site on the same GPCR and in doing so modify the affinity of the receptor for the orthosteric ligand, the potency of the orthosteric ligand, and/or the efficacy of the orthosteric ligand (red and purple circles). Alone, an allosteric modulator has no intrinsic ability to activate the receptor. Positive allosteric modulators (PAM) increase the potency and/or efficacy of orthosteric ligands whereas negative allosteric modulators (NAM) decrease the potency and/or efficacy of orthosteric ligands.

with p65/RelA in HD (chapter 2), biased agonism of CB_1 in the presence of mHtt (chapters 3 and 4), negative allosteric modulation of CB_1 by CBD (chapter 5), and positive allosteric modulation of CB_1 using the compounds GAT211, GAT228, and GAT229 in cell culture (chapter 6) and *in vivo* (chapter 7) models of HD.

CHAPTER 2

THE CYTOKINE AND ENDOCANNBINOID SYSTEMS ARE CO-REGULATED BY NF-κB P65/RELA IN CELL CULTURE AND TRANSGENIC MOUSE MODELS OF HUNTINGTON DISEASE AND IN STRIATAL TISSUE FROM HUNTINGTON DISEASE PATIENTS

Copyright statement

Contribution statement

The manuscript used as the basis for this chapter was written with guidance from Dr. Eileen Denovan-Wright. Data were collected and analyzed by myself with assistance from Jordan Warford and Sarah Hutchings. Critical reagents were provided by Drs. Melanie Kelly and George Robertson.

2.1. INTRODUCTION

Transcriptional dysregulation of a subset of genes is a hallmark pathological feature of Huntington disease (HD) (Glass *et al*., 2000). Transcriptional dysregulation is most prevalent in the caudate and putamen (CPu) and occurs before the onset of motor symptoms and neuronal cell death in HD patients. Several authors have demonstrated that the mutant huntingtin protein (mHtt) interferes with transcription by inhibiting the activity of multiple transcription factors, including Sp1 (Ravache *et al*., 2010), cAMP response element binding protein (CREB) (Cui *et al*., 2006), TATA binding protein (Hogel *et al*., 2012), and NF-κB (nuclear factor κ B) p65/RelA (Marcora and Kennedy, 2010; Ghose *et al*., 2011). Each of these transcription factors participates in the regulation of a subset of genes. Transcriptional dysregulation of a subset of genes is more likely to occur if those genes are co-regulated by mHtt-affected transcription factors (Hogel *et al*., 2012). Therapies that target the cytokine and endocannabinoid systems are being explored for the treatment of HD and both may be co-regulated by p65/RelA. Therefore, we focused on p65/RelA and genes of the cytokine and endocannabinoid systems that may be co-regulated by p65/RelA.

The type 1 cannabinoid receptor (CB_1) is among the genes repressed in the presence of mHtt early in HD progression (Glass *et al*., 2000; Denovan-Wright and Robertson, 2000) and decreased expression of CB_1 in the CPu is thought to contribute to disease pathogenesis (Dowie *et al*., 2009, 2010; Blázquez *et al*., 2011; Mievis *et al*., 2011). Activation of CB_1 is associated with inhibition of excessive neurotransmitter release and increased pro-survival signaling. Consequently, CB_1-mediated signaling is considered neuroprotective and the utility of CB_1-specific ligands for the treatment of neurodegenerative diseases is an area of intense investigation. Recently, we observed that activation of NF-κB p65/RelA increased CB_1 mRNA and protein levels in the ST*Hdh* cell culture model of HD and increased cell viability (Laprairie *et al*., 2013). In addition to CB_1, p65/RelA may regulate the transcription of cytokines, which are often up-regulated in response to inflammatory stimuli *via* NF-κB. In the brain, cytokines such as tumor necrosis factor (TNF)α and chemokine (C-C) motif ligand 5 (CCL5) promote myelination and

neuronal differentiation and therefore, like CB_1, are considered neuroprotective (Arnett *et al*., 2001; Park *et al*., 2009). The activity and expression of the p65/RelA subunit of NF-κB are decreased in several cell culture models of HD (Marcora and Kennedy, 2010; Ghose *et al*., 2011). Therefore, mHtt-dependent repression of p65/RelA may contribute to the transcriptional dysregulation of several genes, including cytokines and several components of the endocannabinoid system.

Understanding the relationship between the endocannabinoid and cytokine systems may provide insight into new treatment strategies for HD. In this study we sought to determine how the levels of p65/RelA, cytokines, and components of the endocannabinoid system were changed in the brain of R6/2 HD mice and the CPu of HD patients. We also wanted to determine whether activation or inhibition of p65/RelA, *via* modulation of cannabinoid tone, would affect mHtt-mediated transcriptional dysregulation of p65/RelA-regulated genes. While other studies have explored changes in cytokine levels, or parts of the endocannabinoid system in HD as separate systems, this study characterized the two systems to determine how they relate to each other through p65/RelA.

2.2. METHODS

2.2.1. ANIMALS AND TISSUE SAMPLES

A colony of R6/2 transgenic HD mice was established and maintained by crossing hemizygous carrier R6/2 males with CBA×C57BlJ/6 females. All mice were originally purchased from The Jackson Laboratory (Bar Harbor, ME). Mice were genotyped as described previously (Hebb *et al*., 2004). All animals were group-housed starting at 3 weeks of age with *ad libitum* access to food and water, and maintained on a 12 h light/dark cycle. All protocols were in accordance with the guidelines detailed by the Canadian Council on Animal Care (CCAC; Ottawa ON: Vol 1, 2nd Ed, 1993; Vol 2, 1984), approved by the Carleton Animal Care Committee at Dalhousie University and efforts were made to minimize the number of animals used. For *in situ* hybridization analysis, mice were anaesthetized with >100 mg/kg sodium pentobarbital,

decapitated, the brains removed and stored at −70°C prior to sectioning. For RNA isolation, animals were anaesthetized, decapitated and the striatum was excised and stored in liquid nitrogen prior to RNA extraction.

Human tissue was obtained from the Harvard Brain Bank, McLean Hospital (Boston, MA, USA) and maintained at −70 °C (Table 2-1).

2.2.2. QUANTITATIVE REVERSE TRANSCRIPTASE PCR (QRT-PCR)

RNA was harvested from the striatal tissue of human HD patients and R6/2 mice, or from ST*Hdh* cells using the Trizol® (Invitrogen, Burlington, ON) extraction method according to the manufacturer's instruction. Reverse transcription reactions were carried out with SuperScript III® reverse transcriptase (+RT; Invitrogen), or without (-RT) as a negative control for use in subsequent PCR experiments according to the manufacturer's instructions. Two micrograms of RNA were used per RT reaction. qRT-PCR was conducted using the LightCycler® system and software (version 3.0; Roche, Laval, QC). Reactions were composed of a primer-specific concentration of $MgCl_2$ (Table 2-2), 0.5 μM each of forward and reverse primers (Table 2-2), 2 μL of LightCycler® FastStart Reaction Mix SYBR Green I, and 1 μL cDNA to a final volume of 20μL with dH_2O (Roche). The PCR program was: 95°C for 10 min, 50 cycles of 95°C 10 s, a primer-specific annealing temperature (Table 2-2) for 5 s, and 72°C for 10 s. Experiments always included sample-matched –RT controls, a no-sample dH_2O control, and a standard control containing product-specific cDNA of a known concentration. cDNA abundance was calculated by comparing the cycle number at which a sample entered the logarithmic phase of amplification (crossing point) to a standard curve generated by amplification of cDNA samples of known concentration (LightCycler Software version 4.1; Roche). Here, qRT-PCR data were normalized to the expression of β-actin (Blázquez *et al.*, 2011).

Table 2-1. Detailed information on human tissue samples used.

Sample number	HD or Control	Age (years)	Sex	Post-mortem interval (h)	Vonsattel grade	CAG Repeat Length*
6124	Control	66	Male	16.9	-	18/22
6096	Control	70	Male	20.9	-	14/15
6078	Control	21	Male	29.9	-	19/24
3688	Control	66	Male	18.7	-	27/32
3740	Control	48	Male	15.4	-	15/18
3826	Control	53	Male	16.3	-	22/27
6190	Control	78	Female	22.7	-	26/29
5570	HD	77	Male	20.1	3	17/39
6033	HD	51	Male	25.6	3	29/56
6019	HD	44	Male	11.3	3	21/49
6024	HD	47	Female	23.9	3	18/46
4255	HD	52	Female	17.5	3	17/48
4424	HD	67	Female	22.0	3	28/51
4470	HD	48	Male	17.6	3	26/52
5137	HD	37	Female	19.7	4	25/41
5709	HD	53	Female	13.0	4	19/48
5172	HD	42	Female	25.6	4	26/54
4822	HD	48	Female	19.6	4	21/47
6071	HD	69	Female	12.5	4	18/49

*CAG repeat length indicated on each allele as "#/#".

Table 2-2. Synthetic oligonucleotides used in this study.

Target	Oligonucleotide Sequence (5' - 3')	Anneal. Temp. (°C)	$MgCl_2$ (mM)	Product length (bp)
CB_1[a]	GGGCAAATTTCCTTGTAGCA GGCTAACGTGACTGAGAAA	58	1	129
CB_2 (Mouse)	GGATGCCGGGAGACAGAAGTGA CCCATGAGCGGCAGGTAAGAAAT	57	2	506
CB_2 (Human)	ATGATCCTGAGTGGTCCCCA CATGCAAAGACCACACTGGC	58	3	191
CCL5	GCTGTTTGCCTACCTCTG TCGAGTGACAAACACGACTGC	57	2	103
FAAH	AAGGTGATTTCGTGGACCCC TTCCAGCCGAACGAGACTTC	58	4	150
FGF basic	CTGCTGGCTTCTAAGTGTGTT TTCTGTCCAGGTCCCGTTTT	59	2	161
IL-1β	GAAATGCCACCTTTTGACAGTG CTGGATGCTCTCATCAGGACA	57	5	117
IL-6	CTGCAAGAGACTTCCATCGAG AGTGGTATAGACAGGTCTGTTGG	57	4	131
MAGL	TTTCCGATGACAGCTTCGGG ACAAATCGCTAGAGGGGCTC	58	2	195
MCP-1	TTAAAAACCTGGATCGGACCCAA GCATTAGCTTCAGATTTACGGGT	57	2	121
p65/RelA (Mouse)[b]	GCGTACACATTCTGGGGAGT CCGAAGCAGGAGCTATCAAC	59	2	175
p65/RelA (Human)	ATAGAAGAGCAGCGTGGGGA GATCTTGAGCTCGGCAGTGT	59	3	156
TNFα	CAGGCGGTGCCTATGTCTC CGATCACCCCGAAGTTCAGTAG	59	3	89
β-actin[a]	AAGGCCAACCGTGAAAAGAT GTGGTACGACCAGAGGCATAC	59	2	110
CB_1 (*in situ*)[c]	ATGTCTCCTTTGATATCTTCGTACT GAATGTCATTTG	52	-	-
FAAH (*in situ*)	GTCAGCCAGATAGGAGGTCACAC AGTTGGTCCCTTTGTTCACTT	52	-	-

[a]Blázquez *et al*., 2011; [b]Cao *et al*., 2006; [c]Denovan-Wright and Robertson, 2000. All other primers self-designed using NCBI primer BLAST.

2.2.3. SDS-PAGE AND WESTERN BLOT

Tissue was homogenized for 1 min using a TissueRuptor (Qiagen, Galthersburg, MD) and protein concentration was determined by Bradford assay (Bio-Rad, Mississauga, ON). Fifty micrograms of protein were resolved on 10% acrylamide gels by SDS-PAGE for 20 min at 75 V and 2.5 h at 120 V. Protein was transferred to 0.2 µm nitrocellulose membrane (Bio-Rad) at 400 mA for 1 h on ice. Membranes were dried overnight before immunoblotting.

Membranes were rinsed once in dH_2O and blocked for 1 h in 20% Odyssey blocking buffer (Li-Cor Biosciences, Lincoln, NE) with shaking at room temperature. Membranes were incubated overnight at 4°C, with shaking, in rabbit anti-p65/RelA (1:500, Abcam, Cambridge, MA, ab7970-1) and mouse anti-β III tubulin (1:20,000, Abcam, ab7751-1) primary antibody solutions diluted in 20% Odyssey blocking buffer. Membranes were washed 3 times, 5 min each, with shaking in PBS containing 0.1% Tween-20 and incubated in donkey anti-rabbit IRdye^{800CW}-conjugated secondary antibody (1:500, Rockland Immunochemicals, Gilbertsville, PA, cat no. 631-731-127) and goat anti-mouse Alexfluor^{680}-conjugated secondary antibody (1:500, Invitrogen, cat no. A31562) for 1 h at room temperature, protected from light, with shaking. Membranes were washed 3 times, 5 min each, with shaking in PBS containing 0.1% Tween-20 and once in PBS alone. Membranes were visualized immediately using the Li-Cor Odyssey imaging system (Li-Cor Biosciences). Relative expression levels were quantified using ImageJ.

2.2.4. BIO-PLEX

Bio-Plex Pro™ premixed 27-plex human cytokine kits (Bio-Rad, Hercules, CA) were used to obtain an overview of inflammatory status in the CPu from HD patients and normal neurological controls. Tissue was weighed and subsequently homogenized in 500 µL of sterile ice-cold PBS containing a protease inhibitor (Sigma-Aldrich) using a handheld homogenizer (Pro Scientific Inc., USA). Homogenates were centrifuged (10,000 *x g*) and the supernatant was immediately frozen at -80°C. On the day of the experiment, standards were reconstituted using the

same PBS homogenization solution as the samples and incubated on ice for 30 min. Reagents, standards, and samples were equilibrated to room temperature before use.

Anti-cytokine conjugated beads (50 µL) were added to a 96-well plate and washed with 120 µL of assay buffer using a bio-plex handheld magnetic washer (Bio-Rad, Hercules, CA). Samples were diluted to final concentration of 500 µg/mL with Bio-Rad sample diluent. Next, 50 µL each of standards, samples, or negative controls (water only) were added to the wells in triplicate and incubated with the conjugated beads for 30 min on a microplate shaker at room temperature (1100 rpm for 1 minute, then 300 rpm 29 minutes). Following three washes, 25 µL of biotinylated detection antibody was added to each well and incubated for 30 min as previously described. This was followed by another series of washes and the addition of 50 µL of strepavidin-phycoerythrin to each well. The plate was protected from light and incubated for 10 min. Lastly, beads were washed three times, re-suspended in assay buffer (1100 rpm for 1 min), and analyzed with the Bio-Plex® 200 Suspension Array System. Data was acquired using Bio-Plex Manager® software version 6.0 with five-parameter logistic regression (5PL) curve fitting (Bio-Rad, Hercules, CA, USA). Data provided by the software as 'concentration in range' (*i.e.* within the linear range of the standards used) were used for analyses.

2.2.5. IN SITU HYBRIDIZATION

Synthetic, antisense oligonucleotide probes were obtained from Sigma-Aldrich (Oakville, ON, Table 2-2). Ten pmol of oligonucleotide probe were radio-labelled at the 3′ end with [α-^{33}P]dATP (2000 Ci/mmol; Mandel Scientific, Guelph, ON) using the reagents and protocol provided in the 3′ end-labelling kit (Amersham Pharmacia Biotech). *In situ* hybridization was performed as described previously using 14 µm coronal sections from R6/2 and age-matched, wild-type mice (Denovan-Wright *et al*., 1998). The sections were exposed to Kodak MR film for 2 weeks at room temperature. Densitometric analysis of *in situ* autoradiographs was performed using Kodak 3D imaging software (Kodak) to determine the optical density (OD) of the radiolabel in the lateral, ventromedial, and dorsomedial striatum and cortex. Measurements were

determined on sections derived from 4 individual animals at each time point. Local background was subtracted from each OD value.

2.2.6. CELL CULTURE

Conditionally immortalized wild-type (ST*Hdh*$^{Q7/Q7}$), heterozygous mutant (ST*Hdh*$^{Q7/Q111}$) or homozygous mutant (ST*Hdh*$^{Q111Q/111}$) mouse striatal progenitor cell lines expressing exon 1 from the human *huntingtin* allele in the mouse *huntingtin* locus were acquired from the Coriell Institute (Camden, NJ) (Trettel *et al*., 2000). Cells were propagated at 33°C, 5% CO_2 in DMEM supplemented with 10% FBS, 2 mM L-glutamine, 10^4 U/mL Pen/Strep, and 400 µg/mL geneticin. For all experiments, cells were serum-starved for 24 h.

The CB_1 agonist arachidonoyl-2'-chloroethylamide (ACEA), the fatty acid amide hydrolase (FAAH) inhibitor URB597, the type 2 cannabinoid receptor (CB_2) agonist HU-308, and the CB_2 antagonist AM630 were dissolved in DMSO (Tocris Bioscience, Ellisville, MI). Interleukin (IL)-1β was dissolved in dH_2O (Sigma-Aldrich). All treatments were for 18 h. Compounds were added directly to serum-free media.

2.2.7. TRANSFECTION AND THE DUAL LUCIFERASE ASSAY

Promoter-reporter plasmids used to study CB_1 promoter activity included: 1) a 1 kb fragment of the human CB_1 promoter, cloned into the *Mlu*I and *Bgl*II sites of the minimal promoter pELS plasmid, driving expression of *Renilla* luciferase (pCNR1) (Cat No. S701885; SwitchGear Genomics, Menlo Park, CA), 2) the pELS plasmid (SwitchGear Genomics), 3) a tandem repeat NF-κB response element promoter driving expression of firefly luciferase in the minimal promoter pTA plasmid (pNF; Cat No. LR0051; Panomics, Santa Clara, CA), and 4) the pTA plasmid (Panomics). The pCMV4-p65 plasmid used to study mHtt-mediated transcriptional dysregulation was obtained from Warner C Greene *via* Addgene (Addgene plasmid 21966) (Ballard *et al*., 1992).

Transfections were performed using Lipofectamine 2000® reagent according to the manufacturer's instructions with 400 ng pCNR1, or pELS (data not shown), and 200 ng pNF or

pTA (data not shown; Invitrogen, Burlington, ON), or 400 ng pCMV4-p65. The dual luciferase assay was performed according to the manufacturer's instructions (Promega, Madison, WI). Luciferase activity data were normalized to total protein content in cell lysates (Cui *et al*., 2006).

2.2.8. STATISTICAL ANALYSES

Statistical analyses were conducted by one- or two-way analysis of variance (ANOVA), as indicated, using GraphPad (v. 5.0, Prism). *Post-hoc* analyses were performed using Bonferroni's or Tukey's tests, as indicated. Homogeneity of variance was confirmed using Bartlett's test. All results are reported as the mean ± the standard error of the mean (SEM).

2.3. RESULTS

2.3.1. P65/RELA LEVELS WERE LOWER IN THE R6/2 HD MOUSE STRIATUM AND IN THE CPU OF LATE-STAGE HD PATIENTS.

Past studies have shown that the levels of p65/RelA are lower in the presence of mHtt in cell culture models of HD (Marcora and Kennedy, 2010; Ghose *et al*., 2011). Here, p65/RelA mRNA levels were lower in 6 and 12 week-old R6/2 HD mice compared to age-matched, wild-type littermates, while p65/RelA protein levels were lower in 12 week-old R6/2 HD mice compared to age-matched, wild-type littermates ($P < 0.01$, Fig. 2-1A-C). Moreover, both p65/RelA mRNA and protein levels were decreased in CPu tissue derived from grades 3 and 4 HD donors ($P < 0.001$, Fig. 2-2A-C).

2.3.2. THE EXPRESSION OF SEVERAL P65/RELA-REGULATED CYTOKINES AND CHEMOKINES WAS REDUCED IN THE HD CPU

p65/RelA regulates the expression of many genes. Specifically, we were interested in genes of the cytokine and endocannabinoid systems. We hypothesized that genes whose expression was regulated by p65/RelA would be repressed in HD. This hypothesis was tested by studying the endocannabinoid system and a representative panel of 27 cytokines. This panel consisted of those cytokines whose protein levels are most-often dysregulated in neuroinflammatory and neurodegenerative states (Bio-Rad). MatInspector software (v.

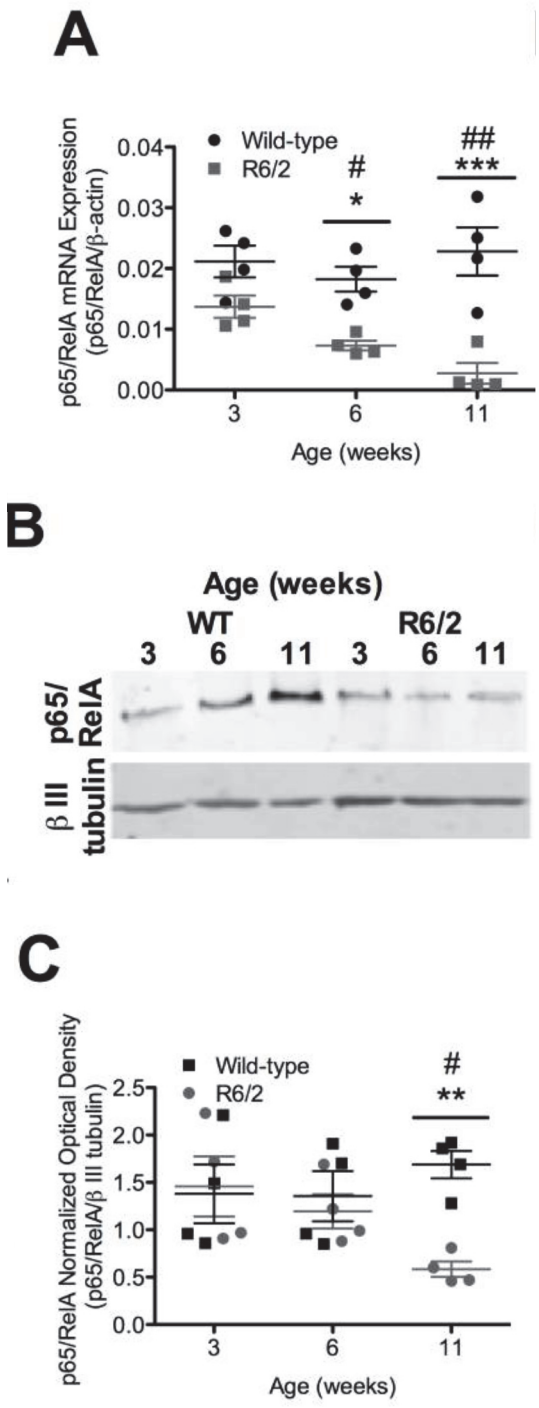

Figure 2-1. p65/RelA mRNA and protein levels were decreased in the striatum of R6/2 HD mice at 6 weeks. The striatum was dissected from 3, 6, and 11 week-old R6/2 HD mice and age-matched wild-type littermates. **A)** p65/RelA mRNA levels were quantified *via* qRT-PCR and normalized to β-actin levels. **B)** A representative blot illustrating p65/RelA and β III tubulin protein detection using SDS-PAGE and western blot (one of four independently conducted experiments). **C)** The relative levels of p65/RelA protein were quantified using densitometry software (ImageJ). *$P < 0.05$, **$P < 0.01$, ***$P < 0.001$ relative to age-matched R6/2 HD mice, #$P < 0.05$, ##$P < 0.01$ R6/2 HD mice relative to 3 week-old mice within genotype, as determined by two-way ANOVA followed by Bonferroni's *post-hoc* test ($n = 4$, mean ± SEM).

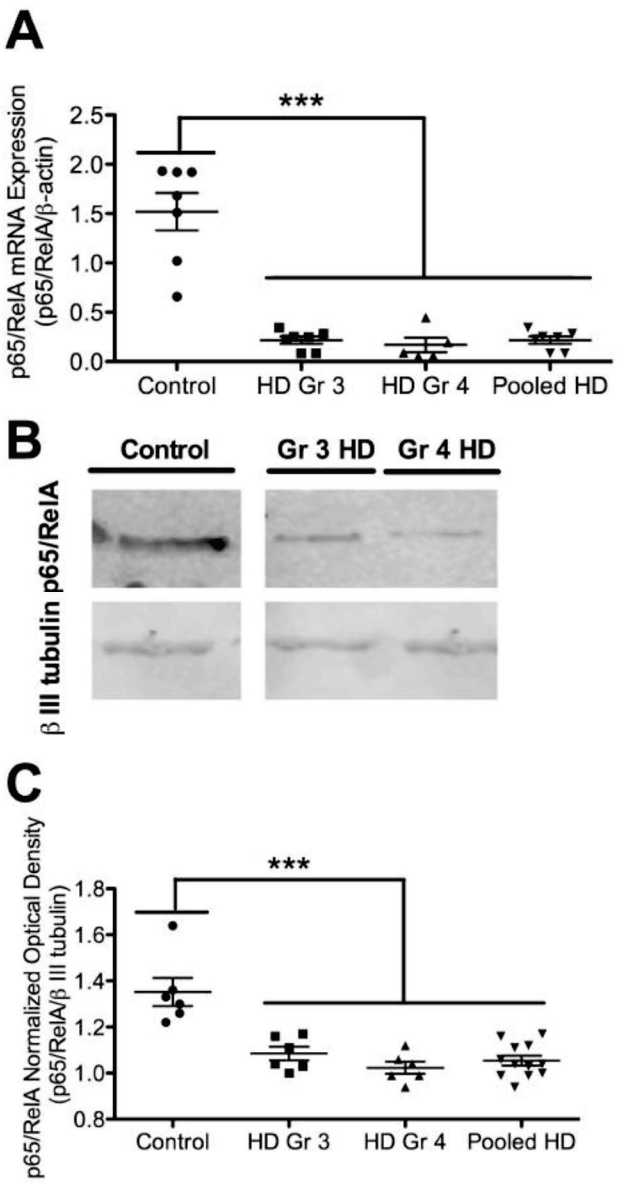

Figure 2-2. p65/RelA mRNA and protein levels were decreased in CPu tissue from HD donors. A) RNA was isolated from the CPu of HD donors and healthy controls. p65/RelA mRNA levels were quantified *via* qRT-PCR and normalized to β-actin levels. **B)** A representative blot illustrating p65/RelA and β III tubulin protein detection using SDS-PAGE and western blot (one of four independently conducted experiments). **C)** The relative levels of p65/RelA protein were quantified using densitometry software (ImageJ). ***$P < 0.001$ relative to control tissue, as determined by one-way ANOVA followed by Tukey's *post-hoc* test ($n = 7$ 'control' and 'HD Gr 3', $n = 5$ 'HD Gr 4', $n = 12$ 'Pooled HD' mean ± SEM).

8.0.6) was used to compare the promoter regions of 27 cytokines, as well as components of the endocannabinoid system (Table 2-3). We found that the human macrophage inflammatory protein (MIP)-1β, IL-8, TNFα, granulocyte macrophage colony-stimulating factor (GM-CSF), IL-1β, CB_1, and CCL5 promoters contained multiple p65/RelA binding sequences within their promoters, and while other promoters also contained NF-κB regulatory elements (*e.g.* CB_2), the sequences of these elements did not correspond to the consensus sequence for p65/RelA. Of the 27 cytokines analyzed, 6 were found to be decreased in grade 3 and 4 HD tissue, relative to control tissue, including: IL-1β ($P < 0.001$), IL-8 ($P < 0.001$), CCL5 ($P < 0.001$), GM-CSF ($P < 0.05$), MIP-1β ($P < 0.05$), and TNFα ($P < 0.05$ grade 3, $P < 0.01$ grade 4 and pooled, Fig. 2-3A-F). These were the same proteins whose gene promoters contained the greatest number of p65/RelA binding sites among the genes included in our *in silico* analyses, thus confirming our hypothesis (Table 2-3). Only the levels of one protein, FGF Basic, were increased in grade 3 and 4 HD tissue, relative to control tissue ($P < 0.05$ grade 3, $P < 0.01$ grade 4 and pooled, Fig. 2-3G). The levels of the remaining 20 cytokines and chemokines included in our multiplex ELISA were unchanged in HD tissue compared to control tissue (Table 2-4).

To determine whether p65/RelA-regulated cytokine expression was dysregulated during HD progression, the mRNA levels of IL-1β, CCL5, TNFα, FGF basic, IL-6, MCP-1 were quantified in striatal tissue from 3, 6, and 11 week-old R6/2 HD mice, and age-matched wild-type littermates. All mouse models of HD are limited by the relatively short time span over which disease progression occurs because HD is a neurodegenerative disease that progressively worsens over the course of many years. R6/2 HD mice are considered a relatively accurate model of early changes in HD pathogenesis (Bari *et al.*, 2013; Blázquez *et al.*, 2011). Although R6/2 HD mice exhibit an early onset of HD symptoms and rapid disease progression, this model was chosen because CB_1 gene expression is decreased early in disease progression in these mice, as it is in HD patients (Denovan-Wright and Robertson, 2000). IL-1β ($P < 0.001$) and

Table 2-3. Several cytokine, chemokine, and endocannabinoid genes contain multiple NF-κB p65 promoter elements

Gene name	Protein	Size of promoter examined (bp)	Sequence Accession number	Number of NF-κB p65 elements	Total number of NF-κB elements
CCL4	**MIP-1β**	**958**	**NM_002984.2**	**4**	**10**
IL8	**IL-8**	**1085**	**NM_000584.3**	**4**	**9**
TNF	**TNFα**	**1028**	**NM_000594.3**	**4**	**4**
CSF2	**GM-CSF**	**1004**	**NM_000758.3**	**3**	**5**
IL1b	**IL-1β**	**964**	**NM_000576.2**	**3**	**4**
CNR1	**CB1**	**902**	**NM_016083.4**	**3**	**3**
CCL5	**CCL5**	**1067**	**NM_002985.2**	**2**	**14**
CSF3	G-CSF	1013	NM_000759.3	2	12
IL6	IL-6	1214	NM_000600.3	2	9
IL9	IL-9	908	NM_000590.1	2	7
CCL2	MCP-1	999	NM_002982.3	2	6
IL13	IL-13	979	NM_002188.2	2	4
IL12	IL-12	1423	NM_000882.3	1	12
MGLL	MAGL	1190	NM_007283.6	1	3
IL4	IL-4	1049	NM_000589.3	1	3
IL7	IL-7	1058	NM_000880.3	0	6
IL15	IL-15	906	NM_172175.2	0	6
1L1ra	IL-1rα	1086	NM_000877.2	0	3
IL5	IL-5	1041	NM_000879.2	0	3
bFGF	**FGF Basic**	**1011**	**NM_002006.4**	**0**	**3**
CCL3	MIP-1α	926	NM_002983.2	0	3
CNR2	CB2	701	NM_001841.2	0	2
IFNG	IFN-γ	907	NM_000619.2	0	2
CXCL10	IP-10	1067	NM_001565.3	0	1
FAAH1	FAAH	919	NM_001441.2	0	1
IL2	IL-2	972	NM_000586.3	0	1
IL10	IL-10	994	NM_000572.2	0	1
CCL11	Eotaxin	1076	NM_002986.2	0	1
VEGF	VEGF	996	NM_003376.5	0	1
IL17	IL-17	1013	NM_002190.2	0	0
PDGFB	PDGF-ββ	992	NM_002608.2	0	0

Regulator elements were defined as:	Consensus Sequence (5' - 3')
NF-κB1 (p105, p50), NF-κB2 (p100, p52)	NGGRNNYYCC
NF-κB RelA (p65)	GGGRNNYYCC HGGARNYYCC

Where H = A, C, or T; R = A or G; Y = C or T; N = A, G, C, or T

Bold font indicates genes whose levels differed in HD tissue compared to healthy controls.

CB, cannabinoid receptor; CCL, Chemokine (C-C) motif ligand; FAAH, fatty acid amide hydrolase; FGF, fibroblast growth factor; GM-CSF, Granulocyte macrophage colony-stimulating factor; IFN, interferon; IL, interleukin; MAGL, monoacyl glycerol lipase; MCP, monocyte chemotactic protein; MIP, macrophage inflammatory protein; PDGF, platelet-derived growth factor; TNF-α, tumor necrosis factor alpha; VEGF, vascular endothelial growth factor.

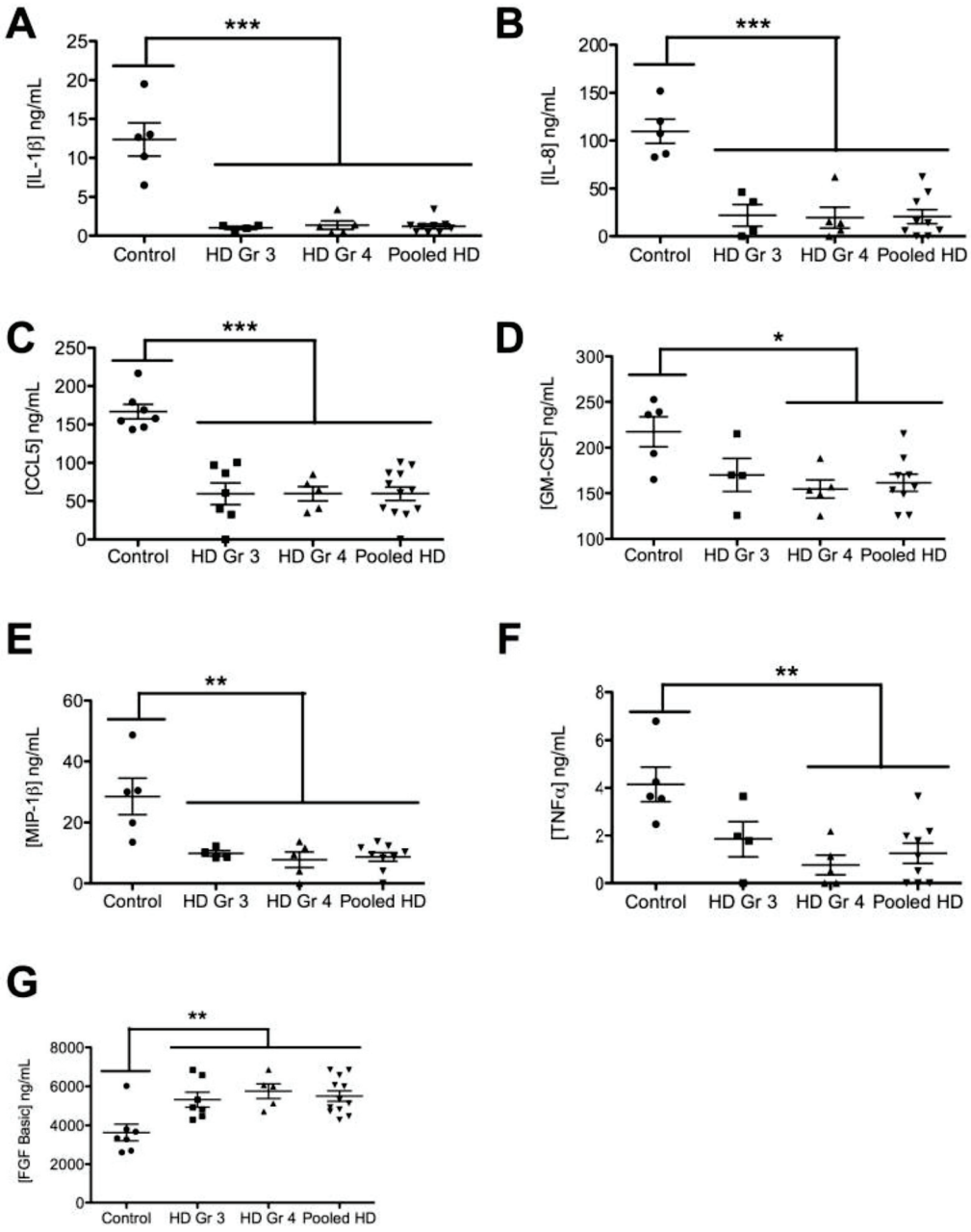

Figure 2-3. Cytokines and chemokines that contain multiple p65/RelA NF-κB promoter regulatory elements were down-regulated in CPu tissue from HD donors. Protein was isolated from the CPu of HD donors and healthy controls. IL-1β **(A)**, IL-8 **(B)**, CCL5 **(C)**, GM-CSF **(D)**, MIP-1β **(E)**, TNFα **(F)**, and FGF basic **(G)** levels were quantified *via* multiplex ELISA (bio-plex). Data were analyzed as concentrations within the range of the standard curve. **P* < 0.05, ***P* < 0.01, ****P* < 0.001 relative to control tissue, as determined by one-way ANOVA followed by Tukey's *post-hoc* test (*n* = 7 'control' and 'HD Gr 3', *n* = 5 'HD Gr 4', *n* = 12 'Pooled HD' mean ± SEM).

Table 2-4. Observed cytokine concentration in human control and HD donor tissue.

Group	*n*	Target	Mean [Target] (ng/mL)	SEM	*P*	Target	Mean [Target] (ng/mL)	SEM	*P*
Control	7	**IL-1β**	**12.37**	**1.80**	**< 0.001**	IL-1rα	57.71	2.24	0.071
HD Gr 3	7		**1.04**	**0.14**			62.61	9.32	
HD Gr 4	5		**1.38**	**0.55**			50.54	2.37	
Pooled HD	12		**1.23**	**0.26**			55.47	5.30	
Control	7	IL-4	6.60	0.66	0.099	IL-5	1.13	0.35	0.094
HD Gr 3	7		7.02	1.72			1.50	0.65	
HD Gr 4	5		6.73	0.45			1.64	0.79	
Pooled HD	12		6.95	0.96			1.56	0.48	
Control	7	IL-7	46.43	9.74	0.091	**IL-8**	**109.65**	**10.64**	**< 0.001**
HD Gr 3	7		48.30	11.92			**22.08**	**8.55**	
HD Gr 4	5		37.57	7.62			**19.68**	**10.95**	
Pooled HD	12		38.90	6.22			**20.75**	**6.41**	
Control	7	IL-10	15.81	1.76	0.072	IL-12	8.16	1.50	0.091
HD Gr 3	7		15.73	2.93			8.09	2.98	
HD Gr 4	5		11.29	3.75			5.82	1.93	
Pooled HD	12		12.31	2.23			6.37	1.81	
Control	7	IL-15	16.37	2.07	0.072	IL-17	183.54	14.65	0.084
HD Gr 3	7		13.38	3.53			174.72	25.91	
HD Gr 4	5		10.47	4.90			150.84	30.83	
Pooled HD	12		10.94	2.53			151.07	18.18	
Control	7	**FGF-b**	**3630.53**	**433.87**	**0.002**	G-CSF	66.81	22.11	0.065
HD Gr 3	7		**5320.91**	**380.94**			53.85	12.51	
HD Gr 4	5		**5755.09**	**377.51**			41.22	6.78	
Pooled HD	12		**5501.82**	**268.20**			42.18	6.44	

Table 2-4 Continued. Observed cytokine concentration in human control and HD donor tissue.

Group	*n*	Target	Mean [Target] (ng/mL)	SEM	*P*	Target	Mean [Target] (ng/mL)	SEM	*P*
Control	7	IL-2	14.14	1.93	0.870	IFN-γ*	0.00	0.00	0.000
HD Gr 3	7		13.58	3.73			0.00	0.00	
HD Gr 4	5		9.83	4.91			0.00	0.00	
Pooled HD	12		11.17	2.61			0.00	0.00	
Control	7	IL-6	164.03	52.26	0.082	MIP-1α	34.10	5.52	0.470
HD Gr 3	7		97.70	26.16			21.50	4.75	
HD Gr 4	5		82.65	10.86			33.41	9.31	
Pooled HD	12		79.80	11.12			27.05	4.85	
Control	7	IL-9	95.64	14.08	0.064	**CCL5**	**166.70**	**9.53**	**<0.001**
HD Gr 3	7		73.83	23.09			**59.57**	**14.22**	
HD Gr 4	5		57.47	24.74			**59.60**	**9.51**	
Pooled HD	12		58.32	14.05			**59.58**	**8.83**	
Control	7	IL-13	19.71	1.57	0.083	IP-10	221.70	11.72	0.100
HD Gr 3	7		16.86	2.89			211.35	49.30	
HD Gr 4	5		12.90	10.11			214.18	29.67	
Pooled HD	12		14.97	4.95			211.44	29.11	
Control	7	Eotaxin	220.46	31.13	0.077	PDGF-ββ	36.32	3.69	0.052
HD Gr 3	7		170.56	43.10			33.74	7.75	
HD Gr 4	5		154.31	70.95			22.89	5.16	
Pooled HD	12		166.37	37.36			25.02	5.08	
Control	7	**GM-CSF**	**219.97**	**16.84**	**0.040**	**TNFα**	**4.15**	**0.61**	**0.002**
HD Gr 3	7		**171.10**	**30.10**			**1.85**	**0.56**	
HD Gr 4	5		**154.70**	**9.21**			**0.77**	**0.41**	
Pooled HD	12		**158.43**	**16.77**			**1.25**	**0.36**	
Control	7	MCP-1	44.76	10.61	0.380	**MIP-1β**	**16.42**	**5.68**	**0.031**
HD Gr 3	7		53.15	14.90			**10.61**	**2.31**	
HD Gr 4	5		67.89	6.05			**7.83**	**2.31**	
Pooled HD	12		53.39	7.41			**9.02**	**1.55**	

Table 2-4 Continued. Observed cytokine concentration in human control and HD donor tissue.

Group	*n*	Target	Mean [Target] (ng/mL)	SEM	*P*
Control	7	VEGF	5.21	1.56	0.050
HD Gr 3	7		7.07	1.70	
HD Gr 4	5		3.83	1.04	
Pooled HD	12		5.02	1.08	

*IFN-γ levels were below the detection threshold.
Bolded regions indicate significant differences ($P < 0.01$) *via* one-way ANOVA followed by Tukey's *post-hoc* test.

CCL5 ($P < 0.05$) mRNA levels were lower in the striatum of 6 and 11 week-old R6/2 HD mice, and TNFα ($P < 0.05$) mRNA levels were lower in the striatum of 11 week-old R6/2 HD mice, compared to age-matched, wild-type littermates or 3 week-old R6/2 HD mice (Fig. 2-4A-C). No change in the mRNA levels of FGF basic, IL-6 or MCP-1 were detected in R6/2 HD mice compared to wild-type mice (Fig. 2-4D-F). Therefore, repression of IL-1β, CCL5, and TNFα mRNA occurred during the same time period as p65/RelA in R6/2 HD mice and resembled the repression of these proteins observed in tissue from the human HD CPu.

2.3.3. The endocannabinoid system was dysregulated in R6/2 HD mice and in the CPu of late-stage HD patients.

We had observed that the promoter of the CB_1 gene, like the cytokines and chemokines analyzed above, contained multiple p65/RelA binding sites (Table 2-3). CB_1 mRNA levels are lower in the lateral striatum of HD mice than wild-type littermates (Denovan-Wright and Robertson, 2000; McCaw *et al*., 2004). We wanted to determine whether this decrease in CB_1 mRNA in HD was specific to the lateral striatum, where steady-state CB_1 levels are normally high, or whether CB_1 mRNA levels were decreased throughout the striatum and cortex. CB_1 mRNA levels were decreased in the lateral striatum of 6 week-old R6/2 HD mice compared to age-matched, wild-type littermates ($P < 0.001$, Fig. 2-5A,B). CB_1 mRNA levels were also reduced in the dorsomedial and ventromedial striatum of 6 week-old R6/2 HD mice compared to age-matched, wild-type littermates ($P < 0.001$, Fig 2-5C,D). Further, the number of CB_1-positive nuclei in the cortex was reduced in 6 week-old R6/2 HD mice compared to age-matched, wild-type littermates ($P < 0.001$, Fig. 2-5E). Therefore, CB_1 levels declined throughout the striatum and cortex of HD mice during the same time period as IL-1β, CCL5, TNFα, and p65/RelA.

Because endocannabinoid tone influences the expression of CB_1 (Laprairie *et al*., 2013), we wanted to examine other components of the endocannabinoid system to determine whether they, too, were dysregulated in HD. FAAH mRNA levels were higher in the cortices of 3, 6, and 11 week-old R6/2 mice compared to wild-type, age-matched littermates ($P < 0.05$, Fig. 2-6A,B).

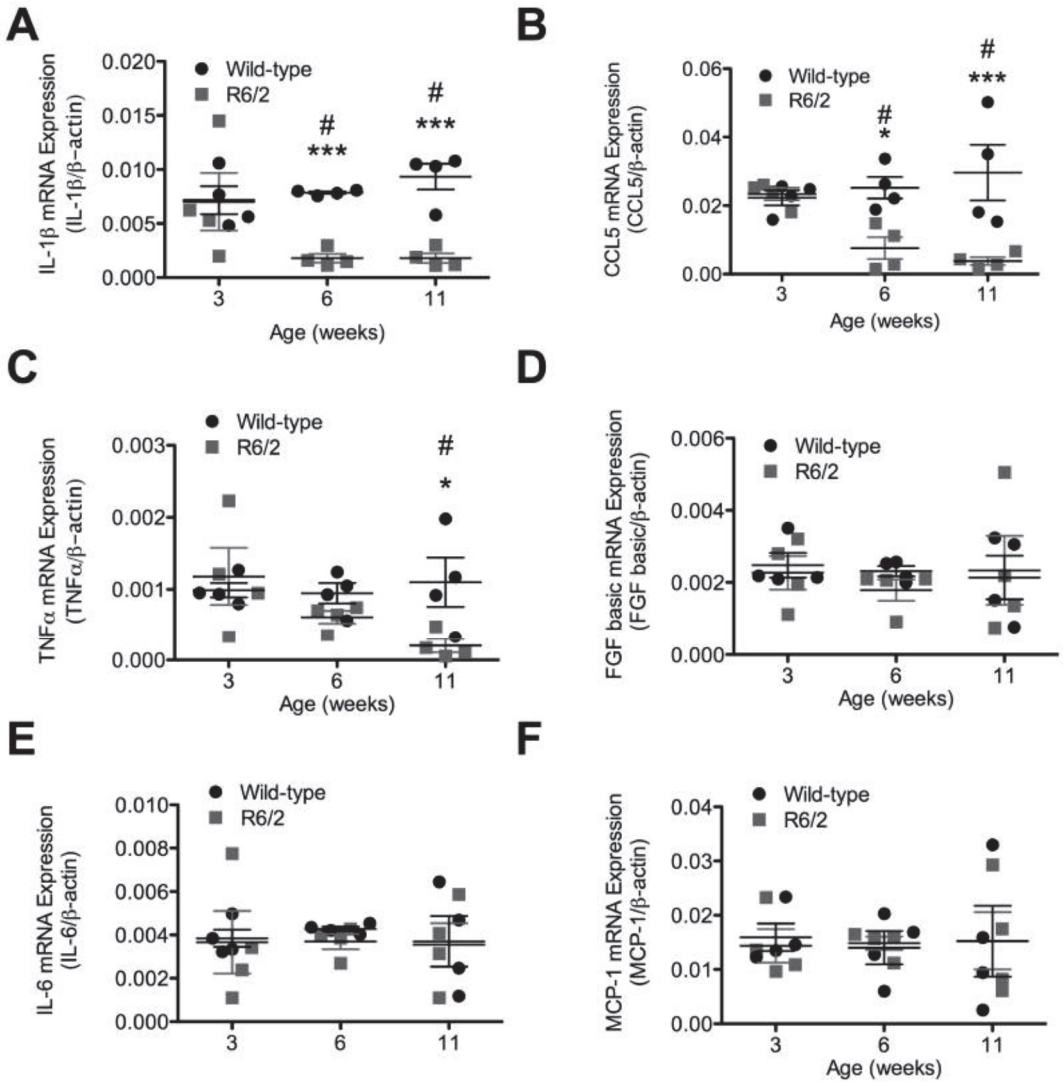

Figure 2-4. IL-1β, CCL5, and TNFα mRNA levels are decreased in the striatum of R6/2 HD mice. The striatum was dissected from 3, 6, and 11 week-old R6/2 HD mice and age-matched wild-type littermates. **A)** IL-1β, **B)** CCL5, **C)** TNFα, **D)** FGF basic, **E)** IL-6, and **F)** MCP-1 mRNA levels were quantified *via* qRT-PCR and normalized to β-actin levels. *$P < 0.05$, ***$P < 0.001$ relative to age-matched R6/2 HD mice, #$P < 0.05$ R6/2 HD mice relative to 3 week-old mice within genotype, as determined by two-way ANOVA followed by Bonferroni's *post-hoc* test ($n = 4$, mean ± SEM).

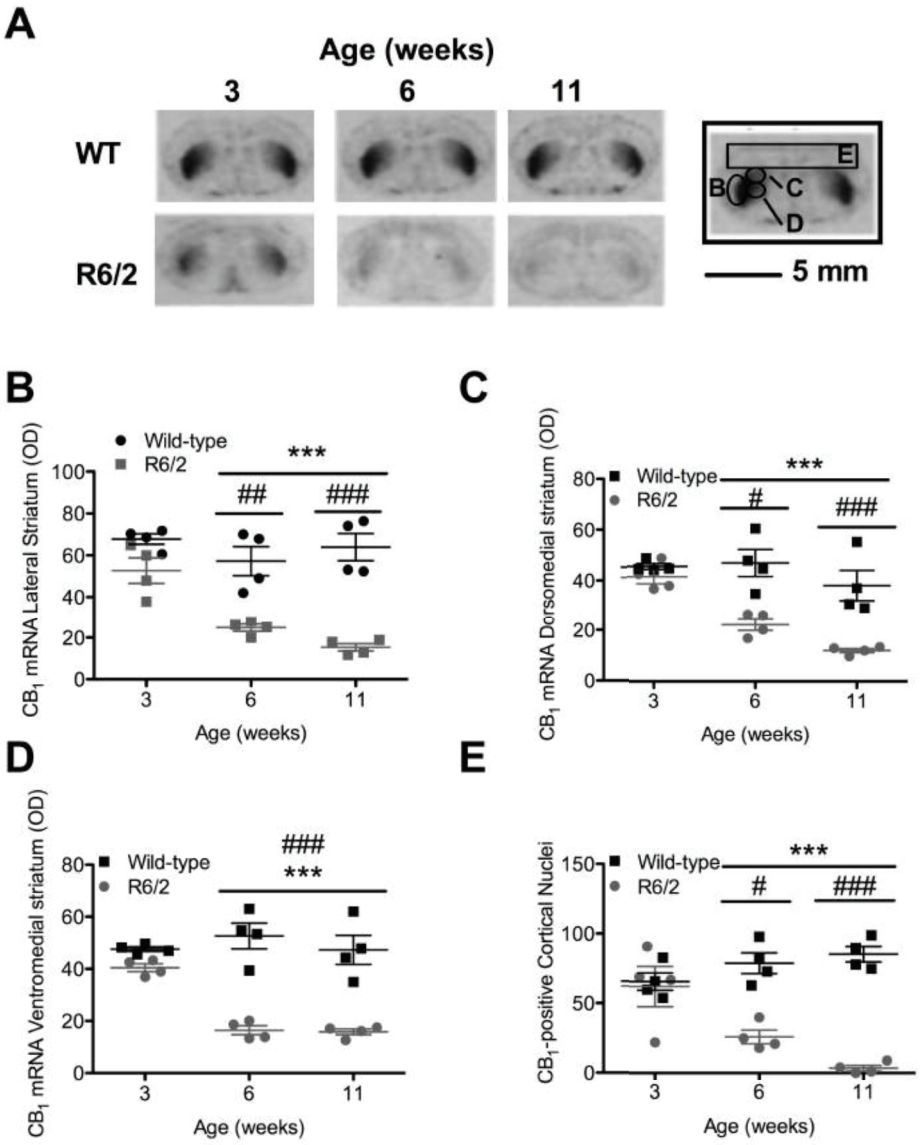

Figure 2-5. CB_1 mRNA levels were decreased in the lateral, dorsomedial, and ventromedial striatum, and cortex of R6/2 HD mice at 6 weeks. *In situ* hybridization was used to detect CB_1 mRNA optical density (OD) in coronal sections from 3, 6, and 11 week-old R6/2 HD mice and age-matched wild-type littermates. **A)** Representative coronal sections illustrate decreased CB_1 levels in the striatum and cortex of R6/2 HD mice during disease progression. The boxed section illustrates the regions from which data were acquired for panels B – E. Background-corrected CB_1 mRNA levels were quantified using densitometry software (Kodak) in the **B)** lateral striatum, **C)** dorsomedial striatum, and **D)** ventromedial striatum. **E)** CB_1-postivie nuclei were counted in the cortex. ***$P < 0.001$ relative to age-matched R6/2 HD mice, #$P < 0.05$, ##$P < 0.01$, ###$P < 0.001$ R6/2 HD mice relative to 3 week-old mice within genotype, as determined by two-way ANOVA followed by Bonferroni's *post-hoc* test ($n = 4$, mean ± SEM).

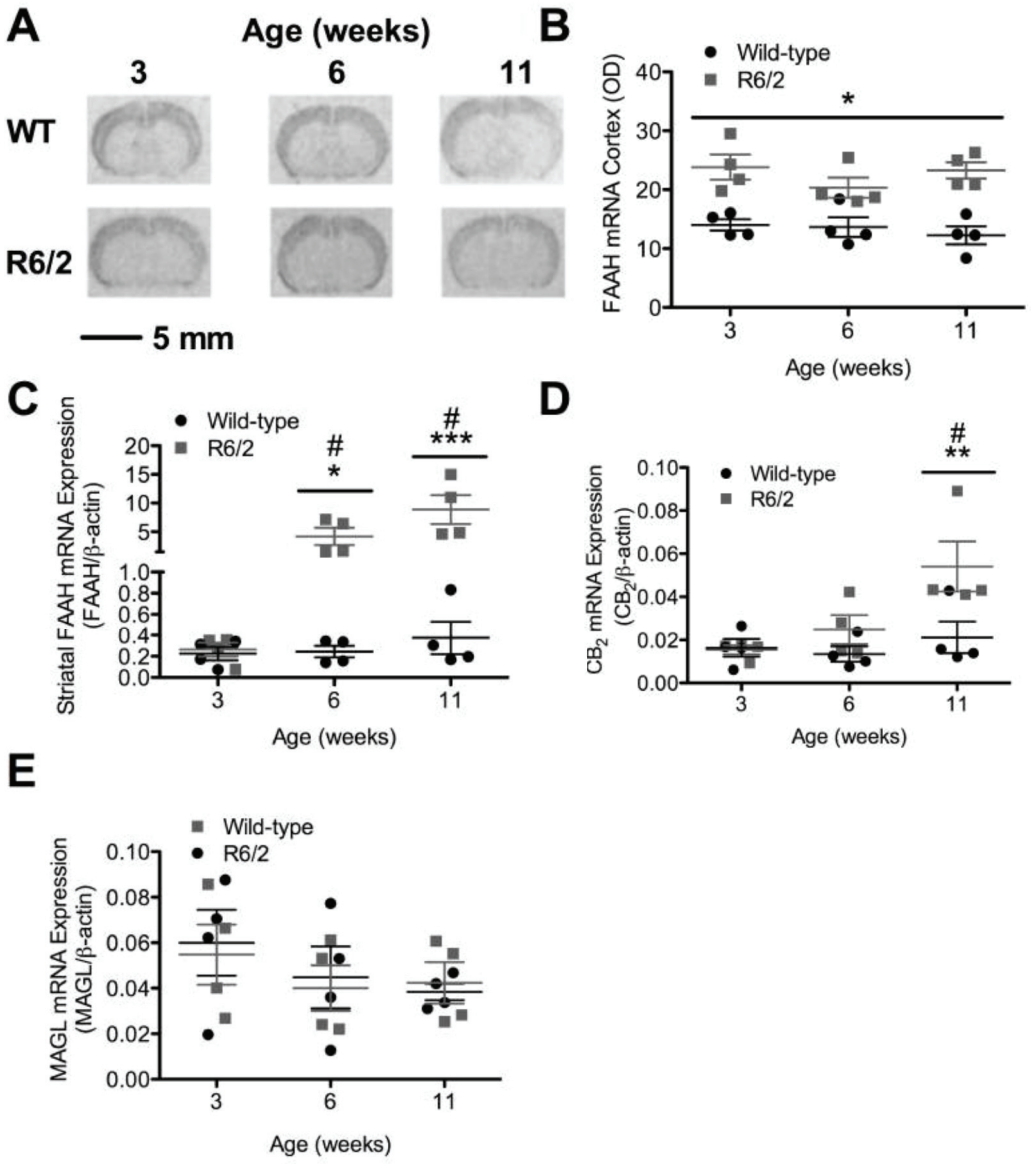

Figure 2-6. FAAH and CB_2 mRNA levels were increased in R6/2 HD mice. A) *In situ* hybridization was used to detect FAAH mRNA optical density (OD) in coronal sections from 3, 6, and 11 week-old R6/2 HD mice and age-matched wild-type littermates. Representative coronal sections illustrate increased FAAH levels in the cortex of R6/2 HD mice during disease progression. **B)** Background-corrected CB_1 mRNA levels were quantified using densitometry software (Kodak) in the cortex. Striatal **C)** FAAH, **D)** CB_2, and **E)** MAGL mRNA levels were quantified *via* qRT-PCR and normalized to β-actin levels. $*P < 0.05$, $**P < 0.01$, $***P < 0.001$ relative to age-matched R6/2 HD mice, $\#P < 0.05$ R6/2 HD mice relative to 3 week-old mice within genotype, as determined by two-way ANOVA followed by Bonferroni's *post-hoc* test (n = 4, mean ± SEM).

FAAH mRNA levels were also higher in the striatum of 6 week-old R6/2 HD mice compared to age-matched, wild-type littermates, as determined by qRT-PCR ($P < 0.05$; Fig. 2-6C).

Additionally, CB_2 mRNA levels were higher in the striatum of 11 week-old R6/2 mice compared to age-matched, wild-type controls ($P < 0.05$, Fig. 2-6D). No change was observed in monacyl glycerol lipase (MAGL) levels in striatal tissue from R6/2 HD mice compared to controls (Fig. 2-6E). Furthermore, CB_1 levels were lower ($P < 0.001$, Fig. 2-7A), while CB_2 ($P < 0.001$, Fig. 2-7B) and FAAH $P < 0.01$, Fig. 2-7C) levels were higher, in the human HD CPu compared to control tissue, suggesting that R6/2 HD mice accurately reflect the dysregulation of the endocannabinoid system observed in human HD tissue.

2.3.4. NF-κB AND CB_1 PROMOTER ACTIVITY WERE INDUCED BY CB_1 AGONISM AND IL-1B TREATMENT IN THE PRESENCE OF MHTT

CB_1 promoter activity and mRNA levels can be increased *via* CB_1 agonism in ST*Hdh*$^{Q7/Q7}$ cells through an NF-κB-dependent mechanism (Laprairie *et al*., 2013). Here, we wanted to determine whether CB_1 promoter activity could be induced in the presence of mHtt *via* CB_1 agonism. We, and others, have found that CB_1 mRNA levels are lower in ST*Hdh*$^{Q7/Q111}$ and $^{Q111/Q111}$ cell culture models of HD (Blázquez *et al*., 2011; Laprairie *et al*., 2013). Both NF-κB and CB_1 promoter activity were lower in the presence of mHtt compared to ST*Hdh*$^{Q7/Q7}$ cells ($P < 0.05$, Fig. 2-8A,B). Further, CB_1 and NF-κB promoter activities were induced in ST*Hdh* cells following treatment with 1 μM ACEA ($P < 0.05$ compared to vehicle-treated cells, Fig. 2-8A,B). Similarly, addition of 5 ng/mL of IL-1β induced NF-κB and CB_1 promoter activity in all ST*Hdh* cell lines compared to vehicle-treated cells ($P < 0.05$, Fig. 2-8A,B). Because CB_2 and FAAH mRNA levels were greater in human HD tissue compared to healthy controls, we wanted to determine whether treatment with a CB_2 agonist or a FAAH inhibitor would also affect NF-κB and CB_1 promoter activity. CB_2 and FAAH were expressed in ST*Hdh* cells and we observed that CB_2 and FAAH mRNA levels were increased in ST*Hdh*$^{Q7/Q111}$ and ST*Hdh*$^{Q111/Q111}$ compared to

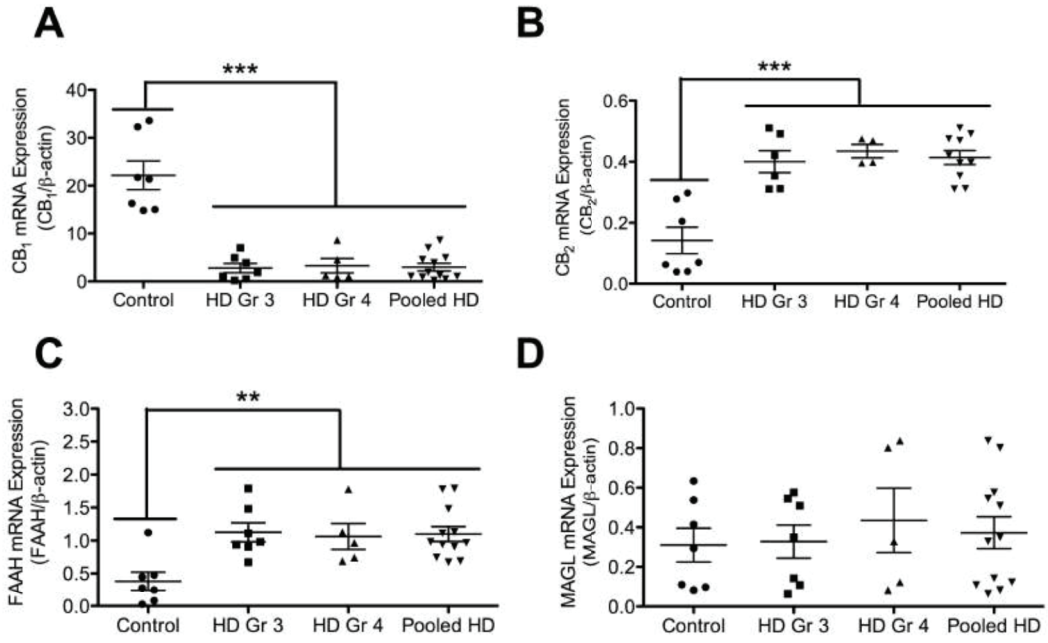

Figure 2-7. CB_1 mRNA levels were decreased, while FAAH and CB_2 levels were increased in CPu tissue from HD donors. RNA was isolated from the CPu of HD donors and healthy controls. **A)** CB_1, **B)** CB_2, **C)** FAAH, and **D)** MAGL mRNA levels were quantified *via* qRT-PCR and normalized to β-actin levels. $^{**}P < 0.01$, $^{***}P < 0.001$ relative to control tissue, as determined by one-way ANOVA followed by Tukey's *post-hoc* test ($n = 7$ 'control' and 'HD Gr 3', $n = 5$ 'HD Gr 4', $n = 12$ 'Pooled HD' mean ± SEM).

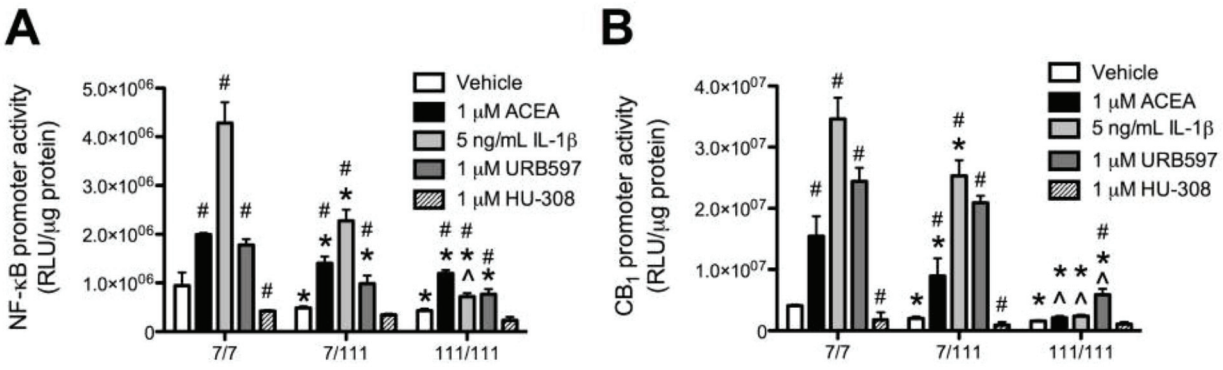

Figure 2-8. NF-κB and CB_1 promoter activity were induced by enhancing cannabinoid tone and inhibited by CB_2 agonism. ST*Hdh*$^{Q7/Q7}$ (7/7), $^{Q7/Q111}$ (7/111), and $^{Q111/Q111}$ (111/111) cells were transfected with 200 ng of pNF plasmid (NF-κB promoter driving the expression of firefly luciferase) and 400 ng of pCNR1 (CB_1 promoter driving the expression of *Renilla* luciferase) and treated with vehicle, 1 μM ACEA (CB_1 agonist), 5 ng/mL IL-1β, 1 μM URB597 (FAAH inhibitor), or 1 μM HU-308 (CB_2 agonist) for 18 h. **A)** NF-κB and **B)** CB_1 promoter activities were assessed *via* the dual luciferase assay and normalized to total protein. *$P < 0.05$ compared to 7/7 cells within treatment, ^$P < 0.05$ compared to 7/111 cells within treatment, #$P < 0.05$ compared to vehicle treatment within genotype, as determined by two-way ANOVA followed by Bonferroni's *post-hoc* test ($n = 6$, mean ± SEM).

ST*Hdh*$^{Q7/Q7}$ cells ($P < 0.05$, Fig. 2-9A,B). Similar to the effects of ACEA, inhibition of FAAH *via* 1 μM URB597 induced NF-κB and CB_1 promoter activity in ST*Hdh* cells ($P < 0.05$, Fig. 2-8A,B). Conversely, activation of CB_2 *via* 1 μM HU-308 decreased both CB_1 and NF-κB promoter activity in all ST*Hdh*$^{Q7/Q7}$ and ST*Hdh*$^{Q7/Q111}$ cells compared to vehicle-treated cells ($P < 0.05$, Fig. 2-8A,B). None of the above treatments affected the promoter activity of the minimal promoter pELS or pTA plasmids (data not shown). Therefore, modulation of cannabinoid tone altered NF-κB-dependent promoter activity in the presence of mHtt.

Next, we wanted to determine whether the cytokines that were repressed in the R6/2 HD striatum were expressed by ST*Hdh* cells, if their expression was decreased in the presence of mHtt, and whether cannabinoid treatment could increase the expression of these cytokines. Using qRT-PCR, we found that while ST*Hdh* cells do not endogenously express IL-1β, IL-6, TNFα, or FGF basic (data not shown), they do express CCL5 and MCP-1 (Fig. 2-10A,B). CCL5 mRNA levels were lower in ST*Hdh*$^{Q7/Q111}$ and ST*Hdh*$^{Q111/Q111}$ cells compared to ST*Hdh*$^{Q7/Q7}$ cells ($P < 0.05$, Fig. 2-10A). CCL5 mRNA levels were increased ~3-fold in all ST*Hdh* cells transfected with pCMV4-p65 or treated with 1 μM ACEA, URB597, or AM630 for 18 h compared to vehicle controls ($P < 0.05$, Fig. 2-10A). CCL5 levels remained lower in p65-transfected, ACEA-, URB597-, and AM630-treated ST*Hdh*$^{Q7/Q111}$ and ST*Hdh*$^{Q111/Q111}$ cells compared to ST*Hdh*$^{Q7/Q7}$ cells ($P < 0.05$, Fig. 2-10A). Co-treatment of cells with 1 μM ACEA and 1 μM AM630 for 18 h resulted in a ~14-fold increase in CCL5 mRNA levels, which was not different between ST*Hdh* cell types ($P < 0.05$, Fig. 2-10A). MCP-1 mRNA levels did not differ between ST*Hdh* cells types and were not changed by any treatment (Fig. 2-10B). Although p65/RelA levels were lower HD tissue (Figs. 2-1 and 2-2), p65/RelA activity was increased both directly and *via* changes in cannabinoid tone in the ST*Hdh* cells expressing mHtt. Therefore, modulation of p65/RelA activity may normalize the levels of some genes that are repressed in the presence of mHtt, despite the repression of these genes by mHtt.

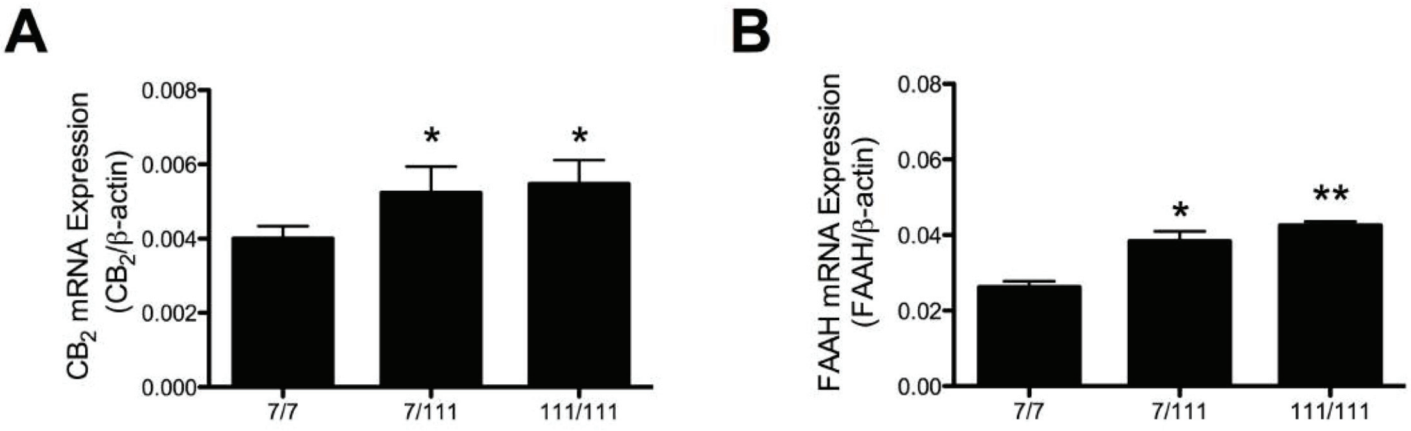

Figure 2-9. CB_2 and FAAH mRNA levels were higher in ST*Hdh*$^{Q7/Q111}$ and $^{Q111/Q111}$ cells than ST*Hdh*$^{Q7/Q7}$ cells. RNA was extracted from ST*Hdh*$^{Q7/Q7}$ (7/7), $^{Q7/Q111}$ (7/111), and $^{Q111/Q111}$ (111/111) cells and **A)** CB_2 and **B)** FAAH mRNA levels were quantified *via* qRT-PCR and normalized to β-actin levels. **P* < 0.05, ***P* < 0.01 compared to 7/7 cells, as determined by one-way ANOVA followed by Tukey's *post-hoc* test (*n* = 6, mean ± SEM).

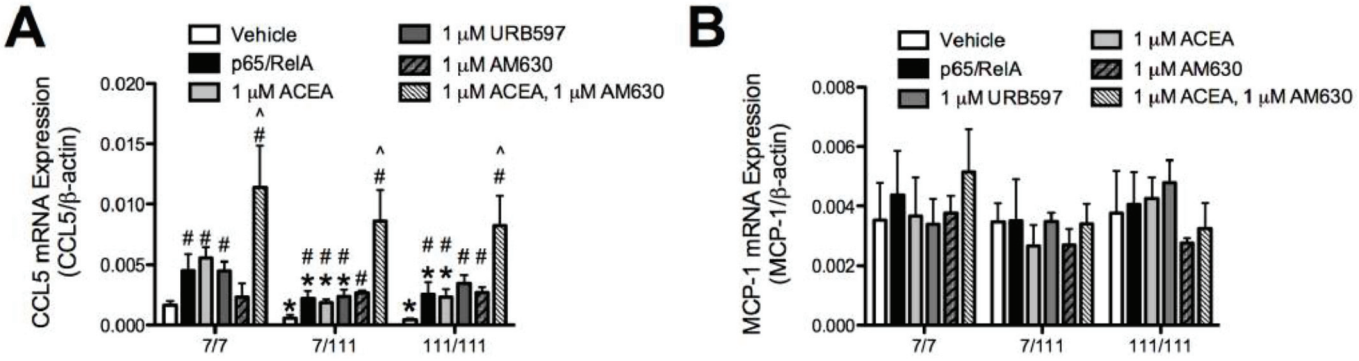

Figure 2-10. CCL5 mRNA expression was induced by overexpressing p65/RelA, activation of CB_1, and inhibition of CB_2. ST*Hdh*$^{Q7/Q7}$ (7/7), $^{Q7/Q111}$ (7/111), and $^{Q111/Q111}$ (111/111) cells were transfected with 400 ng of pCMV4-p65 or treated with vehicle, 1 μM ACEA (CB_1 agonist), 1 μM URB597 (FAAH inhibitor), 1 μM AM630 (CB_2 antagonist), or 1 μM ACEA + 1 μM AM630 for 18 h. **A)** CCL5 and **B)** MCP-1 mRNA levels were quantified *via* qRT-PCR and normalized to β-actin levels. **P* < 0.05 compared to 7/7 cells within treatment, #*P* < 0.05 compared to vehicle treatment within genotype, ^*P* < 0.05 compared to ACEA or AM630 treatment within cell type, as determined by two-way ANOVA followed by Bonferroni's *post-hoc* test (*n* = 6, mean ± SEM).

2.4. DISCUSSION

In this study we found that the expression of IL-1β, IL-8, CCL5, GM-CSF, MIP-1β, TNFα, and CB_1 were repressed in the CPu of grade 3 and 4 HD patients. We also observed that IL-1β, CCL5, TNFα, CB_1 were repressed in R6/2 HD mice, and CCL5 and CB_1 were repressed in ST*Hdh*$^{Q7/Q111}$ and ST*Hdh*$^{Q111/Q111}$ cells. The human gene promoters of each of these cytokines contain more p65/RelA elements, with higher sequence similarity to the p65/RelA element consensus sequence, than the other cytokines analyzed in our study. Therefore, both the cytokine and endocannabinoid systems are regulated, in part, by p65/RelA, which may be repressed in R6/2 HD mice and in the CPu of grade 3 and 4 HD patients.

Other authors have found that the expression and activity of p65/RelA are repressed in the presence of mHtt (Marcora and Kennedy, 2010; Ghose *et al*., 2011). Ghose *et al*. (2011) found that a miRNA that promotes the degradation of p65/RelA mRNA is up-regulated in mHtt-expressing cells and in the striatum of HD mice. Marcora and Kennedy (2010) found that the nuclear translocation of p65/RelA is inhibited in mHtt-expressing cells. Based on our data, we conclude that it is reduced p65/RelA mRNA and protein levels, and not a change in the transcription factor's activity, which contributes to changes in the expression of p65/RelA-regulated genes.

mHtt causes transcriptional dysregulation through a number of mechanisms (Hogel *et al*., 2012). For example, p65/RelA, Sp1 (Ravache *et al*., 2010), CREB (Cui *et al*., 2006), REST (Zuccato *et al*., 2007; Ravache *et al*., 2010), and TBP (Hogel *et al*., 2012) all contribute to the transcriptional regulation of CB_1, and each is affected by mHtt through sequestration, decreased activity at the promoter, or decreased expression. Therefore, increasing p65/RelA activity to affect a subset of genes may reverse some molecular signs of HD, but would not remove the underlying transcriptional dysregulation associated with expression of mHtt.

In contrast to our observations in human HD CPu tissue, most studies published to date have reported no change (Gadavarthi *et al*., 2009; Bouchard *et al*., 2012), or increased levels of

MIP-1β, IL-8, TNFα, GM-CSF, IL-1β (Dalrymple *et al*., 2007) in animal and cell culture models of HD (Chou *et al*., 2008; Nguyen *et al*., 2010; Franciosi *et al*., 2012). Previous studies performed using human samples have found no changes in IL-1β levels, and increased levels of IL-8, MIP-1β, and TNFα in the plasma (Wild *et al*., 2011) and CSF (Bjorqvist *et al*., 2008) of HD patients. Further, one study observed increases in several cytokines, including IL-8, in the CNS of HD patients compared to healthy controls (Silvestroni *et al*., 2009). However, only the mRNA expression, and not the protein levels, of these cytokines were quantified (Silvestroni *et al*., 2009). As in our study, CCL5 levels are decreased in the striatum of symptomatic R6/1 and R6/2 HD mice (Chou *et al*., 2008), GM-CSF levels are decreased in the plasma and cerebrospinal fluid of HD patients (Bjorqvist *et al*., 2008), and FGF basic levels are increased in the CPu of post-mortem HD tissue (Tooyama *et al*., 1993). Because we observed a decrease in CCL5 levels in mouse and human HD tissue and in cultured neuronal cells expressing mHtt, decreased expression of p65/RelA-regulated genes may be a direct consequence of mHtt in neurons. The microglial activation and increased cytokine levels reported elsewhere may be the result of treatment-specific conditions, such as treatment with lipopolysaccharide (Franciosi *et al*., 2012) or cell-specific conditions where microglia and macrophages have been examined in isolation (Ellrichmann *et al*., 2013). To our knowledge, this is the first observation that the levels of a subset of cytokines, that share a common promoter element, are lower in the CPu of HD tissue than in healthy tissue.

Proponents of cannabinoid-based therapies have suggested that cannabinoids might be useful for hyperkinetic and neurodegenerative movement disorders, such as HD (Glass *et al*., 2000; Denovan-Wright and Robertson, 2000). CB_1 promoter activity can be induced *via* p65/RelA in cell culture models of HD (Laprairie *et al*., 2013). Therefore, cannabinoid-based therapies targeting CB_1 may be a pharmacologically tractable means of normalizing p65/RelA-mediated gene expression in HD. CB_1 expression is decreased in the CPu of HD patients and the striatum and cortex of HD mice, while CB_2 levels are increased (Glass *et al*., 2000; Denovan-

Wright and Robertson, 2000; Blázquez *et al*., 2011; Miller and Devi, 2011; Laprairie *et al*., 2013). Based on the observation that cytokine production in the striatal neurons may be suppressed in HD, CB_2 agonists that inhibit cytokine production may aggravate this state (Rajesh *et al*., 2008). Indeed, CB_2 agonism inhibited CB_1 and NF-κB promoter activity, while CB_2 antagonism increased CCL5 levels such that the repressive effect of mHtt was no longer observed *in vitro*. Although CB_1 levels are decreased in HD, CB_1-specific agonists have been shown to increase expression of their cognate receptor (Borner *et al*., 2007; Mukhopadhyay *et al*., 2010; Proto *et al*., 2011; Laprairie *et al*., 2013). Moreover, cannabinoid agonism *via* FAAH inhibition mimicked the effects of CB_1 agonism in ST*Hdh* cells. Widespread changes in endocannabinoid tone that occur in HD could be modulated by FAAH inhibition to produce the beneficial effects of CB_1 agonism (Dowie *et al*., 2009, 2010). Therefore, CB_1-specific agonists, CB_2-specific antagonists, and inhibitors of FAAH, may promote neuronal survival in HD, while CB_2-specific cannabinoid agonists could exacerbate the suppression of p65/RelA-regulated genes in HD.

In this study, we were unable to determine whether changes in the expression of p65/RelA, or genes that may be regulated by p65/RelA, occur early in human HD patients, as a direct consequence of mHtt expression, or occur late, as the result of secondary changes. Furthermore, we were unable to measure cytokine mRNA levels due to a limited amount of human tissue. However, the observation that CCL5 levels were lower in ST*Hdh* neuronal cells expressing mHtt compared to wild-type ST*Hdh* cells supports the hypothesis that the levels of p65/RelA, and genes whose expression may be regulated by p65/RelA, may be decreased *via* mHtt in neurons.

2.4.1. CONCLUSIONS

In conclusion, we found that IL-1β, IL-8, CCL5, GM-CSF, MIP-1β, TNFα, and CB_1 levels were decreased, while CB_2 and FAAH levels were increased, in the CPu of late-stage HD patients. Similarly, IL-1β, CCL5, TNFα, and CB_1 levels were reduced, and CB_2 and FAAH levels were increased, in the striatum of R6/2 HD mice. Our *in silico* analysis of these promoters

provided evidence that these genes were co-regulated by p65/RelA. In cell culture, we observed that CB_1 agonism and CB_2 antagonism normalized p65/RelA and CB_1 promoter activity and cytokine levels *via* p65/RelA in the presence of mHtt. Therefore, cannabinoid-based therapies that activate p65/RelA *via* CB_1 may restore the neuroprotective effects of CB_1 (Laprairie *et al*., 2013), among others, in the HD CPu. The data presented here correlate changes in the cytokine and endocannabinoid systems to changes in p65/RelA levels in HD tissue. The *in vitro* data provide evidence for the possible co-regulation of the cytokine and endocannabinoid systems by p65/RelA in mHtt-expressing neurons. Determining the *in vivo* effects of modulating cytokine levels *via* cannabinoids in HD will provide further evidence to support this premise.

CHAPTER 3

TYPE 1 CANNABINOID RECEPTOR LIGANDS DISPLAY FUNCTIONAL SELECTIVITY IN A CELL CULTURE MODEL OF STRIATAL MEDIUM SPINY PROJECTION NEURONS

Contribution statement

The manuscript used as the basis for this chapter was written with guidance from Drs. Eileen Denovan-Wright, Melanie Kelly, and Denis Dupré. Data were collected and analyzed by myself with technical assistance from Dr. Amina Bagher.

3.1. INTRODUCTION

Cannabinoids are a structurally diverse group of compounds that are broadly classified as endogenous cannabinoids (endocannabinoids) [*e.g.* 2-arachidonoylglycerol (2-AG) and anandamide (*N*-arachidonylethanolamine (AEA)], phytocannabinoids [*e.g.* Δ^9-tetrahydrocannabinol (THC) and cannabidiol (CBD)], and synthetic cannabinoids [*e.g.* WIN55,212-2 (WIN) and CP55,940 (CP)] (Pertwee, 2008).

Cannabinoids mediate their effects through several receptors, including the type 1 cannabinoid receptor (CB_1), which has been intensively studied for its neuromodulatory activity. Many cannabinoids, including 2-AG, AEA, and THC, induce analgesic responses, and their use for chronic and acute pain conditions, such as arthritis and migraine, is being actively explored (Cupini *et al.*, 2008; Bosier *et al.*, 2010; Kinsey *et al*., 2011). Cannabinoids evoke hypolocomotive responses *via* CB_1 and may be useful in the treatment of movement disorders such as tremor, ataxia, Tourette syndrome, Parkinson disease, and Huntington disease (Pazos *et al*., 2008). CBD, acting independently of CB_1, has been shown to have therapeutic potential as an anti-epileptic and anti-inflammatory agent (Costa *et al.*, 2007; Jones *et* al., 2010; Devinsky *et al.,* 2014). Modulation of CB_1 activity in the central nervous system and periphery also affects appetite, glucose and fat metabolism (Cota *et al*., 2003). Cannabinoids may play a therapeutic role in the management of metabolic syndrome, diabetes, and lipodystrophies (Cota *et al*., 2003). Additionally, it is important to understand how psychoactive cannabinoids, such as THC, affect neuronal activity *via* CB_1 and other effectors within the context of substance abuse and addiction (Welch and Eads, 1999; Rubino *et al*., 2006; Pertwee, 2008, Magen *et al*., 2009).

Cannabinoids differ in their affinity for CB_1 and their potency and efficacy of action *via* CB_1 (Kearn *et al*., 1999; Pertwee, 2008; Bosier *et al*., 2010). The classical view of CB_1 activation was that there was a correlation between binding affinity at CB_1 and the potencies of cannabinoids to induce the *in vivo* tetrad responses of anti-nociception, hypoactivity, hypothermia, and catalepsy (Brievogel *et al.*, 1998; Kearn *et al*., 1999; Bosier *et al*., 2008a,b, 2010). Because of this correlation, individual

cannabinoids were expected to be similarly potent in all four tetrad responses (Bosier *et al*., 2010). However, this is not the case for many cannabinoids. THC and WIN, for example, are more potent inducers of hypolocomotion than catalepsy or hypothermia (Ryan *et al*., 1995; Wiley *et al*., 1998). AEA and THC differ in their potencies for anti-nociception and hypolocomotion in the ICR strain of mice (Smith *et al.*, 1994) and in their ability to evoke tolerance and dependence in fatty acid amide hydrolase (FAAH) knockout mice (Falenski *et al*., 2010). Long *et al.* (2009) and Schlosburg *et al*. (2010) observed that selective blockade of AEA or 2-AG catabolism results in sustained analgesia or disruption of analgesia and cross-tolerance to other CB_1 agonists, respectively. CBD, unlike other cannabinoids, does not evoke the tetrad responses (Jones *et al*., 2010). CBD demonstrates low affinity for the CB_1 orthosteric site (Laprairie *et al.*, 2015d). The *in vivo* effects of CBD, including its anti-inflammatory properties, appear to be CB_1-independent (Cota *et al.*, 2007; Magen *et al.*, 2009; Jones *et al.*, 2010; Devinsky *et al.*, 2014). Differences in the potency and efficacy of cannabinoids to evoke various responses *in vivo* may be exploited in the application of these compounds as therapies.

Distinct agonists appear to modulate the signaling specificity of CB_1 through the coupling of different G proteins (Glass and Northrup, 1999; Bosier *et al.*, 2010). CB_1 agonist-selective coupling to $G\alpha_i$, $G\alpha_s$, and $G\alpha_q$ has been demonstrated in cell lines over-expressing CB_1 treated with WIN, CP, and other synthetic cannabinoids (Bonhaus *et al.*, 1998; Lauckner *et al.*, 2005; Mukhopadhyay and Howlett, 2005). The potency of AEA, CP, WIN, and other cannabinoids to stimulate [^{35}S]GTPγS has been evaluated using in rat cerebellar membranes (Welch and Eads, 1999) and N1E-115 cells over-expressing CB_1 (Bosier *et al.*, 2007, 2008b). In these and subsequent studies, WIN and CP were found to be full agonists of $G\alpha_{i/o}$ while AEA and, to a lesser extent, THC were partial agonists (Brievogel *et al.*, 1998; Kearn *et al.*, 1999; Bosier *et al.*, 2008a,b, 2010). It is thought that WIN and CP stabilize functionally different active conformations of CB_1 resulting in a differential interaction and activation of G proteins (Anavi-Goffer *et al*., 2007; Georgieva *et al*., 2008). *In silico* modeling of CB_1-cannabinoid interactions suggests that each cannabinoid interacts with a different subset of residues on the third and fourth

transmembrane helices of CB_1 (Bakshi *et al*., 2007; Varga *et al.*, 2008; Singh *et al*., 2011). Based on these data, Vagra *et al*. (2008) proposed that ligand-specific changes in CB_1 conformation may enhance the binding of different G proteins (*e.g.* $G\alpha_{i/o}$ *versus* $G\alpha_s$) or arrestins, which would in turn facilitate the activation of different signaling pathways downstream of CB_1. Glass and Northrup (1999) used Sf9 cell membrane preparations containing CB_1 and various G proteins to differentiate the $G\alpha_i$- and $G\alpha_o$-mediated effects of CB_1. In this study, the cannabinoids HU210, WIN, and AEA were full agonists of $G\alpha_i$, whereas THC acted as a partial agonist; WIN, AEA, and THC were all partial agonists of $G\alpha_o$ relative to HU210 (Glass and Northrup, 1999). Similar to Vagra *et al*. (2008), the authors concluded that distinct agonists induce unique receptor conformations resulting in ligand-specific CB_1-dependent G protein signaling (Glass and Northrup, 1999). The data presented in these studies suggests that the pharmacological activity of cannabinoids acting through G proteins depends on their affinity for CB_1 as well as the signaling bias of specific cannabinoids.

Beyond G proteins, recruitment of arrestin1 and 2 to CB_1 has also been examined (Jin *et al*., 1999; van der Lee *et al*., 2009; Vrecl *et al*., 2009). These studies report that CB_1 weakly interacts with arrestin2, which facilitates internalization upon stimulation with WIN or CP in HEK cells, AtT20 immortalized mouse anterior pituitary cells, and U2OS human osteosarcoma cells stably-expressing CB_1 (Jin *et al*., 1999; van der Lee *et al*., 2009; Vrecl *et al*., 2009). WIN and CP have been shown to be differentially efficacious activators of tyrosine hydroxylase transcription, ERK1/2 phosphorylation, and JNK activation in neuroblastoma cells (Bosier *et al.*, 2007, 2008a,b). Although these observations were not related to agonist-specific coupling, the authors suggest that the differences between WIN and CP support functional selectivity of cannabinoids at CB_1 (Bosier *et al.*, 2007, 2008a,b). To complicate matters, the functional selectivity of cannabinoid ligands may be cell-type specific because reports of efficacy have varied across model systems and tissues (Cupini *et al*., 2008). Therefore, individual cannabinoids may stabilize specific CB_1 receptor conformations, resulting in a cell- and tissue-specific response (van der Lee *et al*., 2009; Vrecl *et al*., 2009). This is interesting because it may be possible for

cannabinoids to be designed that bias receptor signaling toward desirable effects and away from undesirable ones.

In this study, we wanted to characterize the signaling bias of several cannabinoid ligands in an *in vitro* model of neurons that endogenously express CB_1. The downstream functional selectivity of six compounds from three classes of cannabinoids was examined in the ST*Hdh*$^{Q7/Q7}$ cell culture model of striatal medium spiny projection neurons. This cell culture model was chosen to characterize cannabinoid signaling bias because these cells model the major output of the indirect motor pathway of the striatum where CB_1 levels are highest relative to other regions of the brain (Trettel *et al.*, 2000; Laprairie *et al.*, 2013). ST*Hdh*$^{Q7/Q7}$ cells endogenously express CB_1 and FAAH (Trettel *et al.*, 2000; Laprairie *et al.*, 2013), as well as the dopamine D_2 receptor, enkephalin, and other markers of striatal neurons, making this *in vitro* model system ideally suited to studying cannabinoid signaling in a physiologically relevant context. The endocannabinoids AEA and 2-AG, the phytocannabinoids CBD and THC, and the synthetic cannabinoids WIN and CP, were compared for their ability to activate arrestin2- (β-arrestin1), $G\alpha_{i/o}$-, $G\alpha_s$-, and $G\alpha_q$-dependent pathways in ST*Hdh*$^{Q7/Q7}$ cells. Based on the existing *in vitro* and *in vivo* data for cannabinoid ligands, we hypothesized that endocannabinoids, phytocannabinoids and synthetic cannabinoids would differentially bias CB_1-dependent signaling.

3.2. METHODS

3.2.1. MATERIALS

Cannabinoids used in this study included 2-AG, AEA, WIN, CP, CBD, THC, and the CB_1-selective antagonist O-2050. All cannabinoids were purchased from Tocris Bioscience (Bristol, UK), with the exception of THC, which was purchased from Sigma-Aldrich (Oakville, ON). *Pertussis* and *cholera* toxins (PTx and CTx) were purchased from Sigma-Aldrich. The Gβγ modulator gallein was purchased from EMD Millipore (Billerica, MA). Cannabinoids and gallein were dissolved in DMSO (final concentration of 0.1% in assay media for all assays) and added directly to the media at the concentrations and times indicated. No effects of vehicle alone were observed compared to assay media alone. PTx and

CTx were dissolved in dH_2O (50 ng/mL) and added directly to the media 24 h prior to cannabinoid treatment. Pre-treatment of cells with PTx and CTx inhibits $G\alpha_{i/o}$ and $G\alpha_s$, respectively (Miligan *et al.*, 1989). While treatment with CTx for 30 min or less increases $G\alpha_s$ signaling as measured by increased cAMP levels, 24 h treatment with CTx leads to an irreversible inhibition of ADP-ribosylated $G\alpha_s$ protein and the concomitant elimination of $G\alpha_s$-dependent signaling (Miligan *et al.*, 1989; McKenzie and Miligan, 1991). All experiments included a vehicle treatment control.

3.2.2. CELL CULTURE

ST*Hdh*$^{Q7/Q7}$ cells are a cell line derived from the conditionally immortalized striatal progenitor cells of embryonic day 14 C57BlJ/6 mice (Coriell Institute, Camden, NJ) (Trettel *et al.*, 2000). Cells were grown at 33°C, 5% CO_2 in DMEM supplemented with 10% FBS, 2 mM L-glutamine, 10^4 U/mL Pen/Strep, and 400 μg/mL geneticin. Twenty-four hours of serum deprivation promotes the differentiation of ST*Hdh*$^{Q7/Q7}$ cells into an adult neuron-like phenotype characterized by increased neurite outgrowth, GABA release, and increased expression of CB_1, dopamine D_2 receptors, preproenkephalin, and dopamine and cAMP-related phosphoprotein 32 kDa (DARPP-32), typical of mature medium spiny projection neurons of the indirect motor pathway of the striatum (Trettel *et al.*, 2000; Bagher *et al.*, 2013; Laprairie *et al.*, 2013). These cells are ideally suited for the characterization of cannabinoid ligand bias *in vitro* because they model a neuronal cell type that expresses CB_1 at high levels compared to other cell types in the central nervous system. The striatum is a major site of action of centrally-acting cannabinoid-based therapies (Fernandez-Ruiz *et al.*, 2004).

3.2.3. PLASMIDS

Human CB_1 and arrestin2 (β-arrestin1) were cloned and expressed as either green fluorescent protein^2 (GFP^2) or *Renilla* luciferase (Rluc) fusion proteins at the intracellular C-terminus. CB_1-GFP^2 and arrestin2-GFP^2 were generated using the pGFP^2-N3 plasmid (PerkinElmer, Waltham, MA) as described previously (Hudson *et al.*, 2010). CB_1-Rluc was generated using the pRluc-N3 plasmid (PerkinElmer, Waltham, MA). The arrestin2-Rluc (pcDNA3.1), human ether-a-go-go-related gene-C-terminus GFP^2 and

Rluc fusion constructs (HERG-GFP^2, HERG-Rluc), GFP^2-Rluc fusion construct, and Rluc plasmids have been previously described (Lavoie *et al*., 2002; Dupré *et al*., 2007; Bagher *et al.*, 2013). The $G\alpha_q$ dominant negative mutant [Glu 209 Δ Leu, Asp 277 Δ Asn (Q209L,D277N)] pcDNA3.1 plasmid was obtained from the Missouri S&T cDNA Resource Center (Rolla, MO) (Lauckner *et al.*, 2005). The arrestin2 dominant negative mutant [Val 53 Δ Asp (V53D)] pcDNA3.1 plasmid has been described previously (Dupré *et al.*, 2007). arrestin2-red fluorescent protein (RFP) was provided by Dr. Denis Dupré (Dalhousie University).

3.2.4. BIOLUMINESCENCE RESONANCE ENERGY TRANSFER^2 (BRET^2)

Direct interactions between CB_1 and arrestin2 were quantified *via* BRET^2 (Ramsay *et al.*, 2006). Cells were grown in a 6-well plate and transfected with the indicated GFP^2 and Rluc constructs. Forty-eight h post-transfection cells were washed twice with cold 0.1 M PBS and suspended in 90 µL of 0.1 M PBS supplemented with glucose (1 mg/mL), benzamidine (10 mg/mL), leupeptin (5 mg/mL) and a trypsin inhibitor (5 mg/mL). Cells were dispensed into white 96-well plates and treated as indicated (PerkinElmer). Coelenterazine 400a substrate (50 µM; Biotium, Hayward, CA) was added and light emissions were measured at 460 nm (Rluc) and 510 nm (GFP^2) using a Luminoskan Ascent plate reader (Thermo Scientific, Waltham, MA), with an integration time of 10 s and a photomultiplier tube voltage of 1200 V. BRET efficiency ($BRET_{Eff}$) was determined using previously described methods (James *et al.*, 2006) such that Rluc alone was used to calculate $BRET_{MIN}$ and the Rluc-GFP^2 fusion protein was used to calculate $BRET_{MAX}$.

3.2.5 FLUORESCENCE RESONANCE ENERGY TRANSFER (FRET)

Receptor dimerization was visually assessed *via* FRET according to the methods of Wu *et al*. (2012). Cells were grown in a 6-well plate and transfected with the indicated GFP^2 and RFP constructs. Forty-eight hours post-transfection cells were moved to coverslips and grown for an additional 24 h. Cells were treated as indicated and visualized on a Zeiss 510 Upright Laser Scanning Microscope with 20X and 63X objective lenses. Images were captured using Zen Image Capture 2009 edition (Carl Zeiss

Canada). The following excitation/emission filters were used to directly visualize fluorescence: for GFP^2 492 nm/510 nm, and for RFP 543 nm/565 nm. For FRET, GFP^2 was excited 488 nm, separated by a 488/564 dichromic mirror, with emitted fluorescence being detected by between 502-651 nm (Wu *et al*., 2012). In order to measure endogenous association between CB_1 and arrestin, paraformaldehyde (PFA)-fixed cells were used for the immunocytochemical detection of CB_1 using a *C*-terminal CB_1 primary antibody (1:500; Cayman Chemical Company, Cat No. 10006590, Ann Arbor, MI) and $Alexafluor^{488}$ secondary antibody (donor) and arrestin2 using an arrestin1/2 primary antibody (1:250; Santa Cruz Biotechnology, Santa Cruz, CA) and Cy^3 secondary antibody (acceptor), as described in Knowles *et al*. (1999). Cells were grown on coverslips and treated as indicated. Cells were washed with 0.1 M PBS and fixed with 4% PFA and washed three times with 0.1 M PBS for 5 min each. Cells were incubated with blocking solution (0.1 M PBS, 5% normal goat serum, in dH_2O) for 1 h at room temperature. Cells were incubated with primary antibody solutions directed against *C*-CB_1 (1:500) and arrestin1/2 (1:250) diluted in antibody dilution buffer [0.1 M PBS, 1% (w/v) BSA, in dH_2O] overnight at 4°C. Cells were washed three times with 0.1 M PBS for 5 min each. Cells were incubated in $Alexafluor^{488}$ (1:500) and Cy^3 (1:500) (Rockland Immunochemicals, Gilbertsville, PA) for 1 h at room temperature. Cells were then washed three times with 0.1 M PBS for 5 min each. Microscopy and FRET were then conducted using the same methodology described for FRET in transfected cells. The specificity of the *C*-terminal CB_1 and arrestin1/2 primary antibodies were confirmed using blocking peptide controls (1:500) (Cayman Chemical Company and Santa Cruz Biotechnology). FRET efficiency was calculated in ImageJ by dividing the average pixel intensity at 565 nm for any given image by the intensity at 522 nm for that image, after background subtraction; FRET was visually represented by mapping a pseudo-color look-up table (16 colors, ImageJ) onto the resulting image (Wu *et al*., 2012).

3.2.6 In- and On-cell™ Western and immunocytochemistry

For On-cell™ Western analyses, cells were fixed for 10 min at room temperature with 4% PFA and washed three times with 0.1 M PBS for 5 min each. Cells were incubated with blocking solution (0.1

M PBS, 5% normal goat serum, in dH_2O) for 1 h at room temperature. Cells were incubated with primary antibody solutions directed against *N*-CB_1 (1:500; Cayman Chemical Company, Cat No. 101500) diluted in antibody dilution buffer [0.1 M PBS, 1% (w/v) BSA, in dH_2O] overnight at 4°C. Cells were washed three times with 0.1 M PBS for 5 min each. Cells were incubated in $IR^{CW800dye}$ (1:500; Rockland Immunochemicals) for 1 h at room temperature. Cells were then washed three times with 0.1 M PBS for 5 min each. Cells were allowed to air-dry overnight. On-cell™ data were then collected using the Odyssey Imaging system and software (version 3.0; Li-Cor, Lincoln, NE). These data represented the fraction of CB_1 detected on the plasma membrane. The same cells were then used to quantify total CB_1 protein levels using the In-cell™ Western technique. The On-cell™ CB_1 levels were divided by the In-cell™ (total) CB_1 levels to determine the fraction plasma membrane CB_1. In-cell™ Western analyses and immunocytochemistry were conducted as described above except that 0.3% TritonX-100 was added to the blocking and antibody dilution solutions. Primary antibody solutions were: *N*-CB_1 (1:500), pERK1/2(Tyr205/185) (1:200), ERK1/2 (1:200), pCREB(S133) (1:500), CREB (1:500), pPLCβ3(S537) (1:500), PLCβ3 (1:1000), pAkt(Ser473) (1:500), panAkt (1:1000), arrestin1/2 (1:250), or β-actin (1:2000; Santa Cruz Biotechnology). pERK1/2(Y205/185), pAkt(S473), pCREB(S133), and pPLCβ3(S537) were chosen because phosphorylation at these sites demonstrates activation of the ERK, PI3K/Akt, CREB, and $G\alpha_q$ pathways, respectively. Secondary antibody solutions were: $IR^{CW700dye}$ or $IR^{CW800dye}$ (1:500; Rockland Immunochemicals). In-cell™ Western analyses were then conducted using the Odyssey Imaging system and software (version 3.0; Li-Cor). All experiments measuring CB_1 included an *N*-CB_1 blocking peptide (1:500) control, which was incubated with *N*-CB_1 antibody (1:500). Immunofluorescence observed with the *N*-CB_1 blocking peptide was subtracted from all experimental replicates.

3.2.7. QUANTITATIVE REVERSE TRANSCRIPTASE PCR

RNA was harvested from cells using the Trizol® (Invitrogen, Burlington, ON) extraction method according to the manufacturer's instruction. Reverse transcription reactions were carried out with SuperScript III® reverse transcriptase (+RT; Invitrogen), or without (-RT) as a negative control for use in

subsequent PCR experiments according to the manufacturer's instructions. Two micrograms of RNA were used per RT reaction. qRT-PCR was conducted using the LightCycler® system and software (v. 3.0; Roche, Laval, QC). Reactions were composed of a primer-specific concentration of $MgCl_2$ (Table 3-1), 0.5 μM each of forward and reverse primers (Table 3-1), 2 μL of LightCycler® FastStart Reaction Mix SYBR Green I, and 1 μL cDNA to a final volume of 20μL with dH_2O (Roche). The PCR program was: 95°C for 10 min, 50 cycles of 95°C 10 s, a primer-specific annealing temperature (Table 3-1) for 5 s, and 72°C for 10 s. Experiments always included sample-matched –RT controls, a no-sample dH_2O control, and a standard control containing product-specific cDNA of a known concentration. cDNA abundance was calculated by comparing the cycle number at which a sample entered the logarithmic phase of amplification (crossing point) to a standard curve generated by amplification of cDNA samples of known concentration (LightCycler Software version 4.1; Roche). qRT-PCR data were normalized to the expression of β-actin (Blázquez *et al*., 2011).

3.2.8. STATISTICAL ANALYSES

Statistical analyses were conducted by one- or two-way analysis of variance (ANOVA), as indicated, using GraphPad (v. 5.0, Prism). *Post-hoc* analyses were performed using Bonferroni's or Tukey's tests, as indicated. Homogeneity of variance was confirmed using Bartlett's test. The level of significance was set to $P < 0.001$, < 0.01, or < 0.05, as indicated, and all results are reported as the mean ± the standard error of the mean (SEM) from at least 4 independent experiments. In order to improve the readability of the data, many figures are sub-divided as endocannabinoids (AEA, 2-AG), phytocannabinoids (CBD, THC), and synthetic cannabinoids (CP, WIN).

Table 3-1. Synthetic oligonucleotides used in this study.

Target	Oligonucleotide Sequence (5' - 3')	Annealing Temperature (°C)	$MgCl_2$ (mM)
CB_1[a]	GGGCAAATTTCCTTGTAGCA GGCTAACGTGACTGAGAAA	58	1
ppENK	GCGCGTTCTTCTCTCCTACA GTGCACGCCAGGAAATTGAT	57	3
β-actin[a]	AAGGCCAACCGTGAAAAGAT GTGGTACGACCAGAGGCATAC	59	2
Arrestin2	CACGCAGCCCTCACTCTC GTGTCACGTAGACTCGCCTT	59	2
Arrestin3	AAGGTGAAGCTGGTGGTGTC CCAGTGTGTATCTCGGGTGG	59	2

[a]Blázquez *et al*., 2011. All other primers self-designed in NCBI primer BLAST.

3.3. RESULTS

3.3.1. INTERACTIONS BETWEEN CB_1 AND ARRESTIN2 (B-ARRESTIN1) ARE LIGAND-SPECIFIC.

Initially, we wanted to determine whether the interaction between CB_1 and arrestin2 differed among CB_1 agonists. To do this, $BRET_{Eff}$ was measured between CB_1-GFP^2 and arrestin2-Rluc. Arrestin2 was chosen because it is endogenously expressed by ST*Hdh*$^{Q7/Q7}$ cells (Fig. 3-1A). The amount of donor and acceptor plasmid used, and the ratio of donor to acceptor plasmids, were optimized using a BRET saturation curve at 400 ng CB_1-GFP^2 to 200 ng arrestin2-Rluc (2:1; Fig. 3-1B). Basal $BRET_{Eff}$ between CB_1-GFP^2 and arrestin2-Rluc was approximately 0.2 and greater than $BRET_{Eff}$ between HERG-GFP^2 and arrestin2-Rluc (Fig. 3-1B). We also verified that $BRET_{Eff}$ was independent of time and plasmid expression level for CB_1-GFP^2 and arrestin2-Rluc (Fig. 3-1C). Cells were treated with 1 μM AEA, 2-AG, CBD, THC, CP, or WIN, or 500 nM O-2050, for 0 – 30 min (Fig. 3-2A-C). Treatment with AEA, 2-AG, THC, CP, or WIN increased $BRET_{Eff}$ within 10 min, compared to vehicle treatment and $BRET_{Eff}$ was stable over 30 min (Fig. 3-2A-C). CBD and O-2050 treatment did not change $BRET_{Eff}$ relative to vehicle treatment. In addition, $BRET_{Eff}$ between CB_1-GFP^2 and arrestin2-Rluc was greater in cells treated with 2-AG compared to AEA by 15 min, with THC compared to CBD by 10 min, and with CP compared to WIN by 5 min (Fig. 3-2A-C). The ligand-specific differences in CB_1-arrestin2 association were further analyzed by measuring $BRET_{Eff}$ in cells treated with 0.01 – 5.00 μM AEA, 2-AG, CBD, THC, CP, or WIN in the absence or presence of 500 nM O-2050 for 10 (Fig. 3-2D-F) or 30 min (Fig 3-2G-I). At 10 min, $BRET_{Eff}$ between CB_1-GFP^2 and arrestin2-Rluc was not different in AEA- and 2-AG-treated cells (Fig. 3-2D), while THC and CP were more potent and efficacious ligands than CBD and WIN, respectively (Fig. 3-2E,F). At 30 min, 2-AG was a more efficacious ligand than AEA (Fig. 3-2G). As was observed at 10 min, THC and CP were more potent and efficacious ligands than CBD and WIN, respectively (Fig. 3-2H,I). AEA-, 2-AG-, THC-, WIN-, and CP-mediated recruitment of arrestin2 to CB_1 was inhibited by co-treatment of cells with the CB_1 antagonist O-2050, as demonstrated by a significant rightward shift in the $BRET_{Eff}$ dose-response curves (Fig. 3-2D-J). The EC_{50}, Hill Slope, and E_{max} values

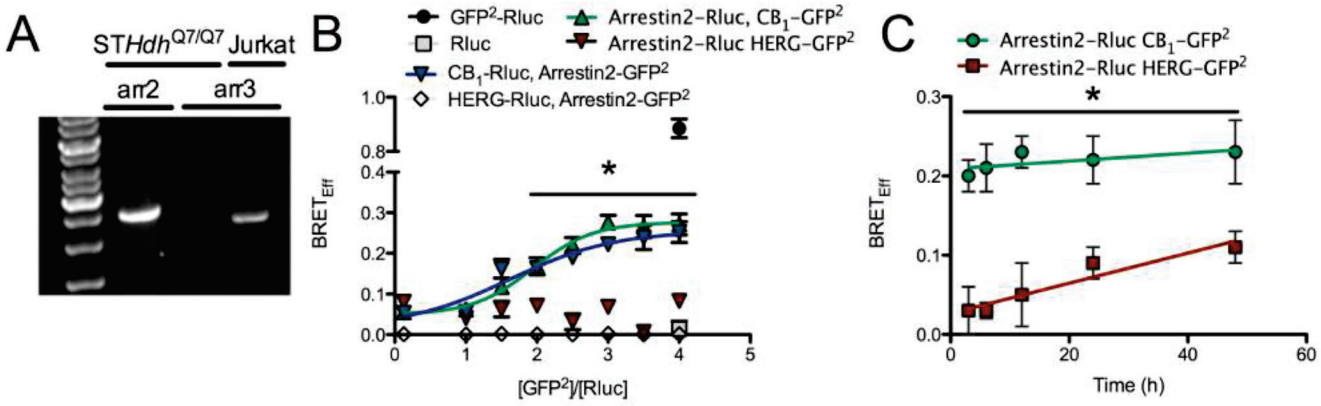

Figure 3-1. Optimization of BRET^2 between arrestin2 (β-arrestin1) and CB$_1$ in ST*Hdh*$^{Q7/Q7}$ cells. A) Representative image demonstrating arrestin2, and not arrestin3, is expressed in ST*Hdh*$^{Q7/Q7}$ cells. PCR products were amplified *via* qRT-PCR and resolved on agarose gels. **B)** Cells were transfected with varying amounts of donor (CB$_1$-Rluc, HERG-Rluc, and arrestin2-Rluc) and acceptor (CB$_1$-GFP^2, HERG-GFP^2, and arrestin-GFP^2) plasmids and BRET$_{Eff}$ was determined. The amount of DNA transfected was kept constant (800 ng) by the addition of pcDNA3.1. The non-interacting HERG receptor and Rluc alone were used as negative controls. GFP^2-Rluc was used as a positive control. **P* < 0.001 compared to HERG-Rluc, arrestin2-GFP^2 and arrestin2-Rluc, HERG-GFP^2 as determined *via* two-way ANOVA followed by Bonferroni's *post-hoc* test. *n* = 6. **C)** Cells were transfected with arrestin2-Rluc and CB$_1$-GFP^2 or arrestin2-Rluc and HERG-GFP^2 plasmids and BRET$_{Eff}$ was measured (Time 0 h = 48 h post-transfection). **P* < 0.001 compared to arrestin2-Rluc, HERG-GFP^2 as determined *via* one-way ANOVA followed by Tukey's *post-hoc* test. *n* = 6.

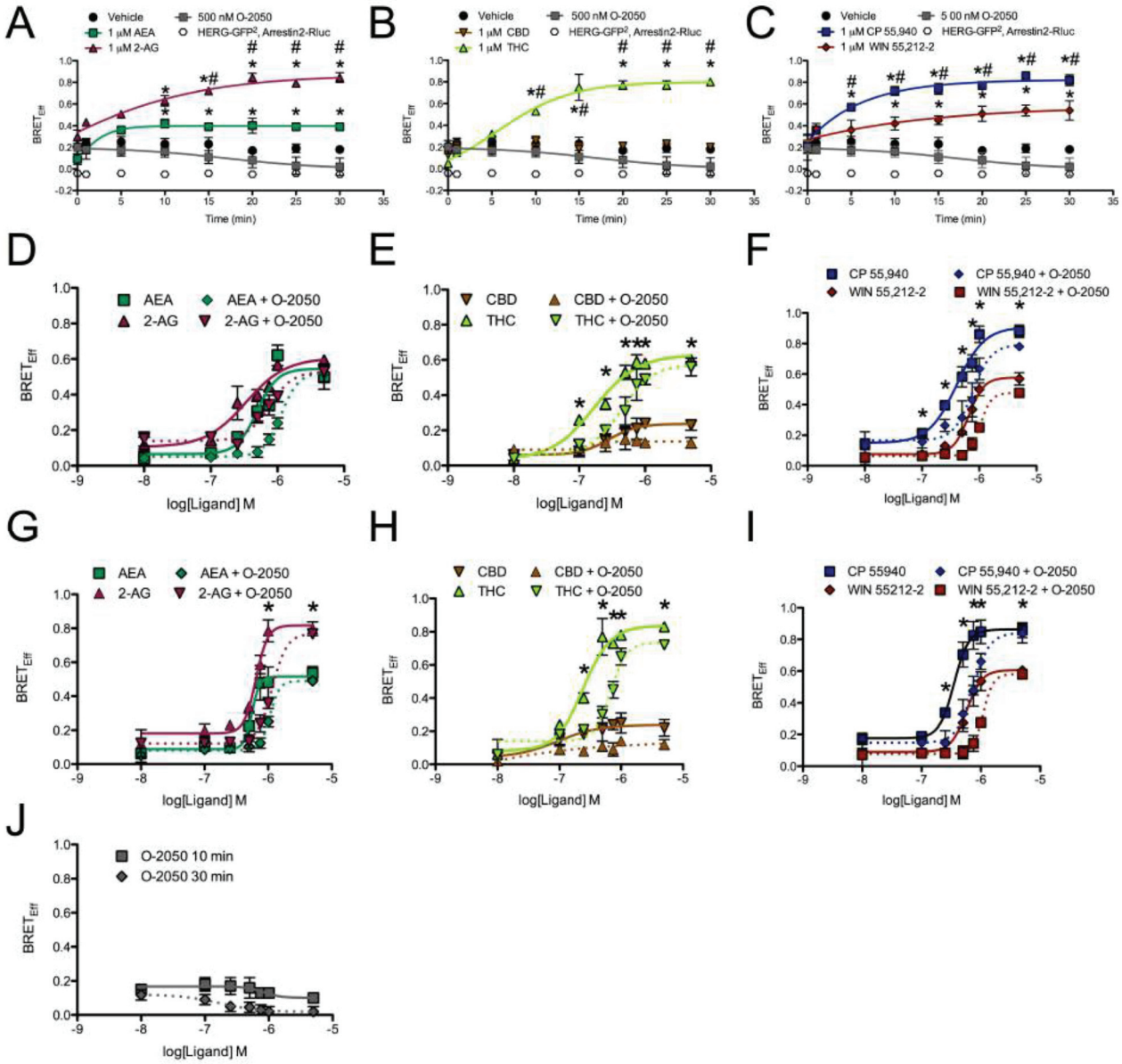

Figure 3-2. 2-AG, THC, and CP treatment enhanced $BRET_{Eff}$ between CB_1-GFP^2 and arrestin2-Rluc. A – C) $BRET_{Eff}$ was measured over 30 min in cells expressing CB_1-GFP^2 or HERG-GFP^2 and arrestin2-Rluc and treated with vehicle, 500 nM O-2050, 1 μM AEA or 2-AG **(A)**, CBD or THC **(B)**, and CP or WIN **(C)**. **D – I)** $BRET_{Eff}$ was measured at 10 **(D – F)** or 30 min **(G – I)** in ST$Hdh^{Q7/Q7}$ cells expressing CB_1-GFP^2 and arrestin2-Rluc and treated with 0.01 – 5.00 μM AEA or 2-AG **(D, G)**, CBD or THC **(E, H)**, and CP or WIN **(F, I)** with or without 500 nM O-2050, and O-2050 alone **(J)**. **A – C)** **P* < 0.001 compared to vehicle, #*P* < 0.001 compared to AEA **(A)** or CBD **(B)** as determined *via* one-way ANOVA followed by Tukey's *post-hoc* test. *n* = 6. **D – I)** **P* < 0.001 compared to 2-AG **(G)**, CBD **(E, H)**, or WIN **(F, I)** as determined *via* one-way ANOVA followed by Tukey's *post-hoc* test. *n* = 6.

Table 3-2. $BRET_{Eff}$ potencies and efficacies of cannabinoid ligands (CB_1-GFP^2, arrestin2-Rluc).

	AEA		2-AG	
	10 min	**30 min**	**10 min**	**30 min**
EC_{50} (μM) (95% CI)	0.49 (0.39 - 0.52)	0.55 (0.44 - 0.69)	0.34 (0.29 - 0.48)	0.54 (0.46 - 0.73)†
Hill Slope ± SEM	1.20 ± 0.21	1.40 ± 0.39	1.40 ± 0.24	1.71 ± 0.31
E_{max} ($BRET_{EFF}$) ± SEM	0.55 ± 0.05	0.52 ± 0.05	0.59 ± 0.05	0.80 ± 0.04*^
	CBD		**THC**	
	10 min	**30 min**	**10 min**	**30 min**
EC_{50} (μM) (95% CI)	0.28 (0.13 - 0.59)	0.09 (0.01 - 0.17)*#	0.17 (0.12 - 0.24)*	0.25 (0.18 - 0.34)*#
Hill Slope ± SEM	1.00 ± 0.64	1.30 ± 0.08	1.32 ± 0.40	1.97 ± 0.62
E_{max} ($BRET_{EFF}$) ± SEM	0.24 ± 0.03*	0.25 ± 0.04*	0.63 ± 0.03	0.83 ± 0.09*†
	WIN 55,212-2		**CP 55,940**	
	10 min	**30 min**	**10 min**	**30 min**
EC_{50} (μM) (95% CI)	0.65 (0.51 - 0.79)#$&	0.57 (0.45 - 0.72)$&	0.37 (0.32 - 0.41)§	0.35 (0.28 - 0.43)
Hill Slope ± SEM	0.90 ± 0.49	1.10 ± 0.57	1.10 ± 0.41	1.00 ± 0.31
E_{max} ($BRET_{EFF}$) ± SEM	0.57 ± 0.04	0.59 ± 0.13	0.91 ± 0.05*	0.86 ± 0.04*

*$P < 0.001$ compared to AEA within time-point, #$P < 0.001$ compared to 2-AG within time-point, $$P < 0.001$ compared to CBD within time-point, &$P < 0.001$ compared to THC within time-point, §$P < 0.001$ compared to WIN within time-point, †$P < 0.001$ compared to 10 min within drug treatment as determine *via* two-way ANOVA followed by Bonferroni's *post-hoc* test. $n = 6$.

generated from these concentration-response relationships were also compared (Table 3-2). THC was more potent than AEA and WIN at 10 min, and more potent than AEA, 2-AG, and WIN at 30 min (Table 3-2). The flat concentration-response relationship observed with CBD demonstrates this ligand had very little effect on the interaction between CB_1-GFP^2 and arrestin2-Rluc because the basal $BRET_{Eff}$ is not significantly different from the E_{max} (Fig. 3-2E,H). 2-AG (30 min), THC (30 min), and CP (10 and 30 min) were more efficacious ligands, while CBD (10 and 30 min) was less efficacious, than AEA for $BRET_{Eff}$ between CB_1-GFP^2 and arrestin2-Rluc (Table 3-2). The $BRET_{Eff}$ E_{max} values were greater at 30 min than 10 min when cells were treated with 2-AG or THC (Table 3-2). No statistically significant changes in Hill Slope were observed. Based on these data we concluded that 1) with the exception of CBD, each ligand promoted interactions between CB_1 and arrestin2, 2) 2-AG, THC, and CP displayed higher maxima than the other cannabinoid ligands tested for enhancing CB_1-arrestin2 interactions, and 3) in the assay, THC and CP were more potent than the other cannabinoid ligands tested at enhancing CB_1-arrestin2 interactions. A final concentration of 1 μM was used for all subsequent experiments because this dose consistently produced a response that approximated the E_{max} observed for $BRET_{Eff}$ for all cannabinoids tested.

Because BRET assays quantify the level of interaction between two proteins, but do not provide data on the localization of protein complexes, FRET analyses were conducted to determine the localization CB_1 and arrestin2 complexes within ST*Hdh*$^{Q7/Q7}$ cells in the presence of the cannabinoids studied. FRET was used to study the interaction between CB_1-GFP^2 and arrestin2-RFP or endogenous CB_1 and arrestin2 detected *via* fluorescent antibodies. A photobleaching experiment was conducted as a control for FRET (Wu *et al*., 2012). Cells were transfected with CB_1-GFP^2 and arrestin2-RFP. As expected, direct excitation of RFP at 543 nm for 5 min eliminated the fluorescent signal at 565 nm in a small, cytoplasmic region of interest (ROI) and the GFP^2 signal in that area was enhanced, while the RFP and GFP^2 signals in a non-photobleached ROI were unchanged (Fig. 3-3A,B) (Wu *et al*., 2012). The specificity of the anti-CB_1 and anti-arrestin1/2 antibodies was analyzed *via* immunohistochemistry in the

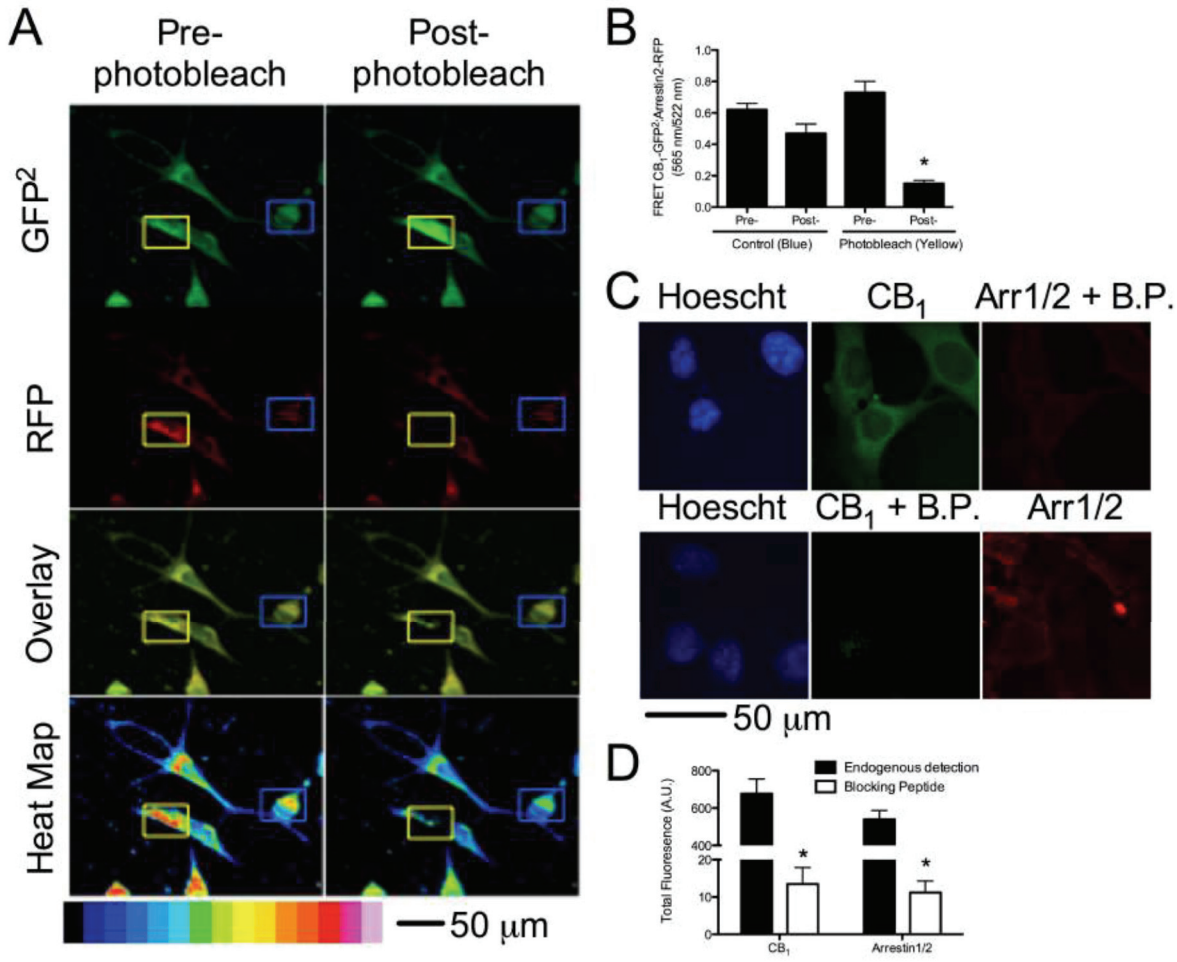

Figure 3-3. Validation of the FRET assay. Cells expressing CB_1-GFP^2 and arrestin2-RFP were photobleached to confirm FRET. **A)** A representative image of photobleaching in cells expressing CB_1-GFP^2 and arrestin2-RFP. The blue box indicates a control area and the yellow box indicates an area that was photobleached. **B)** Quantification of FRET pre- and post-photobleaching. $*P < 0.001$ compared to pre-photobleach (yellow square) as determined *via* unpaired *t*-test. $n = 60$ from 3 independent experiments. **C)** Representative images of immunohistochemical detection of CB_1 and arrestin1/2 in the absence and presence of blocking peptides (B.P.). **D)** Quantification of fluorescence for CB_1 and arrestin1/2 in the absence and presence of blocking peptides. $*P < 0.001$ compared to endogenous detection as determined *via* unpaired *t*-test. $n = 9$ from 3 independent experiments.

absence and presence of CB_1 and arrestin1/2 antibody blocking peptides (Fig. 3-3C). Fluorescence intensity was approximately 60-fold greater than in the absence of blocking peptide for both CB_1 and arrestin1/2 antibodies (Fig. 3-3D) FRET was qualitatively higher in cells treated with all cannabinoids tested (1 μM, 30 min), except CBD, indicating that interactions between CB_1 and arrestin2 had increased in transfected cells overexpressing CB_1-GFP^2 and arrestin2-RFP (Fig. 3-4A) and cells endogenously expressing CB_1 and arrestin2 (Fig. 3-4B). Quantification of total FRET for cells expressing CB_1-GFP^2 and arrestin2-RFP revealed that FRET was greater in cells treated with 1 μM AEA, 2-AG, THC, CP, or WIN for 30 min than in cells treated with vehicle (dotted line) (Fig. 3-4C). Similarly, total FRET between $Alexafluor^{488}$-conjugated antibodies (CB_1) and Cy^3-conjugated antibodies (arrestin2) was greater in cells treated with 1 μM AEA, 2-AG, THC, CP, or WIN for 30 min than in cells treated with vehicle (solid line) (Fig. 3-4C). Total FRET between $Alexafluor^{488}$ and Cy^3 was reduced in cells treated with 1 μM CBD for 30 min relative to vehicle-treated cells (Fig. 3-4C). We also observed that total FRET was greater in cells treated with 2-AG ($Alexafluor^{488}$ and Cy^3 only), THC, or CP, and less in cells treated with CBD, than in cells treated with AEA (Fig. 3-4C). At the plasma membrane, FRET was greater in cells treated with AEA, 2-AG, or WIN ($Alexafluor^{488}$ and Cy^3 only), and less in cells treated with CBD ($Alexafluor^{488}$ and Cy^3 only) or CP, compared to vehicle-treated cells (Fig. 3-4D). FRET was reduced in cells treated with CBD, WIN (CB_1-GFP^2 and arrestin2-RFP only), or CP relative to AEA-treated cells (Fig. 3-4D). Within the cytoplasm, FRET was greater in cells treated with AEA (CB_1-GFP^2 and arrestin2-RFP only), 2-AG, THC, WIN (CB_1-GFP^2 and arrestin2-RFP only), or CP, and less in cells treated with CBD ($Alexafluor^{488}$ and Cy^3 only), than in vehicle-treated cells (Fig. 3-4E). FRET within the cytoplasm was also greater in 2-AG- (CB_1-GFP^2 and arrestin2-RFP only), THC-, and CP-treated cells, and less in CBD- treated cells ($Alexafluor^{488}$ and Cy^3 only), than in AEA-treated cells (Fig. 3-4E). Further comparison of FRET between the plasma membrane (Fig. 3-4D) and cytoplasm (Fig. 3-4E) demonstrates that while 2-AG, THC, and CP all enhanced arrestin2 recruitment to CB_1 to a greater extent than AEA or CBD, THC and CP biased CB_1-arrestin2 complexes toward internalization to a greater extent than 2-AG.

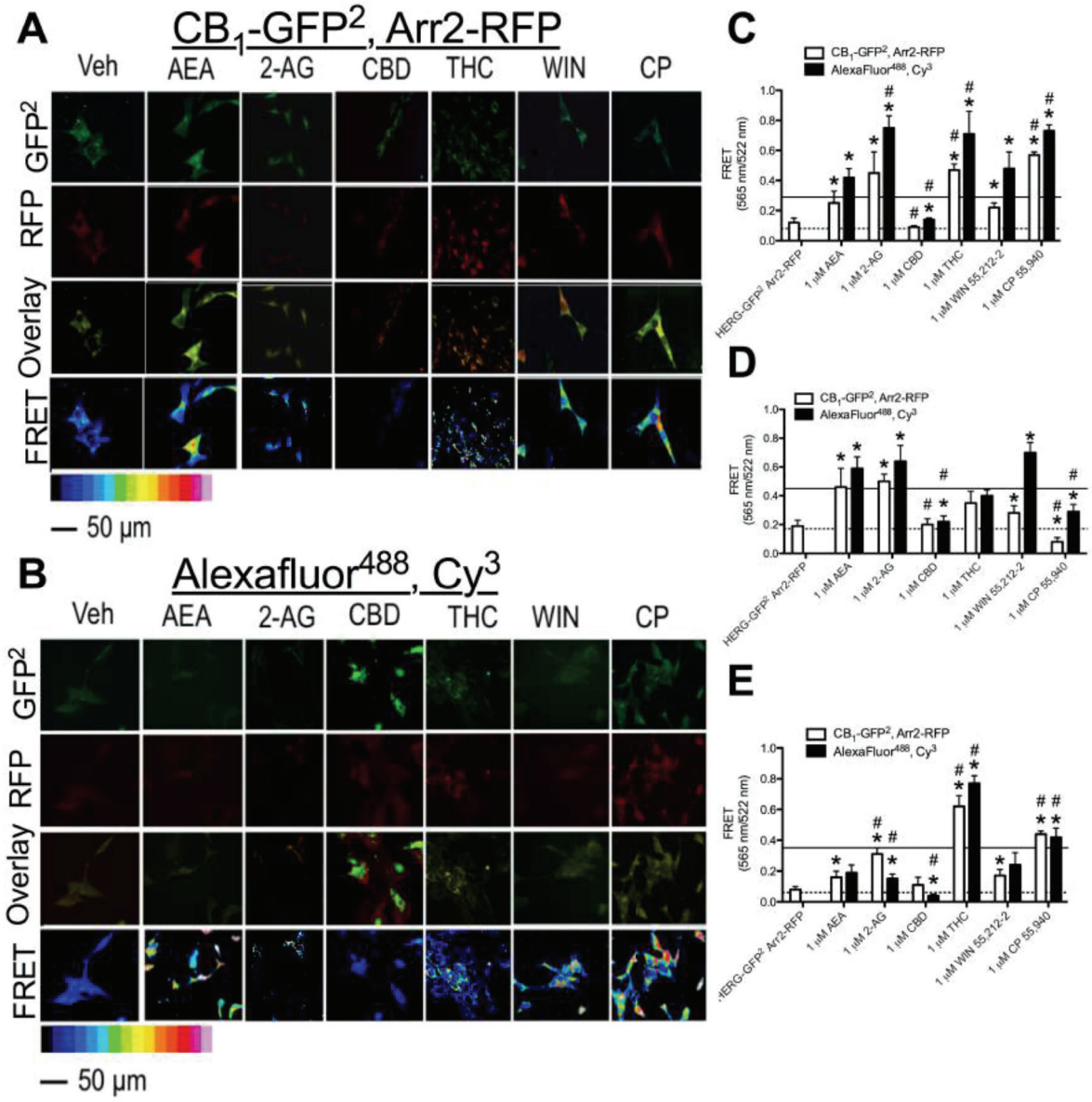

Figure 3-4. 2-AG, THC, and CP treatment enhanced FRET between CB_1-GFP^2 and arrestin2-Rluc. Representative images of FRET between CB_1-GFP^2 and arrestin2-RFP **(A)** or $Alexafluor^{488}$ or Cy^3 **(B)** in cells treated with vehicle or 1 µM AEA, 2-AG, CBD, THC, WIN, or CP for 30 min. **C – E)** Quantification of FRET between CB_1-GFP^2 and arrestin2-RFP and $Alexafluor^{488}$ and Cy^3 from the whole cell **(C)**, at the plasma membrane **(D)**, and in the cytoplasm **(E)**. *$P < 0.001$ compared to vehicle treatment (dotted line represents the mean for CB_1-GFP^2:arrestin2-RFP vehicle-treated cells, solid line represents the mean for $Alexafluor^{488}$:Cy^3 vehicle-treated cells), #$P < 0.001$ compared to AEA as determined *via* two-way ANOVA followed by Bonferroni's *post-hoc* test. $n = 60$ from 3 independent experiments.

No significant difference between 10 and 30 min treatment with any cannabinoid tested was observed (data not shown). Quantification of FRET in the nucleus and dendrites of cells revealed no difference among treatments (data not shown). Cell diameter, cell area, projection length and projection number were not different between treatment groups (n = 50; data not shown). Overall, these data demonstrate that THC and CP appear to bias CB_1 toward arrestin2-mediated internalization to a greater degree than the other cannabinoid ligands tested.

3.3.2. CANNABINOID LIGANDS BIASED INTRACELLULAR SIGNALING.

Because we had observed ligand-specific differences in CB_1-arrestin2 interactions, we wanted to determine whether intracellular signaling differed among cannabinoids. Treatment with AEA or 2-AG for 10 min resulted in a PTx-and O-2050-sensitive increase in ERK phosphorylation compared to vehicle (Fig. 3-5A,B). By 30 min, AEA-mediated ERK phosphorylation was not detected, while O-2050-sensitive ERK phosphorylation persisted in 2-AG-treated cells, and was no longer PTx-sensitive, compared to vehicle treated cells or compared to 10 min treatment (Fig. 3-5A,B). AEA and 2-AG treatment did not change the levels of CREB phosphorylation (Fig. 3-6A,B). AEA and 2-AG treatment did increase O-2050 and PTx-sensitive Akt phosphorylation at 10 and 30 min compared to vehicle treatment (Fig. 3-7A,B). AEA and 2-AG also increased the CB_1- and $G\alpha_q$-dependent phosphorylation PLCβ3 at 10 min compared to vehicle treatment (Fig. 3-8A,B). Treatment with CBD did not change ERK, Akt, or PLCβ3 phosphorylation, but did increase CTx-sensitive CREB phosphorylation at 30 min compared to vehicle treatment and 10 min treatment with CBD (Figs. 3-6C). CBD-mediated CREB phosphorylation was not changed by treatment with O-2050 (Figs. 3-5D,3-6D,3-7D,3-8D). WIN and CP treatment for 10 min resulted in a PTx- and O-2050-sensitive increase in ERK phosphorylation (Fig. 3-5E,F), and CB_1- and $G\alpha_q$-dependent phosphorylation PLCβ3 at 10 min (Fig 3-8E,F), relative to vehicle treatment. As with AEA, ERK phosphorylation was not detected in cells treated with WIN for 30 min (Fig. 3-5E). CP treatment for 30 min resulted in CB_1-dependent, PTx-insensitive ERK phosphorylation compared to

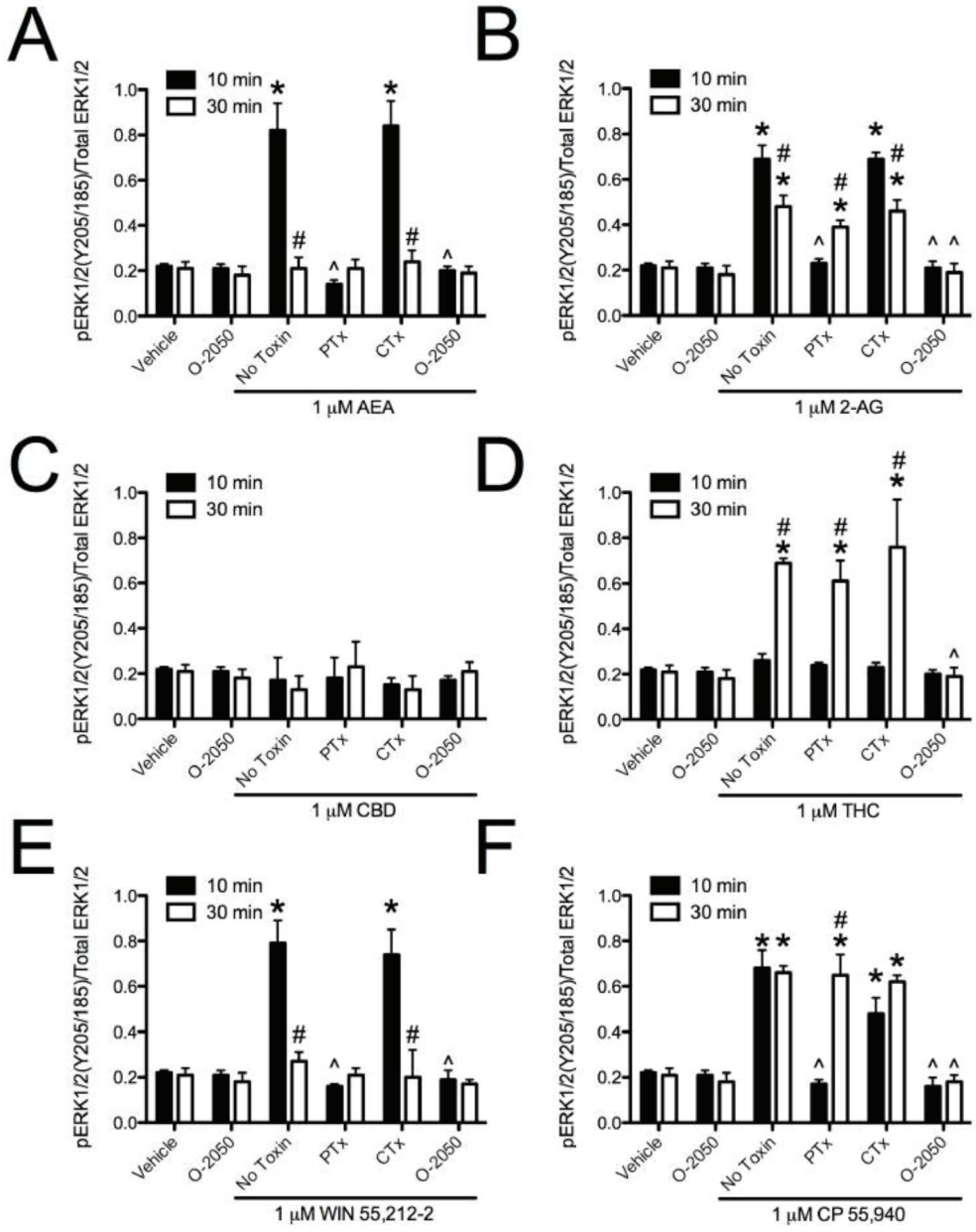

Figure 3-5. Cannabinoid ligands biased CB_1-dependent ERK signaling. ERK phosphorylation [pERK1/2(Y205/185)/Total ERK1/2) was quantified *via* In-cell™ Western in cells treated with 1 μM AEA **(A)**, 2-AG **(B)**, CBD **(C)**, THC **(D)**, WIN **(E)** or CP **(F)** for 10 or 30 min with or without 500 nM O-2050 or 24 h pre-treatment with 50 ng/mL PTx or CTx. *$P < 0.001$ compared to vehicle treatment within time-point, ^$P < 0.001$ compared to 'No Toxin' treatment within time-point, #$P < 0.001$ compared to 10 min within drug and toxin treatment as determined *via* two-way ANOVA followed by Bonferroni's *post-hoc* test. $n = 4$.

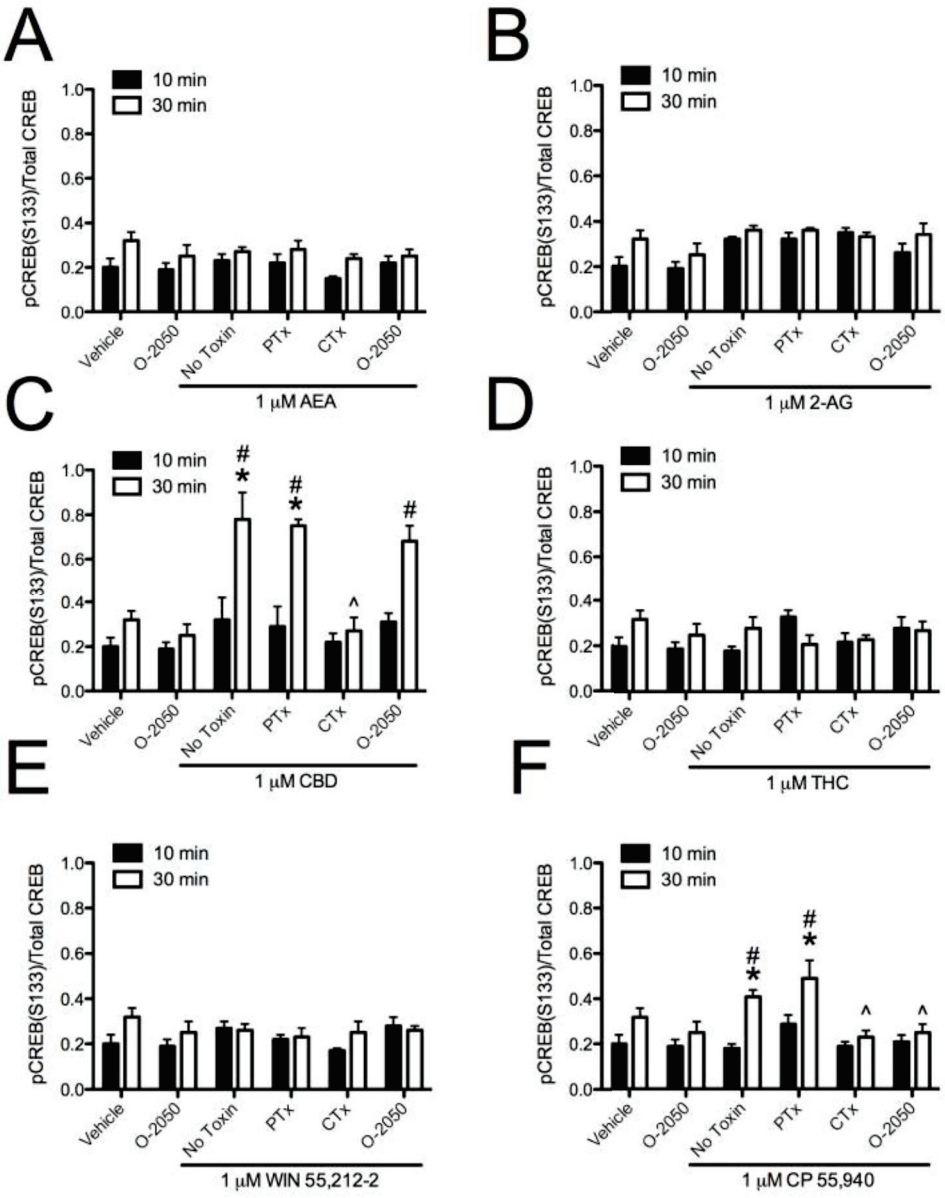

Figure 3-6. Cannabinoid ligands biased CB_1-dependent CREB signaling. CREB phosphorylation [pCREB(S133)/Total CREB] was quantified *via* In-cell™ Western in cells treated with 1 μM AEA **(A)**, 2-AG **(B)**, CBD **(C)**, THC **(D)**, WIN **(E)** or CP **(F)** for 10 or 30 min with or without 500 nM O-2050 or 24 h pre-treatment with 50 ng/mL PTx or CTx. **P* < 0.001 compared to vehicle treatment within time-point, ^*P* < 0.001 compared to 'No Toxin' treatment within time-point, #*P* < 0.001 compared to 10 min within drug and toxin treatment as determined *via* two-way ANOVA followed by Bonferroni's *post-hoc* test. *n* = 4.

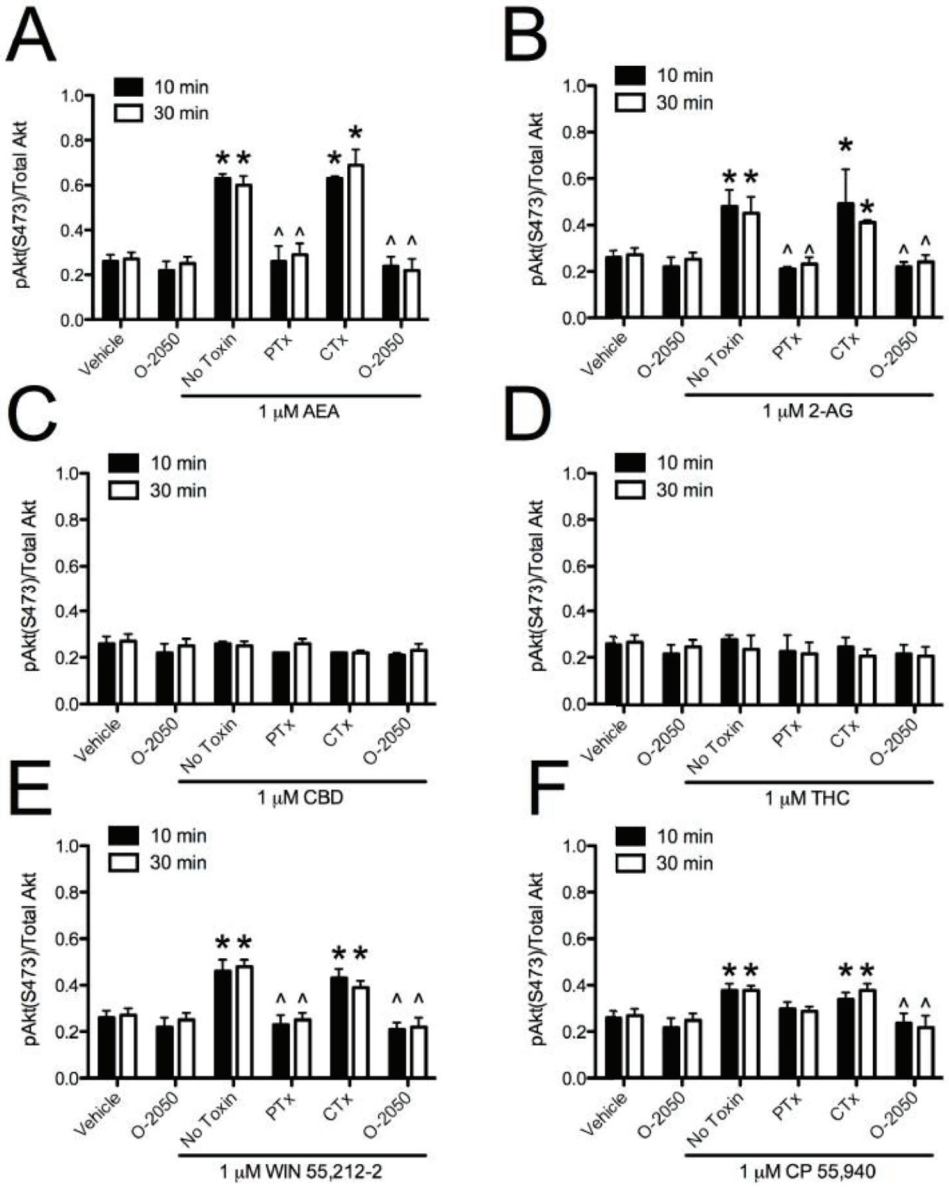

Figure 3-7. Cannabinoid ligands biased CB_1-dependent Akt signaling. Akt phosphorylation [pAkt(S473)/Total Akt] was quantified *via* In-cell™ Western in cells treated with 1 μM AEA **(A)**, 2-AG **(B)**, CBD **(C)**, THC **(D)**, WIN **(E)** or CP **(F)** for 10 or 30 min with or without 500 nM O-2050 or 24 h pre-treatment with 50 ng/mL PTx or CTx. **P* < 0.001 compared to vehicle treatment within time-point, ^*P* < 0.001 compared to 'No Toxin' treatment within time-point, #*P* < 0.001 compared to 10 min within drug and toxin treatment as determined *via* two-way ANOVA followed by Bonferroni's *post-hoc* test. *n* = 4.

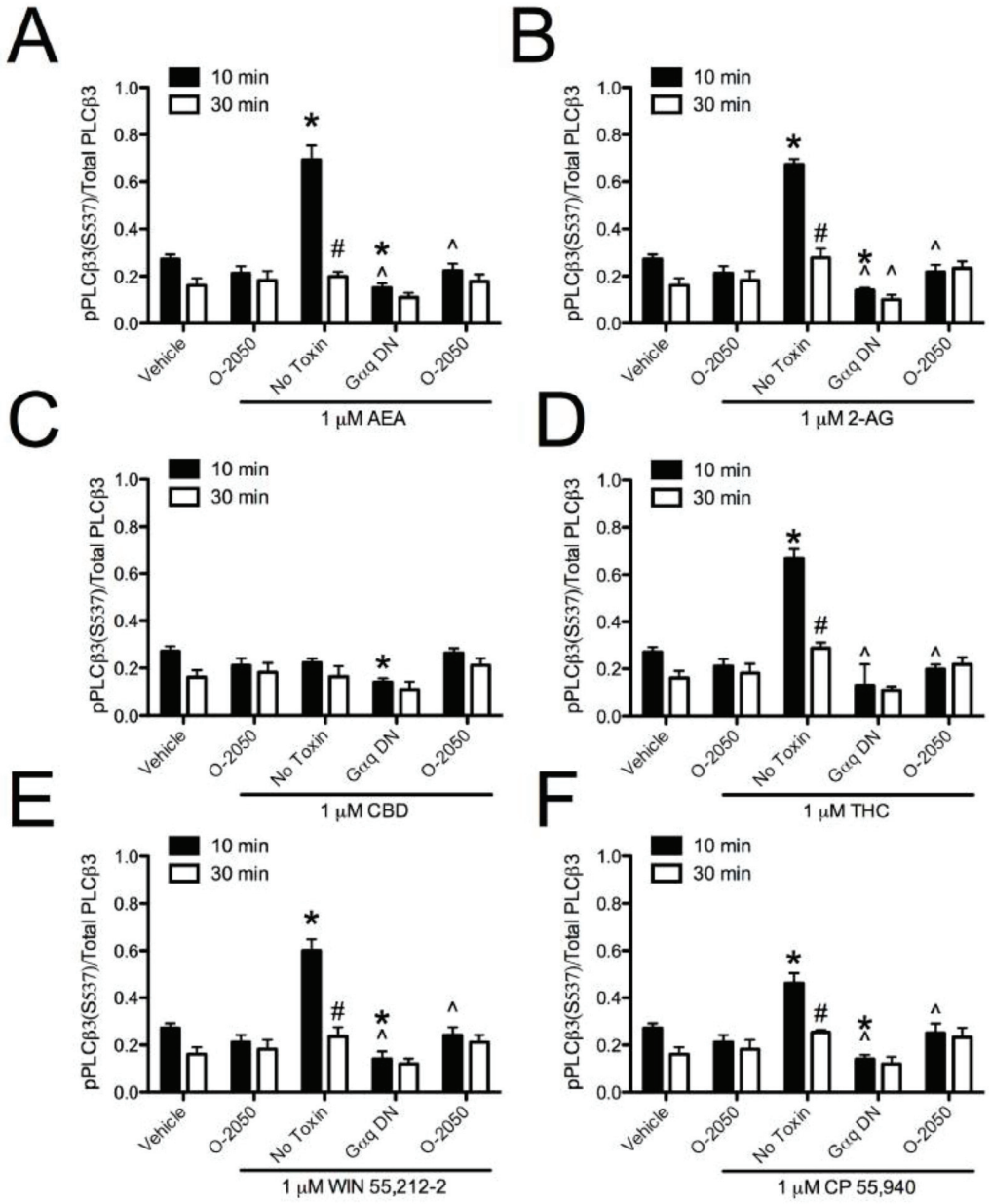

Figure 3-8. Cannabinoid ligands biased CB_1-dependent PLCβ3 signaling. PLCβ3 [pPLCβ3(S537)/Total PLCβ3] was quantified *via* In-cell™ Western in cells treated with 1 μM AEA **(A)**, 2-AG **(B)**, CBD **(C)**, THC **(D)**, WIN **(E)** or CP **(F)** for 10 or 30 min with or without 500 nM O-2050 or expressing $G\alpha_q$ dominant negative (Gαq DN). *$P < 0.001$ compared to vehicle treatment within time-point, ^$P < 0.001$ compared to 'No Toxin' treatment within time-point, #$P < 0.001$ compared to 10 min within drug and toxin treatment as determined *via* two-way ANOVA followed by Bonferroni's *post-hoc* test. $n = 4$.

vehicle treatment, as was observed with 2-AG and THC (Fig. 3-5F). WIN treatment did not alter CREB phosphorylation, but CP treatment for 30 min did increase O-2050- and CTx-sensitive CREB phosphorylation relative to vehicle treatment and 10 min treatment with CP (Fig. 3-6E,F). CP-dependent CREB phosphorylation was less than CBD-dependent CREB phosphorylation (Fig. 3-6C,F). Both WIN and CP treatment for 10 and 30 min increased Akt phosphorylation compared to vehicle treatment, but less than either AEA or 2-AG (Fig. 3-7A,B,E,F). Therefore, AEA, 2-AG, WIN, and CP treatment resulted in $G\alpha_{i/o}$-dependent, transient, ERK phosphorylation (Daigle *et al*., 2008), $G\alpha_q$-dependent, transient PLCβ3 phosphorylation, and persistent Akt phosphorylation. THC treatment also resulted in $G\alpha_q$-dependent, transient PLCβ3 phosphorylation. Further, treatment with 2-AG, THC, and CP, the ligands that enhanced $BRET_{Eff}$ and FRET between CB_1 and arrestin2 more than the other cannabinoids tested, resulted in persistent (30 min), $G\alpha_{i/o}$-independent ERK phosphorylation. Finally, CBD and CP treatment enhanced $G\alpha_s$-mediated CREB phosphorylation, although CBD did so independent of CB_1. AEA, 2-AG, THC, WIN, and CP increased the phosphorylation of ERK, CREB, Akt, or PLCβ3 *via* CB_1 because these effects were blocked by the CB_1-selective antagonist O-2050 (Pertwee, 2008).

Sustained and $G\alpha_{i/o}$-independent ERK phosphorylation occurs *via* arrestin2 (Shenoy *et al.*, 2007; Ahn *et al*., 2013). We tested this possibility by treating cells over-expressing an arrestin2 dominant negative (arrestin2 V53D) with 1 μM 2-AG, THC, or CP with or without 50 ng/mL PTx (Fig. 3-9A-C). We observed that PTx-insensitive ERK phosphorylation was sustained at each time point above the levels observed before drug treatment in cells treated with 2-AG (Fig. 3-9A), and for 12 h in cells treated with THC (Fig. 3-9B) or CP (Fig. 3-9C). However, levels of phosphorylated ERK did not differ from basal levels (0 h) in cells expressing arrestin2 V53D. Based on these data, the sustained ERK phosphorylation observed with 2-AG, THC, and CP occurred *via* arrestin2-mediated signaling.

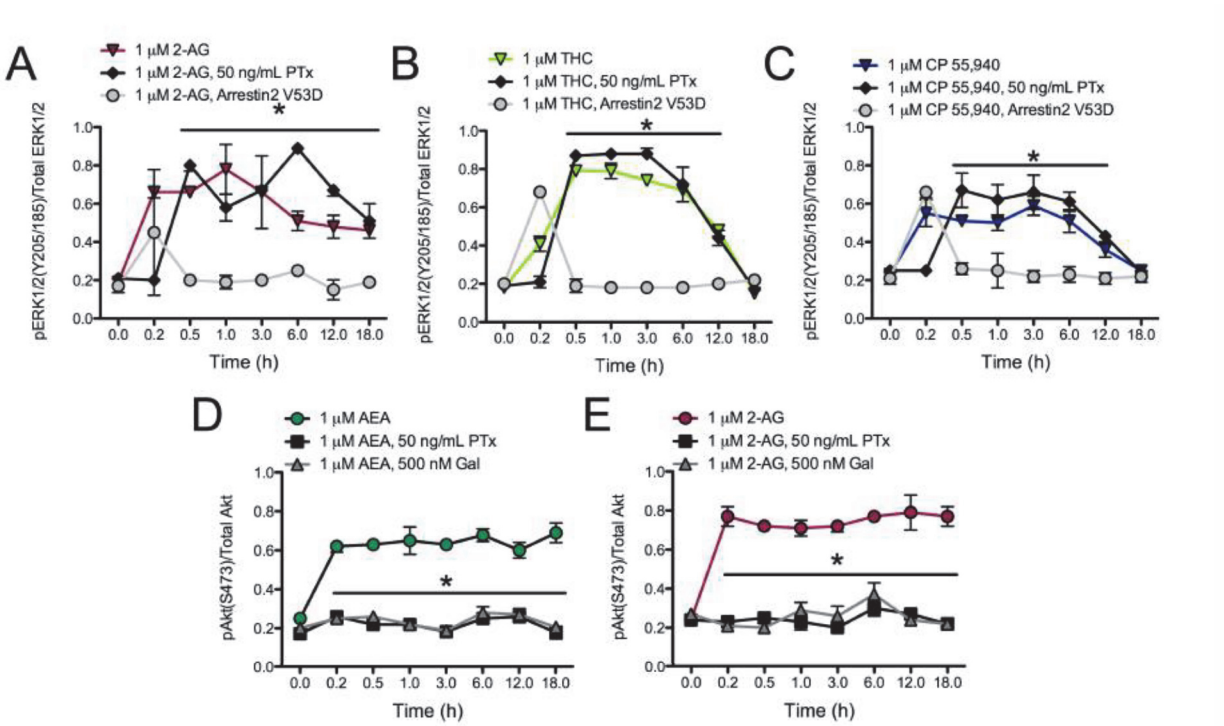

Figure 3-9. Sustained ERK phosphorylation was arrestin2-dependent and sustained Akt phosphorylation was $G\alpha_{i/o}$- and $G\beta\gamma$-dependent. A – C) ERK phosphorylation [pERK1/2(Y205/185)/Total ERK] was measured over 18 h in cells treated with 1 μM 2-AG **(A)**, THC **(B)**, or CP **(C)** with or without 50 ng/mL PTx or in the presence of an arrestin2 dominant negative mutant (arrestin2 V53D). **P* < 0.001 compared to treatment in the presence of arrestin2 V53D, within time-point as determined *via* one-way ANOVA followed by Tukey's *post-hoc* test. *n* = 4. **D,E)** Akt phosphorylation [pAkt(S473)/Total Akt] was measured over 18 h in cells treated with 1 μM AEA **(D)** or 2-AG **(E)** with or without 50 ng/mL PTx or 500 nM gallein (Gal). **P* < 0.001 compared to cannabinoid treatment alone, within time-point as determined *via* one-way ANOVA followed by Tukey's *post-hoc* test. *n* = 4.

We had also observed PTx-sensitive Akt phosphorylation in cells treated with AEA or 2-AG for 10 or 30 min. Akt phosphorylation is not commonly associated with activation of $G\alpha_{i/o}$-mediated signaling (Shenoy *et al*., 2006), but does occur *via* $G\beta\gamma$-dependent activation, which is typically associated with $G\alpha_{i/o}$ (Obara *et al*., 2008). To determine whether this was occurring in our model system, cells were treated with 1 μM AEA or 2-AG with or without 50 ng/mL PTx or 500 nM of the $G\beta\gamma$ inhibitor gallein (Fig. 3-9D,E). Co-treatment of AEA- (Fig. 3-9D) or 2-AG- (Fig. 3-9E) treated cells with PTx or gallein prevented Akt phosphorylation over the 18 h time period analyzed. Therefore, AEA- and 2-AG-dependent Akt phosphorylation was mediated by $G\alpha_{i/o}$ and $G\beta\gamma$.

3.3.3. The functional selectivity of cannabinoid ligands altered the expression and localization of CB_1 receptors.

Arachidonyl-2'-chloroethylamide (ACEA), methanandamide, and AEA increased the steady-state levels of CB_1 mRNA and protein *via* Akt and NF-κB (Laprairie *et al*., 2013). Akt activation was observed in AEA-, 2-AG-, WIN-, and CP-treated cells and not in THC- and CBD-treated cells. We hypothesized that this increase in CB_1 levels was unique to those cannabinoids that increased Akt phosphorylation. To test this hypothesis, cells were treated with 1 μM AEA, 2-AG, CBD, THC, WIN, or CP with or without 50 ng/mL PTx or CTx, or 500 nM O-2050 for 18 h and CB_1 mRNA levels were quantified relative to β-actin (Fig. 3-10A). AEA and 2-AG, and to a lesser extent WIN, increased CB_1 mRNA levels relative to vehicle treatment, while CBD, THC, and CP treatment did not change CB_1 mRNA levels (Fig. 3-10A). The increase in CB_1 mRNA levels may have been lower in WIN-treated cells, and absent in CP-treated cells, because Akt phosphorylation was lower in WIN- and CP-treated cells relative to AEA- and 2-AG-treated cells (Fig. 3-7), resulting in insufficient activation of this signaling pathway. In addition, the increase in CB_1 mRNA levels was blocked by treatment with O-2050 or PTx and therefore occurred through CB_1 and $G\alpha_{i/o}$ (Fig. 3-10A). Thus, AEA, 2-AG, and WIN treatment biased CB_1 signaling toward activation of $G\alpha_{i/o}$ signaling, resulting in increased CB_1 mRNA levels.

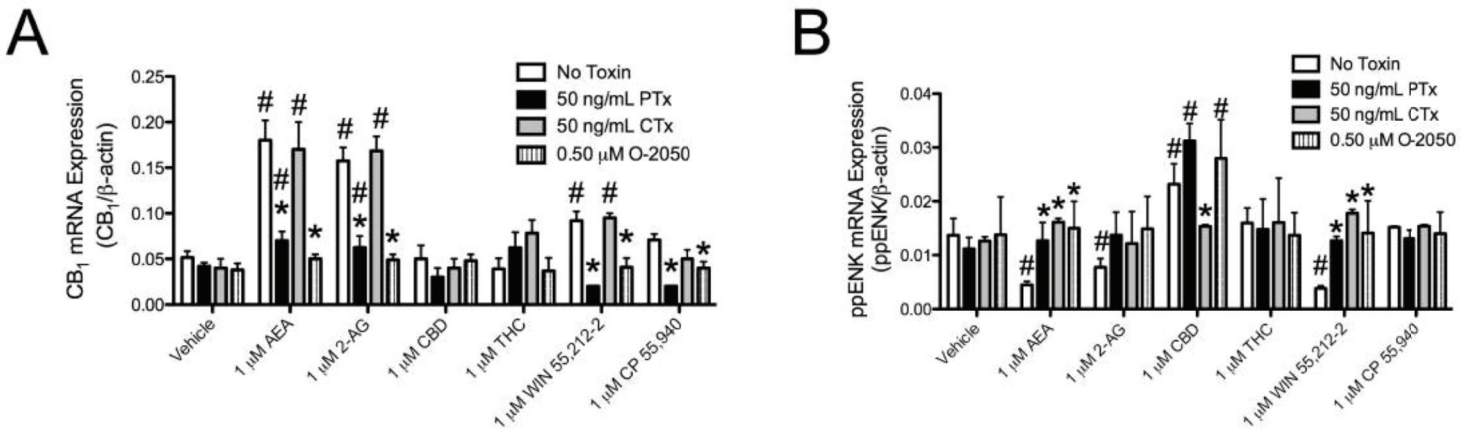

Figure 3-10. AEA and 2-AG treatment increased CB_1 mRNA levels *via* $G\alpha_{i/o}$, while CBD increased ppENK mRNA levels *via* $G\alpha_s$. CB_1 **(A)** and ppENK **(B)** mRNA levels were quantified using qRT-PCR in samples from cells treated with 1 μM AEA, 2-AG, CBD, THC, WIN or CP for 18 h with or without 500 nM O-2050 or 24 h pre-treatment with 50 ng/mL PTx or CTx. CB_1 and ppENK levels were normalized to β-actin. *$P < 0.001$ compared to 'No Toxin' within treatment group, #$P < 0.001$ compared to vehicle within toxin treatment as determined *via* two-way ANOVA followed by Bonferroni's *post-hoc* test. $n = 4$.

CBD and CP treatment increased CREB phosphorylation (Fig. 3-6C,F). Therefore, we wanted to know if treatment with CBD or CP increased preproenkephalin (ppENK) expression, which is known to be CREB-dependent (Simpson *et al*., 1995; Gu *et al*., 1996). ppENK mRNA levels were quantified in cells treated with 1 μM AEA, 2-AG, CBD, THC, WIN, or CP with or without 50 ng/mL PTx or CTx, or 500 nM O-2050 for 18 h. AEA, 2-AG, and WIN treatment were associated with a CB_1-dependent decrease in ppENK mRNA levels, while CBD treatment increased ppENK mRNA levels, compared to vehicle treatment (Fig. 3-10B). The CBD-mediated increase in ppENK mRNA levels was CB_1-independent because it was not inhibited by O-2050 (Fig. 3-10B). CP treatment did not affect ppENK mRNA levels (Fig. 3-10B). CBD treatment resulted in greater CREB phosphorylation than CP treatment (Fig. 3-6C,F). Therefore, CP treatment may have failed to increase ppENK mRNA levels because the magnitude of CREB phosphorylation was too low. Based on these data, AEA-, 2-AG-, and WIN-dependent activation of $G\alpha_{i/o}$ (through CB_1) inhibited CREB-mediated gene expression, while CBD-mediated, CB_1-independent activation of $G\alpha_s$ increased CREB-mediated gene expression.

Increased CB_1 mRNA levels translated to increased CB_1 protein abundance, as determined *via* On- and In-cell™ Western analyses. Treatment with 1 μM AEA or 2-AG resulted in increased CB_1 levels within 3 h compared to the 0 h measurement, or vehicle treatment within the time point, and this increase was still observed at 18 h (Fig. 3-11A). In contrast, treatment with 1 μM THC or CP resulted in decreased CB_1 levels by 6 h (THC) and 12 h (CP) compared to the 0 h measurement or vehicle control (Fig. 3-11B,C). Treatment with 1 μM CBD or WIN did not change CB_1 protein levels (Fig. 3-11B,C). CB_1 localization was also analyzed over an 18 h treatment period. The fraction of CB_1 receptors at the membrane of AEA- and 2-AG-treated cells was decreased between 0.5 and 3 h, compared to the 0 h time point or vehicle-treated cells, which returned to basal levels by 6 h (Fig. 3-11D). A decrease in the fraction of CB_1 receptors at the membrane was also observed in THC- and WIN-treated cells between 1 and 12 h (THC) and at 1 h (WIN), compared to the 0 h time point or vehicle-treated cells, which returned to basal levels by 18 h (THC) and 3 h (WIN) (Fig. 3-11E,F). Treatment with CBD increased the fraction

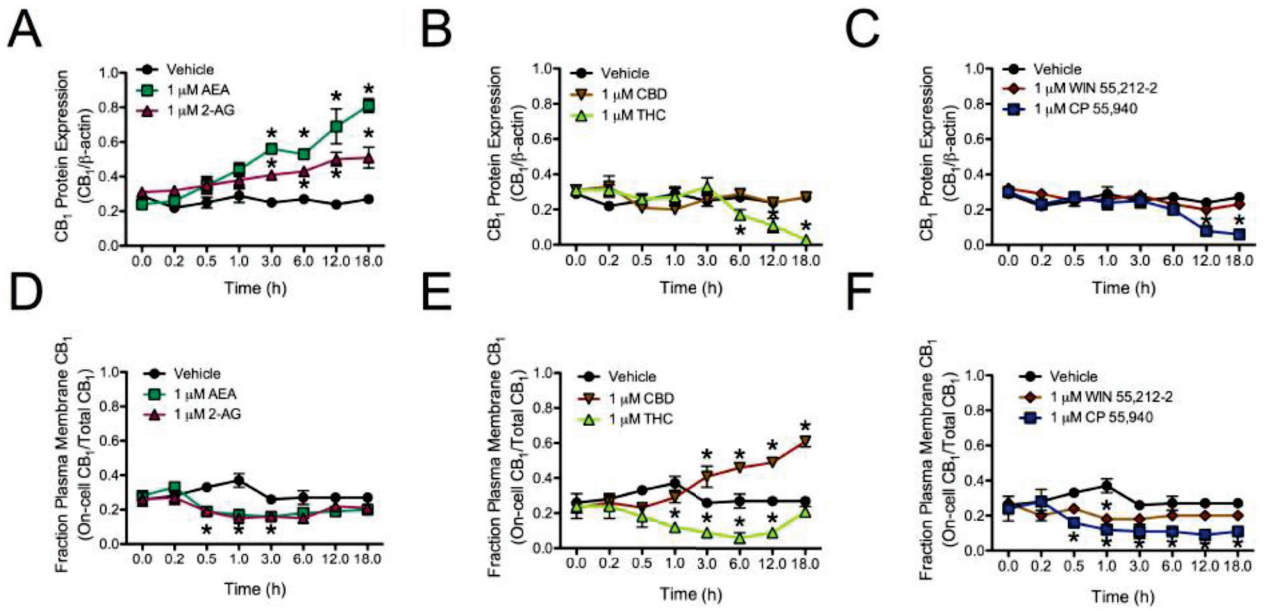

Figure 3-11. AEA and 2-AG treatment increased CB_1 protein levels, while THC and CP treatment promoted CB_1 degradation. A – C) CB_1 protein levels (relative to β-actin) were determined using In-cell™ Western assays in cells treated with vehicle, 1 μM AEA or 2-AG **(A)**, CBD or THC **(B)**, and WIN or CP **(C)** for 18h. **D – F)** The percentage of cell surface CB_1 receptors relative to total CB_1 receptor levels was determined using On- and In-cell™ Western assays in cells treated with vehicle, 1 μM AEA or 2-AG **(D)**, CBD or THC **(E)**, and WIN or CP **(F)** for 18h. *$P < 0.001$ compared to vehicle treatment within time point and 0 h time point within treatment as determined *via* two-way ANOVA followed by Bonferroni's *post-hoc* test. $n = 4$.

of CB_1 receptors at the membrane between 3 and 18 h, relative to the 0 h time point or vehicle-treated cells (Fig. 3-11E). In contrast, treatment with CP resulted in a sustained decrease in the fraction of CB_1 receptors at the membrane beginning at 0.5 h and persisting to 18 h, compared to the 0 h time point and vehicle-treated cells (Fig. 3-11F). CB_1 receptor localization was also examined *via* confocal microscopy in cells expressing CB_1-GFP^2 and treated with 1 μM AEA, THC, or CBD for 10 min, 30 min, 1, 3, 6, 12, or 18 h. Similar to the observations made in figure 3-11D, CB_1-GFP^2 localization shifted from the plasma membrane to the cytoplasm and back to the plasma membrane in cells treated with AEA for 18 h (Fig. 3-12). In contrast to AEA-treated cells, CB_1-GFP^2 was first internalized and subsequently degraded, as indicated by decreased fluorescence, in THC-treated cells (Fig. 3-12). In CBD-treated cells CB_1-GFP^2 fluorescence at the plasma membrane gradually increased over the 18 h observed (Fig. 3-12). Similarly, CB_1-GFP^2 was localized to the plasma membrane in cells treated with 500 nM O-2050 for 3 h (Fig. 3-12). Therefore, while AEA and THC treatment affected CB_1 signaling and internalization, CBD did not affect CB_1 internalization and CBD-mediated signaling was CB_1-independent.

In summary, the endocannabinoids AEA and 2-AG facilitated an increase in CB_1 mRNA and protein *via* $G\alpha_{i/o}$ and $G\beta\gamma$. WIN also activated $G\alpha_{i/o}$ and $G\beta\gamma$ signaling, but to a lesser extent than AEA and 2-AG. Treatment with the phytocannabinoid, THC, and the synthetic cannabinoid, CP, did not alter CB_1 mRNA levels, but did lead to a decrease in CB_1 protein levels over the 18 h time period analyzed. CP also enhanced $G\alpha_s$ signaling *via* CB_1. CBD-mediated $G\alpha_s$ signaling occurred independent of CB_1 as observed elsewhere (Jones *et al*., 2010).

3.4. DISCUSSION

3.4.1. CB_1-MEDIATED INTRACELLULAR SIGNALING WAS LIGAND-SPECIFIC.

The goal of this study was to compare the CB_1-mediated functional selectivity of six cannabinoids in a cell line that models striatal medium spiny projection neurons endogenously expressing CB_1. Each ligand displayed functional selectivity for a subset of intracellular signaling pathways (see

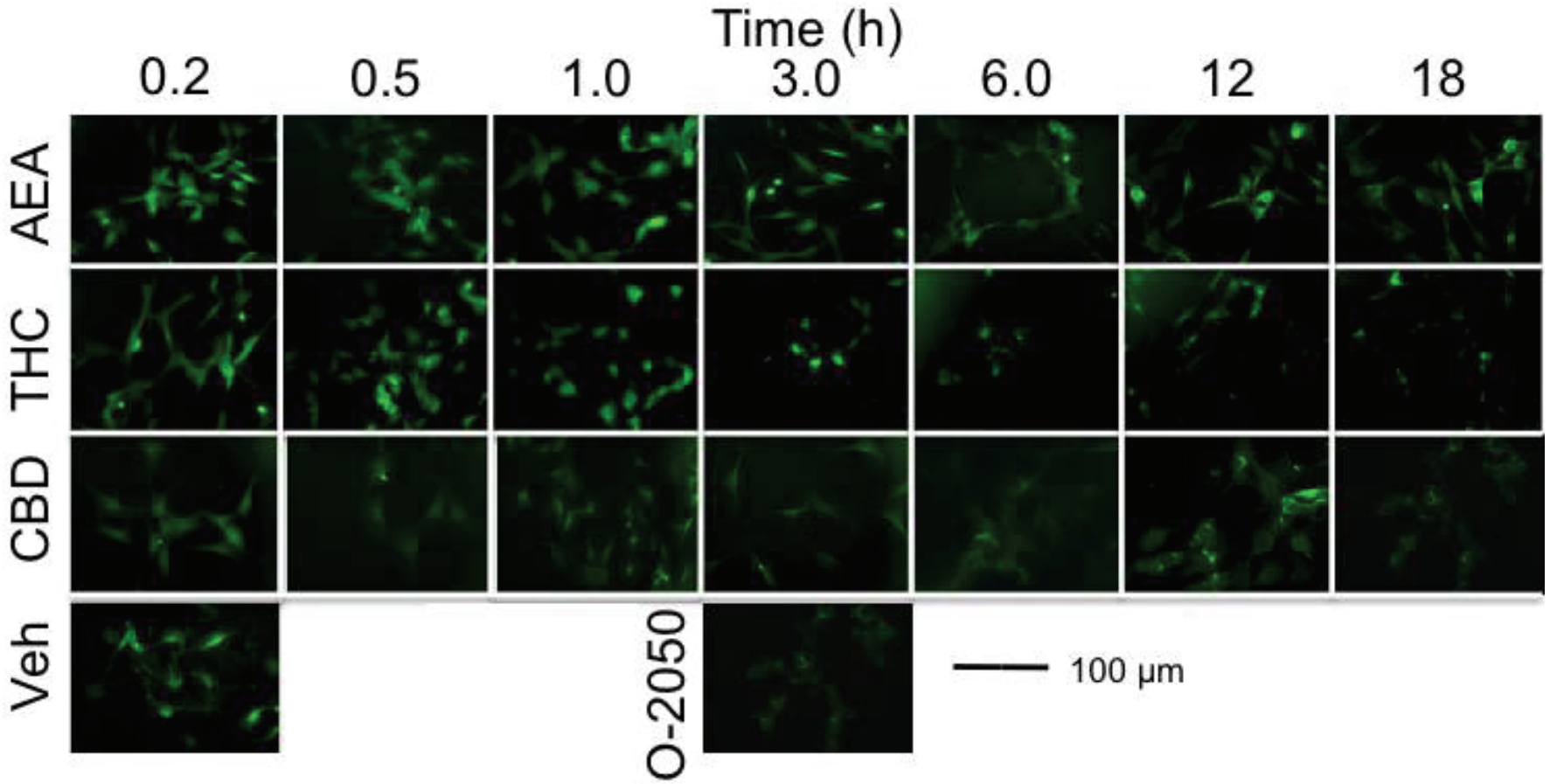

Figure 3-12. CB_1 localization was assessed in cells expressing CB_1-GFP^2. Representative images of ST*Hdh*$^{Q7/Q7}$ cells expressing CB_1-GFP^2 and treated with vehicle, 1 µM AEA, THC, or CBD for the length of time indicated and 500 nM O-2050 for 3 h. Images are from 1 of 4 independent experiments.

summary in figure 3-13). With the exception of CBD-dependent $G\alpha_s$ signaling, this functional selectivity was CB_1-dependent.

2-AG, THC, and CP enhanced the interaction between CB_1 and arrestin2 to a greater extent than other cannabinoids tested suggesting a high degree of interaction between the population of CB_1 and arrestin2 molecules in the *in vitro* system following 30 min treatment with these compounds. The relative $BRET_{Eff}$ was a conservative estimate of the interaction between CB_1 and arrestin2 because endogenous CB_1 and arrestin2 would have competed with their labeled counterparts in ST*Hdh*$^{Q7/Q7}$ cells in the BRET assays. These observations differ from previous reports that CB_1 weakly interacts with arrestins in U2OS, CHO, and HEK cell heterologous expression systems treated with WIN or CP for 5 min (van der Lee *et al.,* 2009) or 2 h (Vrecl *et al*., 2009). Previous studies also observed that recruitment of arrestins to CB_1 occurred over a wider range of ligand concentrations ($1x10^{-10}$ – $1x10^{-6}$ M) (van der Lee *et al.,* 2009; Vrecl *et al*., 2009) than that observed here ($1x10^{-8}$ – $1x10^{-5}$ M). The variability between our results and previous reports may reflect differences between the functionality of CB_1 in ST*Hdh*$^{Q7/Q7}$ cells and CB_1 over-expression in U2OS, CHO, or HEK cells (Vrecl *et al*., 2009). In addition, $BRET^2$ is a more sensitive assay for detecting protein-protein interactions compared to the Tango and PathHunter reporter assays used previously (van der Lee *et al.,* 2009). Moreover, previous studies examined the recruitment of arrestin3 (β-arrestin2) in HEK cells (Vrecl *et al*., 2009) and not arrestin2.

At 1 μM AEA, 2-AG, WIN, and CP promoted CB_1 signaling toward $G\alpha_{i/o}$-mediated ERK phosphorylation to a greater degree than other cannabinoids tested. The consequence of this functional selectivity is that transient ERK signaling was enhanced by endocannabinoids compared to other cannabinoids tested, whereas sustained ERK signaling from 10 – 30 min through arrestin2 was enhanced by 2-AG, THC, and CP and not by AEA, CBD, or WIN. Other studies have also reported that transient ERK activation occurs *via* $G\alpha_{i/o}$ in the N18TG2 mouse neuronal cell line (Dalton *et al*., 2012), and in HEK cells stably-expressing CB_1 (Daigle *et al*., 2008). In our studies CB_1 receptors recruited arrestin2 leading to sustained ERK signaling, whereas previous studies have found that sustained ERK signaling

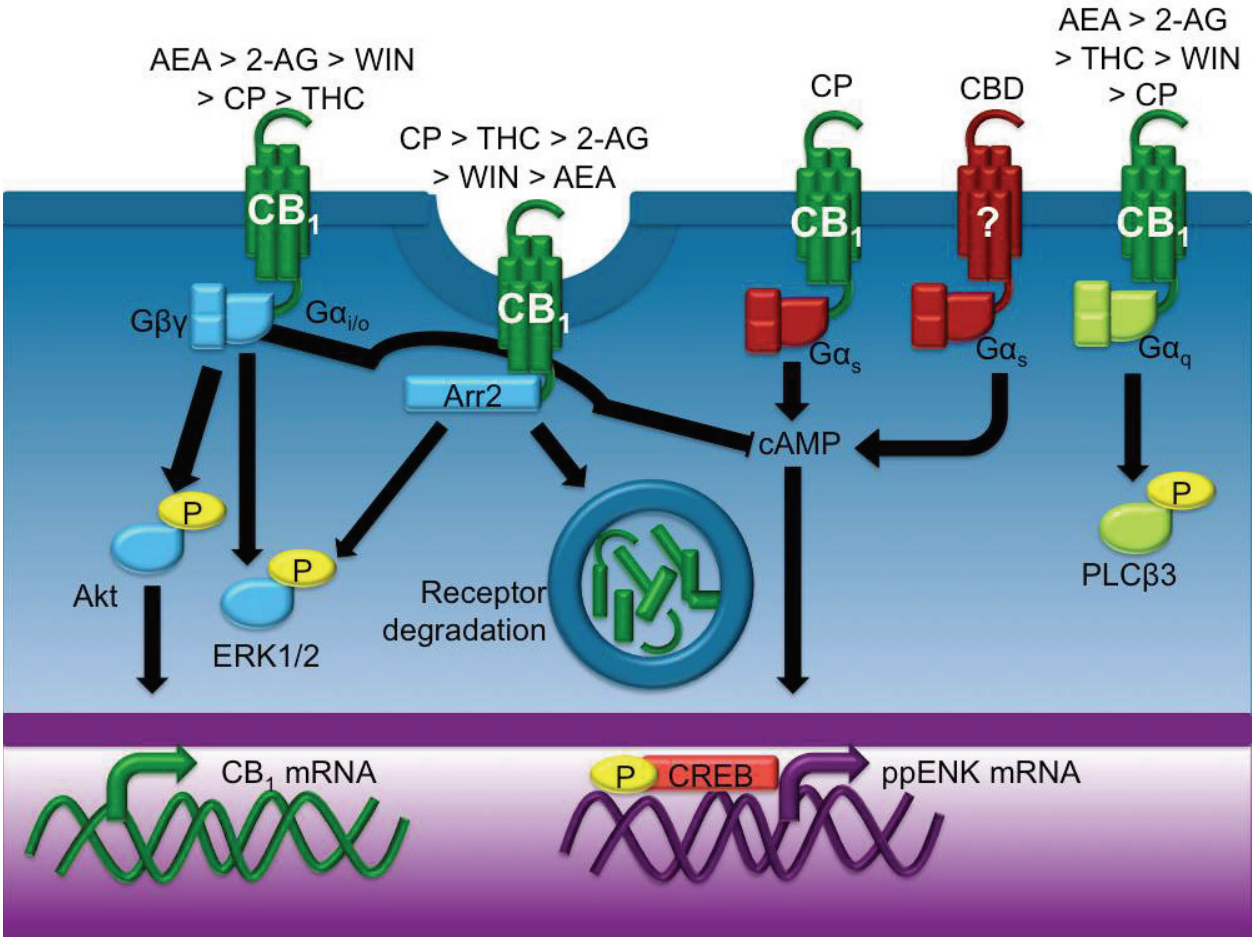

Figure 3-13. Cannabinoid ligands biased CB_1-dependent signal transduction. Each cannabinoid tested here biased CB_1 signaling toward different pathways. The endocannabinoids AEA and 2-AG promoted $G\alpha_{i/o}$-dependent ERK and Akt activation more effectively than other cannabinoids tested. THC and CP were the most efficacious ligands with regard to CB_1-arrestin2 interactions, but 2-AG, WIN, and AEA also promoted interactions between CB_1 and arrestin2 above the level observed in vehicle-treated cells. CBD appeared to inhibit the internalization of CB_1. CBD, and to a lesser extent CP, treatment enhanced $G\alpha_s$-dependent CREB phosphorylation independent of CB_1, whereas CP-dependent CREB phosphorylation of CB_1-dependent. AEA, 2-AG, THC, WIN, and CP promoted $G\alpha_q$-dependent, transient PLCβ3 activation.

is receptor tyrosine kinase-dependent (Dalton *et al*., 2012).

AEA and 2-AG activated Akt *via* $G\alpha_{i/o}$- and $G\beta\gamma$-dependent pathways. This resulted in increased CB_1 mRNA and protein levels. Although WIN and CP treatment also resulted in $G\alpha_{i/o}$-dependent ERK phosphorylation and $G\beta\gamma$-dependent Akt phosphorylation, the magnitude of $G\beta\gamma$ activation was less following WIN and CP treatment than that observed in AEA and 2-AG treatment. The net result was that WIN and CP treatment did not lead to significantly increased CB_1 mRNA and protein levels.

In addition to activation of $G\alpha_{i/o}$, AEA, 2-AG, WIN, THC, and CP enhanced transient $G\alpha_q$-coupled PLCβ3 phosphorylation. Few studies have examined direct coupling of CB_1 to $G\alpha_q$ (Lauckner *et al*., 2005; McIntosh *et al*., 2007). Coupling of CB_1 to $G\alpha_q$ has been reported in HEK cells stably-expressing CB_1 (Lauckner *et al*., 2005) and human trabecular meshwork cells (McIntosh *et al*., 2007). In these studies, the authors observed transient, $G\alpha_q$-dependent Ca^{2+} efflux following stimulation of CB_1 with WIN (Lauckner *et al*., 2005; McIntosh *et al*., 2007), which is an indirect measure of $G\alpha_q$ coupling. In support of studies that have indirectly measured CB_1 coupling to $G\alpha_q$ *via* Ca^{2+} efflux, the work here measured PLCβ3 activation, which is a direct effect of $G\alpha_q$. Because $G\alpha_q$ signaling may affect cellular function, future studies examining CB_1 signaling should determine whether CB_1 couples to $G\alpha_q$ in other model systems.

CBD treatment resulted in $G\alpha_S$-signaling and CREB-dependent expression of ppENK (Costa *et al.*, 2007; Magen *et al*., 2009). CBD signaling was independent of CB_1 as demonstrated by the inability of the direct antagonist O-2050 to block agonist-dependent $G\alpha_s$ signaling, as reported elsewhere (Jones *et al*., 2010). Although CBD has a relatively low affinity for CB_1 (Devinsky *et al*., 2014), CBD has been shown to act as an agonist and antagonist at the type 2 cannabinoid receptor, an adenosine A_{2A} agonist, a $5HT_{1A}$ agonist, and a modulator of FAAH and monoacylglycerol lipase activity (MAGL) (Costa *et al.,* 2007; Mechoulam *et al.*, 2007; Jones *et* al., 2010; Devinsky *et al.*, 2014). ST*Hdh*$^{Q7/Q7}$ cells express adenosine A_{2A} and $5HT_{1A}$ receptors and FAAH (Trettel *et al.,* 2000; Laprairie *et al*., 2013). The inability of O-2050 to block $G\alpha_s$ signaling indicates that CBD acted at non-CB_1 targets in ST*Hdh*$^{Q7/Q7}$ cells. In our assays,

CBD treatment increased CB_1 levels at the plasma membrane, but did not affect CB_1-dependent signaling through $G\alpha_{i/o}$ or $G\alpha_q$. CBD is being investigated for its utility as an anti-epileptic (Jones *et al*., 2010) anti-inflammatory (Magen *et al*., 2009) and for its neuromodulatory activities *in vivo* (Costa *et al*., 2007; Jones *et al*., 2010). CBD has a relatively safe side effect profile compared to THC and other cannabinoids (Costa *et al*., 2007; Jones *et al*., 2010). The fact that we observed that CBD selectively increased CREB-dependent gene expression may also have therapeutic potential in neurodegenerative diseases where CREB-dependent gene expression is dysregulated (Jones *et al*., 2010; Laprairie *et al*., 2013; Devinsky *et al.*, 2014).

Unlike CBD, CP-dependent CREB phosphorylation occurred *via* CB_1. Although CB_1 does not typically signal through $G\alpha_s$, CP could promote a conformational change in the receptor that favours $G\alpha_s$ binding. Alternatively, CP treatment may promote the dimerization of CB_1 with other GPCRs that signal through $G\alpha_s$. CB_1 is known to homodimerize with CB_1 and CB_1 splice variants (Bagher *et al*., 2013), and heterodimerize with other receptors including the dopamine D_2 receptor (Hudson *et al*., 2010; Przybyla and Watts, 2010; Laprairie *et al.*, 2013). ST*Hdh*$^{Q7/Q7}$ cells express dopamine D_2 receptors and CB_1-D_2 dimerization could contribute to the actions of CP in these cells (Przybyla and Watts, 2010).

3.4.2. CB_1-MEDIATED SIGNALING HAD IMMEDIATE AND SUSTAINED COMPONENTS

In addition to observing cannabinoid functional selectivity, CB_1 signaling was also time-dependent. $G\alpha_{i/o}$ and $G\alpha_q$ signaling were transient, being detected at 10 min and returning to basal levels at 30 min. Transient CB_1-dependent activation of $G\alpha_{i/o}$ and $G\alpha_q$ signaling has been observed elsewhere in HEK cells stably-expressing CB_1 (Lauckner *et al*., 2005; Daigle *et al*., 2008). In contrast, $G\alpha_s$ signaling was not detected before 30 min. The association between CB_1 and arrestin2 peaked shortly after 10 min for all ligands tested and remained high for 30 min relative to vehicle control demonstrating that the pleiotropically-coupled CB_1 receptor switches between G protein signaling and arrestin signaling within approximately 30 min of ligand administration and this switch is ligand-specific. Over an 18 h treatment period THC, CP, and 2-AG treatment resulted in CB_1 receptor internalization (beginning at 30 min), but

only THC and CP treatment resulted in decreased CB_1 receptor protein levels (beginning at 12 h). This difference may be due to the higher affinity of THC and CP for CB_1 compared to 2-AG (Pertwee *et al*., 2010), which implies that 2-AG is a 'fast-off' cannabinoid relative to THC or CP (Jin *et al.*, 1999; van der Lee *et al.*, 2009; Singh *et al*., 2011). *In vivo*, 2-AG is approximately 1,000 times more abundant than AEA (Kondo *et al.*, 1998; Sugiura *et al.*, 1999; Pertwee *et al*., 2010). 2-AG is likely to have a greater effect on the arrestin-mediated recycling of CB_1 between the membrane and intracellular space relative to AEA. Overall, the functional selectivity displayed by the six cannabinoids tested here in an *in vitro* model of striatal neurons supports the hypothesis that individual ligands promote unique conformational changes in the CB_1 receptor that lead to functionally divergent intracellular effects, such as G protein-coupled signaling, arrestin recruitment, receptor trafficking and gene expression (Glass and Northrup, 1999; Jin *et al*., 1999; Varga *et al.*, 2008; van der Lee *et al*., 2009; Vrecl *et al*., 2009).

3.4.3. THE EFFECT OF CANNABINOIDS IS BRAIN REGION- AND AGONIST-SPECIFIC.

We observed increased CB_1 mRNA and protein levels following 18 h treatment with 2-AG or AEA in an *in vitro* cell culture model of striatal neurons. *In vivo*, CB_1 receptor binding does not differ between FAAH knockout mice and wild-type littermates in the striatum, hippocampus, or cerebellum when treated with vehicle or AEA for 5 consecutive days (Falenski *et al.*, 2010). Further, CB_1 receptor binding decreases in these brain regions of FAAH knockout mice treated with THC for 5 consecutive days (Falenski *et al.*, 2010). MAGL knockout mice and mice treated for 6 days with the MAGL inhibitor JZL184 display decreased CB_1 receptor binding in the cortex, hippocampus, and periaqueductal gray, but no difference in the striatum (Schlosberg *et al.*, 2010). *In vivo* then, alteration of CB_1 level depends on brain region, animal genotype, duration of treatment, and the cannabinoid ligand (Long *et al.*, 2009; Falenski *et al.*, 2010; Schlosberg *et al.*, 2010). Inhibition of MAGL (5 days), the principle regulator of 2-AG levels, results in functional antagonism of CB_1, whereas inhibition of FAAH, the principal regulator of AEA levels, maintains CB_1 signaling (Long *et al.*, 2009; Falenski *et al.*, 2010; Schlosberg *et al.*, 2010). Sub-chronic or chronic exposure to exogenous cannabinoids, such as THC, and high potency

cannabinoids decreases CB_1 receptor binding (Long *et al.*, 2009; Falenski *et al.*, 2010; Schlosberg *et al.*, 2010). Downregulation and desensitization of CB_1 receptor following repeated THC or WIN treatment are more pronounced in the hippocampus compared to the striatum (Sim-Selley *et al.*, 2006; Lazenka *et al*., 2013). CB_1 desensitization and arrestin3 (β-arrestin2) recruitment also vary widely between brain regions (Nguyen *et al.*, 2012). FAAH knockout mice show less CB_1 downregulation and desensitization following AEA treatment compared to THC treatment (Falenski *et al.*, 2010). CB_1 internalization is also promoted by WIN more than methanandamide in primary rat hippocampal neurons (Coutts *et al*., 2001). THC-mediated desensitization is faster than WIN-, CP-, and 2-AG-mediated desensitization in HEK cells stably-expressing CB_1 and primary neuronal cultures (Wu *et al*., 2008). In contrast, AEA-mediated CB_1 desensitization is slower than that of WIN-, CP-, and 2-AG (Wu *et al*., 2008). Endogenous cannabinoids, specifically AEA, may have a different effect on CB_1 levels than other cannabinoids. We do not yet know whether there is a difference in the brain region-specific effect on CB_1 mRNA and protein levels under various treatment regimens *in vivo*.

There is the potential to exploit signaling bias at CB_1. Effects such as receptor internalization *via* arrestin2, $G\alpha_{i/o}$-mediated increases in CB_1, $G\alpha_q$-mediated modulation of Ca^{2+} release, $G\alpha_s$-mediated CREB activation, and CB_1 protein downregulation could be selected or avoided according to their usefulness in different disease states. This could lead to the development of therapeutics that avoid the psychoactive effects of cannabinoids and promote their neuroprotective effects.

CHAPTER 4

BIASED TYPE 1 CANNABINOID RECEPTOR SIGNALING INFLUENCES NEURONAL VIABILITY IN A CELL CULTURE MODEL OF HUNTINGTON DISEASE.

Copyright statement

Contribution statement

The manuscript used as the basis for this chapter was written with guidance from Drs. Eileen Denovan-Wright, Amina Bagher, and Melanie Kelly. All data were collected and analyzed by myself.

4.1. INTRODUCTION

Expression of mutant huntingtin protein (mHtt) causes a myriad of molecular and cellular changes that ultimately cause progressive worsening of the symptoms of Huntington disease (HD). Early in HD progression, levels of type 1 cannabinoid receptor (CB_1) mRNA and protein decrease in medium spiny projection neurons of the caudate and putamen (Denovan-Wright and Robertson, 2000; Glass *et al*., 2000; Van Laere *et al*., 2010). CB_1 transcription is inhibited by mHtt (McCaw *et al*., 2004; Laprairie *et al*., 2013). The reduction in CB_1 and loss of CB_1 function have been shown to contribute to the cognitive, behavioural, and motor deficits of HD pathology in animal models of HD (Blázquez *et al*., 2011; 2015; Chiarlone *et al*., 2014). Furthermore, rescue of CB_1 gene expression in the striatum using viral transduction prevents the loss of excitatory synaptic markers and reduces dendritic spine loss in animal models of HD (Naydenov *et al*., 2014). The benefit of adeno-associated viral CB_1 delivery in HD provides strong proof for the concept of treating HD through enhancing CB_1 function. However, gene-based therapies specifically for CB_1 or other single alterations in gene expression, are unlikely to be used clinically for HD in the near future because of the invasive nature of delivery and because the potential adverse effects of gene therapy are still being investigated. The more-effective gene-based therapies for HD will target the underlying cause of the disease: the *mHtt* gene and encoded protein, and not secondarily lost cellular components (Kumar *et al.,* 2015). In contrast, pharmacological strategies aimed at elevating CB_1 levels and/or signaling through the remaining pool of CB_1 receptors has significant therapeutic potential for the treatment and management of HD.

CB_1 is activated by cannabinoids, which are a structurally diverse group of ligands that includes endogenously occurring cannabinoids (endocannabinoids) such as anandamide (AEA) and 2-arachidonoylglycerol (2-AG), phytocannabinoids from *Cannabis sativa* such as Δ^9-tetrahydrocannabinol (THC) and synthetic cannabinoids such as CP55,940 (CP) and WIN55,212-2 (WIN) (Pertwee, 2008). Activation of CB_1 in the brain results in inhibition of neurotransmitter

release from presynaptic glutamatergic and GABAergic neurons and activation of pro-survival signaling cascades such as ERK and Akt (Fernández-Ruiz, 2009). We have reported that AEA, and structurally-related compounds, increase the expression of CB_1 *via* CB_1 through $G\alpha_{i/o}$ and $G\beta\gamma$ signaling in a cell culture model expressing normal *huntingtin* (ST*Hdh*$^{Q7/Q7}$) and cells expressing mHtt (ST*Hdh*$^{Q111/Q111}$) (Laprairie *et al*., 2013). Importantly, this cell culture model endogenously expresses CB_1 and other components of the endocannabinoid system. Increasing levels of CB_1 improved neuronal viability in this cell culture model (Laprairie *et al*., 2013), lending further support to the strategy of enhancing signaling through the pool of CB_1 that are retained in the presence of mHtt and elevating CB_1 levels in these cells despite transcriptional repression *via* mHtt.

Not all cannabinoids increase CB_1 levels. THC and CP treatment promote arrestin-dependent CB_1 internalization and reduce CB_1-dependent downstream signaling (Laprairie *et al*., 2014a). Functional selectivity (*i.e.* signaling bias) describes the receptor- and ligand-dependent enhancement of certain signal transduction pathways and the simultaneous diminution of other signal transduction pathways at a single receptor (Luttrell *et al*., 2015). Functional selectivity occurs *via* a GPCR ligand that preferentially activates one effector (*e.g.* $G\alpha_{i/o}$) more potently and efficaciously than another (*e.g.* arrestin) through ligand-specific changes in GPCR conformation or dimerization with other GPCRs (Christopoulos, 2014). Signaling bias could be exploited for enhancement of CB_1 function in HD while limiting detrimental adverse on-target effects (Laprairie *et al*., 2014a). Cannabinoids display signaling bias (Laprairie *et al*., 2014a; Khajehali *et al*., 2015). Endocannabinoids acting at CB_1 are $G\alpha_{i/o}$-biased whereas THC and CP are arrestin-biased in ST*Hdh*$^{Q7/Q7}$ cells (Laprairie *et al*., 2014). In this study, we wanted to determine how the bias of different classes of cannabinoids affected neuronal viability. We hypothesized that $G\alpha_{i/o}$-biased cannabinoids improve neuronal viability, whereas arrestin-biased cannabinoids reduce – or have no effect on – cell viability. The functional selectivity of 6 cannabinoids [AEA, 2-AG, THC, cannabidiol (CBD), WIN, and CP] between $G\alpha_{i/o}$-, $G\alpha_s$, $G\alpha_q$, $G\beta\gamma$, arrestin pathways was

examined in ST*Hdh*$^{Q7/Q7}$ and ST*Hdh*$^{Q111/Q111}$ cells and compared to cannabinoid-dependent changes in ATP level, GABA release, metabolic activity and cell death.

4.2. MATERIALS AND METHODS

4.2.1 DRUGS

Drugs were dissolved in ethanol (THC) or DMSO [2-AG, 8-OH-DPAT ($5HT_{1A}$ agonist), AEA, CP, CBD, gallein (Gβγ inhibitor), haloperidol (D_2 antagonist), O-2050 (CB_1 antagonist), quinpirole (D_2 agonist), WAY 100635 ($5HT_{1A}$ antagonist), WIN] and diluted to final solvent concentrations of 0.1%. 2-AG, AEA, CP, CBD, O-2050, and WIN were purchased from Tocris Bioscience (Bristol, UK). 8-OH-DPAT, haloperidol, quinpirole, THC, and WAY 100635 were purchased from Sigma-Aldrich (Oakville, ON, CAN). The Gβγ modulator gallein was purchased from EMD Millipore (Billerica, MA). *Pertussis* toxin (PTx) and *Cholera* toxin (CTx) (Sigma-Aldrich) were dissolved in dH_2O (50 ng/mL) and added directly to the media 24 h prior to cannabinoid treatment. Pre-treatment of cells with PTx and CTx inhibits $G\alpha_{i/o}$ and $G\alpha_s$, respectively (Milligan *et al*., 1989). While treatment with CTx for 30 min or less increases $G\alpha_s$ signaling as measured by increased cAMP levels, 24 h treatment with CTx leads to an irreversible inhibition of ADP-ribosylated $G\alpha_s$ protein and the concomitant elimination of $G\alpha_s$-dependent signaling (Miligan *et al.*, 1989; McKenzie and Miligan, 1991). All experiments included a vehicle treatment control.

4.2.2. CELL CULTURE

ST*Hdh*$^{Q7/Q7}$ and ST*Hdh*$^{Q111/Q111}$ cells are derived from the conditionally immortalized striatal progenitor cells of embryonic day 14 C57BlJ/6 mice (Coriell Institute, Camden, NJ) (Trettel *et al*., 2000). ST*Hdh*$^{Q111/Q111}$ cells express exon 1 of the mutant human *huntingtin* gene containing 111 CAG repeats knocked into the mouse *huntingtin* locus (Trettel *et al.,* 2000). ST*Hdh*$^{Q7/Q7}$ and ST*Hdh*$^{Q111/Q111}$ cells endogenously express CB_1 and dopamine D_2 receptor (Paoletti *et al.*, 2008). Cells were maintained at 33°C, 5% CO_2 in DMEM supplemented with 10% FBS, 2 mM L-glutamine, 10^4 U mL^{-1} Pen/Strep, and 400 μg mL^{-1} geneticin. Cells were

serum-deprived for 24 h prior to experiments to promote differentiation (Trettel *et al*., 2000; Laprairie *et al*., 2014a,b).

4.2.3. PLASMIDS AND TRANSFECTION

Human CB_1-green fluorescent protein^2 (GFP^2) C-terminal fusion protein was generated using the pGFP^2-N3 (PerkinElmer, Waltham, MA) plasmid, as described previously (Bagher *et al*., 2013). Human arrestin2 (β-arrestin1)-*Renilla* luciferase II (Rluc) C-terminal fusion protein was generated using the pcDNA3.1 plasmid and provided by Dr. Denis J Dupré (Dalhousie University, NS, CAN). The GFP^2-Rluc fusion construct, and Rluc plasmids have also been described (Bagher *et al*., 2013). The $G\alpha_q$ dominant negative mutant [Glu 209 Δ Leu, Asp 277 Δ Asn (Q209L,D277N)] pcDNA3.1 plasmid was obtained from the Missouri S&T cDNA Resource Center (Rolla, MO) (Lauckner *et al*., 2005).

Cells were grown in 6 well plates and transfected with 200 ng of the Rluc fusion plasmid and 400 ng of the GFP^2 fusion plasmid according to previously described protocols (Laprairie *et al*., 2014a) using Lipofectamine 2000® according to the manufacturer's instructions (Invitrogen, Burlington, ON). Transfected cells were maintained for 48 h prior to experimentation.

4.2.4. BIOLUMINESCENCE RESONANCE ENERGY TRANSFER^2 (BRET^2)

Interactions between CB_1 and arrestin2 were quantified *via* BRET^2 according to previously described methods (James *et al*., 2006; Laprairie *et al*., 2014a). BRET efficiency ($BRET_{Eff}$) was determined such that Rluc alone was used to calculate $BRET_{MIN}$ and the Rluc-GFP^2 fusion protein was used to calculate $BRET_{MAX}$ using previously described methods (James *et al*., 2006).

4.2.5. ON- AND IN-CELL™ WESTERN

On-cell™ western analyses were completed as described previously (Laprairie *et al*., 2014a) using primary antibody directed against *N*-CB_1 (1:500; Cayman Chemical Company, Ann Arbor, MI, USA, Cat No. 101500). All experiments measuring CB_1 included an *N*-CB_1 blocking peptide (1:500) control, which was incubated with *N*-CB_1 antibody (1:500). Immunofluorescence

observed with the *N*-CB_1 blocking peptide was subtracted from all experimental replicates. In-cell™ western analyses were conducted as described previously (Laprairie *et al*., 2014a). Primary antibody solutions were: *N*-CB_1 (1:500), pERK1/2(Tyr205/185) (1:500), ERK1/2 (1:500), pCREB(S133) (1:500), CREB (1:500), pPLCβ3(S537) (1:500), PLCβ3 (1:1000), pAkt(S473) (1:500), Akt (1:1000), or β-actin (1:2000; Santa Cruz Biotechnology). Secondary antibody solutions were: $IR^{CW700dye}$ or $IR^{CW800dye}$ (1:500; Rockland Immunochemicals).

4.2.6. ATP QUANTIFICATION, Γ-AMINO BUTYRIC ACID (GABA) ELISA, AND CELL VIABILITY ASSAYS

The CellTiter-Glo® ATP quantification assay was used according to the manufacturer's instructions (Promega). The GABA ELISA assay was conducted according to the manufacturer's instructions for mouse cell culture media (Novatein Biosciences, Boston, MA, USA). GABA levels were reported as ΔGABA relative to GABA in vehicle-treated cells. Viability assays (calcein-AM [Cal-AM], ethidium homodimer-1 [EthD-1]) were conducted according to the manufacturer's instructions (Live/Dead Cytotoxicity Assay, Life Technologies, Burlington, ON). Cal-AM fluorescence is an indicator of cellular esterase activity and mitochondrial respiration. Cal-Am fluorescence (460/510 nm) is reported as % esterase activity relative to vehicle-treated ST*Hdh*$^{Q7/Q7}$ cells (100%). EthD-1 fluorescence is an indicator of membrane permeability and cell death. EthD-1 fluorescence (530/620 nm) is reported as % membrane permeability relative to ST*Hdh*$^{Q7/Q7}$ cells treated with 70% methanol for 30 min (100%). All measurements of viability (ATP, GABA, calcein-AM, EthD-1) were made 18 h following cannabinoid treatment.

4.2.7. STATISTICAL ANALYSES

All experiments were conducted alongside WIN as a reference ligand. While it is often considered ideal to choose the endogenous receptor agonist as a reference ligand (Kenakin and Christopoulos, 2013), WIN was chosen as a reference ligand for these studies because 1) it is a widely used reference compound to study CB_1-dependent signaling (Lauckner *et al*., 2005), 2) it acted as an agonist in all assays with non-significant differences in EC_{50} observed between assays, and 3) we wanted determine whether the two endogenous cannabinoids, AEA and 2-AG, were

inherently biased either in wild-type (ST*Hdh*$^{Q7/Q7}$) or mHtt-expressing (ST*Hdh*$^{Q111/Q111}$) cells. Concentration-response curves (CRC) for ERK, BRET^2 (CB_1/ arrestin2), CREB, PLCβ3, and Akt are presented as % of WIN E_{max} in ST*Hdh*$^{Q7/Q7}$ cells (Griffin *et al*., 2007).

CRCs were fit to non-linear regression with variable slope (four parameter) model to determine pEC_{50} and E_{max} (Table 4-1), or global non-linear regression using the operational model (Black and Leff, 1983; Ehlert *et al.*, 2011; Kenakin *et al*., 2011) (eq. 1) to estimate the transduction coefficient [logR (τ/ K_A)], change in transducer coefficient relative to the reference ligand (ΔlogR), and bias factor (ΔΔlogR) (Prism v. 5.0, GraphPad Software Inc., San Diego, CA), as indicated. In eq. 1 E is the response, E_{max} is the maximal response, [A] is agonist concentration, n is transducer slope, τ is agonist efficacy, and K_A is the agonist's affinity for the receptor (Kenakin *et al*., 2011). In order to obtain a global least-squares fit of the data to the operational model, n was constrained to 1 and logK_A was shared between both ST*Hdh*$^{Q7/Q7}$ and ST*Hdh*$^{Q111/Q111}$ datasets and constrained to be greater than -15 (Griffin *et al.*, 2007; Ehlert, 2015). Relative activity (ΔlogR) was calculated in Prism as the difference between transduction coefficients [logR (τ/ K_A)] values for two ligands, a 'test' ligand and a reference ligand (here WIN) as measured between sample-matched replicates (Kenakin *et al.*, 2011) (eq. 2). In eq. 3 Bias factor (*i.e.* log bias, ΔΔlogR) is the difference between response 1 (R_1) and response 2 (R_2) (Kenakin *et al.*, 2011). All calculations of ΔΔlogR are reported using pERK response ($G\alpha_{i/o}$) as R_1. Statistical analyses were two-way analysis of variance (ANOVA) (Prism). *Post-hoc* analyses were performed using Bonferroni's test. Homogeneity of variance was confirmed using Bartlett's test. The level of significance was set to $P < 0.01$ where ANOVA was utilized or $P < 0.05$ where non-overlapping confidence intervals (CI) were used to determine significance. Results are reported as the mean ± the standard error of the mean (SEM) from at least 4 independent experiments.

$$E = \frac{E_{max}[A]^n\tau^n}{[A]^n\tau^n+([A]+K_A)^n} \quad \textbf{(1)}$$

$$\Delta logR = \log(\tau/K_A)_{Test\ compound} - log(\tau/K_A)_{Ref\ compound} \quad \textbf{(2)}$$

$$log\ bias = \Delta\Delta logR = \Delta\Delta\log(\tau/K_A)_{R1-R2} = \Delta log(\tau/K_A)_{R1} - \Delta log(\tau/K_A)_{R2} \quad \textbf{(3)}$$

4.3. RESULTS

4.3.1. CANNABINOID-DEPENDENT SIGNALING IN THE PRESENCE OF MHTT.

ST*Hdh*$^{Q7/Q7}$ (Fig. 4-1A-E) and ST*Hdh*$^{Q111/Q111}$ (Fig. 4-1F-J) cells were treated with 10 nM – 10 µM WIN, CP, 2-AG, AEA, THC, CBD, or THC+CBD (1:1) and $G\alpha_{i/o}$- (ERK1/2), arrestin2, $G\alpha_s$- (CREB), $G\alpha_q$- (PLCβ3), and Gβγ-dependent (Akt) signaling were measured. The coupling of each of these signaling pathways to CB_1 and their respective G proteins or arrestin2 has been tested previously (Laprairie *et al*., 2014a). The agonist effects of all cannabinoids tested were CB_1-dependent, except for CBD (see below).

For pERK1/2 ($G\alpha_{i/o}$), the E_{max} observed for all cannabinoids was reduced by approximately 50% in ST*Hdh*$^{Q111/Q111}$ cells compared to ST*Hdh*$^{Q7/Q7}$ cells, with no change in pEC_{50} observed between ST*Hdh*$^{Q7/Q7}$ and ST*Hdh*$^{Q111/Q111}$ cells (Table 4-1; Fig. 4-1A,F). This is consistent with our earlier finding that the E_{max} for pERK relative to total ERK (*i.e.* raw data without reference ligand) following arachidonoyl-2'-chloroethylamide (ACEA) treatment is 50% lower in ST*Hdh*$^{Q111/Q111}$ cells expressing mHtt compared to ST*Hdh*$^{Q7/Q7}$ cells (Laprairie *et al*., 2013). The pERK E_{max} values were greater in WIN- and AEA-treated STHdhQ$^{7/Q7}$ cells compared to 2-AG-, CP-, THC-treated ST*Hdh*$^{Q7/Q7}$ cells; CBD and THC+CBD displayed no agonist activity in ST*Hdh*$^{Q7/Q7}$ cells (Table 4-1; Fig. 4-1A). In contrast, the pERK E_{max} values were not different in 2-AG-, AEA-, WIN-, and CP-treated ST*Hdh*$^{Q111/Q111}$ cells the pERK E_{max} was lower in THC- and THC+CBD-treated ST*Hdh*$^{Q111/Q111}$ cells compared to WIN; CBD did not elicit an

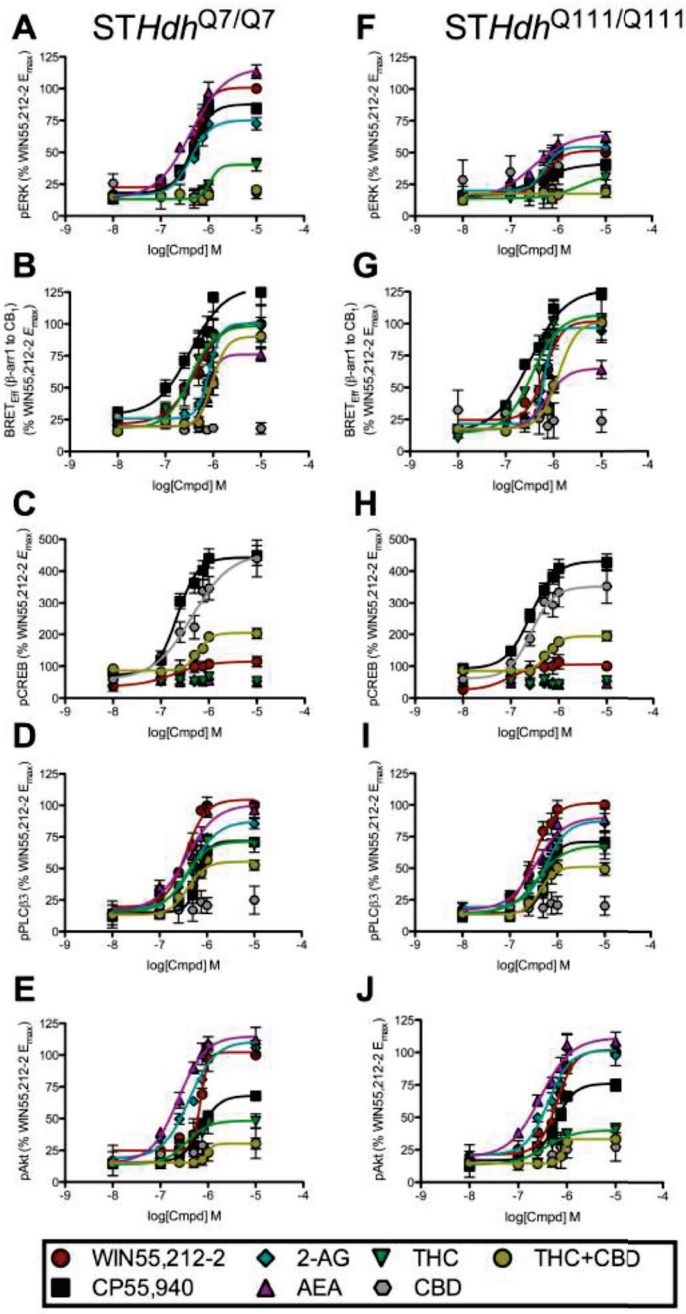

Figure 4-1. Functional selectivity of cannabinoids in wild-type and mHtt-expressing cells. ST*Hdh*$^{Q7/Q7}$ **(A-E)** and ST*Hdh*$^{Q111/Q111}$ **(F-J)** cells were treated with 10 – 10,000 nM WIN, CP, 2-AG, AEA, THC, CBD, or THC+CBD (1:1) and ERK1/2 phosphorylation (10 min) **(A,F)**, arrestin2 recruitment (30 min) **(B,G)**, CREB phosphorylation (30 min) **(C,H)**, PLCβ3 phosphorylation (10 min) **(D,I)**, or Akt phosphorylation (10 min) **(E,J)** were measured and expressed relative to WIN E_{max} in ST*Hdh*$^{Q7/Q7}$ cells. ERK1/2, CREB, PLCβ3, and Akt phosphorylation were measured *via* In-cell western™. Arrestin2 recruitment was measured *via* BRET^2. CRCs were fit to the Black-Leff global non-linear regression using the operational model. $N = 4$.

Table 4-1. pEC_{50} and E_{max} of cannabinoid ligands at CB_1 in ST*Hdh*$^{Q7/Q7}$ and ST*Hdh*$^{Q111/Q111}$ cells.

		ERK response (Gαi/o)				BRET response (arrestin2)				CREB response (Gαs)				PLCβ3 response (Gαq)				Akt response (Gβγ)			
		pEC_{50}		E_{max} (%)		pEC_{50}		E_{max} (%)		pEC_{50}		E_{max} (%)		pEC_{50}		E_{max} (%)		pEC_{50}		E_{max} (%)	
WIN	ST*Hdh*$^{Q7/Q7}$	6.3	± 0.4	101	± 4.0	6.2	± 0.5	102	± 3.6	6.7	± 0.2	115	± 10	6.5	± 0.8	105	± 5.9	6.2	± 0.8	102	± 6.4
	ST*Hdh*$^{Q111/Q111}$	6.3	± 0.9	51.5	± 4.1*	6.1	± 0.3	102	± 4.3	7.0	± 0.3	105	± 6.1	6.5	± 0.7	102	± 5.3	6.2	± 0.4	102	± 5.6
CP	ST*Hdh*$^{Q7/Q7}$	6.3	± 0.6	88.0	± 4.7†	7.4	± 0.2†	128	± 4.0†	6.6	± 0.5	443	± 3.6†	6.2	± 0.4	71.8	± 2.9†	6.2	± 0.5	68.1	± 2.7†
	ST*Hdh*$^{Q111/Q111}$	6.4	± 0.5	41.4	± 4.7*	6.9	± 0.1†	126	± 5.1†	6.6	± 0.7	432	± 5.1†	6.2	± 0.4	70.8	± 4.1†	6.2	± 0.7	76.0	± 4.2†
2-AG	ST*Hdh*$^{Q7/Q7}$	6.4	± 0.6	75.2	± 3.6†	6.1	± 0.7	101	± 2.7	N.C.		N.C.		6.3	± 0.6	87.4	± 4.8	6.4	± 0.8	111	± 5.7
	ST*Hdh*$^{Q111/Q111}$	6.3	± 0.6	54.5	± 3.6*	6.2	± 0.3	96.7	± 3.9	N.C.		N.C.		6.2	± 0.6	87.4	± 3.6	6.4	± 0.7	102	± 4.5
AEA	ST*Hdh*$^{Q7/Q7}$	6.4	± 0.8	117	± 5.9†	6.1	± 0.4	76.1	± 2.0†	N.C.		N.C.		6.4	± 0.9	101	± 5.1	6.6	± 0.9	115	± 5.2
	ST*Hdh*$^{Q111/Q111}$	6.5	± 1.7	64.5	± 5.9*†	6.1	± 0.7	65.0	± 4.6†	N.C.		N.C.		6.4	± 0.8	90.2	± 4.8	6.5	± 0.4	111	± 2.8
THC	ST*Hdh*$^{Q7/Q7}$	6.0	± 1.0	40.3	± 2.4†	6.4	± 0.5	98.8	± 3.8	N.C.		N.C.		6.5	± 1.4	71.4	± 6.2†	6.5	± 1.0	48.3	± 6.7†
	ST*Hdh*$^{Q111/Q111}$	5.5	± 1.5	33.8	± 4.7*†	6.4	± 0.4	107	± 9.8	N.C.		N.C.		6.4	± 1.5	67.9	± 5.2†	6.5	± 1.5	40.1	± 5.2†
CBD	ST*Hdh*$^{Q7/Q7}$	N.C.		N.C.		N.C.		N.C.		6.2	± 0.6	445	± 13.1†	N.C.		N.C.		N.C.		N.C.	
	ST*Hdh*$^{Q111/Q111}$	N.C.		N.C.		N.C.		N.C.		6.4	± 0.8	348	± 24.1†	N.C.		N.C.		N.C.		N.C.	
THC + CBD	ST*Hdh*$^{Q7/Q7}$	N.C.		N.C.		6.0	± 0.5	90.2	± 3.0	6.2	± 0.9	204	± 4.4†	6.4	± 0.7	55.4	± 3.3†	6.0	± 0.5	30.3	± 3.2†
	ST*Hdh*$^{Q111/Q111}$	5.0	± 1.1†	17.6	± 2.3†	5.9	± 0.5	102	± 3.4	6.2	± 1.1	194	± 2.9†	6.4	± 1.1	51.1	± 2.8†	6.1	± 0.6	33.2	± 2.7†

Determined using non-linear regression analysis (4 parameters) in GraphPad v. 5.0. E_{max} (%) is the maximal agonist effect relative to E_{max} for WIN in ST*Hdh*$^{Q7/Q7}$ cells for each measurement. Data are expressed as mean ± S.E.M. N.C., not converged.

*$P < 0.01$ compared to ST*Hdh*$^{Q7/Q7}$ within ligand and measurement. †$P < 0.01$ compared to WIN within cell type and measurement, as determined using two-way ANOVA followed by Bonferroni's *post-hoc* test ($n = 4$).

agonist response (Table 4-1; Fig. 4-1F). THC+CBD-treated ST*Hdh*$^{Q111/Q111}$ cells also displayed a lower pEC_{50} in the pERK assay (Table 4-1; Fig. 4-1F).

CB_1 is known to interact with arrestin2, which mediates receptor internalization, recycling, and degradation (Sim-Selley and Martin, 2002; Laprairie *et al*., 2014a). Unlike pERK, no differences in E_{max} and pEC_{50} were observed for arrestin2 assays. CP displayed higher pEC_{50} and E_{max} values than WIN, while no differences in pEC_{50} and E_{max} were observed between WIN, 2-AG and THC, and AEA displayed lower E_{max} values for arrestin2 recruitment in both cell lines (Table 4-1; Fig. 4-1B,G). CBD was not an agonist of arrestin2 recruitment. In the THC+CBD-treated cells, the E_{max} and pEC_{50} of $BRET_{Eff}$ were both reduced compared to THC-treated cells (Table 4-1). These data are consistent CBD acting as a negative allosteric modulator of THC-dependent effects at CB_1 (see ch. 5).

The observed E_{max} and pEC_{50} for pCREB ($G\alpha_S$) was not different in ST*Hdh*$^{Q7/Q7}$ cells treated with WIN, CP, CBD, or THC+CBD, relative to ST*Hdh*$^{Q111/Q111}$ cells (Table 4-1; Fig. 4-1C,H). AEA and 2-AG did not evoke a pCREB response. CP, CBD, and THC+CBD treatment resulted in higher E_{max} values for pCREB than WIN treatment in both cell lines. pCREB pEC_{50} and E_{max} values were higher in CP- and CBD-treated cells compared to THC+CBD-treated cells (Table 4-1; Fig. 4-1C,H). Because CB_1-dependent $G\alpha_S$ signaling is uncommon, this was examined further (see below).

CB_1 can also couple to $G\alpha_q$ to modulate Ca^{2+}- and PLCβ3-dependent signaling (Lauckner *et al*., 2005). No differences were observed for PLCβ3 phosphorylation between ST*Hdh*$^{Q7/Q7}$ and ST*Hdh*$^{Q111/Q111}$ cells (Table 4-1; Fig. 4-1D,I). pPLCβ3 E_{max} values were greater in WIN-, 2-AG-, and AEA-treated cells compared to CP- and THC-treated cells, with no change in pEC_{50} (Table 4-1; Fig. 4-1D,I). CBD was not an agonist of PLCβ3 phosphorylation.

In the case of pAkt ($G\beta\gamma$), no differences were observed between ST*Hdh*$^{Q7/Q7}$ and ST*Hdh*$^{Q111/Q111}$ cells (Table 4-1; Fig. 4-1E,J). pAkt E_{max} values were greater in WIN-, 2-AG-, and AEA-treated cells compared to CP-treated cells, which were in turn greater compared to THC-

treated cells (Table 4-1; Fig. 4-1E,J). pAkt pEC_{50} values did not differ between agonists. CBD was not an agonist of Akt phosphorylation.

4.3.2. Operational model analysis of cannabinoid transduction coefficients (logR) and relative activity (ΔlogR) in the presence of mHtt.

The operational model global non-linear regression (eq. 1) was used to analyze concentration-response data for cannabinoid signaling bias in ST*Hdh*$^{Q7/Q7}$ and ST*Hdh*$^{Q111/Q111}$ cells. CBD only displayed agonist activity for pCREB and these data were therefore omitted from global non-linear regression analyses of pERK, arrestin2, pPLCβ3, and pAkt assays. The transduction coefficient [logR (τ/ K_A)] for the ERK response was lower in THC- and THC+CBD-treated cells compared to WIN-treated cells, and was lower in THC- and THC+CBD-treated ST*Hdh*$^{Q111/Q111}$ cells compared to ST*Hdh*$^{Q7/Q7}$ cells (Table 4-2). logR for arrestin2 was also lower in THC- (only ST*Hdh*$^{Q111/Q111}$) and THC+CBD-treated cells compared to WIN-treated cells, was lower in THC- and THC+CBD-treated ST*Hdh*$^{Q111/Q111}$ cells compared to ST*Hdh*$^{Q7/Q7}$ cells, and was higher in THC- and THC+CBD-treated cells compared to the ERK response (Table 4-2). logR for the CREB response was higher in CP-treated cells, and lower in THC+CBD-treated cells, compared to WIN, was lower in WIN-treated ST*Hdh*$^{Q111/Q111}$ cells compared to ST*Hdh*$^{Q7/Q7}$ cells, and was lower in WIN-treated cells compared to the ERK response (Table 4-2). logR for the PLCβ3 response was lower in CP- (only ST*Hdh*$^{Q7/Q7}$), AEA-, THC-, and THC+CBD-treated cells, compared to WIN, was lower in CP-, AEA-, and THC-treated ST*Hdh*$^{Q111/Q111}$ cells compared to ST*Hdh*$^{Q7/Q7}$ cells, and was lower in AEA- and THC-treated cells compared to the ERK response (Table 4-2). Finally, logR for the Akt response was lower in CP-, THC-, and THC+CBD-treated cells, was lower in THC- and THC+CBD-treated ST*Hdh*$^{Q111/Q111}$ cells compared to ST*Hdh*$^{Q7/Q7}$ cells, and was lower in THC-treated ST*Hdh*$^{Q7/Q7}$ cells compared to the ERK response (Table 4-2).

Relative activity (ΔlogR) was calculated using WIN as the reference ligand (eq. 2). WIN was chosen as a reference ligand, rather than the endocannabinoids 2-AG and AEA (Kenakin and Christopoulos, 2013), because it displayed activity in all assays and we wanted to quantify the

Table 4-2. Transduction coefficients and relative activity of cannabinoid ligands at CB_1 in ST*Hdh*$^{Q7/Q7}$ and ST*Hdh*$^{Q111/Q111}$ cells.

		ERK response (G*α*i/o)				BRET response (arrestin2)			
		logR (τ/K_A)		ΔlogR (τ/K_A)[a]		logR (τ/K_A)		ΔlogR (τ/K_A)[a]	
WIN	ST*Hdh*$^{Q7/Q7}$	6.35	(6.33-6.37)	Reference ligand		6.41	(6.36-6.46)	Reference ligand	
	ST*Hdh*$^{Q111/Q111}$	6.33	(6.28-6.38)	Reference ligand		6.41	(6.38-6.44)	Reference ligand	
CP	ST*Hdh*$^{Q7/Q7}$	6.30	(6.26-6.34)	-0.04	(-0.09-0.01)	6.46	(6.41-6.52)	0.05	(-0.03-0.13)
	ST*Hdh*$^{Q111/Q111}$	6.22	(6.17-6.27)	-0.11	(-0.22-0.02)	6.47	(6.42-6.49)	0.06	(-0.01-0.11)
2-AG	ST*Hdh*$^{Q7/Q7}$	6.28	(6.20-6.36)	-0.07	(-0.14-0.00)	6.15	(5.91-6.37)	-0.23	(-0.24- -0.22)*†
	ST*Hdh*$^{Q111/Q111}$	6.28	(6.21-6.35)	-0.05	(-0.11-0.01)	6.27	(6.36-6.38)	-0.13	(-0.23- -0.03)*
AEA	ST*Hdh*$^{Q7/Q7}$	6.35	(6.34-6.36)	0.00	(-0.01-0.01)	6.09	(5.82-6.37)	-0.31	(-0.33- -0.29)*†
	ST*Hdh*$^{Q111/Q111}$	6.42	(6.36-6.48)	0.09	(-0.02-0.20)	6.22	(6.07-6.37)	-0.18	(-0.26- -0.10)*†
THC	ST*Hdh*$^{Q7/Q7}$	4.48	(4.43-4.54)*	-1.83	(-2.97- -0.69)*	6.41	(6.40-6.42)†	0.00	(-0.01-0.01)†
	ST*Hdh*$^{Q111/Q111}$	3.26	(3.22-3.30)*^	-3.01	(-4.43- -1.59)*	4.98	(4.94-5.02)*^†	-1.43	(-1.47- -1.39)*^†
CBD	ST*Hdh*$^{Q7/Q7}$		N.C.		N.C.		N.C.		N.C.
	ST*Hdh*$^{Q111/Q111}$		N.C.		N.C.		N.C.		N.C.
THC + CBD	ST*Hdh*$^{Q7/Q7}$	2.06	(1.91-2.21)*	-4.29	(-5.95- -2.63)*	0.83	(-1.91-1.95)*†	-5.58	(-5.60- -5.56)*
	ST*Hdh*$^{Q111/Q111}$	0.35	(-2.01-3.69)*^	-1.40	(-2.77- -0.33)*	4.83	(4.77-4.89)*^†	-1.58	(-1.64- -1.52)*^†

Determined using the operational model global non-linear regression analysis (Eq. 1, 2) in GraphPad v. 5.0. Data are expressed as mean with 95% CI. N.C., not converged. [a]ΔlogR (τ/K_A) calculated as logR (τ/K_A) test ligand - logR (τ/K_A) reference ligand within cell type, where **WIN** is the reference ligand and ΔlogR (τ/K_A) 'WIN' = 0.

*$P < 0.05$ compared to WIN within cell type and measurement, ^$P < 0.05$ compared to ST*Hdh*$^{Q7/Q7}$ within ligand and measurement, †$P < 0.05$ compared to ERK (G*α*i/o) within cell type, as determined using non-overlapping CIs ($n = 4$).

Table 4-2 Continued. Transduction coefficients and relative activity of cannabinoid ligands at CB_1 in ST*Hdh*$^{Q7/Q7}$ and ST*Hdh*$^{Q111/Q111}$ cells.

		CREB response (G*α*s)				PLCβ3 response (G*α*q)			
		logR (τ/K_A)		ΔlogR (τ/K_A)[a]		logR (τ/K_A)		ΔlogR (τ/K_A)[a]	
WIN	ST*Hdh*$^{Q7/Q7}$	3.43	(3.32-3.54)†	Reference ligand		6.54	(6.32-6.72)	Reference ligand	
	ST*Hdh*$^{Q111/Q111}$	2.22	(2.20-2.24)^†	Reference ligand		6.51	(6.34-6.66)	Reference ligand	
CP	ST*Hdh*$^{Q7/Q7}$	6.47	(6.46-6.48)*	3.01	(2.91-3.11)*†	5.77	(5. 67-5.87)*†	-0.77	(-0.92- -0.62)*†
	ST*Hdh*$^{Q111/Q111}$	5.07	(5.06-5.08)*	2.85	(2.55-3.04)*†	6.32	(4.35-8.29)^	-0.21	(-0.48-0.06)^
2-AG	ST*Hdh*$^{Q7/Q7}$		N.C.		N.C.	6.01	(4.66-7.36)	-0.53	(-0.88- -0.18)*†
	ST*Hdh*$^{Q111/Q111}$		N.C.		N.C.	5.76	(4.99-6.53)	-0.71	(-1.46-0.04)
AEA	ST*Hdh*$^{Q7/Q7}$		N.C.		N.C.	6.31	(6.08-6.54)	-0.23	(-0.47-0.01)
	ST*Hdh*$^{Q111/Q111}$		N.C.		N.C.	5.41	(4.52-5.94)*^†	-1.13	(-1.99- -0.27)*†
THC	ST*Hdh*$^{Q7/Q7}$		N.C.		N.C.	5.45	(5.23-5.67)*†	-1.09	(-1.31- -0.87)*
	ST*Hdh*$^{Q111/Q111}$		N.C.		N.C.	4.33	(3.80-4.86)*^†	-2.18	(-2.69- -1.67)*^
CBD	ST*Hdh*$^{Q7/Q7}$	3.34	(3.29-3.39)	-0.09	(-0.22-0.04)		N.C.		N.C.
	ST*Hdh*$^{Q111/Q111}$	2.27	(2.24-2.30)	0.03	(-0.01-0.07)		N.C.		N.C.
THC + CBD	ST*Hdh*$^{Q7/Q7}$	0.26	(-0.40-1.92)*	-3.19	(-3.21- -3.17)*	0.57	(-1.43-1.91)*	-5.97	(-6.20- -5.74)*
	ST*Hdh*$^{Q111/Q111}$	3.28	(3.27-3.30)*†	1.06	(1.04-1.08)*^†	4.25	(3.55-4.95)*^	-2.27	(-2.95- -1.59)*^

Determined using the operational model global non-linear regression analysis (Eq. 1, 2) in GraphPad v. 5.0. Data are expressed as mean with 95% CI. N.C., not converged. [a]ΔlogR (τ/K_A) calculated as logR (τ/K_A) test ligand - logR (τ/K_A) reference ligand within cell type, where **WIN** is the reference ligand and ΔlogR (τ/K_A) 'WIN' = 0.

*$P < 0.05$ compared to WIN within cell type and measurement, ^$P < 0.05$ compared to ST*Hdh*$^{Q7/Q7}$ within ligand and measurement, †$P <$ 0.05 compared to ERK (G*α*i/o) within cell type, as determined using non-overlapping CIs ($n = 4$).

Table 4-2 Continued. Transduction coefficients and relative activity of cannabinoid ligands at CB_1 in ST*Hdh*$^{Q7/Q7}$ and ST*Hdh*$^{Q111/Q111}$ cells.

		Akt response (Gβγ)			
		logR (τ/K_A)		ΔlogR (τ/K_A)[a]	
WIN	ST*Hdh*$^{Q7/Q7}$	6.18	(5.98-6.40)	Reference ligand	
	ST*Hdh*$^{Q111/Q111}$	6.21	(6.13-6.29)	Reference ligand	
CP	ST*Hdh*$^{Q7/Q7}$	5.94	(5.92-5.96)*†	-0.24	(-0.26- -0.22)*†
	ST*Hdh*$^{Q111/Q111}$	5.84	(5.31-6.37)	-0.37	(-0.91-0.17)
2-AG	ST*Hdh*$^{Q7/Q7}$	6.22	(6.19-6.25)	0.02	(-0.01-0.05)
	ST*Hdh*$^{Q111/Q111}$	6.14	(5.96-6.32)	-0.07	(-0.25-0.11)
AEA	ST*Hdh*$^{Q7/Q7}$	6.32	(6.27-6.37)	0.14	(-0.03-0.25)*
	ST*Hdh*$^{Q111/Q111}$	6.25	(5.73-6.77)	0.04	(-0.47-0.55)
THC	ST*Hdh*$^{Q7/Q7}$	5.35	(5.32-5.38)*†	-0.83	(-0.86- -0.80)*†
	ST*Hdh*$^{Q111/Q111}$	4.00	(3.87-4.13)*^	-2.21	(-2.32- -2.10)*^†
CBD	ST*Hdh*$^{Q7/Q7}$	N.C.		N.C.	
	ST*Hdh*$^{Q111/Q111}$	N.C.		N.C.	
THC + CBD	ST*Hdh*$^{Q7/Q7}$	0.31	(-1.39-2.01)*†	-5.87	(-5.97- -5.77)*
	ST*Hdh*$^{Q111/Q111}$	3.59	(3.50-3.68)*^	-2.62	(-2.72- -2.52)*^

Determined using the operational model global non-linear regression analysis (Eq. 1, 2) in GraphPad v. 5.0. Data are expressed as mean with 95% CI. N.C., not converged. [a]ΔlogR (τ/K_A) calculated as logR (τ/K_A) test ligand - logR (τ/K_A) reference ligand within cell type, where **WIN** is the reference ligand and ΔlogR (τ/K_A) 'WIN' = 0.

*$P < 0.05$ compared to WIN within cell type and measurement, ^$P < 0.05$ compared to ST*Hdh*$^{Q7/Q7}$ within ligand and measurement, †$P < 0.05$ compared to ERK (Gαi/o) within cell type, as determined using non-overlapping CIs ($n = 4$).

relative activity and bias of 2-AG and AEA in ST*Hdh*$^{Q7/Q7}$ and ST*Hdh*$^{Q111/Q111}$ cells. The ΔlogR for ERK response was lower in THC- and THC+CBD-treated cells compared to WIN (ΔlogR = 0) (Table 4-2). The ΔlogR for arrestin2 was lower in 2-AG, AEA, THC- and THC+CBD-treated cells compared to WIN, and compared to the ERK response (Table 4-2). The ΔlogR for arrestin2 was lower in THC-treated ST*Hdh*$^{Q111/Q111}$ cells, and higher in THC+CBD-treated ST*Hdh*$^{Q111/Q111}$ cells, compared to ST*Hdh*$^{Q7/Q7}$ cells (Table 4-2). The ΔlogR for the CREB response was higher in CP- (both cell types) and THC+CBD- treated ST*Hdh*$^{Q111/Q111}$ cells, and lower in THC+CBD-treated ST*Hdh*$^{Q7/Q7}$ cells, compared to WIN (Table 4-2). The ΔlogR for the CREB response was higher in CP- (both cell types) and THC+CBD-treated ST*Hdh*$^{Q111/Q111}$ cells compared to the ERK response, and was greater in THC+CBD-treated ST*Hdh*$^{Q111/Q111}$ cells compared to ST*Hdh*$^{Q7/Q7}$ cells (Table 4-2). The ΔlogR for the PLCβ3 response was lower in CP- (only ST*Hdh*$^{Q7/Q7}$), 2-AG- (only ST*Hdh*$^{Q7/Q7}$), AEA- (only ST*Hdh*$^{Q111/Q111}$), THC- and THC+CBD-treated cells compared to WIN, and compared to the ERK response for CP, 2-AG, and AEA treatments (Table 4-2). The ΔlogR for the PLCβ3 response was lower in THC- and THC+CBD-treated ST*Hdh*$^{Q111/Q111}$ cells compared to ST*Hdh*$^{Q7/Q7}$ cells (Table 4-2). Finally, the ΔlogR for the Akt response was lower in CP- (only ST*Hdh*$^{Q7/Q7}$), AEA- (only ST*Hdh*$^{Q7/Q7}$), THC-, and THC+CBD-treated cells compared to WIN, and compared to the ERK response for CP and THC (Table 4-2). ΔlogR values for the Akt response were lower and higher in THC- and THC+CBD-treated ST*Hdh*$^{Q111/Q111}$ cells, respectively, compared to ST*Hdh*$^{Q7/Q7}$ cells (Table 4-2).

Summarizing the data in table 4-2 we observed that the rank order of τ/K_A and relative activity (ΔlogR) for pERK was AEA > WIN > CP (ST*Hdh*$^{Q7/Q7}$) > 2-AG > CP (ST*Hdh*$^{Q111/Q111}$) > THC ≥ THC+CBD. For arrestin2 this order was CP > THC ≥ WIN > 2-AG = AEA > THC (ST*Hdh*$^{Q111/Q111}$) > THC+CBD. For pCREB this order was CP > WIN (ST*Hdh*$^{Q7/Q7}$) > CBD (ST*Hdh*$^{Q7/Q7}$) > THC+CBD (ST*Hdh*$^{Q111/Q111}$) > CBD (ST*Hdh*$^{Q111/Q111}$) > WIN (ST*Hdh*$^{Q111/Q111}$) ≥ THC+CBD (ST*Hdh*$^{Q7/Q7}$). For pPLCβ3 the order was WIN > CP (ST*Hdh*$^{Q111/Q111}$) > AEA (ST*Hdh*$^{Q7/Q7}$) > 2-AG (ST*Hdh*$^{Q7/Q7}$) > CP (ST*Hdh*$^{Q7/Q7}$) > 2-AG (ST*Hdh*$^{Q7/Q7}$) > THC

(ST*Hdh*$^{Q7/Q7}$) > AEA (ST*Hdh*$^{Q7/Q7}$) > THC (ST*Hdh*$^{Q7/Q7}$) > THC+CBD. And for pAkt the order was AEA ≥ 2-AG = WIN > CP > THC > THC+CBD.

4.3.3. Operational model analysis of cannabinoid-dependent system bias (ΔΔlogR) in the presence of mHtt.

Bias values (ΔΔlogR) were calculated from the relative activity data (ΔlogR) in order to characterize functional selectivity in ST*Hdh*$^{Q7/Q7}$ and ST*Hdh*$^{Q111/Q111}$ cells (eq. 3) (Fig. 4-2A-D). Because CB_1 is classically considered a $G\alpha_{i/o}$-coupled receptor (Kondo *et al.,* 1998; Lauckner *et al*., 2005), all comparisons were made using $G\alpha_{i/o}$-dependent ERK1/2 signaling (pERK) as $\Delta\log R_1$. Based on these data, CP evoked $G\alpha_S$- and arrestin2-biased signaling compared to $G\alpha_{i/o}$, and $G\alpha_{i/o}$-biased signaling compared to $G\alpha_q$ or $G\beta\gamma$ in both cell types tested here (*i.e.* $G\alpha_S$ > arrestin2 > $G\alpha_{i/o}$ > $G\alpha_q$ > $G\beta\gamma$) (Fig. 4-2A-D). 2-AG evoked $G\alpha_{i/o}$-biased signaling compared to arrestin2 (in ST*Hdh*$^{Q7/Q7}$ cells) and $G\alpha_q$ (more so in ST*Hdh*$^{Q111/Q111}$ cells), and $G\beta\gamma$-biased signaling compared to $G\alpha_{i/o}$ (in ST*Hdh*$^{Q7/Q7}$ cells) (*i.e.* $G\beta\gamma$ > $G\alpha_{i/o}$ >-arrestin2 > $G\alpha_q$) (Fig. 4-2A-D). Like 2-AG, AEA evoked $G\alpha_{i/o}$-biased signaling compared to arrestin2 and $G\alpha_q$ (more so in ST*Hdh*$^{Q111/Q111}$ cells), and $G\beta\gamma$-biased signaling compared to $G\alpha_{i/o}$ (in ST*Hdh*$^{Q7/Q7}$ cells) (*i.e.* $G\beta\gamma$ > $G\alpha_{i/o}$ > arrestin2 > $G\alpha_q$) (Fig. 4-2A-D). THC evoked arrestin2-, $G\alpha_q$-, and $G\beta\gamma$-biased signaling compared to $G\alpha_{i/o}$, in both cell types (*i.e.* arrestin2 > $G\alpha_q$ = $G\beta\gamma$ > $G\alpha_{i/o}$) (Fig. 4-2A-D). CBD treatment only produced a significant activation of $G\alpha_S$-dependent CREB phosphorylation and bias values could not be calculated for this ligand. The combination THC+CBD evoked $G\alpha_S$-biased signaling compared to $G\alpha_{i/o}$ and $G\alpha_{i/o}$-biased signaling compared to arrestin2, $G\alpha_q$, or $G\beta\gamma$ (more so in ST*Hdh*$^{Q7/Q7}$ cells) (*i.e.* $G\alpha_S$ > $G\alpha_{i/o}$ > arrestin2 = $G\alpha_q$ = $G\beta\gamma$) (Fig. 4-2A-D).

Each cannabinoid analyzed here displayed unique functional selectivity for different signaling pathways. Overall, the bias factor of 2-AG and AEA was shifted toward $G\alpha_{i/o}$-dependent ERK phosphorylation, and the bias factor of THC+CBD was shifted away from $G\alpha_{i/o}$-

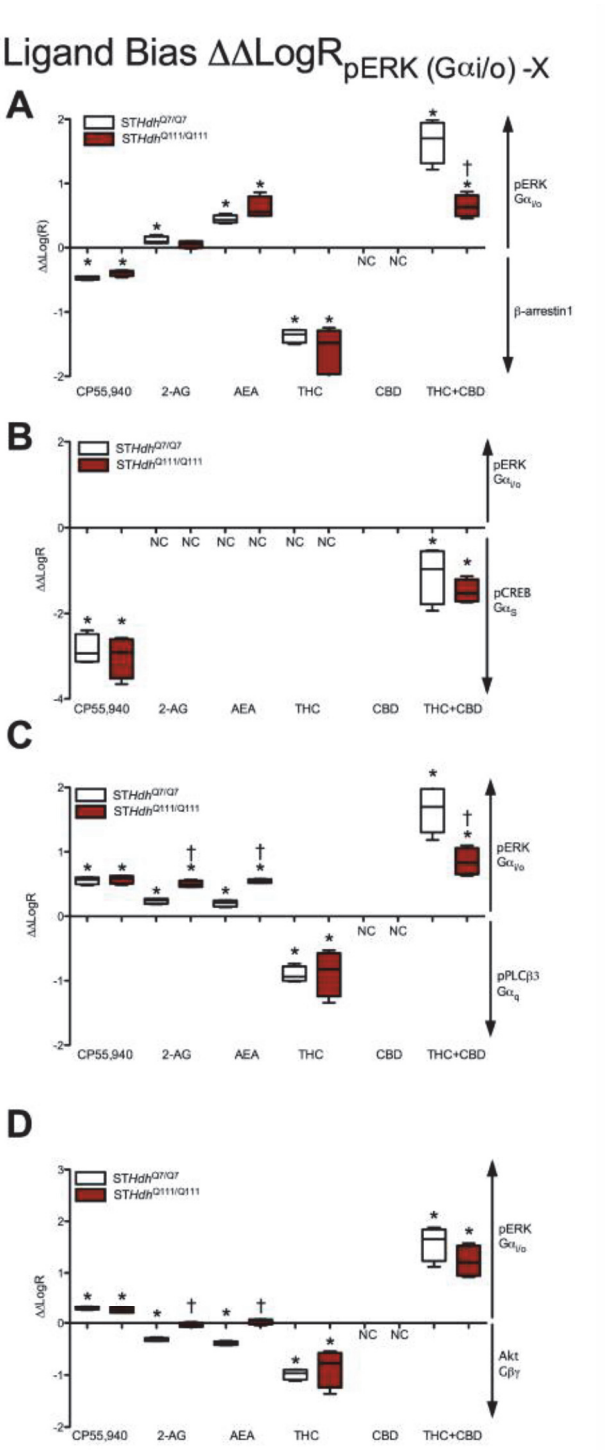

Figure 4-2. Calculated bias factor of cannabinoids in wild-type and mHtt-expressing cells. Ligand bias (ΔΔLogR) was calculated using eq. 2 as the difference between the ERK ($G\alpha_{i/o}$) response and a second response X: **A)** arrestin2 (ß-arrestin1), **B)** $G\alpha_s$, **C)** $G\alpha_q$, or **D)** Gβγ, Data are displayed as the mean with the minimum and maximum (box) and 95% confidence intervals (error bars). **P* < 0.01 compared to 0 (*i.e.* no bias), †*P* < 0.01 compared to ST*Hdh*$^{Q7/Q7}$ cells within ligand. *N* = 4.

dependent ERK phosphorylation, in ST*Hdh*$^{Q111/Q111}$ cells. The reduced pERK E_{max} in mHtt-expressing ST*Hdh*$^{Q111/Q111}$ cells compared to ST*Hdh*$^{Q7/Q7}$ cells (Table 4-1) may result from lower CB_1 levels (50%) (Laprairie *et al.*, 2013). An important advantage of using the operational model to estimate the relative activity and ligand bias is that this model negates the effects of differences in receptor density (Kenakin *et al*., 2011). Therefore, differences in bias between ST*Hdh*$^{Q7/Q7}$ and ST*Hdh*$^{Q111/Q111}$ cells were likely mHtt-dependent and not the result of changes in agonist potency or efficacy.

4.3.4. CANNABINOID-SPECIFIC CHANGES IN CELLULAR FUNCTION AND VIABILITY.

Treatment of ST*Hdh*$^{Q7/Q7}$ cells with WIN, 2-AG, AEA, or THC resulted in a small increase in ATP, whereas treatment with CP, CBD, or THC+CBD resulted in a decrease in ATP (Fig. 4-3A). In ST*Hdh*$^{Q111/Q111}$ cells, basal ATP levels were approximately 50% lower than basal ATP levels in ST*Hdh*$^{Q7/Q7}$ cells. ATP levels increased in ST*Hdh*$^{Q111/Q111}$ cells treated with WIN, 2-AG, AEA, or THC and decreased with CP or CBD (Fig. 4-3E). THC+CBD treatment resulted in higher ATP levels in ST*Hdh*$^{Q111/Q111}$ cells. CP and CBD were the only cannabinoids tested that evoked $G\alpha_S$-biased (CREB) signaling in ST*Hdh* cells. The lower ATP levels observed in cells treated with CP or CBD may have resulted from cAMP production. However, given that cells expressing mHtt are deficient in ATP (Sadri-Vakili *et al.*, 2006; Laprairie *et al*., 2013), cannabinoids that exaggerate this state may exacerbate cellular pathology.

Excessive glutamate release from cortical neurons and GABA release from striatal medium spiny projection neurons are both observed in HD (Benn *et al*., 2007; Botelho *et al*., 2014). Compounds that limit neurotransmitter release may, therefore, be beneficial in HD, whereas compounds that enhance neurotransmitter release may exacerbate HD pathophysiology. GABA release was inhibited by WIN, 2-AG, AEA, CP, and THC in ST*Hdh*$^{Q7/Q7}$ and ST*Hdh*$^{Q111/Q111}$ cells (Fig. 4-3B,F). CBD treatment was associated with enhanced GABA release in ST*Hdh*$^{Q7/Q7}$ and ST*Hdh*$^{Q111/Q111}$ cells and the EC_{50} and E_{max} of this response were reduced in the presence of THC (THC+CBD) (Fig. 4-3B,F). Therefore, CBD treatment may enhance excessive

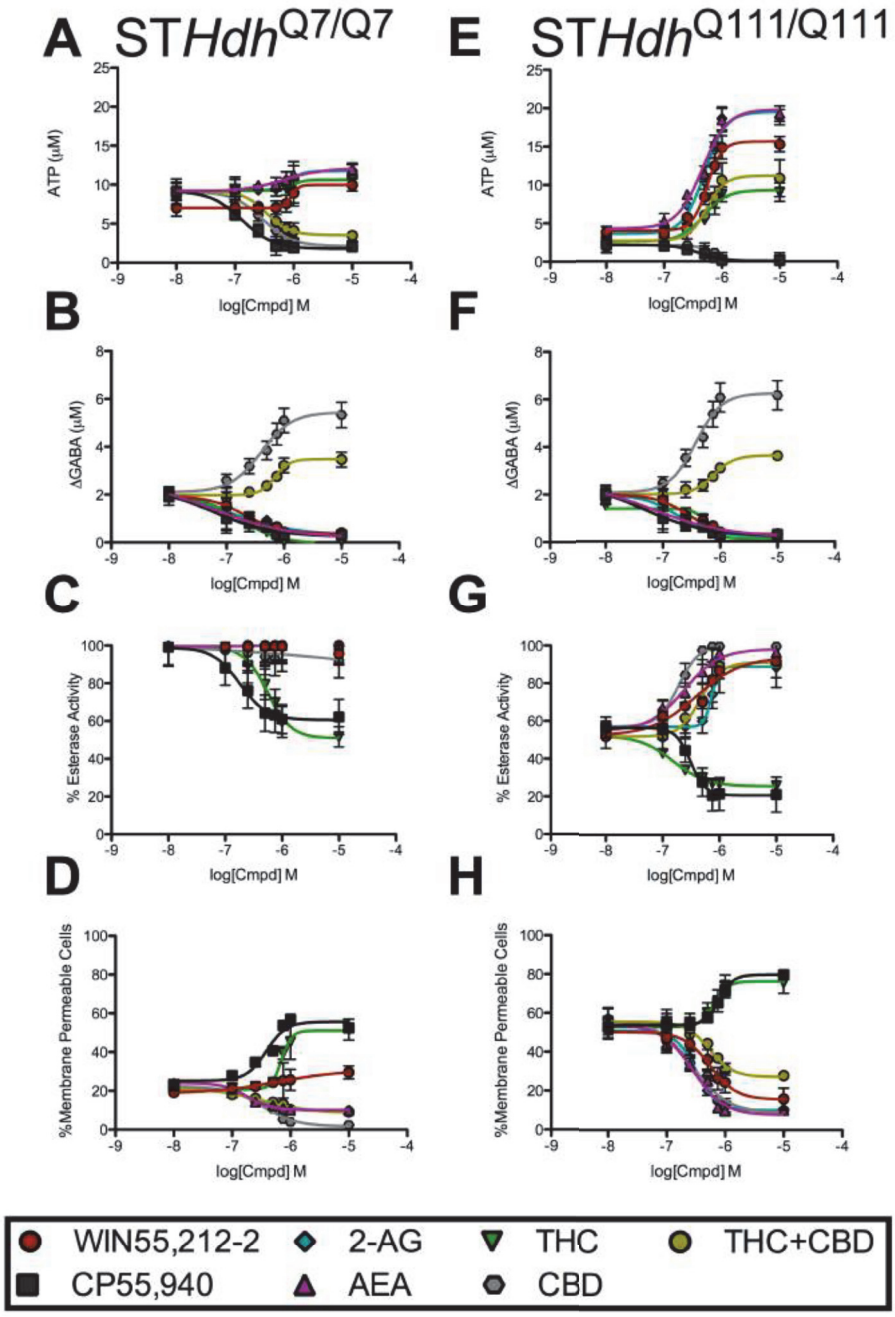

Figure 4-3. Changes in functionality and viability in wild-type and mHtt-expressing cells treated with cannabinoids. ST*Hdh*$^{Q7/Q7}$ **(A-D)** and ST*Hdh*$^{Q111/Q111}$ **(E-H)** cells were treated with 10 – 10,000 nM WIN, CP, 2-AG, AEA, THC, CBD, or THC+CBD (1:1) for 30 min and ATP **(A,E)**, change in GABA release compared to vehicle treatment (ΔGABA) **(B,F)**, % cellular esterase activity compared to vehicle treatment **(C,G)**, and % membrane permeable cells compared to vehicle treatment **(D,H)** were measured. [ATP] was determined using the CellTiter Glo assay (Promega). [GABA] in cell culture media was determined using GABA ELISA assay (Novatein Biosciences). % cellular esterase activity (calcein AM cleavage) and % membrane permeable cells (ethidium homodimer-1 penetration) were determined using the Live/Dead cytotoxicity assay (Invitrogen). CRCs were fit using non-linear regression models. $N = 4$.

neurotransmitter release in HD, whereas other cannabinoids tested here limited neurotransmitter release.

Cell viability was measured by cal-AM fluorescence, which is an indicator of esterase activity and mitochondrial respiration that is positively correlated with viability, and EthD-1 fluorescence, which is an indicator of membrane permeability and cell death and therefore negatively correlated with viability (MacCoubrey *et al*., 1990). Basal cal-AM fluorescence (% esterase activity) was 60% less in ST*Hdh*$^{Q111/Q111}$ cells compared to ST*Hdh*$^{Q7/Q7}$ cells (Fig. 4-3C,G). Cal-AM fluorescence was decreased by 40% in ST*Hdh*$^{Q7/Q7}$ and ST*Hdh*$^{Q111/Q111}$ cells treated with CP or THC and increased by 40% in ST*Hdh*$^{Q111/Q111}$ cells treated with WIN, 2-AG, AEA, or CBD (Fig. 4-3C,G). Basal EthD-1 fluorescence (% membrane permeable cells) was 40% greater in ST*Hdh*$^{Q111/Q111}$ cells compared to ST*Hdh*$^{Q7/Q7}$ cells (Fig. 4-3D,H). EthD-1 fluorescence was increased by 30% in ST*Hdh*$^{Q7/Q7}$ and ST*Hdh*$^{Q111/Q111}$ cells treated with CP or THC (Fig. 4-3D,H). EthD-1 fluorescence was decreased by 20% in AEA- and CBD-treated ST*Hdh*$^{Q7/Q7}$ cells, and by 40% in WIN-, 2-AG-, AEA-, and CBD-treated ST*Hdh*$^{Q111/Q111}$ cells (Fig. 4-3D,H). The effect of CBD predominated over that of THC for both cal-AM and EthD-1 fluorescence in both cell lines. Therefore, in these viability assays, the CP and THC (which both displayed arrestin2 bias) appeared harmful whereas other cannabinoids improved viability in ST*Hdh*$^{Q111/Q111}$ cells.

Functional CB_1 residing at the plasma membrane undergo internalization following ligand binding and arrestin recruitment (Blair *et al*., 2009). Total CB_1 levels were higher in WIN-, 2-AG-, and AEA-treated ST*Hdh*$^{Q7/Q7}$ and ST*Hdh*$^{Q111/Q111}$ cells, compared to vehicle, while total CB_1 levels were lower in CP- and THC-treated ST*Hdh*$^{Q7/Q7}$ and ST*Hdh*$^{Q111/Q111}$ cells (Fig. 4-4A). The fraction of CB_1 at the plasma membrane and total CB_1 was assayed in ST*Hdh*$^{Q7/Q7}$ and ST*Hdh*$^{Q111/Q111}$ cells treated with various cannabinoids for 12 h (Fig. 4-4A,B). The fraction of CB_1 at the plasma membrane was lower in WIN-, 2-AG-, CP-, and THC-treated cells, and higher in CBD-treated cells (Fig. 4-4B). CP and THC – and to a lesser extent WIN and 2-AG – displayed

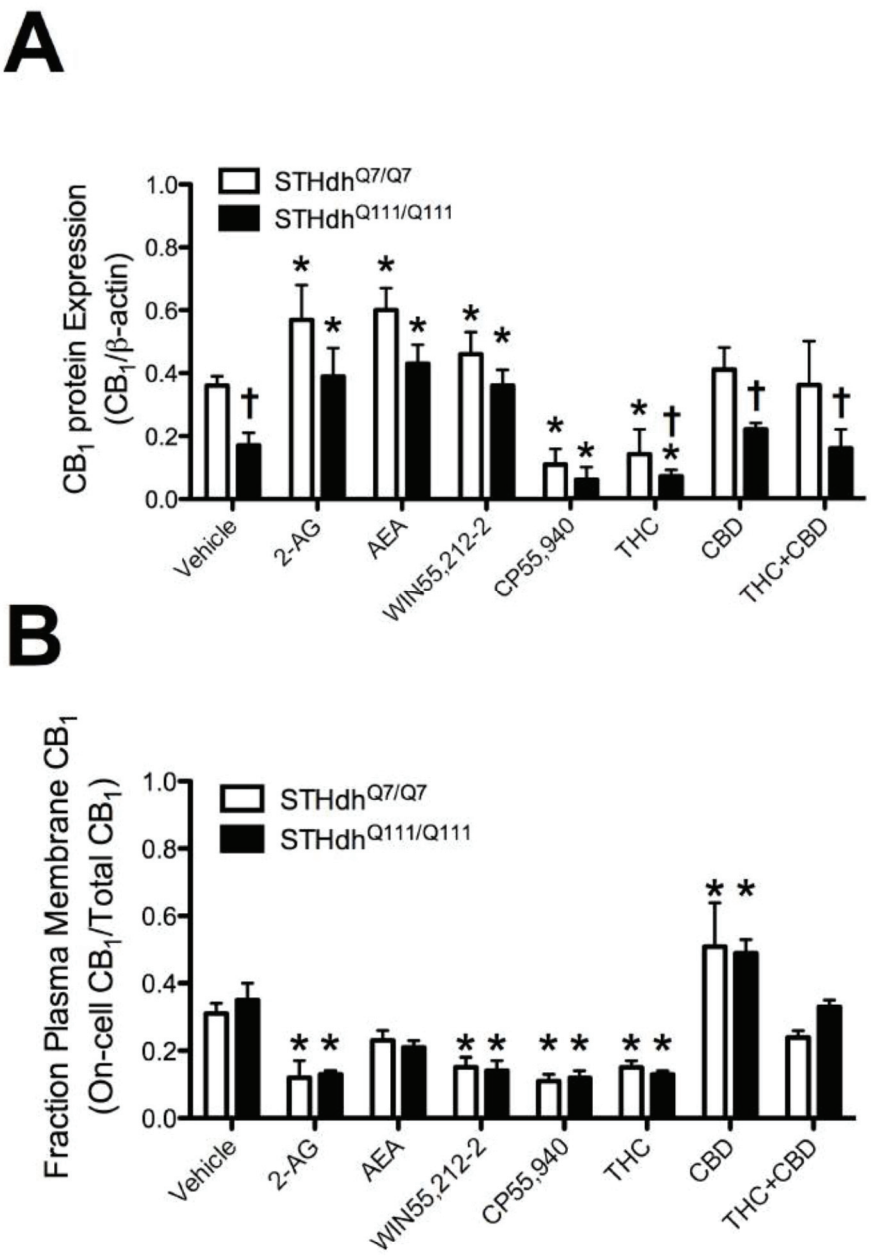

Figure 4-4. Long-term exposure to cannabinoids affected CB_1 localization and levels. ST*Hdh*$^{Q7/Q7}$ and ST*Hdh*$^{Q111/Q111}$ cells were treated with 1.0 μM 2-AG, AEA, WIN, CP, THC, CBD, or THC+CBD (1:1) for 18 h and total CB_1 levels **(A)** and the fraction of CB_1 at the plasma membrane **(B)**. **A)** Total CB_1 levels were determined using In-cell western™ and expressed relative to β-actin levels. $N = 8$. **B)** The fraction of CB_1 at the plasma membrane was determined using On- and In-cell western™. $N = 8$. *$P < 0.01$ compared to vehicle-treated cells within cell type, †$P < 0.01$ compared to ST*Hdh*$^{Q7/Q7}$ cells within treatment group, as determined using two-way ANOVA followed by Bonferroni's *post-hoc* analysis.

greater arrestin2 bias than AEA or CBD. The mechanism of cannabinoid-dependent induction of CB_1 expression has been described previously (Laprairie *et al*., 2013). Here, it is important to note that treatment with cannabinoids that evoked $G\alpha_{i/o}$-and $G\beta\gamma$-biased signaling (2-AG, AEA) was associated with higher CB_1 levels, whereas treatment with CP and THC (arrestin2-biased cannabinoids) was associated with lower CB_1 levels, suggesting that cannabinoids that are functionally selective for arrestin2 may reduce the available pool of CB_1 receptors. The effects of THC and CBD were neutralized by one another (Fig. 4-4A,B).

4.3.5. MECHANISM OF CP- AND CBD-DEPENDENT $G\alpha_S$ SIGNALING.

CBD is known to modulate the activity of many cellular GPCRs, including CB_1, the type 2 cannabinoid receptor (CB_2) (Hayakawa *et al*., 2008), the serotonin $5HT_{1A}$ receptor (Russo *et al*., 2005), GPR55 (Ryberg *et al*., 2007), and the μ- and δ-opioid receptors (Kathmann *et al*., 2006). Here, CBD treatment resulted in CB_1-independent CREB phosphorylation (Fig. 4-5). CREB phosphorylation was highest 30 min after CBD treatment and was sustained for the duration of the experiment (60 min) (Fig. 4-5A). Treatment of ST*Hdh*$^{Q7/Q7}$ cells with the $5HT_{1A}$ agonist 8-OH-DPAT resulted in a dose-dependent increase in CREB phosphorylation that was competitively inhibited by the $5HT_{1A}$ antagonist WAY 100635 and CBD (Fig. 4-5B). Treatment of ST*Hdh*$^{Q7/Q7}$ cells with CBD alone also resulted in a dose-dependent increase in CREB phosphorylation, with less potency and efficacy than the full agonist 8-OH-DPAT (Fig. 4-5C). CBD-dependent CREB phosphorylation was not inhibited by the CB_1 antagonist O-2050, but was inhibited by WAY 100635 (Fig. 4-5C), indicating that CBD activated CREB *via* $5HT_{1A}$. It is not known whether the partial agonism of $5HT_{1A}$ by CBD is functionally antagonistic of serotonergic signaling *in vivo* and whether this would play a role in CBD-based treatments of neurological disorders.

Unexpectedly, we observed a switch in signaling following continued drug exposure for CP. At 10 min CP treatment produced $G\alpha_{i/o}$-dependent ERK phosphorylation that returned to

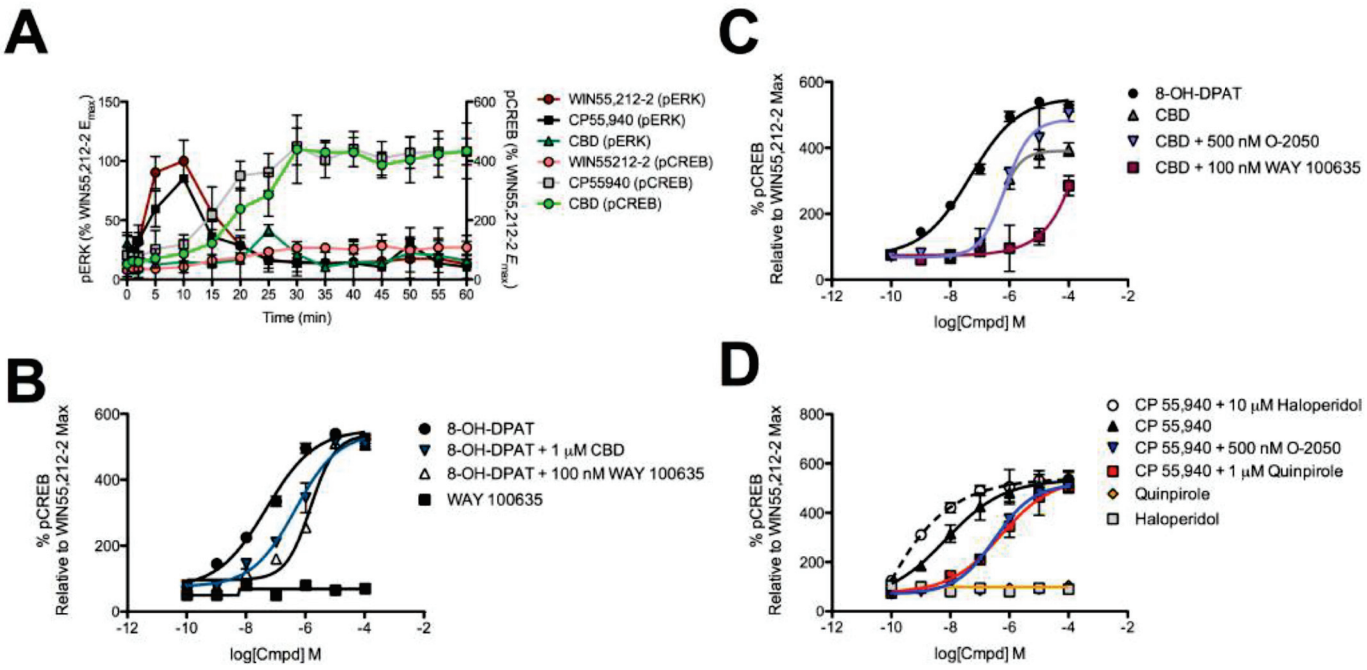

Figure 4-5. CB_1-independent CREB signaling. A) Time course of ERK and CREB signaling. ST*Hdh*$^{Q7/Q7}$ cells were treated with 1 μM WIN55,212-2, CP55940, or CBD for 0 – 60 min, and ERK (left y-axis) or CREB (right y-axis) phosphorylation was measured *via* In-Cell Western. N = 4. **B,C)** $5HT_{1A}$-dependent CREB signaling. ST*Hdh*$^{Q7/Q7}$ cells were treated with 0.1–100,000 nM 8-OH-DPAT, WAY-100,635, or CBD, ± 1 μM CBD, 100 nM WAY-100,635, or 500 nM O-2050 for 30 minutes, and CREB phosphorylation was measured *via* In-Cell Western. N = 4. **D)** D_2-dependent CREB signaling ST*Hdh*$^{Q7/Q7}$ cells were treated with 0.1–100,000 nM CP, quinpirole, or haloperidol, ± 10 μM haloperidol, 1 μM quinpirole, or 500 nM O-2050 for 30 minutes and CREB phosphorylation was measured *via* In-Cell Western. Concentration-response curves were fit using non-linear regression models. N = 4. All data are expressed relative to WIN E_{max} in ST*Hdh*$^{Q7/Q7}$ cells.

basal levels by 25 min; and at 30 min CP treatment produced $G\alpha_s$-dependent CREB phosphorylation (Fig. 4-5A). ST*Hdh* cells endogenously express D_2 (Paoletti *et al.*, 2008) and heterodimerization of CB_1 and D_2 is known to lead to a switch in coupling *from* $G\alpha_{i/o}$ *to* $G\alpha_s$ following treatment with CP (Glass and Felder, 1997; Kearn *et al*., 2005). Therefore, we hypothesized that CP could be functionally selective for CB_1/D_2 heterodimer signaling to explain the switch from $G\alpha_{i/o}$ to $G\alpha_s$. Co-treatment of ST*Hdh*$^{Q7/Q7}$ cells with CP and 1 μM quinpirole (a D_2 agonist) shifted the CRC for CREB phosphorylation right, as did co-treatment with O-2050 (a competitive antagonist of CB_1), while co-treatment with 10 μM haloperidol (a D_2 antagonist) shifted the CRC left (Fig. 4-5D). Quinpirole and haloperidol did not effect CREB phosphorylation alone (Fig. 4-5D). From these data, we suggest that CP selectively enhanced either physical heterodimerization between CB_1/D_2 or functional signaling through these receptors with a subsequent switch from $G\alpha_{i/o}$ *to* $G\alpha_s$ (Kearn *et al*., 2005).

4.4. DISCUSSION

4.4.1. CORRELATIONS BETWEEN FUNCTIONAL SELECTIVITY AND CELLULAR VIABILITY

In this study, we described the biased signaling properties of 6 cannabinoids in the ST*Hdh* cell culture model of striatal medium spiny projection neurons. System bias shifted toward $G\alpha_{i/o}$ for 2-AG and AEA in ST*Hdh*$^{Q111/Q111}$ cells (mHtt-expressing) cells compared to ST*Hdh*$^{Q7/Q7}$ cells. Treatment of ST*Hdh*$^{Q111/Q111}$ cells with cannabinoids that signalled *via* CB_1 and were functionally selective for $G\alpha_{i/o}$ and $G\beta\gamma$ (2-AG, AEA) was associated with the greatest improvement in ATP production, inhibition of GABA release, cellular metabolic activity (esterase activity), and cell death (membrane permeability). In contrast, ligands that preferentially enhanced arrestin2 recruitment (THC and CP) reduced cellular viability in both ST*Hdh*$^{Q7/Q7}$ and ST*Hdh*$^{Q111/Q111}$ cells as determined by the same measures. We have previously observed that derivatives of AEA normalize CB_1 levels in ST*Hdh*$^{Q111/Q111}$ cells *via* $G\alpha_{i/o}$, $G\beta\gamma$, Akt, and NF-κB and that normalization of CB_1 was associated with improved cell function and viability (Laprairie *et al*., 2013, 2014b). Recently, three studies have demonstrated that increasing CB_1 levels in

medium spiny projection neurons in the R6/2 mouse model of HD *via* adenovirus-mediated overexpression normalizes brain-derived neurotrophic factor levels, reduces striatal atrophy and prevents decreases in dendritic spine density and levels of excitatory synaptic markers such as synaptophysin and vesicular glutamate transporter, but does not improve deficits in motor coordination (Chiarlone *et al*., 2014; Naydenov *et al*., 2014; Blázquez *et al*., 2015). In accordance with this, knockdown or knockout of CB_1 in medium spiny projection neurons of R6/2, N171-82Q, or $Hdh^{Q150/Q150}$ HD mice further reduces the pool of CB_1 and exacerbates deficits in motor control, enhances striatal atrophy, reduces survival (Blázquez *et al*., 2011; Mievis *et al.*, 2011; Horne *et al*., 2013). Further, individuals with HD and a variant of the CB_1 gene (*CNR1* rs4707436), that is associated with lower levels of CB_1, begin displaying motor-related symptoms of HD earlier than individuals with HD and normal *CNR1* (Kloster *et al*., 2013). Together, these studies and our data provide support for $G\alpha_{i/o}$- and $G\beta\gamma$-selective activation of CB_1 in order to maintain CB_1 levels and the cellular function and viability of cells expressing mHtt (Blázquez *et al*., 2011, 2015; Mievis *et al.*, 2011; Horne *et al*., 2013; Chiarlone *et al*., 2014; Naydenov *et al*., 2014).

4.4.2. Use of THC and CBD in HD

Despite a lack of clinical evidence, patients suffering from HD may be seeking medical marijuana or acquiring it from other sources in an attempt to relieve some of the symptoms of their disease (Müller-Vahl *et al.*, 1999; Meisel and Friedman, 2012; Koppel *et al*., 2014). Most medically available and tested illicit marijuana contains a high concentration of THC relative to other cannabinoids, such as CBD (De Backer *et al.*, 2012). Here, we observed that THC reduced cellular function and viability in cells expressing mHtt whether THC was used alone or in a 1:1 combination with CBD. Similarly, treatment of R6/1 and R6/2 mouse models with 10 mg/kg THC is associated with worsening of HD signs and symptoms (Dowie *et al*., 2010). However, others have reported improvement in motor control and reduced striatal atrophy in R6/1 and R6/2 HD treated for 6 weeks with 2 mg/kg THC beginning at 4 weeks of age (Blázquez *et al.*, 2011),

suggesting that the deleterious effects of THC in HD are dose- and time course-dependent. CBD alone displayed mixed beneficial and negative effects in ST*Hdh*$^{Q7/Q7}$ and ST*Hdh*$^{Q111/Q111}$ cells. CBD is known to act through a number of effectors, including as a negative allosteric modulator at CB_1 and a partial agonist at $5HT_{1A}$ (Pazos *et al.,* 2013; Laprairie *et al*., 2015d). It is unclear which effects of CBD predominate *in vivo* normally and in HD and how the combinations of any or all of the at least 65 cannabinoids found in marijuana (McPartland *et al.*, 2015) influence one another's pharmacokinetics and pharmacodynamics (Sagredo *et al.*, 2011; Valdeolivas *et al*., 2012). Further, the utility of CBD in HD remains controversial, with some studies reporting no effects in animal models and human trials (Consroe *et al*., 1991; Valdeolivas *et al*., 2012), or positive effects in animal models (Sagredo *et al*., 2007, 2011). Overall, the use of THC or marijuana may exacerbate the signs and symptoms of HD *via* further downregulation of CB_1 and reduced cellular viability.

4.4.3. CONCLUSIONS

$G\alpha_{i/o}$- and $G\beta\gamma$-selective CB_1 ligands are likely to be the most therapeutically useful cannabinoids in the treatment of HD. However, highly potent synthetic cannabinoids, such as WIN, may produce unwanted psychoactive effects and their chronic use is likely to result in receptor desensitization or downregulation (Sim-Selley and Martin, 2002; Blair *et al*., 2009). Endocannabinoids, which we observed to enhance $G\alpha_{i/o}$- and $G\beta\gamma$-dependent signaling in the ST*Hdh* cell culture system, are rapidly metabolized *in vivo* and consequently have limited efficacy when they are directly administered (Devane *et al.,* 1992; Kondo *et al*., 1998). The inhibitor of endocannabinoid catabolism URB597 has demonstrated limited efficacy at improving motor control deficits in R6/2 HD mice (Dowie *et al*., 2010), but additional studies are needed to understand how elevating endocannabinoid levels affects the signs and symptoms of HD *in vivo*. An alternative means of enhancing endogenous CB_1 signaling is with the use of positive allosteric modulators (PAMs) of CB_1. PAMs bind to a site on the receptor that is distinct from the site of endogenous ligand binding (*i.e.* the orthosteric site) and enhance the binding and efficacy of the

endogenous ligands that are produced and regulated through intrinsic control mechanisms (Pamplona *et al.*, 2012; Wootten *et al*., 2013). CB_1 PAMs are more likely to increase $G\alpha_{i/o}$ and pro-survival endocannabinoids and less likely to produce the psychotropic effects associated with cannabinoid agonists because they are unable to directly activate CB_1. Our *in vitro* study of cannabinoid functional selectivity leads us to conclude that enhancement of endocannabinoid-dependent CB_1 activation is the most likely means of treating the signs of symptoms of HD by targeting CB_1.

CHAPTER 5

CANNABIDIOL IS A NEGATIVE ALLOSTERIC MODULATOR OF THE TYPE 1 CANNABINOID RECEPTOR.

Copyright statement

This chapter has been previously published in: Laprairie RB, Bagher AM, Kelly MEM, Denovan-Wright EM (2015). Cannabidiol is a negative allosteric modulator of the type 1 cannabinoid receptor. *Br J Pharmacol* **172**: 4790 – 4805. The manuscript has been modified to meet formatting requirements. Re-use is permitted with copyright permission (Appendix A).

Contribution statement

The manuscript used as the basis for this chapter was written with guidance from Drs. Eileen Denovan-Wright and Melanie Kelly. Technical assistance was provided by Dr. Amina Bagher.

5.1. INTRODUCTION

The majority of available drugs that target G protein-coupled receptors (GPCR) act at the receptor's orthosteric site – the site at which the endogenous ligand binds (Christopoulos and Kenakin, 2002). The type 1 cannabinoid receptor (CB_1) is the most abundant GPCR in the central nervous system and is expressed throughout the periphery (reviewed in Ross, 2007; Pertwee, 2008). Orthosteric ligands of CB_1 have been touted as possible treatments for anxiety and depression, epilepsy, neurodegenerative diseases such as Huntington disease and Parkinson disease, and chronic pain (Pertwee, 2008; Piscitelli *et al*., 2012), and have been tested in the treatment of addiction, obesity, and diabetes (Pertwee, 2008; Piscitelli *et al*., 2012). Despite their therapeutic potential, orthosteric agonists of CB_1 are limited by their potential psychomimetic effects while orthosteric antagonists of CB_1 are limited by their depressant effects (Ross, 2007).

An allosteric binding site is a distinct domain from the orthosteric site that can bind to small molecules or other proteins in order to modulate receptor activity (Wootten *et al*., 2013). All class A, B, and C GPCRs investigated to date possess allosteric binding sites (Wootten *et al*., 2013). Ligands that bind to receptor allosteric sites may be classified as *allosteric agonists* that can activate a receptor independent of other ligands, *allosteric modulators* that alter the potency and efficacy of the orthosteric ligand but cannot activate the receptor alone, and *mixed agonist/modulator ligands*. As therapeutics, allosteric modulators, unlike allosteric agonists and mixed agonist/modulator ligands, are attractive because they lack intrinsic efficacy (Ross, 2007; Wootten *et al*., 2013). Therefore, the effect ceiling of an allosteric modulator is determined by the endogenous or exogenous orthosteric ligand (Wooten *et al*., 2013). In contrast, exogenous orthosteric ligands may produce adverse effects through supra-physiological over activation or downregulation of a receptor (Wootten *et al*., 2013). Unlike orthosteric ligands, allosteric modulators of CB_1 may not produce these undesirable side effects because their efficacy depends on the presence of orthosteric ligands, such as the two major endocannabinoids anandamide and 2-arachidonoylglycerol (2-AG) (Ross, 2007; Wootten *et al*, 2013).

To date, the best-characterized allosteric modulators of CB_1 are the positive allosteric modulator (PAM) lipoxin A_4 (Pamplona *et al*., 2012) and the negative allosteric modulators (NAM) Org27569 and PSNCBAM-1 (Price *et al*., 2005; Horswill *et al*., 2007; Wang *et al*., 2011; Ahn *et al*., 2013). Org27569 and PSNCBAM-1 reduce the efficacy and potency of CB_1 agonists WIN55,212-2 and CP55,940 to stimulate $GTP\gamma S^{35}$, enhance $G\alpha_{i/o}$-dependent signaling and arrestin recruitment, and inhibit CB_1 internalization and cAMP accumulation at submicromolar concentrations (Price *et al*., 2005; Horswill *et al*., 2007; Wang *et al*., 2011; Ahn *et al*., 2013; Cawston *et al*., 2013). The well-characterized NAM activities of Org27569 and PSNCBAM-1 are the archetypes against which novel CB_1 NAMs are compared.

Cannabidiol (CBD) is known to modulate the activity of many cellular effectors, including CB_1, the type 2 cannabinoid receptor (CB_2) (Hayakawa *et al*., 2008), the serotonin $5HT_{1A}$ receptor (Russo *et al*., 2005), GPR55 (Ryberg *et al*., 2007), the μ- and δ-opioid receptors (Kathmann *et al*., 2006), the transient receptor potential cation channel subfamily V 1 (TRPV1) (Bisogno *et al*., 2001), the peroxisome proliferator-activated receptor γ (PPARγ) (Campos *et al*., 2012), and fatty acid amide hydrolase (FAAH) (Bisogno *et al*., 2001). With regard to cannabinoid receptor-specific effects, several *in vitro* and *in vivo* studies have reported that CBD acts as an antagonist of cannabinoid agonists at CB_1 at concentrations well below the reported affinity (K_i) for CBD to the orthosteric agonist site of CB_1 (Pertwee *et al.*, 2002; Ryan *et al*., 2007; Thomas *et al*., 2007; McPartland *et al*., 2014). We recently reported that the effects of CBD on intracellular signaling were largely CB_1-independent (Laprairie *et al*., 2014a). However, CBD inhibited CB_1 internalization *in vitro* at submicromolar concentrations where no other CB_1-dependent effect on signaling was observed (Laprairie *et al*., 2014a). Given these similarities with Org27569 and PSNCBAM-1 inhibition of CB_1 internalization, and existing *in vivo* data suggesting CBD can act as a potent antagonist of CB_1 agonists, we hypothesized that CBD had NAM activity at CB_1.

The objective of this study was to determine whether CBD had NAM activity at CB_1 in cell culture. The NAM activity of CBD was tested for arrestin2, $G\alpha_q$ (PLCβ3), and $G\alpha_{i/o}$

(ERK1/2) pathways using 2-AG and Δ^9-tetrahydrocannabinol (THC) as the orthosteric probes and compared to the competitive antagonist O-2050 (Hudson *et al*., 2010; Laprairie *et al*., 2014a). While some studies have suggested O-2050 may be a partial agonist of CB_1 (Wiley *et al*., 2011, 2012), several groups have noted the competitive antagonistic activity of O-2050 at CB_1 (Canals and Milligan, 2008; Higuchi *et al.,* 2010; Ferreira *et al.*, 2012; Anderson *et al*., 2013). Allosteric effects of CBD were studied using an operational model of allosterism (Keov *et al*., 2011). Using this operational model, we were able to estimate ligand co-operativity (α), changes in efficacy (β), and orthosteric and allosteric ligand affinity (K_A and K_B) (Keov *et al*., 2011) and support our hypothesis that CBD displayed NAM activity at CB_1. HEK293A and ST*Hdh*$^{Q7/Q7}$ cells were used to test our hypothesis. HEK293A cells represent a well-characterized heterologous expression system to study CB_1 signaling while ST*Hdh*$^{Q7/Q7}$ cells model the major output of the indirect motor pathway of the striatum where CB_1 levels are highest relative to other regions of the brain (Trettel *et al*., 2000; Laprairie *et al*., 2013, 2014a,b), making this cell line ideally suited to studying endocannabinoid signaling in a more physiologically relevant context.

5.2. METHODS

5.2.1. DRUGS

Drug stocks were made up in ethanol (THC) or DMSO [2-AG, CBD, and (6aR,10aR)-3-(1-methanesulfonylamino-4-hexyn-6-yl)-6a,7,10,10a-tetrahydro-6,6,9-trimethyl-6H-dibenzo[b,d]pyran (O-2050), *N*-(Piperidin-1-yl)-5-(4-iodophenyl)-1-(2,4-dichlorophenyl)-4-methyl-1*H*-pyrazole-3-carboxamide (AM251)] and diluted to final solvent concentrations of 0.1%. 2-AG, CBD, and O-2050 were purchased from Tocris Bioscience (Bristol, UK). THC was purchased from Sigma-Aldrich (Oakville, ON).

5.2.2. CELL CULTURE

HEK293A cells were from the American Type Culture Collection (ATCC, Manaassas, VI). Cells were maintained at 37°C, 5% CO_2 in DMEM supplemented with 10% FBS and 10^4 U/mL Pen/Strep.

ST*Hdh*$^{Q7/Q7}$ cells are derived from the conditionally immortalized striatal progenitor cells of embryonic day 14 C57BlJ/6 mice (Coriell Institute, Camden, NJ) (Trettel *et al*., 2000). Cells were maintained at 33°C, 5% CO_2 in DMEM supplemented with 10% FBS, 2 mM L-glutamine, 10^4 U/mL Pen/Strep, and 400 µg/mL geneticin. Cells were serum-deprived for 24 h prior to experiments to promote differentiation (Trettel *et al*., 2000; Laprairie *et al*., 2013, 2014a,b).

5.2.3. PLASMIDS AND TRANSFECTION

Human CB_1, CB_{1A}, CB_{1B}, and arrestin2 (β-arrestin1) were cloned and expressed as either green fluorescent protein^2 (GFP^2) or *Renilla* luciferase (Rluc) fusion proteins. CB_1-GFP^2, and arrestin2-Rluc were generated using the pGFP^2-N3 and pcDNA3.1 plasmids (PerkinElmer, Waltham, MA) as described previously (Hudson *et al*., 2010; Laprairie *et al*., 2014a). The GFP^2-Rluc fusion construct, and Rluc plasmids have been previously described (Laprairie *et al*., 2014a).

The human CB_1 receptor was mutagenized at two cysteine residues (Cys-98 and Cys-107). Mutagenesis was conducted as described previously (Laprairie *et al*. 2013) with the cysteine residues being mutated to alanines (C98A, C107A) or serines (C98S, C107S) using the CB_1-GFP^2 fusion plasmid and the following forward and reverse primers: CB_1^{C98A}-GFP^2 forward 5'-AAC ATC CAG GCT GGG GAG AAC T-3', reverse 5'-AGT TCT CCC CAG CCT GGA TGT T-3'; and CB_1^{C107A}-GFP^2 forward 5'-GAC ATA GAG GCT TTC ATG GTC-3', reverse 5'-GAC CAT GAA AGC CTC TAT GTC-3'; CB_1^{C98S}-GFP^2 forward 5'-AAC ATC CAG TCT GGG GAG AAC T-3', reverse 5'-AGT TCT CCC CAG ACT GGA TGT T-3'; and CB_1^{C107S}-GFP^2 forward 5'-GAC ATA GAG TCT TTC ATG GTC-3', reverse 5'-GAC CAT GAA AGA CTC TAT GTC-3'. Mutagenesis was confirmed by sequencing (GeneWiz, Camden, NJ).

Cells were grown in 6 well plates and transfected with 200 ng of the Rluc fusion plasmid and 400 ng of the GFP^2 fusion plasmid according to previously described protocols (Laprairie *et al*., 2014a) using Lipofectamine 2000® according to the manufacturer's instructions (Invitrogen, Burlington, ON). Transfected cells were maintained for 48 h prior to experimentation.

5.2.4. BIOLUMINESCENCE RESONANCE ENERGY TRANSFER^2 (BRET^2)

Interactions between CB_1 and arrestin2 were quantified *via* $BRET^2$ according to previously described methods (Laprairie *et al*., 2014a). BRET efficiency ($BRET_{Eff}$) was determined as previously described (James *et al*., 2006; Laprairie *et al*., 2014a) such that Rluc alone was used to calculate $BRET_{MIN}$ and the Rluc-GFP^2 fusion protein was used to calculate $BRET_{MAX}$.

5.2.5. ON- AND IN-CELL™ WESTERN

On-cell™ western analyses were completed as described previously (Laprairie *et al*., 2014a) using primary antibody directed against *N*-CB_1 (1:500; Cayman Chemical Company, Ann Arbor, MI, Cat No. 101500). All experiments measuring CB_1 included an *N*-CB_1 blocking peptide control (1:500; Cayman Chemical Company), which was incubated with *N*-CB_1 antibody (1:500). Immunofluorescence observed with the *N*-CB_1 blocking peptide was subtracted from all experimental replicates. In-cell™ western analyses were conducted as described previously (Laprairie *et al*., 2014a). Primary antibody solutions were: *N*-CB_1 (1:500), pERK1/2(Tyr205/185) (1:200), ERK1/2 (1:200), pPLCβ3(S537) (1:500), PLCβ3 (1:1000), or β-actin (1:2000) (all from Santa Cruz Biotechnology, Santa Cruz, CA). Secondary antibody solutions were: $IR^{CW700dye}$ or $IR^{CW800dye}$ (1:500; Rockland Immunochemicals, Gilbertsville, PA). Quantification was completed using the Odyssey Imaging system and software (v. 3.0; Li-Cor, Lincoln, NE).

5.2.6. DATA ANALYSIS AND CURVE FITTING

Data are presented as the mean ± the standard error of the mean (SEM) or mean and 95% confidence interval, as indicated, from at least 4 independent experiments. All data analysis and curve fitting was carried out using GraphPad Prism (v. 5.0). Concentration-response curves (CRC) were fit with the non-linear regression with variable slope (4 parameters), Gaddum/Schild EC_{50} shift model, or operational model of allosterism (eq. 1) (Keov *et al.,* 2011) and are shown in each figure according to the best-fit model as determined by R^2 value (GraphPad Prism v. 5.0). Pharmacological statistics were obtained from non-linear regression models as indicated in

figures and tables. Global curve fitting of allosterism data was carried out using the following operational model (Hudson *et al*., 2014; Keov *et* al., 2011; Smith *et al.,* 2011):

$$E= \frac{E_{max}(\tau_A[A](K_B+\alpha\beta[B])+\tau_B[B]K_A)^n}{([A]K_B+K_AK_B+[B]K_A+\alpha[A][B])^n+(\tau_A[A](K_B+\alpha\beta[B])+\tau_B[B]K_A)^n} \quad \textbf{(1)}$$

where E is the measured response, A and B are the orthosteric and allosteric ligand concentrations, respectively, E_{max} is the maximum system response, α is a measure of the allosteric co-operativity on ligand binding, β is a measure of the allosteric effect on efficacy, K_A and K_B are estimates of the binding of the orthosteric and allosteric ligands, respectively, n represents the Hill slope, and τ_A and τ_B represent the abilities of the orthosteric and allosteric ligands to directly activate the receptor (Smith *et al*., 2011). To fit experimental data to this equation, E_{max} and n were constrained to 1.0 and 1.0, respectively, and global estimates of α, β, K_A, K_B, τ_A and τ_B were calculated.

Relative receptor activity (RA) was calculated according to equation 2 (Christopoulos and Kenakin, 2002):

$$RA= \frac{(E_{max}\%)(EC_{50\ Agonist\ Alone})}{(E_{max\ Agonist\ Alone}\%)(EC_{50})} \quad \textbf{(2)}$$

where E_{max} % is the E_{max} of the concentration-response curve in the presence of a given concentration of CBD, EC_{50} is the EC_{50} (μM) in the presence of a given concentration of CBD; $E_{max\ Agonist\ Alone}$ % is the E_{max} in the absence of CBD; $EC_{50\ Agonist\ Alone}$ is the EC_{50} (μM) in the absence of CBD. Statistical analyses were one- or two-way analysis of variance (ANOVA), as indicated, using GraphPad. *Post-hoc* analyses were performed using Dunnett's multiple comparisons, Bonferroni's or Tukey's tests, as indicated. Homogeneity of variance was confirmed using Bartlett's test. The level of significance was set to $P < 0.001$ or < 0.01, as indicated. To improve the readability of the data, all figures have been laid out such that data from HEK293A cells appears above data from ST*Hdh*$^{Q7/Q7}$ cells, and data for O-2050 appears before data for CBD (Figs. 5-2,-4,-5).

5.3. RESULTS

5.3.1. CB_1 INTERNALIZATION AND KINETIC EXPERIMENTS

We had previously observed that CBD reduced CB_1 internalization in ST*Hdh*$^{Q7/Q7}$ cells (Laprairie *et al*., 2014a). Here, we sought to determine how CBD affected the kinetics of CB_1 internalization and arrestin2 recruitment in ST*Hdh*$^{Q7/Q7}$ cells. The fraction of CB_1 at the plasma membrane was concentration-dependently decreased by THC (Fig. 5-1A) and 2-AG in ST*Hdh*$^{Q7/Q7}$ cells (Fig. 5-1B). The efficacy and potency of THC- and 2-AG-dependent CB_1 internalization were reduced by increasing concentrations of CBD (Fig. 5-1A,B). BRET[2] between arrestin2-Rluc and CB_1-GFP[2] was measured every 10 s for 4 min in ST*Hdh*$^{Q7/Q7}$ cells treated with 1 μM THC (Fig. 5-1C) or 2-AG (Fig. 5-1D). Increasing concentrations of CBD decreased the rate of association between arrestin2 and CB_1 over 4 min (Fig. 5-1E) and decreased maximal $BRET_{Eff}$ observed at 10 min (Fig. 5-1C-E). The fraction of CB_1 at the plasma membrane was also reduced in ST*Hdh*$^{Q7/Q7}$ cells treated with 1 μM THC (Fig. 5-1F) or 2-AG (Fig. 5-1G) over 60 min. CBD alone increased the fraction of CB_1 at the membrane (Fig. 5-1F-H). The rates of CB_1 internalization, and the maximum fraction of CB_1 internalized were reduced by increasing concentrations of CBD (Fig. 5-1F-H). Similarly, Cawston *et al*. (2013) observed that the rate of arrestin recruitment to CB_1 was reduced by the allosteric modulator Org27569. Therefore, CBD delayed interactions between CB_1 and arrestin2 and increased the pool of receptors present at the plasma membrane at sub-micromolar concentrations, which is similar to the actions of the previously described CB_1 allosteric modulator Org27569 (Cawston *et al*., 2013).

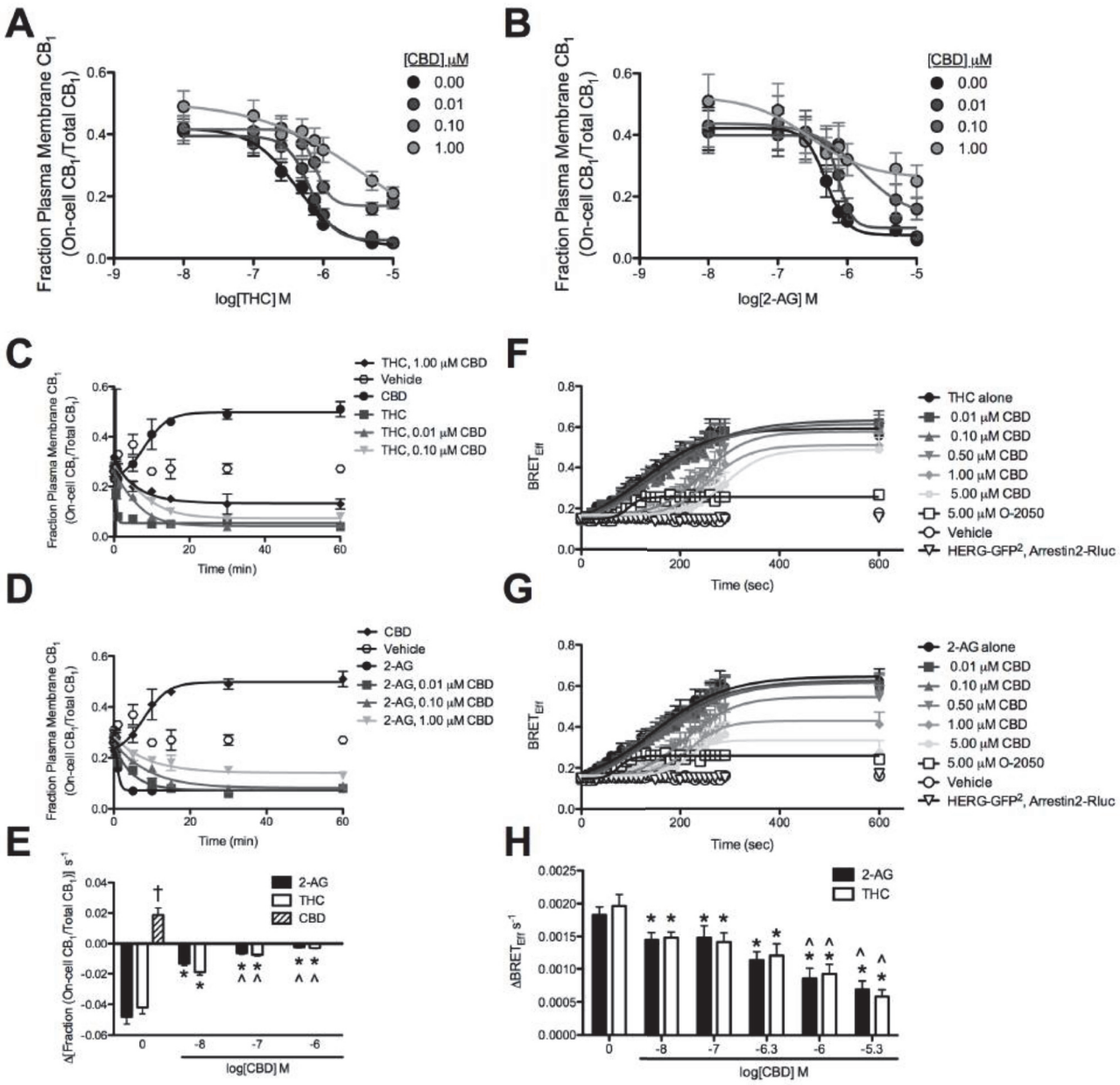

Figure 5-1. CBD reduced the rate and maximal $BRET_{Eff}$ between CB_1 and arrestin2 and CB_1 internalization in THC- and 2-AG-treated ST*Hdh*$^{Q7/Q7}$ cells. A,B) ST*Hdh*$^{Q7/Q7}$ cells were treated with THC **(A)** or 2-AG **(B)** ± CBD for 10 min and the fraction of CB_1 at the plasma membrane was quantified using On- and In-cell™ western analyses. Data were fit to a non-linear regression model with variable slope. **C-E)** ST*Hdh*$^{Q7/Q7}$ cells were transfected with arrestin2-Rluc- and CB_1-GFP^2-containing plasmids and $BRET^2$ was measured every 10 s for 4 min (240 sec) and again at 10 min (600 sec) after treatment with THC **(C)** or 2-AG **(D)** ± O-2050 or CBD. Data were fit to a non-linear regression model with variable slope. **E)** The rate of arrestin2 recruitment to CB_1 was measured as the change in $BRET_{Eff}$ s^{-1} during the first 4 min. **F-H)** ST*Hdh*$^{Q7/Q7}$ cells were treated with THC **(F)** or 2-AG **(G)** ± CBD for 60 min and the fraction of CB_1 at the plasma membrane was quantified using On- and In-cell™ western analyses. Data were fit to a non-linear regression model with variable slope. **H)** The rate of CB_1 internalization was measured as the change in the Fraction On-cell CB_1/Total CB_1 min^{-1} prior to plateau. †$P <$ 0.01 compared to 2-AG or THC alone, *$P < 0.01$ compared to 0 CBD within orthosteric ligand treatment, ^$P <$ 0.01 compared to 0.01 μM CBD (log[CBD] M = -8) within orthosteric ligand treatment, as determined *via* two-way ANOVA followed by Bonferroni's *post-hoc* test. $N = 6$.

5.3.2. CB_1-ARRESTIN2 $BRET^2$ EXPERIMENTS

2-AG and THC enhance the interaction between CB_1 and arrestin2, as indicated by $BRET^2$ in ST*Hdh*$^{Q7/Q7}$ cells (Laprairie *et al*., 2014a). Here, we used HEK293A cells as a heterologous expression system for CB_1 and arrestin2 to determine whether CBD acted as a NAM of CB_1. Treatment of HEK293A cells with 0.01 – 5.00 μM THC or 2-AG for 30 min produced a concentration-dependent increase in $BRET_{Eff}$ between arrestin2-Rluc and CB_1-GFP^2 (Fig. 5-2A-D). The CB_1 antagonist O-2050 (0.01 – 5.00 μM) produced a concentration-dependent rightward shift in the THC and 2-AG CRCs that were best fit using the Gaddum/Schild EC_{50} non-linear regression model indicative of competitive antagonism (Fig. 5-2A,B). CBD (0.01 – 5.00 μM) treatment produced a concentration-dependent rightward and downward shift in the THC and 2-AG CRCs that were best fit using the operational model of allosterism (eq.1, Fig. 5-2C,D). The rightward shift in EC_{50} was significant at 1.00 μM and 0.50 μM CBD for THC- and 2-AG-treated cells, respectively (Table 5-1). The decrease in E_{max} was significant at 0.10 and 0.50 μM for THC- and 2-AG-treated cells, respectively (Table 5-1). The Hill coefficient (*n*) was less than 1 at 0.10 and 0.50 μM for THC- and 2-AG-treated cells, respectively (Table 5-1). Relative receptor activity (eq. 2) was significantly reduced at 0.01μM for THC- and 2-AG-treated cells (Table 5-1). Schild analyses of these data demonstrated that while O-2050 behaved as a competitive antagonist, inhibition of $BRET_{Eff}$ by CBD was non-linear for THC- and 2-AG-treated HEK293A cells (Fig. 5-2E, Table 5-2). These data demonstrated that CBD behaved as a NAM of THC- and 2-AG-mediated arrestin2 recruitment to CB_1 in the HEK293A heterologous expression system.

The NAM properties of CBD on CB_1-arrestin2 interactions were confirmed in the ST*Hdh*$^{Q7/Q7}$ cell culture model of medium spiny projection neurons. As in HEK293A cells, O-2050 treatment produced a concentration-dependent rightward shift in the THC and 2-AG CRCs that were best fit using the Gaddum/Schild EC_{50} non-linear regression model indicative of competitive antagonism (Fig. 5-2F,G), and CBD treatment produced a concentration-dependent rightward and downward shift in the THC and 2-AG CRCs that were best fit using the operational

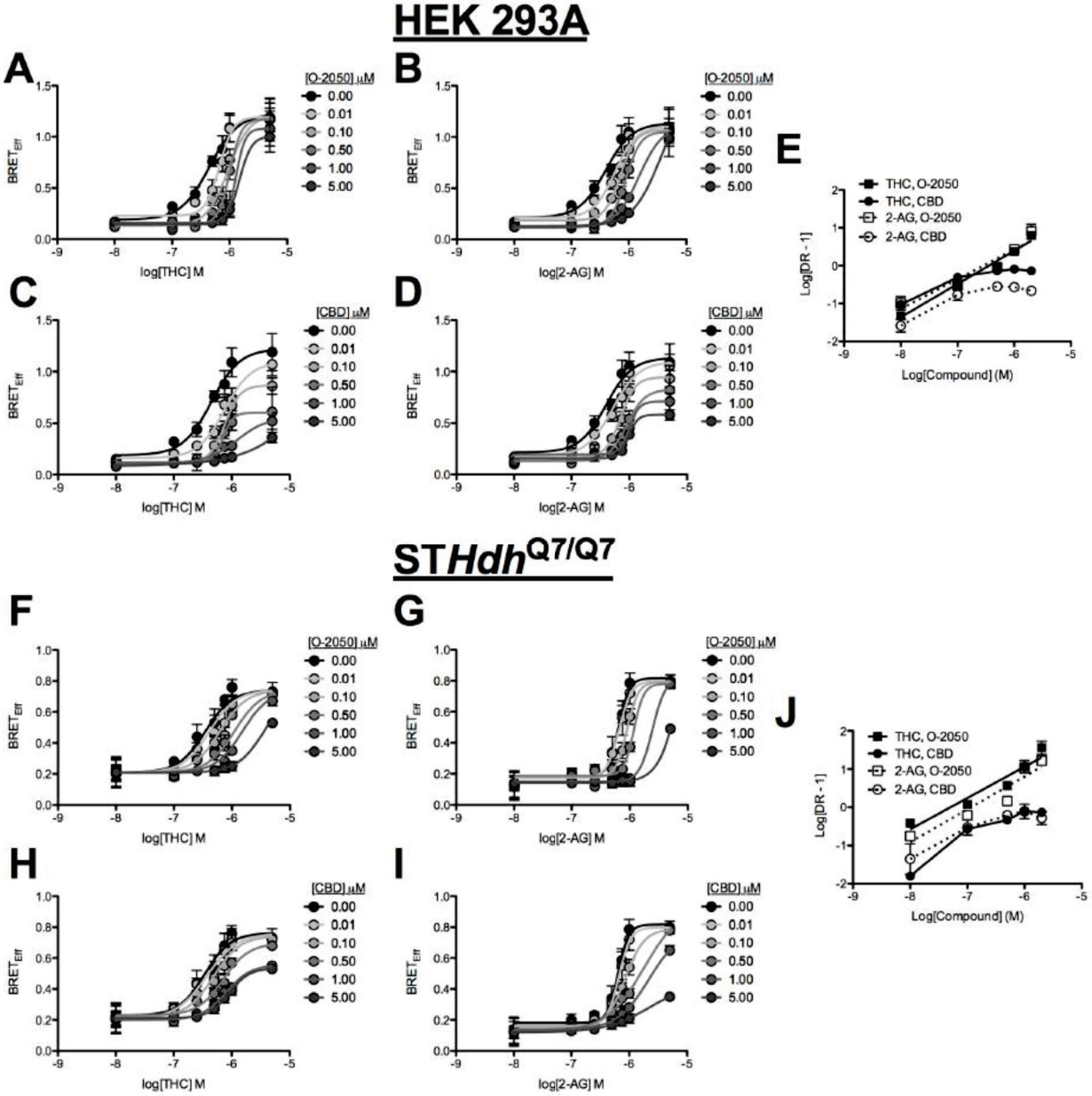

Figure 5-2. CBD was a NAM of arrestin2 recruitment to CB_1 following THC and 2-AG treatment. HEK293A **(A-E**) and ST*Hdh*$^{Q7/Q7}$ **(F-J)** cells were transfected with arrestin2-Rluc- and CB_1-GFP^2-containing plasmids and BRET^2 was measured 30 min after treatment with 2-AG or THC ± O-2050 or CBD. CRCs were fit using Gaddum/Schild EC_{50} shift **(A,B,F,G)** and operational model of allosterism **(C,D,H,I)** non-linear regression models. **E,J)** Schild regressions were plotted as the logarithm of 2-AG or THC concentration against the logarithm of the concentration-response at $EC_{50} - 1$. $N = 6$.

Table 5-1. Effect of CBD on Arrestin-2 recruitment in HEK293A and ST*Hdh*$^{Q7/Q7}$ cells.

Data are mean ±S.E.M. or with 95% CI of six independent experiments.

Agonist	[CBD] (μM)	EC_{50} μM (95% CI)[a]	E_{max} (95% CI)[a,b]	n (95% CI)[a,c]	RA ± S.E.M.[d]
HEK293A					
THC	*DMSO*	0.44 (0.27 - 0.72)	1.22 (0.99 - 1.46)	1.00 (0.89 - 1.06)	1.00 ± 0.0
	0.01	0.75 (0.53 - 1.06)	1.09 (0.90 - 1.29)	0.76 (0.65 - 0.89)	0.50 ± 0.05*
	0.10	0.77 (0.64 - 0.92)	0.87 (0.75 - 0.89)†	0.63 (0.46 - 0.85)†	0.39 ± 0.04*
	0.50	0.71 (0.49 - 1.03)	0.60 (0.41 - 0.80)†	0.55 (0.43 - 0.69)†	0.29 ± 0.05*
	1.00	1.29 (0.89 - 1.41)†	0.56 (0.35 - 0.77)†	0.38 (0.26 - 0.41)†	0.15 ± 0.03*
	5.00	1.41 (1.04 - 1.77)†	0.15 (0.09 - 0.31)†	0.17 (0.08 - 0.24)†	0.04 ± 0.03*
2-AG	*DMSO*	0.39 (0.23 - 0.67)	1.13 (0.91 - 1.36)	1.00 (0.86 - 1.13)	1.00 ± 0.0
	0.01	0.52 (0.36 - 0.75)	1.10 (0.92 - 1.28)	0.81 (0.68 - 1.05)	0.72 ± 0.04*
	0.10	0.71 (0.59 - 0.86)	0.95 (0.82 - 1.07)	0.78 (0.73 - 0.93)	0.46 ± 0.07*
	0.50	0.91 (0.69 - 1.08)†	0.83 (0.59 - 1.09)†	0.64 (0.51 - 0.74)†	0.31 ± 0.02*
	1.00	1.00 (0.87 - 1.16)†	0.71 (0.63 - 0.79)†	0.33 (0.21 - 0.53)†	0.24 ± 0.04*
	5.00	1.09 (0.87 - 1.18)†	0.58 (0.52 - 0.64)†	0.27 (0.18 - 0.37)†	0.18 ± 0.02*
ST*Hdh*$^{Q7/Q7}$					
THC	*DMSO*	0.34 (0.21 - 0.46)	0.76 (0.65 - 0.88)	1.00 (0.93 - 1.31)	1.00 ± 0.0
	0.01	0.37 (0.18 - 0.56)	0.76 (0.58 - 0.93)	0.87 (0.54 - 1.24)	0.91 ± 0.3
	0.10	0.49 (0.32 - 0.66)	0.74 (0.63 - 0.86)	0.81 (0.43 - 1.07)	0.68 ± 0.1*
	0.50	0.72 (0.50 - 0.94)†	0.70 (0.59 - 0.79)	0.80 (0.35 - 1.06)	0.43 ± 0.1*
	1.00	0.80 (0.56 - 1.05)†	0.54 (0.48 - 0.64)†	0.74 (0.36 - 0.95)	0.31 ± 0.1*
	5.00	0.91 (0.70 - 1.17)†	0.50 (0.48 - 0.59)†	0.65 (0.30 - 0.84)†	0.26 ± 0.0*
2-AG	*DMSO*	0.64 (0.56 - 0.73)	0.82 (0.74 - 0.90)	1.00 (0.71 - 1.37)	1.00 ± 0.0
	0.01	0.66 (0.52 - 0.84)	0.80 (0.65 - 0.94)	0.89 (0.70 - 1.09)	0.94 ± 0.2
	0.10	0.86 (0.69 - 1.08)	0.78 (0.68 - 0.89)	0.56 (0.32 - 0.83)	0.72 ± 0.2*
	0.50	1.80 (1.42 - 2.18)†	0.76 (0.65 - 1.05)	0.29 (0.14 - 0.42)†	0.34 ± 0.1*
	1.00	2.18 (2.06 - 3.53)†	0.74 (0.68 - 1.04)	0.25 (0.16 - 0.38)†	0.27 ± 0.1*
	5.00	2.20 (1.95 - 3.55)†	0.44 (0.25 - 0.57)†	0.25 (0.18 - 0.37)†	0.16 ± 0.0*

[a]Determined using non-linear regression with variable slope (4 parameter) analysis; [b]Maximal agonist effect $BRET_{Eff}$; [c]Hill coefficient; [d]Relative Activity, as determined in eq. 2.

†Significantly different from the DMSO vehicle as determined by non-overlapping CI.

*$P < 0.01$ compared to DMSO vehicle as determined by one-way ANOVA followed by Dunnett's multiple comparison.

model of allosterism (Fig. 5-2H,I) in ST*Hdh*$^{Q7/Q7}$ cells. The rightward shift in EC_{50} was significant at 0.50 μM CBD for THC- and 2-AG-treated cells (Table 5-1). The decrease in E_{max} was significant at 1.00 and 5.00 μM for THC- and 2-AG-treated cells, respectively (Table 5-1). The Hill coefficient (*n*) was less than 1 at 5.00 and 0.50 μM for THC- and 2-AG-treated cells, respectively (Table 5-1). Relative receptor activity (Eq. 2) was significantly reduced at 0.10 μM for both THC- and 2-AG-treated cells (Table 5-1). The Schild regression for these data demonstrated that O-2050 modeled competitive antagonism for THC- and 2-AG-treated ST*Hdh*$^{Q7/Q7}$ cells (greater slope and R^2) (Fig. 5-2J, Table 5-2). CBD alone displayed weak partial agonist activity in this assay at concentrations > 2 μM (Fig. 5-3). Taken together these data indicate that CBD behaved as a NAM of THC- and 2-AG-mediated arrestin2 recruitment to CB_1 at concentrations below its reported affinity to CB_1 in a cell culture model endogenously expressing CB_1 (Pertwee, 2008).

5.3.3. CB_1-MEDIATED PHOSPHORYLATION OF PLCB3

THC and 2-AG treatment both result in a concentration-dependent increase in PLCβ3 phosphorylation in HEK293A cells (Fig. 5-4A-D) and ST*Hdh*$^{Q7/Q7}$ cells (Laprairie *et al*., 2014a) (Fig. 5-4F-I). O-2050 treatment resulted in a concentration-dependent rightward shift in the THC and 2-AG CRCs (Fig. 5-4A,B,F,G), while CBD treatment resulted in a rightward and downward shift in the THC and 2-AG CRCs, in both cell lines (Fig. 5-4C,D,H,I). O-2050 CRCs were best fit with the Gaddum/Schild EC_{50} model, while CBD CRCs were best fit with the operational model of allosterism. The rightward shift in EC_{50} was significant at 0.50 μM CBD for THC- and 2-AG-treated HEK293A cells (Table 5-3) and 0.50 and 1.00 μM CBD for THC- and 2-AG-treated ST*Hdh*$^{Q7/Q7}$ cells, respectively (Table 5-3). The decrease in E_{max} was significant at 1.00 and 0.50 μM for HEK293A and ST*Hdh*$^{Q7/Q7}$ cells, respectively (Table 5-3). The Hill coefficient (*n*) was less than 1 at 0.50 μM for THC- and 2-AG-treated in both HEK293A and ST*Hdh*$^{Q7/Q7}$ cells (Tables 5-1 and 5-3). Relative receptor activity was significantly reduced at 0.10 μM for THC- and 2-AG-treated HEK293A and ST*Hdh*$^{Q7/Q7}$ cells (Table 5-3).

Table 5-2. Schild analysis of Arrestin-2, PLCβ3, AND ERK modulation by CBD.

Data are mean ±S.E.M. or with 95% CI of six independent experiments.

HEK293A				
Agonist	Slope[a]	R^2	pA_2 (μM) ± S.E.M.[b]	IC_{50} (μM) (95% CI)[c]
BRET[2] (Arrestin-2-Rluc and CB_1-GFP[2])				
THC, O-2050	1.02 ± 0.11	0.89	0.84 ± 0.06	0.42 (0.22 - 0.64)
THC, CBD	0.54 ± 0.06*	0.62	-	0.31 (0.19 - 0.37)
2-AG, O-2050	1.06 ± 0.06	0.95	0.38 ± 0.04**	0.57 (0.29 - 0.67)
2-AG, CBD	0.54 ± 0.07*	0.41	-	0.36 (0.21 - 0.47)
$G\alpha_q$-coupled Phosphorylation of PLCβ3				
THC, O-2050	0.99 ± 0.05	0.90	1.04 ± 0.13	0.45 (0.35 - 0.58)
THC, CBD	0.59 ± 0.09*	0.68	-	0.39 (0.29 - 0.51)
2-AG, O-2050	1.03 ± 0.07	0.96	0.29 ± 0.03**	0.58 (0.31 - 0.73)
2-AG, CBD	0.48 ± 0.07*	0.38	-	0.31 (0.17 - 0.46)
$G\alpha_{I/O}$-coupled Phosphorylation of ERK1/2				
2-AG, O-2050	0.93 ± 0.15	0.88	0.26 ± 0.03	0.39 (0.09 - 0.46)
2-AG, CBD	0.15 ± 0.02*	0.62	-	0.26 (0.19 - 0.59)
ST*Hdh*$^{Q7/Q7}$				
BRET[2] (Arrestin-2-Rluc and CB_1-GFP[2])				
THC, O-2050	0.92 ± 0.09	0.95	0.83 ± 0.21	0.35 (0.27 - 0.46)
THC, CBD	0.34 ± 0.10*	0.78	-	0.23 (0.16 - 0.27)
2-AG, O-2050	0.97 ± 0.10	0.99	0.35 ± 0.13**	0.52 (0.45 - 0.59)
2-AG, CBD	0.35 ± 0.13*	0.70	-	0.63 (0.57 - 0.89)††
Phosphorylation of PLCβ3				
THC, O-2050	1.05 ± 0.17	0.97	0.93 ± 0.15	0.79 (0.42 - 0.85)
THC, CBD	0.22 ± 0.08*	0.70	-	0.94 (0.62 - 1.19)
2-AG, O-2050	1.02 ± 0.05	0.99	0.36 ± 0.09**	0.83 (0.46 - 1.17)
2-AG, CBD	0.29 ± 0.05*	0.71	-	0.96 (0.75 - 1.25)
Phosphorylation of ERK1/2				
2-AG, O-2050	1.06 ± 0.11	0.97	0.36 ± 0.06	0.87 (0.57 - 0.99)
2-AG, CBD	0.17 ± 0.08*	0.60	-	0.27 (0.18 - 0.36)†

[a,b,c]Determined using non-linear regression analysis with a Gaddum/Schild EC_{50} shift for data presented in Figs 5-1 - 5-3. IC_{50} determined at 1 μM agonist. pA_2 was not determined where Schild slope was different from 1 and was estimated by global non-linear regression analysis.

†Significantly different from the same agonist treatment; ††significantly different from the same modulator treatment; as determined by non-overlapping CI.

*$P < 0.01$ compared to the same agonist treatment; **$P < 0.01$ compared to the same modulator treatment; as determined by one-way ANOVA followed by Dunnett's multiple comparison.

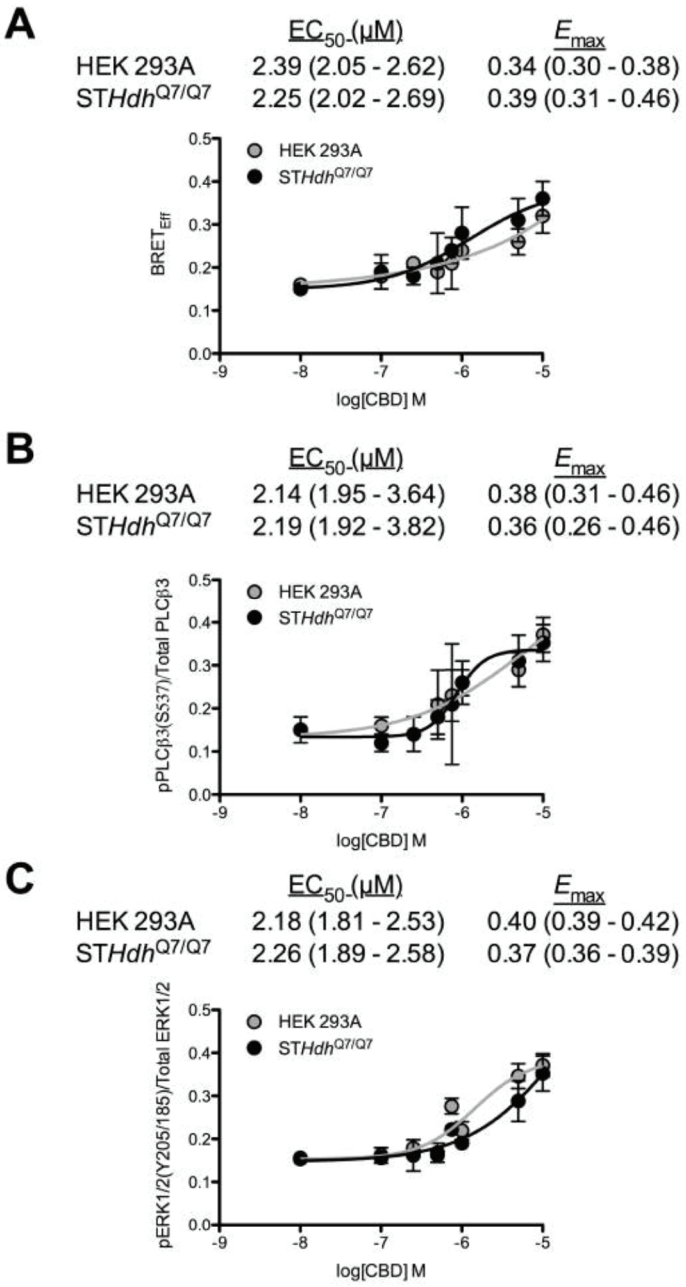

Figure 5-3. CBD displayed weak partial agonist activity at concentrations > 2 µM. A) HEK293A and ST*Hdh*$^{Q7/Q7}$ cells were transfected with arrestin2-Rluc- and CB_1-GFP^2 and BRET^2 was measured 30 min after treatment with CBD. **B,C)** HEK293A cell expressing CB_1-GFP^2 and ST*Hdh*$^{Q7/Q7}$ cells were treated with CBD and total and phosphorylated PLCβ3 **(B)** and ERK1/2 **(C)** levels were determined using In-cell™ western. CRCs were fit using non-linear regression with variable slope (4 parameter). $N = 4$. EC_{50} and E_{max} are presented as mean (95% CI). Note the y-axis scale is from 0.0 – 0.5.

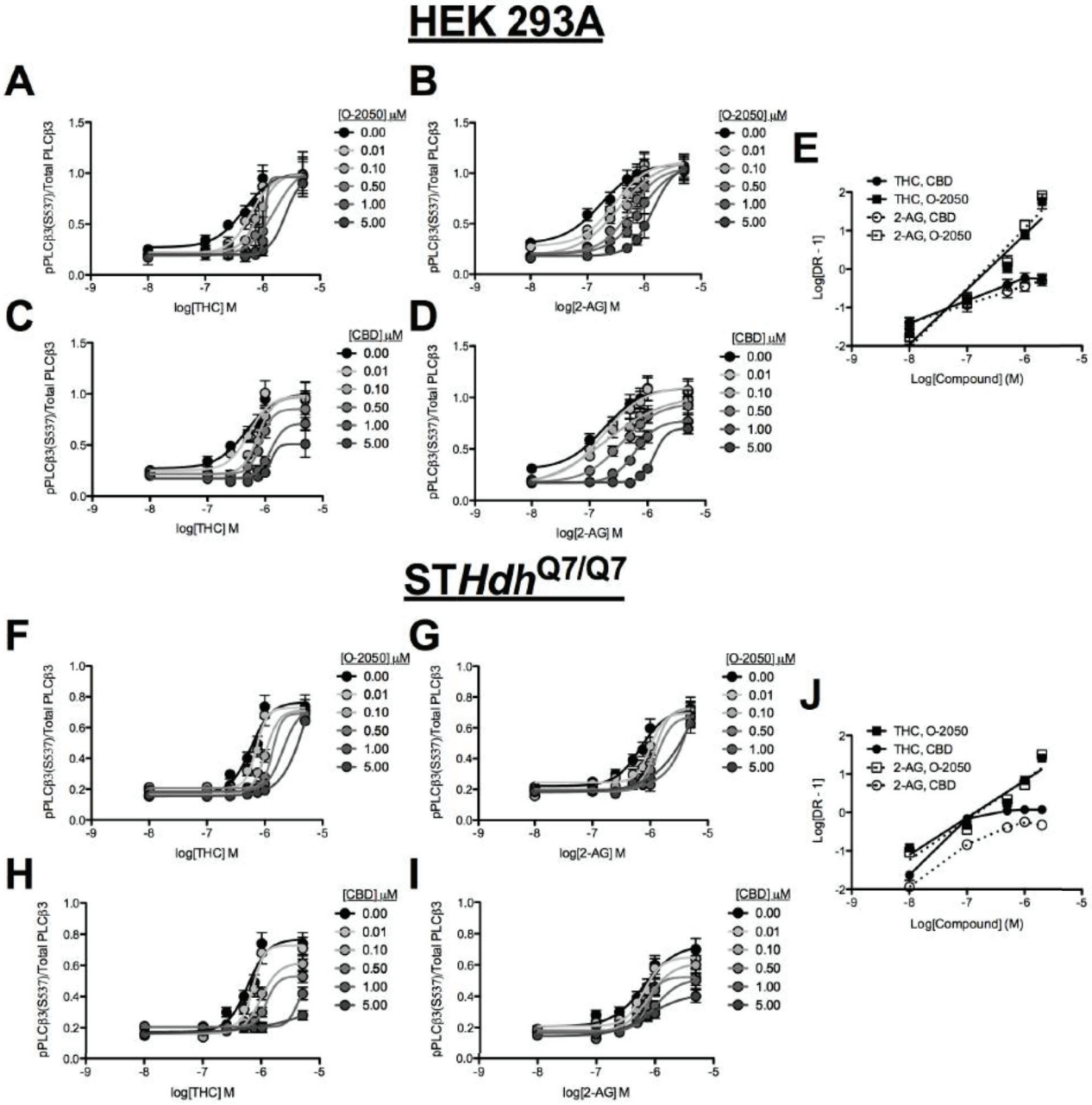

Figure 5-4. CBD was a NAM of CB_1-dependent PLCβ3 phosphorylation following THC and 2-AG treatment. HEK293A cell expressing CB_1-GFP[2] **(A-E)** and ST*Hdh*$^{Q7/Q7}$ cells **(F-J)** were treated with 2-AG or THC ± O-2050 or CBD and total and phosphorylated PLCβ3 levels were determined using In-cell™ western. CRCs were fit using Gaddum/Schild EC_{50} shift **(A,B,F,G)** and operational model of allosterism **(C,D,H,I)** non-linear regression models. **E,J)** Schild regressions were plotted as the logarithm of 2-AG or THC concentration against the logarithm of the concentration-response at $EC_{50} - 1$. $N = 6$.

The Schild regression for these data demonstrated that O-2050 modeled competitive antagonism for THC- and 2-AG-treated ST*Hdh*$^{Q7/Q7}$ cells, while CBD did not (Fig. 5-4E,J, Table 5-2). As with arrestin2 recruitment, CBD alone was a weak partial agonist at concentrations > 2 μM (Fig. 5-3). In the presence of 2-AG or THC, CBD was a NAM of PLCβ3 phosphorylation in HEK293A cells overexpressing CB_1 and ST*Hdh*$^{Q7/Q7}$ cells endogenously expressing CB_1.

5.3.4. CB_1-MEDIATED PHOSPHORYLATION OF ERK1/2

2-AG is a potent and efficacious agonist of ERK1/2 phosphorylation in ST*Hdh*$^{Q7/Q7}$ cells, whereas THC is a weak partial agonist of this response (Laprairie *et al*., 2014a). 2-AG treatment produced a concentration-dependent increase in ERK1/2 phosphorylation in both HEK293A and ST*Hdh*$^{Q7/Q7}$ cells (Fig. 5-5A,B,D,E). O-2050 treatment resulted in a concentration-dependent rightward shift in the 2-AG CRCs (Fig. 5-5A,D), while CBD treatment resulted in a rightward and downward shift in the 2-AG CRCs, in both cell lines (Fig. 5-5B,E). O-2050 CRCs were best fit with the Gaddum/Schild EC_{50} model, while CBD CRCs were best fit with the operational model of allosterism. The rightward shift in EC_{50} was significant at 0.50 and 1.00 μM CBD for HEK293A and ST*Hdh*$^{Q7/Q7}$ cells, respectively (Table 5-4). The decrease in E_{max} was significant at 5.00 and 1.00 μM for HEK293A and ST*Hdh*$^{Q7/Q7}$ cells, respectively (Table 5-4). The Hill coefficient (n) was less than 1 at 0.10 and 0.01 μM CBD for HEK293A and ST*Hdh*$^{Q7/Q7}$ cells, respectively (Table 5-4). Relative receptor activity was significantly reduced at 0.10 and 0.01 μM for 2-AG-treated HEK293A and ST*Hdh*$^{Q7/Q7}$ cells, respectively (Table 5-4). The Schild regression for these data demonstrated that O-2050 modeled competitive antagonism in HEK293A (Fig. 5-5C) and ST*Hdh*$^{Q7/Q7}$ (Fig. 5-5F) cells, whereas CBD did not (greater slope and R^2) (Table 5-2). CBD was a NAM of 2-AG-mediated ERK1/2 phosphorylation in HEK293A cells overexpressing CB_1 and ST*Hdh*$^{Q7/Q7}$ cells endogenously expressing CB_1 at lower concentrations than those reported for CB_1 agonist activity (Mechoulam *et al*., 2007; McPartland *et al*., 2014) (Fig. 5-3).

Table 5-3. Effect of CBD on PLCβ3 activation in HEK293A and ST*Hdh*$^{Q7/Q7}$ cells.

Data are mean ±S.E.M. or with 95% CI of six independent experiments.

Agonist	[CBD] (μM)	EC_{50} μM (95% CI)[a]	E_{max} (95% CI)[a,b]	n (95% CI)[a,c]	RA ± S.E.M.[d]
HEK293A					
THC	*DMSO*	0.47 (0.27 - 0.69)	1.01 (0.82 - 1.20)	1.00 (0.76 - 1.26)	1.00 ± 0.0
	0.01	0.58 (0.34 - 0.81)	0.98 (0.80 - 1.17)	0.83 (0.70 - 1.13)	0.79 ± 0.17
	0.10	0.76 (0.59 - 0.97)	0.97 (0.81 - 1.13)	0.73 (0.67 - 0.93)	0.60 ± 0.08*
	0.50	0.86 (0.70 - 1.07)†	0.85 (0.70 - 1.00)	0.54 (0.41 - 0.72)†	0.46 ± 0.05*
	1.00	1.23 (0.85 - 1.80)†	0.71 (0.63 - 0.79)†	0.36 (0.18 - 0.51)†	0.27 ± 0.03*
	5.00	1.26 (0.82 - 1.58)†	0.51 (0.41 - 0.61)†	0.16 (0.04 - 0.26)†	0.19 ± 0.02*
2-AG	*DMSO*	0.48 (0.28 - 0.72)	1.09 (0.90 - 1.29)	1.00 (0.86 - 1.15)	1.00 ± 0.0
	0.01	0.63 (0.37 - 0.96)	1.11 (0.91 - 1.30)	0.92 (0.81 - 1.02)	0.84 ± 0.07
	0.10	0.83 (0.58 - 1.03)	1.03 (0.74 - 1.32)	0.84 (0.74 - 1.00)	0.60 ± 0.07*
	0.50	1.11 (0.95 - 1.35)†	0.95 (0.80 - 1.10)	0.57 (0.46 - 0.79)†	0.41 ± 0.08*
	1.00	1.62 (1.23 - 1.51)†	0.78 (0.67 - 0.88)†	0.22 (0.07 - 0.36)†	0.23 ± 0.01*
	5.00	2.48 (1.72 - 3.22)†	0.60 (0.54 - 0.66)†	0.13 (0.04 - 0.24)†	0.12 ± 0.06*
ST*Hdh*$^{Q7/Q7}$					
THC	*DMSO*	0.58 (0.42 - 0.79)	0.77 (0.65 - 0.89)	1.00 (0.71 - 1.25)	1.00 ± 0.0
	0.01	0.72 (0.61 - 0.85)	0.73 (0.63 - 0.82)	0.54 (0.44 - 0.82)	0.77 ± 0.3
	0.10	0.99 (0.78 - 1.22)	0.62 (0.54 - 0.69)	0.51 (0.42 - 0.78)	0.48 ± 0.1*
	0.50	1.22 (0.85 - 1.57)†	0.53 (0.48 - 0.58)†	0.55 (0.23 - 0.64)†	0.33 ± 0.1*
	1.00	4.00 (2.76 - 4.32)†	0.49 (0.37 - 0.52)†	0.51 (0.17 - 0.62)†	0.10 ± 0.0*
	5.00	>5.00 †	-	< 0.50 †	0.03 ± 0.0*
2-AG	*DMSO*	0.66 (0.40 - 0.85)	0.73 (0.59 - 0.87)	1.00 (0.70 - 1.18)	1.00 ± 0.0
	0.01	0.67 (0.48 - 0.86)	0.65 (0.56 - 0.74)	0.77 (0.55 - 0.89)	0.88 ± 0.2
	0.10	0.78 (0.58 - 1.01)	0.61 (0.52 - 0.70)	0.57 (0.34 - 0.74)	0.71 ± 0.2*
	0.50	0.87 (0.63 - 0.92)	0.52 (0.46 - 0.58)†	0.39 (0.15 - 0.58)†	0.60 ± 0.1*
	1.00	1.04 (0.87 - 1.61)†	0.51 (0.43 - 0.56)†	0.39 (0.12 - 0.50)†	0.45 ± 0.1*
	5.00	1.78 (1.07 - 2.05)†	0.42 (0.32 - 0.51)†	0.36 (0.09 - 0.49)†	0.21 ± 0.0*

[a]Determined using non-linear regression with variable slope (4 parameter) analysis; [b]Maximal agonist effect $BRET_{Eff}$; [c]Hill coefficient; [d]Relative Activity, as determined in eq. 2.

†Significantly different from the DMSO vehicle as determined by non-overlapping CI.

*$P < 0.01$ compared to DMSO vehicle as determined by one-way ANOVA followed by Dunnett's multiple comparison.

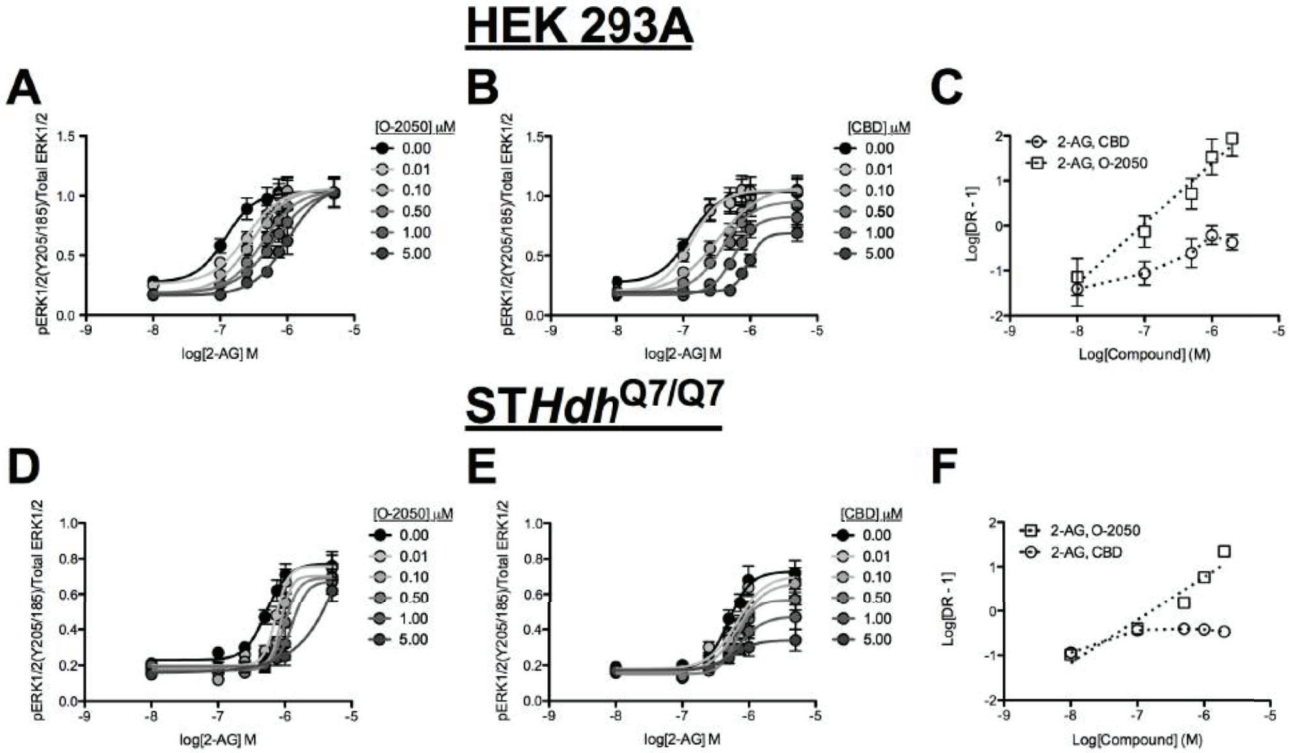

Figure 5-5. CBD was a NAM of CB_1-dependent ERK1/2 phosphorylation following 2-AG treatment. HEK293A cell expressing CB_1-GFP[2] **(A-C**) and ST*Hdh*$^{Q7/Q7}$ cells **(D-F)** were treated with 2-AG ± O-2050 or CBD and total and phosphorylated ERK1/2 levels were determined using In-cell™ western. CRCs were fit using Gaddum/Schild EC_{50} shift **(A,D)** and operational model of allosterism **(B,E)** non-linear regression models. **C,F)** Schild regressions were plotted as the logarithm of 2-AG or THC concentration against the logarithm of the concentration-response at $EC_{50} - 1$. $N = 6$.

Therefore, CBD behaved as a NAM in these cell lines for arrestin2 recruitment, PLCβ3 and ERK1/2 phosphorylation.

5.3.5. OPERATIONAL MODELING OF ALLOSTERISM

While O-2050 acted as a competitive orthosteric antagonist, CBD acted as a NAM in arrestin2, PLCβ3, and ERK1/2 assays. Global curve fitting of data to the operational model of allosterism was used to assess the NAM activity of CBD. Data were fit to this model by constraining E_{max} and n (Hill slope) to 1.0 and 1.0, respectively. In this way, the allosteric co-operativity coefficient for ligand binding (α) was found to be less than 1.0 (0.37), with no significant difference between cell lines, orthosteric ligands, or assays (Table 5-5) indicating that CBD acted as a NAM to reduce the binding of THC and 2-AG. CBD also reduced the efficacy of the orthosteric ligand because β (co-operativity coefficient for ligand efficacy) was consistently less than 1 (0.44). Based on the estimated value of orthosteric ligand affinity (K_A) and the ability of the orthosteric ligand to activate CB_1 (τ_A), 2-AG (241 nM) and THC (97 nM) were able to directly activate CB_1 within a similar concentration range to previously published data (reviewed in Pertwee, 2008). CBD did not display agonist activity, as shown by the estimate of τ_B, but exhibited a greater estimated affinity (304 nM) for CB_1 (K_B) than would be predicted for the orthosteric site (reviewed in Pertwee, 2008). β and αβ can be used to assess ligand bias (functional selectivity) for allosteric modulators (Keov *et al*., 2011). No differences in β and αβ were observed in HEK293A cells in all assays (Table 5-5). In ST*Hdh*$^{Q7/Q7}$ cells, β and αβ were reduced in PLCβ3 assays compared to arrestin2 recruitment and ERK assays, indicating that CBD was a functionally selective inhibitor of arrestin2 and ERK1/2 pathways (Table 5-5). Overall, CBD was a NAM of orthosteric ligand binding and efficacy at CB_1.

5.3.6. NEGATIVE ALLOSTERIC MODULATION OF ANTAGONIST BINDING

If CBD reduced the binding of orthosteric agonists to CB_1, as predicted by the operational model of allosterism, then CBD should also reduce the binding of CB_1 inverse agonists and antagonists. In order to test this hypothesis, ST*Hdh*$^{Q7/Q7}$ cells were treated with the

Table 5-4. Effect of CBD on ERK activation in HEK293A and ST*Hdh*$^{Q7/Q7}$ cells.

Data are mean ±S.E.M. or with 95% CI of six independent experiments.

Agonist	[CBD] (μM)	EC_{50} μM (95% CI)[a]	E_{max} (95% CI)[a,b]	n (95% CI)[a,c]	RA ± S.E.M.[d]
HEK293A					
2-AG	*DMSO*	0.12 (0.07 - 0.22)	1.03 (0.89 - 1.17)	1.00 (0.97 - 1.07)	1.00 ± 0.0
	0.01	0.13 (0.08 - 0.22)	1.05 (0.92 - 1.18)	0.91 (0.82 - 1.03)	0.96 ± 0.09
	0.10	0.33 (0.19 - 0.47)	1.09 (0.90 - 1.28)	0.63 (0.57 - 0.72)†	0.40 ± 0.06*
	0.50	0.39 (0.26 - 0.58)†	0.96 (0.82 - 1.10)	0.39 (0.29 - 0.58)†	0.30 ± 0.05*
	1.00	0.57 (0.45 - 0.72)†	0.83 (0.73 - 0.93)	0.27 (0.17 - 0.39)†	0.17 ± 0.05*
	5.00	0.95 (0.81 - 1.11)†	0.69 (0.61 - 0.76)†	0.19 (0.11 - 0.30)†	0.09 ± 0.02*
ST*Hdh*$^{Q7/Q7}$					
2-AG	*DMSO*	0.50 (0.37 - 0.68)	0.73 (0.63 - 0.83)	1.00 (0.91 - 1.22)	1.00 ± 0.0
	0.01	0.66 (0.44 - 0.99)	0.70 (0.58 - 0.83)	0.78 (0.57 - 0.83)†	0.74 ± 0.2*
	0.10	0.69 (0.48 - 0.95)	0.67 (0.56 - 0.77)	0.79 (0.56 - 0.77)†	0.67 ± 0.1*
	0.50	0.77 (0.52 - 0.87)	0.57 (0.48 - 0.65)	0.73 (0.63 - 0.87)†	0.56 ± 0.1*
	1.00	0.84 (0.69 - 1.21)†	0.47 (0.37 - 0.57)†	0.70 (0.46 - 0.81)†	0.44 ± 0.1*
	5.00	1.27 (0.81 - 1.47)†	0.33 (0.26 - 0.41)†	0.57 (0.27 - 0.72)†	0.30 ± 0.1*

[a]Determined using non-linear regression with variable slope (4 parameter) analysis; [b]Maximal agonist effect $BRET_{Eff}$; [c]Hill coefficient; [d]Relative Activity, as determined in eq. 2.

†Significantly different from the DMSO vehicle as determined by non-overlapping CI.

*$P < 0.01$ compared to DMSO vehicle as determined by one-way ANOVA followed by Dunnett's multiple comparison.

Table 5-5. Operational model analysis of CBD at CB_1 in the presence of THC or 2-AG.

Data are mean ±S.E.M. or with 95% CI of six independent experiments.

HEK293A

	$BRET_{Eff}$		pPLCβ3		pERK1/2
Agonist	THC	2-AG	THC	2-AG	2-AG
Modulator	CBD	CBD	CBD	CBD	CBD
-logα	0.47 ± 0.06	0.53 ± 0.07	0.47 ± 0.12	0.57 ± 0.11	0.48 ± 0.13
-logβ	0.25 ± 0.09	0.41 ± 0.03	0.28 ± 0.07	0.42 ± 0.09	0.30 ± 0.07
$log\tau_A$[a]	1.14 ± 0.26	1.04 ± 0.19	1.01 ± 0.20	1.12 ± 0.18	1.02 ± 0.12
$log\tau_B$[b]	0.21 ± 0.04	0.13 ± 0.05	0.25 ± 0.10	0.15 ± 0.06	0.06 ± 0.04
K_A[a] (nM)	128 (56.7 - 159)	262 (197 - 308)	91.9 (82.2 - 103)	255 (176 - 328)	236 (195 - 275)
K_B[b] (nM)	270 (148 - 349)	352 (272 - 409)	268 (197 - 292)	326 (279 - 382)	318 (255 - 369)
αβ	0.19	0.11	0.18	0.10	0.17

ST*Hdh*$^{Q7/Q7}$

	$BRET_{Eff}$		pPLCβ3		pERK1/2
Agonist	THC	2-AG	THC	2-AG	2-AG
Modulator	CBD	CBD	CBD	CBD	CBD
-logα	0.31 ± 0.09	0.23 ± 0.12	0.46 ± 0.18	0.38 ± 0.15	0.42 ± 0.13
-logβ	0.25 ± 0.08	0.33 ± 0.09	0.60 ± 0.12*	0.58 ± 0.09*	0.27 ± 0.06
$log\tau_A$[a]	0.78 ± 0.21	0.81 ± 0.17	0.81 ± 0.17	0.79 ± 0.12	0.74 ± 0.18
$log\tau_B$[b]	0.31 ± 0.11	0.21 ± 0.09	0.29 ± 0.12	0.18 ± 0.07	0.19 ± 0.05
K_A[a] (nM)	95.7 (58.6 - 118)	237 (181 - 294)	72.3 (59.1 - 107)	255 (178 - 318)	198 (137 - 238)
K_B[b] (nM)	278 (148.4 - 335)	333 (291 - 376)	259 (194 - 280)	315 (281 - 362)	329 (241 - 346)
αβ	0.28	0.28	0.09	0.11	0.20

All values estimated using the operational model of allosterism described in eq. 1. [a]$log\tau_A$ and K_A determined for THC or 2-AG; [b]$log\tau_B$ and K_B determined for CBD.

*$P < 0.01$ compared to $BRET_{Eff}$ with the same agonist as determined by one-way ANOVA followed by Dunnett's multiple comparison.

CB_1 inverse agonist AM251 (Pertwee, 2005) and CBD and ERK phosphorylation was measured (Fig. 5-6A). CBD treatment resulted in a rightward and upward shift in the AM251 CRC (Fig. 5-6A). CBD CRCs were best fit with the operational model of allosterism. To further test our hypothesis, ST*Hdh*$^{Q7/Q7}$ cells were treated with 2-AG and 500 nM O-2050, 500 nM CBD, or 500 nM O-2050 *and* 500 nM CBD (Fig. 5-6B). Treatment of ST*Hdh*$^{Q7/Q7}$ cells with 2-AG, O-2050 and CBD produced a CRC that was shifted right and down relative to 2-AG alone and left relative to 2-AG and O-2050, indicating that CBD had reduced the competitive antagonistic activity of O-2050 and reduced the efficacy of 2-AG (Fig. 5-6B). Therefore, CBD was a NAM of orthosteric ligand binding as demonstrated by the reduced potency and efficacy of the CB_1 inverse agonist AM251 and the antagonist O-2050.

5.3.7. MUTAGENESIS OF CB_1

The CB_1 splice variants CB_{1A} and CB_{1B} differ in the first 89 amino acids of the *N*-terminus relative to CB_1. We compared the allosteric activity of CBD in ST*Hdh*$^{Q7/Q7}$ cells expressing CB_1, CB_{1A} and CB_{1B} using $BRET^2$. $BRET_{Eff}$ did not differ between CB_1-GFP^2, CB_{1A}-GFP^2, and CB_{1B}-GFP^2-expressing cells treated with 0.01 – 5.00 μM THC or 2-AG ± 0.5 μM O-2050 or 5.00 μM CBD (Fig. 5-7A,B). Therefore, the allosteric activity of CB_1 is not contained within amino acids 1 – 89 that differ between CB_1, CB_{1A}, and CB_{1B}, but is associated with the conserved residues common to all three variants (Bagher *et al*., 2013; Fay and Farrens, 2013). Fay and Farrens (2013) previously reported that Cys-98 and Cys-107 in the extracellular *N*-terminus of CB_1 contribute to the allosteric activity of Org27569 and PSNCBAM-1. They suggested that these residues form a disulfide bridge, which contribute to allosteric modulator activity of Org27569 and PSNCBAM-1 (Fay and Farrens, 2013). We hypothesized that these residues might similarly influence the allosteric activity of CBD. We wanted to determine whether it was the polarity of Cys-98 and Cys-107 or the formation of a disulfide bridge that contributed to allosteric activity.

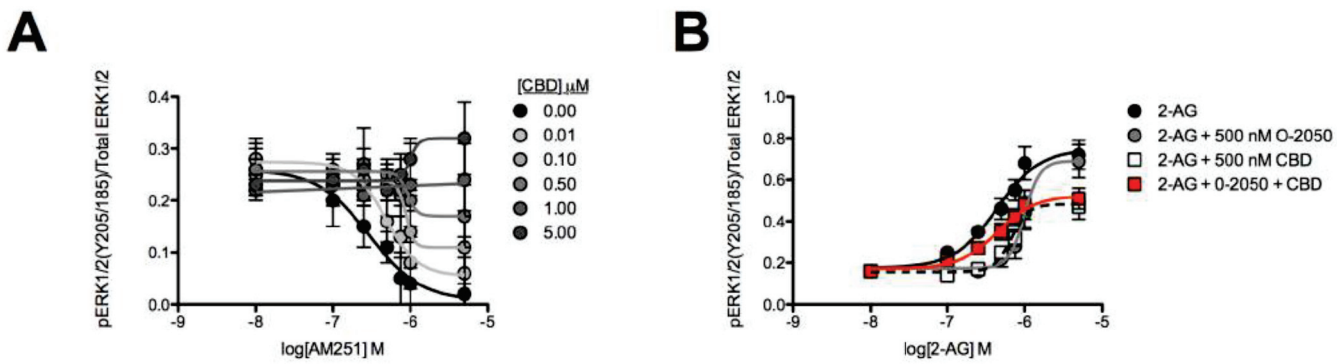

Figure 5-6. CBD was a NAM of AM251-depenendent inverse agonism and O-2050 antagonism. ST*Hdh*$^{Q7/Q7}$ cells were treated with AM251 ± CBD **(A)** or 2-AG ± O-2050, CBD, or O-2050 and CBD **(B)** and total and phosphorylated ERK1/2 levels were determined using In-cell™ western. CRCs were fit using the operational model of allosterism **(A)** or non-linear regression with variable slope (4 parameters) **(B)** models. $N = 6$.

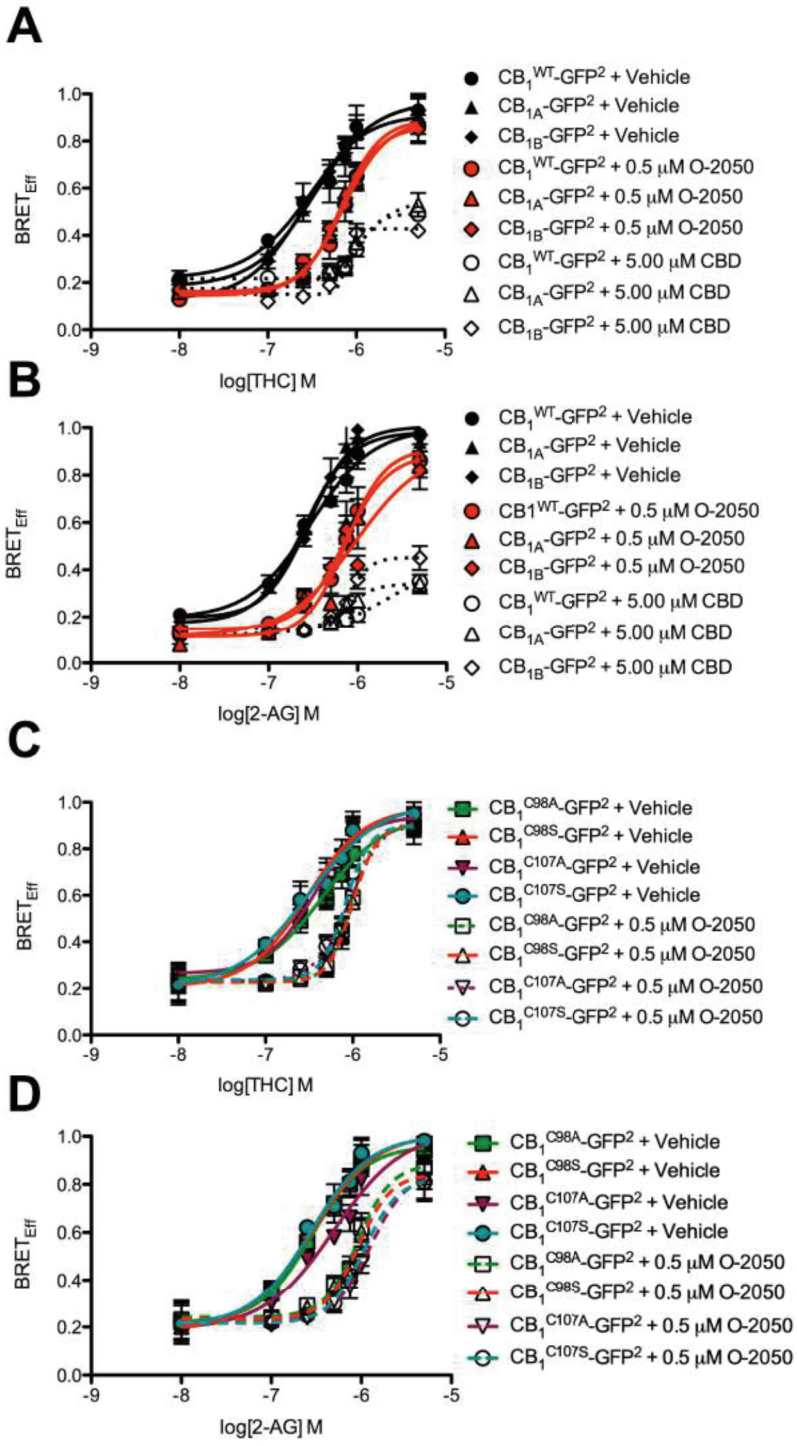

Figure 5-7. The distal N-terminus of CB_1 does not effect the activity of CBD, and Cys-98 and Cys-107 do not affect the activity of orthosteric ligands, at CB_1. ST*Hdh*$^{Q7/Q7}$ cells were transfected with arrestin2-Rluc- and CB_1^{WT}-GFP^2-, CB_{1A}-GFP^2-, CB_{1B}-GFP^2- **(A,B)**, CB_1^{C98A}-GFP^2-, and CB_1^{C98S}-GFP^2-, CB_1^{C107A}-GFP^2-, and CB_1^{C107S}-GFP^2-containing plasmids **(C,D)** and $BRET^2$ was measured 30 min after treatment with THC **(A,C)** or 2-AG **(B,D)** ± O-2050 or CBD. CRCs were fit using non-linear regression with variable slope (4 parameter). $N = 4$.

Each of these residues was individually mutagenized to Ala or Ser in the CB_1-GFP^2 plasmid (CB_1^{WT}-GFP^2, CB_1^{C98A}-GFP^2, CB_1^{C107A}-GFP^2, CB_1^{C98S}-GFP^2, CB_1^{C107S}-GFP^2) and transfected with arrestin2-Rluc into ST*Hdh*$^{Q7/Q7}$ cells. Treatment of CB_1^{WT}-, CB_1^{C98A}-, CB_1^{C107A}-, CB_1^{C98S}-, or CB_1^{C107S}-expressing cells with 0.01 – 5.00 μM THC or 2-AG alone resulted in a response that did not differ between CB_1 mutants or between THC and 2-AG treatments (Fig. 5-8A,B). Further, the competitive antagonistic activity of 0.50 μM O-2050 was not different in CB_1 mutant expressing-cells treated with 0.01 – 5.00 μM THC or 2-AG (Fig. 5-7C,D). Together, these data indicated that mutation of Cys-98 or Cys-107 did not alter CB_1 response to orthosteric ligand. Treatment of CB_1^{WT}-expressing cells with 0.01 – 5.00 μM THC or 2-AG and 5.00 μM CBD resulted in a rightward and downward shift in the $BRET_{Eff}$ CRCs (Fig. 5-8A,B). Similarly, treatment of CB_1^{C98A}- or CB_1^{C107A}-expressing cells with 0.01 – 5.00 μM THC or 2-AG and 5.00 μM CBD resulted in a rightward and downward shift in the $BRET_{Eff}$ CRCs compared to vehicle treatment (Table 5-6). The magnitude of the rightward and downward shift was less pronounced in CB_1^{C98A}- and CB_1^{C107A}- compared to CB_1^{WT}-, CB_1^{C98S}-, and CB_1^{C107S}-expressing cells treated with CBD (Table 5-6; Fig. 5-8A,B). The presence of a polar Ser or Cys at positions 98 or 107 was sufficient to recover the wild-type response to CBD. Therefore, the allosteric activity of CBD at CB_1 depended in part on the presence of polar residues at positions 98 and 107, independent of a disulfide bridge. Additional residues common to CB_1, CB_{1A}, and CB_{1B} may also contribute to the allosteric effect of CBD (Fig. 5-7C).

5.4. DISCUSSION

5.4.1. CANNABIDIOL BEHAVES AS A NEGATIVE ALLOSTERIC MODULATOR OF CB_1

In this study, we provide *in vitro* evidence for the non-competitive negative allosteric modulation of CB_1 by CBD. CBD treatment resulted in negative co-operativity ($\alpha < 1$) and reduced orthosteric ligand (THC and 2-AG) efficacy ($\beta < 1$) at concentrations lower than the predicted affinity of CBD for the orthosteric binding site at CB_1 [304 nM (this study) *versus* > 4 μM (reviewed in Pertwee, 2008)]. As a NAM of CB_1 orthosteric ligand-dependent effects, CBD

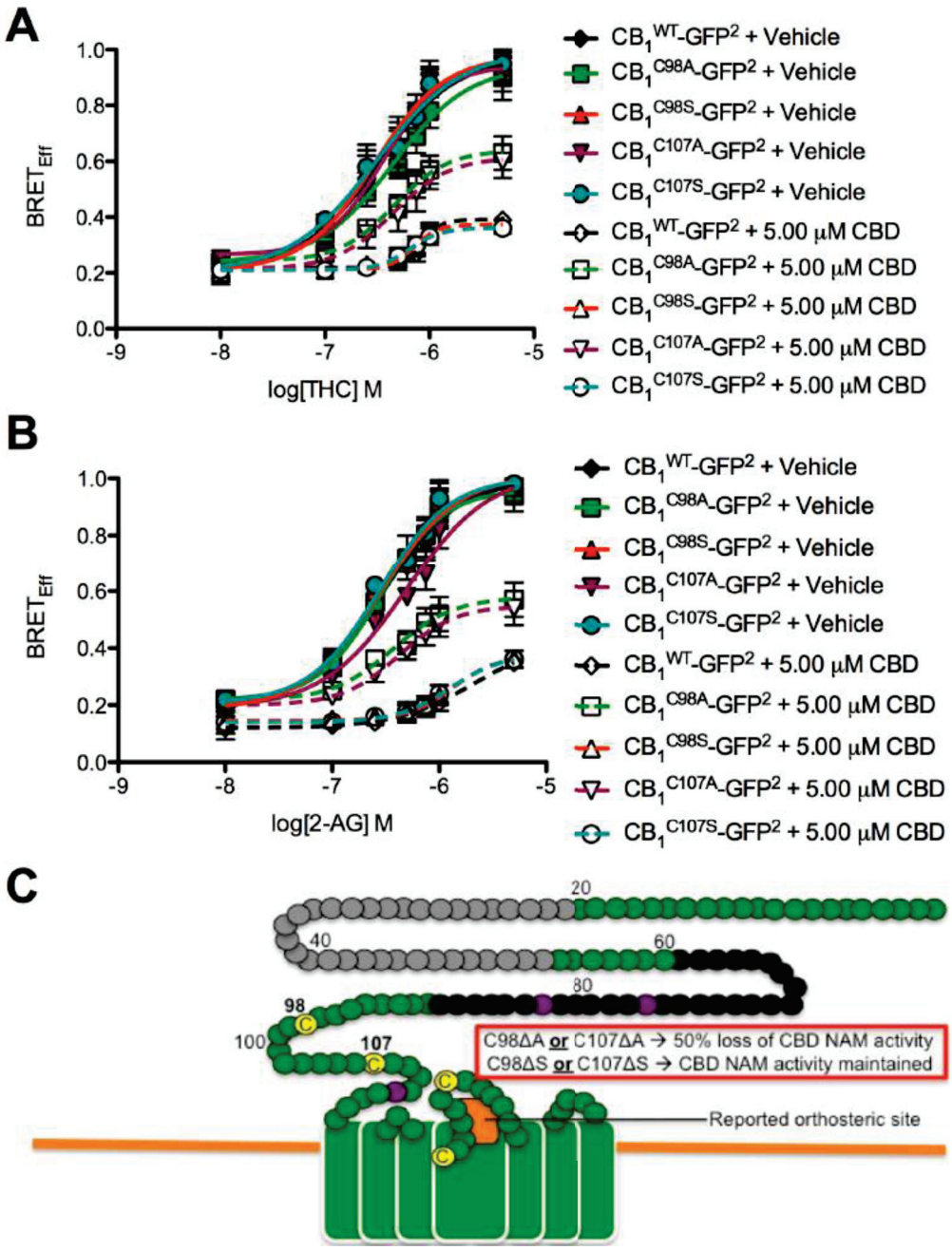

Figure 5-8. Cys-98 and Cys-107 coordinate the negative allosteric modulatory activity of CBD at CB_1. **A,B)** ST*Hdh*$^{Q7/Q7}$ cells were transfected with arrestin2-Rluc- and CB_1^{C98A}-GFP^2-, and CB_1^{C98S}-GFP^2-, CB_1^{C107A}-GFP^2-, and CB_1^{C107S}-GFP^2-containing plasmids and $BRET^2$ was measured 30 min after treatment with THC **(A)** or 2-AG **(B)** ± CBD. CRCs were fit using non-linear regression with variable slope (4 parameter) $N = 4$. **C)** Schematic of the membrane-proximal region of CB_1 summarizing data presented in this figure (adapted from Fay and Farrens, 2013). Our observations and previous studies suggest that Cys-98 and Cys-107 contribute to CB_1 allosterism, while the orthosteric site is near the second extracellular loop (orange box). In this diagram green represents extracellular surface of CB_1. Black circles represent residues unique to the *N*-terminus of CB_{1A}. Grey circles represent residues unique to the *N*-terminus of CB_{1B}. Yellow circles represent Cys. Purple circles represent *N*-glycosylated residues. Residues mutated in this study are marked in bold. Non-bold numbers indicate amino acid number relative to *N*-terminus.

Table 5-6. Effect of CBD on Arrestin-2 recruitment to mutant CB_1 in ST*Hdh*$^{Q7/Q7}$ cells.

Data are mean with 95% CI of four independent experiments.

Agonist	Receptor	Modulator	EC_{50} μM (95% CI)[a]	E_{max} (95% CI)[a,b]
THC	CB_1^{WT}	*DMSO*	0.34 (0.21 - 0.46)	0.96 (0.75 - 1.01)
		5.00 μM CBD	0.91 (0.70 - 1.17)†	0.30 (0.24 - 0.49)†
	CB_1^{C98A}	*DMSO*	0.35 (0.26 - 0.57)	0.94 (0.78 - 1.11)
		5.00 μM CBD	0.55 (0.37 - 0.67)^	0.64 (0.54 - 0.74)†^
	CB_1^{C107A}	*DMSO*	0.36 (0.23 - 0.46)	0.94 (0.82 - 1.07)
		5.00 μM CBD	0.56 (0.48 - 0.67)†^	0.61 (0.54 - 0.73)†^
	CB_1^{C98S}	*DMSO*	0.30 (0.17 - 0.41)	0.98 (0.83 - 1.12)
		5.00 μM CBD	0.97 (0.79 - 1.10)†	0.37 (0.32 - 0.42)†
	CB_1^{C107S}	*DMSO*	0.31 (0.16 - 0.48)	1.00 (0.82 - 1.18)
		5.00 μM CBD	0.91 (0.80 - 1.02)†	0.36 (0.31 - 0.41)†
2-AG	CB_1^{WT}	*DMSO*	0.64 (0.56 - 0.73)	0.82 (0.74 - 0.90)
		5.00 μM CBD	2.20 (1.95 - 3.55)†	0.44 (0.25 - 0.57)†
	CB_1^{C98A}	*DMSO*	0.62 (0.54 - 0.78)	0.96 (0.84 - 1.09)
		5.00 μM CBD	1.37 (1.09 - 1.59)†^	0.67 (0.59 - 0.71)†^
	CB_1^{C107A}	*DMSO*	0.59 (0.43 - 0.69)	1.03 (0.89 - 1.18)
		5.00 μM CBD	1.42 (1.23 - 1.64)†^	0.66 (0.58 - 0.72)†^
	CB_1^{C98S}	*DMSO*	0.68 (0.59 - 0.74)	1.01 (0.90 - 1.12)
		5.00 μM CBD	2.32 (1.97 - 2.57)†	0.37 (0.24 - 0.50)†
	CB_1^{C107S}	*DMSO*	0.67 (0.59 - 0.79)	1.00 (0.90 - 1.11)
		5.00 μM CBD	2.28 (2.14 - 2.40)†	0.38 (0.24 - 0.52)†

†Significantly different from DMSO vehicle within receptor group as determined by non-overlapping CI.
^Significantly different from response to 5.00 μM CBD and DMSO vehicle in CB_1^{WT} vehicle as determined by non-overlapping CI.

reduced both G protein-dependent signaling and arrestin2 recruitment, which explains both the diminished signaling and diminished BRET observed between CB_1-GFP^2 and arrestin2-Rluc. In contrast to the NAM activity of CBD, and as shown previously, O-2050 acted as a competitive orthosteric antagonist of CB_1 (Canals and Milligan, 2008; Higuchi *et al.,* 2010; Hudson *et al.*, 2010; Ferreira *et al.*, 2012; Anderson *et al*., 2013; Laprairie *et al*., 2014a) rather than a partial agonist (Wiley *et al*., 2011, 2012). To directly test the hypothesis that a disulfide bridge between Cys-98 and Cys-107 regulates the activity of CB_1 allosteric modulators, these residues were mutagenized to either Ala or Ser (Fay and Farrens, 2013). Mutation of these residues to Ala (non-polar) decreased the NAM activity of CBD at CB_1, but not the activity of THC, 2-AG, or O-2050. The NAM activity of CBD depended upon the presence of polar (Ser or Cys) residues at CB_1 positions 98 and 107, rather than a disulfide bridge, because replacement of either Cys residue with Ser did not change CBD NAM activity. These findings suggest that the *N*-terminal, extracellular residues Cys-98 and Cys-107 either partially regulate the allosteric activity of CBD at CB_1 directly, or the communication between the allosteric and orthosteric sites of CB_1.

Allosteric modulators are probe-dependent, that is, the activity of the allosteric modulator depends on the orthosteric probe being used (reviewed in Christopoulos and Kenakin, 2002). Org27569 and PSNCBAM-1 both display probe-dependence because they are more potent modulators of CP55,940 binding and CP55,940-mediated CB_1 activation than WIN55,212-2 binding and WIN55,212-2-mediated CB_1 activation (Baillie *et al*., 2013). 2-AG was chosen as an orthosteric probe in this study because it is the most abundant endocannabinoid in the brain, and therefore 2-AG would be the predominant endogenous orthosteric ligand if exogenous CBD was administered (Sugiura *et al*., 1999). THC and CBD are the most abundant phytocannabinoids in marijuana and are used together in varying ratios both medicinally and recreationally in marijuana (Thomas *et al*., 2007). Therefore, THC was selected as an alternative orthosteric probe. In HEK293A cells, CBD did not display probe-dependence (Table 5-2). In ST*Hdh*$^{Q7/Q7}$ cells, CBD was a more potent NAM of CB_1-dependent arrestin2 recruitment when THC was the

orthosteric probe compared to 2-AG (Table 5-2). No probe-dependence was observed for PLCβ3 and ERK1/2 signaling. BRET was used in this study to directly measure the association of CB_1 and arrestin2, which may be a more sensitive method for detecting probe-dependence than In-cell™ western assays that measured PLCβ3 or ERK1/2.

ST*Hdh*$^{Q7/Q7}$ cells express several effector proteins that CBD has been shown to modulate, including CB_1, $5HT_{1A}$, GPR55, μ-opioid receptors, PPARγ and FAAH, suggesting that CBD could have acted independently of CB_1 (Trettel *et al*., 2000; Lee *et al*., 2007; Laprairie *et al*., 2014a). However, the NAM activity of CBD was also observed in HEK293A cells that heterologously express CB_1, but do not express $5HT_{1A}$, GPR55, and μ-opioid receptors demonstrating that these effectors did not alter the actions of CBD (Ryberg *et al*., 2007). HEK293A cells do express PPARγ, but modulation of this nuclear receptor would not affect arrestin and G protein assays used over the duration of these experiments. Importantly, the NAM activity of CBD at CB_1 was dependent on the cannabinoid agonists 2-AG and THC, suggesting that CBD was acting at CB_1. FAAH inhibition would have enhanced, not diminished, cannabinoid efficacy, which was not observed here. Therefore, the NAM activity of CBD at CB_1 documented in this study adds to the mechanisms of action through which chronic CBD mediates its effects *in vivo*.

No significant signaling bias was observed for CBD in HEK293A cells because allosteric ligand efficacy (β) and co-operativity (αβ) were not different among arrestin, PLCβ3, and ERK1/2 assays (Table 5-5). In ST*Hdh*$^{Q7/Q7}$ cells, we observed that CBD was biased for PLCβ3 signaling compared to ERK signaling and arrestin2 recruitment as indicated by reduced β and αβ values (Table 5-5). Previous studies have reported that Org27569 is also biased against ERK and arrestin signaling (Ahn *et al*., 2012, 2013; Baillie *et al*., 2013). The observation that CBD-dependent bias was observed in ST*Hdh*$^{Q7/Q7}$ cells compared to HEK293A cells suggests that heterologous expression systems may underrepresent ligand bias (Ahn *et al*., 2013; Baillie *et al*., 2013).

5.4.2. CANNABIDIOL COMPARED TO OTHER NEGATIVE ALLOSTERIC MODULATORS OF CB_1

Based on the functional effects of CBD on PLCβ3, ERK, arrestin2 recruitment and CB_1 internalization, CBD behaved like the well-characterized allosteric modulators Org27569 and PSNCBAM-1 *in vitro* (Horswill *et al*., 2007; Cawston *et al*., 2013). At higher concentrations (> 2 μM), CBD was able to enhance PLCβ3 and ERK phosphorylation, and arrestin2 recruitment, as well as limit CB_1 internalization, suggesting that CBD may behave as a weak partial agonist at high concentrations, as observed elsewhere (reviewed in Mechoulam *et al*., 2007; McPartland *et al*., 2014). In this study, the primary affect of CBD at CB_1 was negative allosteric modulation at concentrations below 1 μM. The studies by Price *et al*. (2005) and Baillie *et al.* (2013) demonstrated that Org27569 and PSNCBAM-1 paradoxically reduce orthosteric ligand efficacy and potency while increasing orthosteric ligand binding affinity and duration. It is thought that, in general, increased ligand binding results in rapid desensitization of receptors (Price *et al.*, 2005; Ahn *et al*., 2013). In this study, we did not directly test receptor desensitization, or duration of ligand binding. We did, however, estimate ligand co-operativity and found that CBD, unlike Org27569 and PSNCBAM-1, displayed negative co-operativity for ligand binding ($\alpha < 1$) (Price *et al.*, 2005; Ahn *et al*., 2013). Org27569 and PSNCBAM-1 increase the CB_1 receptor pool at the cell surface, and in doing so may potentiate CB_1 signaling (Cawston *et al*., 2013). *In vivo*, Org27569 reduces food intake similar to the CB_1 inverse agonist rimonabant (Gamage *et al*., 2014). However, the *in vivo* actions of Org27569 are CB_1-independent, suggesting that the *in vitro* pharmacology of Org27569 does not correlate with *in vivo* observations (Gamage *et al*., 2014). Like Org27569, CBD may mediate a subset of its *in vivo* actions through non-CB_1 targets (Campos *et al*., 2012). For example, the anxiolytic and antidepressant actions of CBD may be $5HT_{1A}$-dependent, while the antipsychotic activity of CBD may be TRPV1-dependent (Bisogno *et al*., 2001; Russo *et al*., 2005; Ryberg *et al*., 2007; Campos *et al*., 2012). Regardless of whether CBD has alternative targets *in vivo*, the work shown here demonstrates that CBD can alter the

activity of common endo- and phytocannabinoids at CB_1 and this action is likely to be therapeutically important.

5.4.3. CONCLUSIONS

In this *in vitro* study, the NAM activity of the well-known phytocannabinoid, CBD, was characterized for the first time. The data presented here support the hypothesis that CBD binds to a distinct, allosteric site on CB_1 that is functionally distinct from the orthosteric site for 2-AG and THC. Using an operational model of allosteric modulation to fit the data (Keov *et al*., 2011), we observed that CBD reduced the potency and efficacy of THC and 2-AG at concentrations lower than the predicted affinity of CBD for the orthosteric site of CB_1. Future *in vivo* studies should test whether the NAM activity of CBD explains the 'antagonist of agonists' effects reported elsewhere (Thomas *et al*., 2007). Indeed, the NAM activity of CBD may explain its utility as an anti-psychotic, anti-epileptic and anti-depressant. In conclusion, the identification of CBD as a CB_1 NAM provides new insights into the compound's medicinal value, and may be useful in the development of novel, CB_1-selective synthetic allosteric modulators or drug combinations.

CHAPTER 6

CHARACTERIZATION OF THE NOVEL POSITIVE ALLOSTERIC MODULATOR OF THE TYPE 1 CANNABINOID RECEPTOR GAT211, AND ITS ENANTIOMERS GAT228 AND GAT229

Copyright statement

Portions of this chapter are being prepared for submission in: Laprairie RB, Cascio MG, Kulkarni PM, Kelly MEM, Pertwee RG, Straiker A, Denovan-Wright EM, Thakur GA (2016). Characterization of the novel positive allosteric modulator of the type 1 cannabinoid receptor GAT211, and its enantiomers GAT228 and GAT229. *J Biol* Chem. **In preparation.** The manuscript has been modified to meet formatting requirements.

Contribution statement

The manuscript used as the basis for this chapter was written with guidance from Drs. Eileen Denovan-Wright, Roger Pertwee, and Ganesh Thakur. Data were collected by myself and Drs. Maria Cascio and Alex Straiker. Critical reagents were provided by Pushkar Kulkarni and Drs. Melanie Kelly and Ganesh Thakur.

6.1. INTRODUCTION

The type 1 cannabinoid receptor (CB_1) is the most abundant G protein-coupled receptor (GPCR) in the central nervous system and is expressed in many peripheral tissues as well (Ross, 2007). CB_1 is activated by the endogenous ligands anandamide (AEA) and 2-arachdonoylglycerol (2-AG), as well as plant-derived cannabinoids, such as Δ^9-tetrahydrocannabinol, and synthetic cannabinoids (Pertwee, 2008). Activation of CB_1 directly regulates neurotransmission, synapse formation, nociception, metabolism, and reproduction, and is implicated in the diverse pathologies associated with these functions. Given the involvement of CB_1 in multiple pathological conditions, orthosteric agonists and antagonists of CB_1 have been developed for the treatment of neurological disorders, neurodegenerative diseases, chronic pain management, addiction, and obesity (Pertwee, 2008; Piscitelli *et al*., 2012). Unfortunately, the clinical utility of these compounds is limited by their psychotropic side effects (Pertwee, 2008; Piscitelli *et al*., 2012).

Allosteric modulators of CB_1 may have greater therapeutic potential than existing orthosteric ligands because allosteric modulators lack intrinsic efficacy in the absence of an orthosteric ligand, and are therefore unlikely to produce the supraphysiological activation, desensitization, or downregulation of CB_1 associated with psychotropic side effects (Ross, 2007; Wootten *et al*, 2013). The binding of an allosteric modulator induces a conformational change in the receptor that affects the receptor's affinity for, and efficacy of activation by, the orthosteric ligand. Allosteric modulators that enhance orthosteric ligand binding and receptor activation are referred to as positive allosteric modulators (PAM), whereas allosteric modulators that reduce orthosteric ligand binding and receptor activation are referred to as negative allosteric modulators (NAM) (Wootten *et al*., 2013). The known CB_1 allosteric modulators Org27569 and PSNCBAM-1 paradoxically enhance the affinity and reduce the efficacy of orthosteric cannabinoid ligands, such as CP55940 (Price *et al*., 2005; Horswill *et al*., 2007; Wang *et al*., 2011; Ahn *et al*., 2013; Cawston *et al*., 2013). Org27569 and PSNCBAM-1 also display some inverse agonist activity *in*

vitro, suggesting these compounds are not pure allosteric ligands (Wang *et al*., 2011; Ahn *et al*., 2013). Another CB_1 allosteric modulator, lipoxin A_4, has been shown to act as a moderate PAM of orthosteric ligand signaling (Pamplona *et al*., 2012). Given the potential therapeutic utility of allosteric modulators, there is increasing demand for the development of novel, efficacious, potent, and CB_1-specific PAMs.

In this study we describe the pharmacological activity of the racemic compound GAT211 (first described as 'compound A' Astra-Zeneca; Adam *et al.*, 2007), and its enantiomers GAT228 (*R*) and GAT229 (*S*), as allosteric modulators of CB_1 orthosteric ligand binding and signaling. The activity of GAT211, GAT228, and GAT229 was evaluated *in vitro* in HEK293A and Neuro2a cells. GAT211 displayed properties consistent with both positive allosteric modulation of CB_1 and partial agonist activity of CB_1 *via* an allosteric site (*i.e.* ago-PAM). Assessment of each of the enantiomers revealed that the allosteric agonist activity was attributed to GAT228 (*R*), while the potent PAM activity was attributed to GAT229 (*S*). Therefore, GAT211, GAT228, and GAT229 represent novel CB_1 PAMs that display enantiomer-specific activity.

6.2. METHODS

6.2.1. DRUGS

GAT211, GAT228, and GAT229 were synthesized and provided by the laboratory of Dr. Ganesh A Thakur (Northeastern University) (Fig. 6-1). 2-AG, AEA, and (-)-*cis*-3-[2-Hydroxy-4-(1,1-dimethylheptyl)phenyl]-*trans*-4-(3-hydroxypropyl)cyclohexanol (CP55,940; CP) were purchased from Tocris Bioscience (Bristol, UK). *Pertussis* toxin (PTx) was purchased from Sigma-Aldrich (Oakville, ON). Cannabinoids were dissolved in DMSO (final concentration of 0.1% in assay media for all assays) and added directly to the media at the concentrations and times indicated. No effects of vehicle alone were observed compared to assay media alone. PTx was dissolved in dH_2O (50 ng/mL) and added directly to the media 24 h prior to cannabinoid treatment.

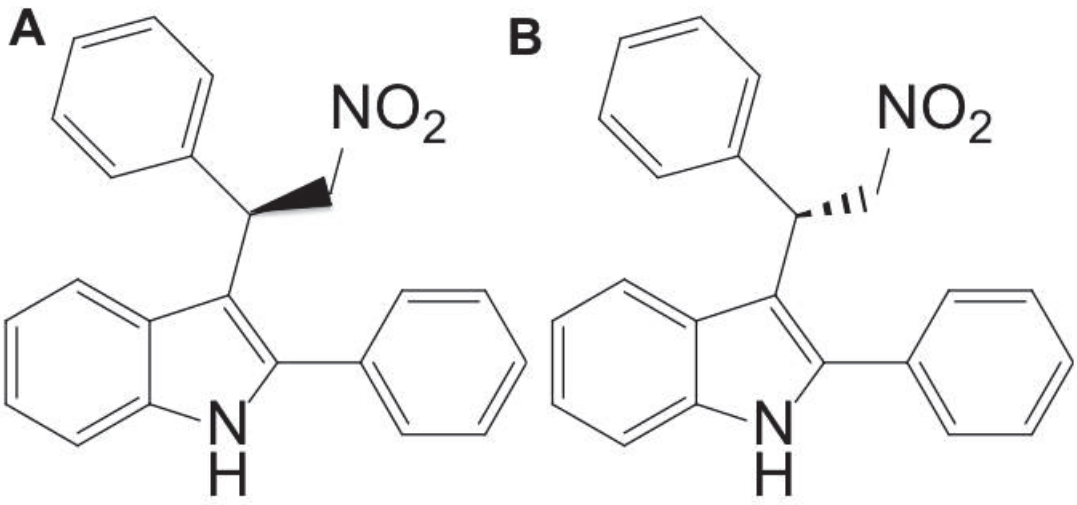

Figure 6-1. Structures of GAT228 (*R*) and GAT228 (*S*). Structures of the GAT211 (racemic) enantiomers **A)** GAT228 and **B)** GAT229.

6.2.2. CELL CULTURE

Human embryonic kidney (HEK) 293A, and Neuro2a cells were from the American Type Culture Collection (ATCC, Manaassas, VI). HEK293A cells do not endogenously express CB_1 (Daigle *et al*., 2008) and were transfected with 400 ng of the hCB_1-GFP^2-expressing plasmid described below using Lipofectamine 2000 according to the manufacturer's instructions (Invitrogen, Burlington, ON, CAN). Cells were maintained at 37°C, 5% CO_2 in DMEM supplemented with 10% FBS and 10^4 U/mL Pen/Strep.

HEK293A Cignal Lenti CRE (HEK-CRE) reporter cells were provided by Dr. Christopher J Sinal (Dalhousie University, NS, CAN). The HEK-CRE cells stably-express the firefly luciferase gene driven by tandem repeat elements of the cAMP transcriptional response element (Qiagen, Toronto, ON, CAN). Thus, luciferase activity is directly proportional to the level cAMP/PKA pathway activation or inhibition. HEK-CRE cells were maintained at 37°C, 5% CO_2 in DMEM supplemented with 10% FBS, 10^4 U/mL Pen/Strep, and 200 µg/mL puromycin.

6.2.3. PLASMIDS

Human CB_1-green fluorescent protein^2 (GFP^2) and arrestin2-*Renilla* luciferase (Rluc) (β-arrestin1) were cloned as fusion proteins at the C-terminus. hCB_1-GFP^2 was generated using the $pGFP^2$-N3 plasmid (PerkinElmer, Waltham, MA) as described previously (Bagher *et al*., 2013). arrestin2-Rluc was generated using the pcDNA3.1 plasmid (PerkinElmer, Waltham, MA) as described previously (Laprairie *et al*., 2014a, 2015a,d). The GFP^2-Rluc fusion construct, and Rluc plasmids have also been described (Bagher *et al*., 2013).

6.2.4. BIOLUMINESCENCE RESONANCE ENERGY TRANSFER^2 (BRET^2)

Direct interactions between CB_1 and arrestin2 were quantified *via* $BRET^2$ (James *et al*., 2006). Cells were transfected with the indicated GFP^2 and Rluc constructs using Lipofectamine 2000, according to the manufacturer's instructions (Invitrogen) and treated as previously described (Laprairie *et al*., 2014a). Briefly, 48 h post-transfection cells were washed twice with cold 0.1 M PBS and suspended in BRET buffer [0.1 M PBS supplemented with glucose (1

mg/mL), benzamidine (10 mg/mL), leupeptin (5 mg/mL) and a trypsin inhibitor (5 mg/mL)]. Cells were treated with compounds as indicated (PerkinElmer) and coelenterazine 400a substrate (50 μM; Biotium, Hayward, CA) was added. Light emissions were measured at 460 nm (Rluc) and 510 nm (GFP^2) using a Luminoskan Ascent plate reader (Thermo Scientific, Waltham, MA), with an integration time of 10 s and a photomultiplier tube voltage of 1200 V. BRET efficiency ($BRET_{Eff}$) was determined using previously described methods (Bagher *et al*., 2013; Laprairie *et al*., 2014a).

6.2.5. IN-CELL™ WESTERNS

Cells were fixed for 10 min at room temperature with 4% paraformaldehyde and washed three times with 0.1 M PBS for 5 min each. Cells were incubated with blocking solution (0.1 M PBS, 20% Odyssey blocking buffer, and 0.1% TritonX-100) for 1 h at room temperature. Cells were incubated with primary antibody solutions directed against pERK1/2(Tyr205/185) (1:200), ERK1/2 (1:200), pPLCβ3(S537) (1:500), PLCβ3 (1:1000), (Santa Cruz Biotechnology) diluted in blocking solution overnight at 4°C. Cells were washed three times with 0.1 M PBS for 5 min each. Cells were incubated in $IR^{CW700dye}$ or $IR^{CW800dye}$ (1:500; Rockland Immunochemicals) and washed three times with 0.1 M PBS for 5 min each. Analyses were conducted using the Odyssey Imaging system and software (version 3.0; Li-Cor).

6.2.6. CAMP LUCIFERASE REPORTER ASSAY

HEK-CRE cells were transfected with CB_1-GFP^2. Twenty-four hours post-transfection cells were cells were dispensed into 96-well plates (10,000 cells/well) and treated as indicated (PerkinElmer) for 24 h. Media was aspirated from cells and cells were lysed with passive lysis buffer for 20 min at room temperature (Promega, Oakville, ON, CAN). Fifty microliters of cell lysate were mixed with luciferase assay reagent (50 μM; Promega, Oakville, ON, CAN) and light emissions were measured at 460 nm using a Luminoskan Ascent plate reader (Thermo Scientific, Waltham, MA), with an integration time of 10 s and a photomultiplier tube voltage of 1200 V. Data are presented as % inhibition relative to orthosteric agonist alone.

6.2.7. DATA ANALYSIS AND CURVE FITTING

Data are presented as the mean ± the standard error of the mean (SEM) or mean and 95% confidence interval, as indicated, from at least 4 independent experiments. All data analysis and curve fitting was carried out using GraphPad Prism (v. 5.0). Concentration-response curves (CRC) were fit with the non-linear regression with variable slope (4 parameters), or operational model of allosterism (eq. 1) (Keov *et al.,* 2011) and are shown in each figure according to the best-fit model (GraphPad Prism v. 5.0). Pharmacological statistics were obtained from non-linear regression models as indicated in figures and tables. Global curve fitting of allosterism data was carried out using the following operational model (Hudson *et al*., 2014; Keov *et* al., 2011; Smith *et al.,* 2011):

$$E= \frac{E_{max}(\tau_A[A](K_B+\alpha\beta[B])+\tau_B[B]K_A)^n}{([A]K_B+K_AK_B+[B]K_A+\alpha[A][B])^n+(\tau_A[A](K_B+\alpha\beta[B])+\tau_B[B]K_A)^n} \quad \textbf{(1)}$$

where E is the measured response, [A] and [B] are the orthosteric and allosteric ligand concentrations, respectively, E_{max} is the maximum system response, α is a measure of the allosteric co-operativity on ligand binding, β is a measure of the allosteric effect on efficacy, K_A and K_B are estimates of the binding of the orthosteric and allosteric ligands, respectively, n represents the Hill slope, and τ_A and τ_B represent the abilities of the orthosteric and allosteric ligands to directly activate the receptor (Smith *et* al., 2011). To fit experimental data to this equation, $\log\tau_A$ and $\log\tau_B$ were constrained to be shared and between 0 and 10 and logα, logβ, and $\log K_A$, $\log K_B$, E_{max}, and n were shared between all datasets.

Statistical analyses were unpaired *t*-test, one- or two-way analysis of variance (ANOVA), as indicated, using GraphPad. *Post-hoc* analyses were performed using Dunnett's multiple comparisons, Bonferroni's or Tukey's tests, as indicated. Homogeneity of variance was confirmed using Bartlett's test.

6.3. RESULTS

6.3.1. RADIOLIGAND BINDING

The effect of GAT211 and the enantiomers GAT228 and GAT229 on CB_1 orthosteric ligand dissociation binding was assessed in the membranes of CHO cells stably-expressing hCB_1 by our collaborators at the University of Aberdeen: Drs. Roger Pertwee and Maria Cascio. GAT211 (1 μM) increased the $t_{½}$ for [^{3}H]CP dissociation from CHO cell membranes [$t_{½}$ DMSO: 6.16 (3.99-13.09) min; $t_{½}$ 1 μM GAT211: 22.38 (14.99-44.16) min; non-overlapping 95% CI]. Increased binding time (*i.e.* a reduced rate of dissociation) is consistent with the allosteric enhancement of orthosteric ligand binding expected for PAMs. GAT211 enhanced [^{3}H]CP binding at 100 nM and 1 μM in CHO cells expressing hCB_1. In contrast, GAT228 only enhanced [^{3}H]CP binding at 1 μM in CHO cells expressing hCB_1, but reduced [^{3}H]CP binding at 10 μM. GAT229 enhanced [^{3}H]CP binding from 1 nM – 10 μM in CHO cells expressing hCB_1, to a greater degree than either GAT211 or GAT228. GAT211-dependent displacement of [^{3}H]CP was also assessed in CHO cells expressing hCB_2. [^{3}H]CP binding at hCB_2 was only reduced by 30% at 10 μM GAT211, and not at lower concentrations. These data from our collaborators are consistent with the racemic compound GAT211 acting as a CB_1-specific PAM of orthosteric ligand binding. While GAT228 enhanced orthosteric ligand binding at some concentrations, it also displaced the orthosteric ligand at higher concentrations. In contrast, GAT229 behaved as a pure PAM of orthosteric ligand binding and enhanced [^{3}H]CP binding more than GAT211 or GAT228.

6.3.2. OPERATIONAL MODEL OF ALLOSTERISM

GAT211, GAT228, and GAT229 each enhanced the binding of orthosteric ligands to hCB_1. In order to determine how GAT211 and its enantiomers modulated hCB_1-dependent signaling, HEK293A cells were transfected with hCB_1-GFP^2 and arrestin2-Rluc, treated with 1 nM – 10 μM CP ± 1 nM – 10 μM GAT211, GAT228, or GAT229 and arrestin2 recruitment to hCB_1 was quantified *via* BRET^2 (Fig. 6-2A-C). The observed concentration-response data were

fit and analyzed using the operational model of allosterism (eq.1), which allowed us to estimate the affinity of these compounds, as well as their modulation of CP potency and efficacy. GAT211 enhanced the potency (α) and efficacy (β) of CP-dependent arrestin2 recruitment in a concentration-dependent manner with an estimated affinity of 7.76 nM, but displayed negligible intrinsic efficacy (τ_B) (Table 6-1; Fig. 6-2A). GAT229 was a more potent (α) and efficacious (β) enhancer of CP-dependent arrestin2 recruitment than GAT211, with an estimated affinity of 7.932 nM and negligible intrinsic efficacy (τ_B) (Table 6-1; Fig. 6-2C). In contrast, GAT228 reduced the potency (α) and efficacy (β) of CP-dependent arrestin2 recruitment in a concentration-dependent manner with an estimated affinity of 6.68 nM, and displayed greater intrinsic efficacy (τ_B) than GAT211 (Table 6-1; Fig. 6-2B).

The ability of GAT211 and its enantiomers to modulate CP-dependent inhibition of cAMP accumulation was also determined. HEK-CRE cells were transfected with hCB_1-GFP[2], treated with 1 nM – 10 μM CP ± 1 nM – 10 μM GAT211, GAT228, or GAT228 and cAMP activity was quantified (Fig. 6-2D-F). The observed concentration-response data were fit and analyzed using the operational model of allosterism (eq.1). GAT211 enhanced the potency (α) and efficacy (β) of CP-dependent cAMP inhibition in a concentration-dependent manner with an estimated affinity of 7.61 nM, with minimal intrinsic efficacy (τ_B) (Table 6-1; Fig. 6-2D). GAT229 was a more potent (α) and efficacious (β) enhancer of CP-dependent cAMP inhibition than GAT211, with an estimated affinity of 7.72 nM, and displayed less intrinsic efficacy (τ_B) than GAT211 (Table 6-1; Fig. 6-2F). GAT228 reduced the potency (α) and efficacy (β) of CP-dependent cAMP inhibition in a concentration-dependent manner with an estimated affinity of 6.58 nM, and displayed greater intrinsic efficacy (τ_B) than GAT211 (Table 6-1; Fig. 6-2E).

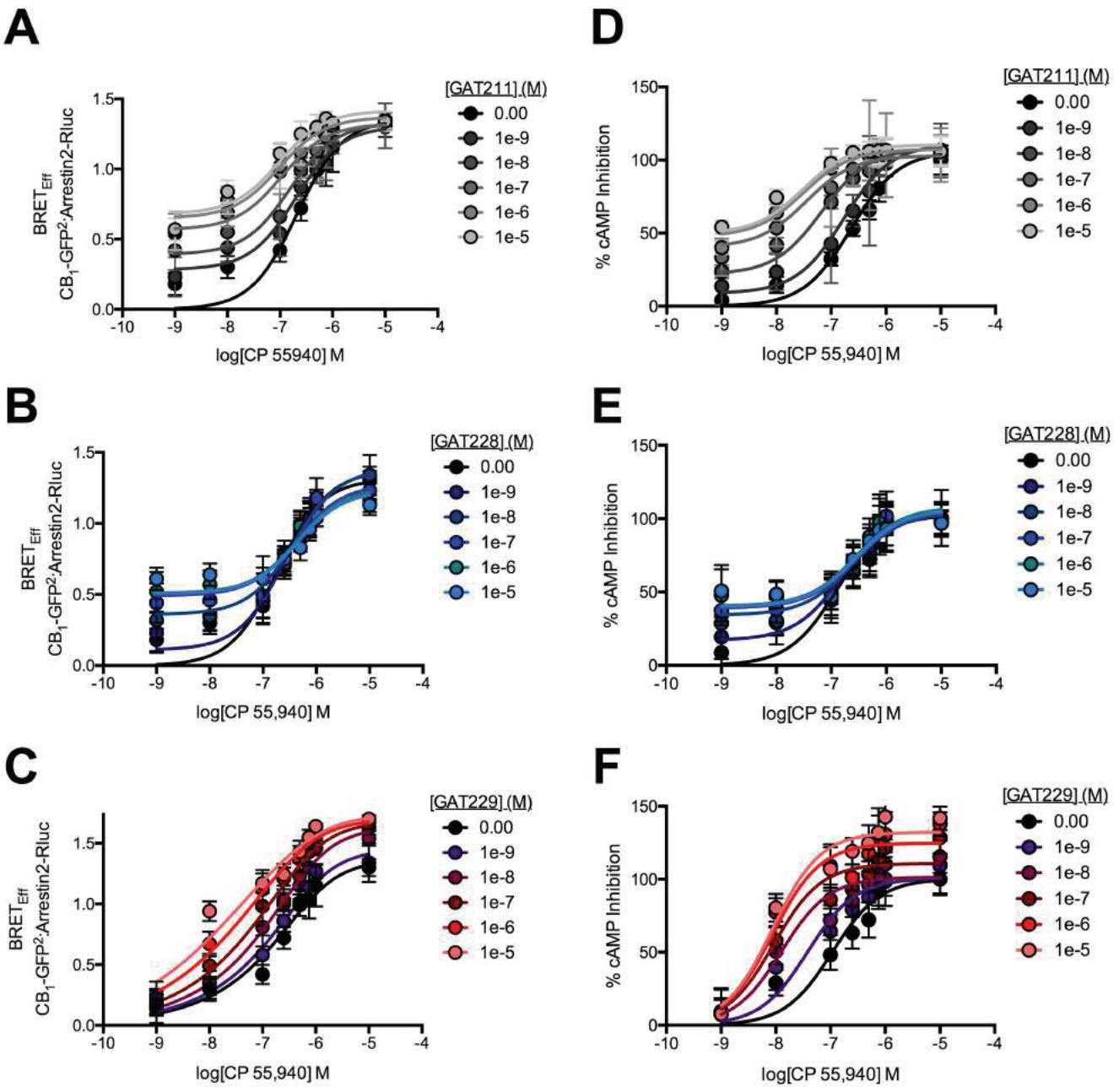

Figure 6-2. GAT211, GAT228, and GAT229 modulated CP- and CB_1-dependent arrestin2 recruitment and cAMP inhibition. A-C) HEK293A cells were transfected with arrestin2-Rluc- and CB_1-GFP^2-containing plasmids and $BRET^2$ was measured 30 min after treatment with CP ± GAT211, GAT228, or GAT229. **D-F)** HEK-CRE cells were transfected with CB_1-GFP^2-containing plasmid and cAMP levels were measured as relative light units 24 h after treatment with CP ± GAT211, GAT228, or GAT229. CRCs were fit using the operational model of allosterism. Data are presented as the mean ± SEM. Further analysis of these data presented in table 6-1. *N* = 4.

Table 6-1. Operational model of allosterism for GAT211, GAT228, and GAT229.

	$BRET_{Eff}$			cAMP		
	GAT211	GAT228	GAT229	GAT211	GAT228	GAT229
logα	1.06 ± 0.08	-1.26 ± 0.46^	1.74 ± 0.06^	0.76 ± 0.16	-1.68 ± 0.69^	1.52 ± 0.04^*
logβ	3.29 ± 0.63	-2.63 ± 0.66^	5.01 ± 0.39^	3.31 ± 0.13	-3.07 ± 0.93^	3.25 ± 0.57
$log\tau_A$[a]	2.40 ± 0.41	2.63 ± 0.66	2.36 ± 0.32	2.68 ± 0.29	2.91 ± 0.82	2.15 ± 0.16
$log\tau_B$[b]	0.34 ± 0.07	2.14 ± 0.85^	0.02 ± 0.06^	0.43 ± 0.05	2.34 ± 0.40^	0.15 ± 0.03^
K_A[a] (nM)	6.80 (0.52 - 29.9)	6.73 (1.46 -29.4)	6.83 (2.21 - 10.9)	6.93 (1.41 - 22.8)	6.94 (2.87 - 34.3)	6.86 (2.09 - 21.11)
K_B[b] (nM)	7.76 (2.97 - 24.5)	6.68 (1.02 - 39.2)	7.93 (3.31 - 70.5)	7.61 (1.68 - 29.7)	6.58 (0.40 - 27.8)	7.72 (1.61 - 15.01)
αβ	2.24×10^4	1.29×10^{-4}	5.62×10^6	1.17×10^4	1.78×10^{-5}	5.89×10^4

All values estimated using the operational model of allosterism described in Keov *et al*. (2011) for the data presented in figure 6-2. [a]$log\tau_A$ and K_A determined for CP; [b]$log\tau_B$ and K_B determined for GAT211, GAT228, or GAT229.

^$P < 0.001$ compared to GAT211 within assay; *$P < 0.001$ compared to $BRET_{Eff}$ with the same compound, as determined by one-way ANOVA followed by Dunnett's multiple comparison.

The coefficient αβ is used to identify functional selectivity between arrestin2 recruitment and G protein signaling (Keov *et al*., 2011). Although no statistical comparisons can be made, GAT211 was functionally selective for arrestin2 recruitment over $G\alpha_{i/o}$ signaling (cAMP) [2.24 x 10^4 (arrestin2) > 1.17 x 10^4 (cAMP)]. GAT229 did not display functional selectivity between arrestin2 and cAMP [5.62 x 10^4 (arrestin2) ≈ 5.89 x 10^4 (cAMP)]. GAT228 was functionally selective for arrestin2 recruitment over cAMP [1.29 x 10^{-4} (arrestin2) > 1.78 x 10^{-5} (cAMP)] (Table 6-1). In both assays, CP displayed high intrinsic efficacy (τ_A) compared to GAT211 and its enantiomers, and similar estimated affinity (K_A) to previous studies (Table 6-1) (reviewed in Pertwee, 2008). Based on these data, GAT211 and GAT229 were $G\alpha_{i/o}$-biased CB_1 PAMs, whereas GAT228 was an arrestin-biased CB_1 allosteric partial agonist.

6.3.3. BRET^2

In order to further understand GAT211-dependent modulation of hCB_1-dependent arrestin2 recruitment, HEK293A and Neuro2a cells were transfected with hCB_1-GFP^2 and arrestin2-Rluc, treated with 1 nM – 10 μM 2-AG, AEA, or CP ± 1 nM – 10 μM GAT211, GAT228, or GAT228 and arrestin2 recruitment to hCB_1 was quantified *via* BRET^2 (Fig. 6-3). The observed concentration-response data were fit and analyzed using the non-linear regression (4 parameter) model. GAT211 (1 μM) shifted the BRET^2 CRCs leftward and upward in the presence of 2-AG, AEA, and CP in HEK293A (Fig. 6-3A-C) and Neuro2a cells (Fig. 6-3E-G). GAT228 (1 μM) did not shift the BRET^2 CRC relative to orthosteric ligands alone (Fig. 6-3). GAT229 (1 μM) shifted the BRET^2 CRCs leftward and upward in the presence of 2-AG, AEA, and CP in HEK293A (Fig. 6-3A-C) and Neuro2a cells (Fig. 6-3E-G) to a greater extent than GAT211. When HEK293A or Neuro2a cells were treated with 1 nM – 10 μM GAT211, GAT228, or GAT228, both GAT211 and GAT228 increased arrestin2 recruitment in a concentration-dependent manner, whereas GAT229 did not (Fig. 6-3D,H). Therefore, the racemic compound GAT211 demonstrated mixed PAM/partial agonist activity for arrestin2 recruitment in both HEK293A and Neuro2a cells for both synthetic (CP) and endogenous (2-AG, AEA)

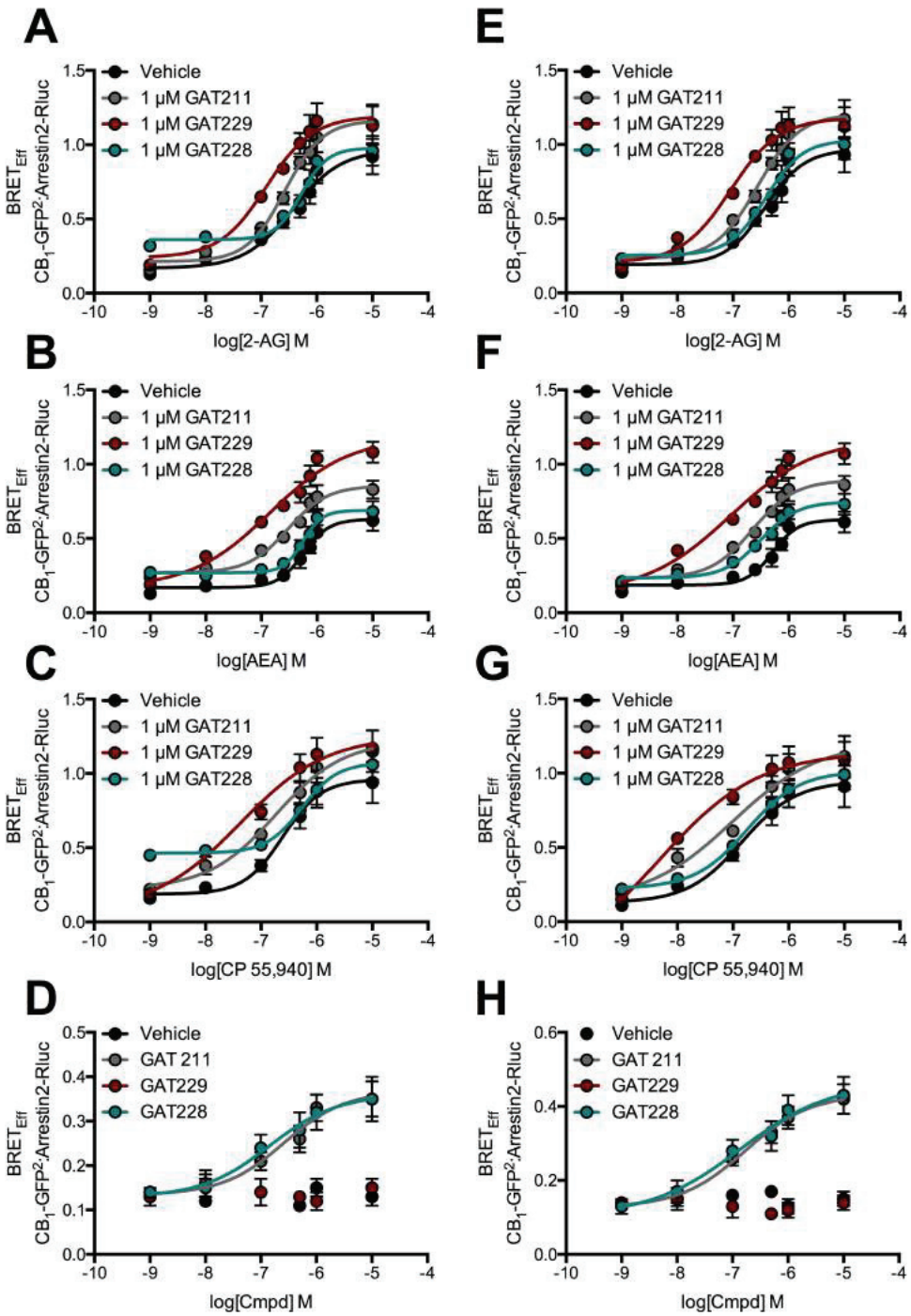

Figure 6-3. GAT211, GAT228, and GAT229 modulated cannabinoid- and CB_1-dependent arrestin2 recruitment in HEK 293A and Neuro2a cells. HEK 293A **(A-D)** or Neuro2a **(E-H)** cells were transfected with arrestin2-Rluc- and CB_1-GFP^2-containing plasmids and $BRET^2$ was measured 30 min after treatment with 1 nM – 10 μM 2-AG, AEA, or CP ± 1 μM GAT211, GAT228, or GAT229 **(A-C,E-G)**, or 1 nM – 10 μM GAT211, GAT228, or GAT229 **(D,H)** CRCs were fit using to a non-linear regression model with variable slope. Data are presented as the mean ± SEM. Further analysis of these data presented in tables 4 and 5. *N* = 4.

cannabinoids. The partial agonist activity was accounted for in GAT228, whereas our data indicate GAT229 acted as a CB_1 PAM.

6.3.4. ERK1/2 AND PLCB3 PHOSPHORYLATION

GAT211-dependent modulation of CB_1-dependent signaling was further assessed in HEK293A transfected with hCB_1-GFP[2], and Neuro2a cells endogenously expressing CB_1, treated with 1 nM – 10 μM 2-AG, AEA, or CP ± 1 nM – 10 μM GAT211, GAT228, or GAT228. ERK (Fig. 6-4) and PLCβ3 phosphorylation (Fig. 6-5) were quantified *via* In-cell™ western. The observed concentration-response data were fit and analyzed using the non-linear regression (4 parameter) model. As was observed for arrestin2 recruitment, GAT211 (1 μM) shifted ERK and PLCβ3 CRCs leftward and upward in the presence of 2-AG, AEA, and CP in HEK293A (Figs. 6-4A-C, 6-5A-C) and Neuro2a cells (Figs. 6-4E-G, 6-5E-G). GAT228 (1 μM) did not shift the CRCs relative to orthosteric ligands alone (Figs. 6-4,-5). GAT229 (1 μM) shifted the CRCs leftward and upward in the presence of 2-AG, AEA, and CP in HEK293A (Figs. 6-4A-C, 6-5A-C) and Neuro2a cells (Figs. 6-4E-G, 6-5E-G) to a greater extent than GAT211. Treatment with 1 nM – 10 μM GAT211 or GAT228 increased ERK and PLCβ3 phosphorylation in a concentration-dependent manner, whereas GAT229 treatment did not (Figs. 6-4D,H, 6-5D,H). These data provide additional evidence for GAT211 acting as a mixed PAM/partial agonist, GAT228 acting as a partial agonist, and GAT229 acting as a CB_1 PAM.

6.3.5. DETERMINATION OF ALLOSTERIC POTENCY AND EFFICACY

The potency of GAT211, GAT228, and GAT229 were estimated in HEK293A cells transfected with hCB_1 and treated with 500 nM CP + 1 nM – 10 μM GAT211, GAT228, or GAT228 (Fig. 6-6, Table 6-2). Similar experiments were also conducted with 500 nM 2-AG or AEA + 1 nM – 10 μM GAT211, GAT228, or GAT228 (CRCs not shown, Table 6-3). GAT229 was a more potent (pEC_{50}) enhancer of arrestin2 recruitment than GAT211 or GAT228 (Fig. 6-6A), and a more potent enhancer or ERK (Fig. 6-6B) and PLCβ3 phosphorylation (Fig. 6-6C)

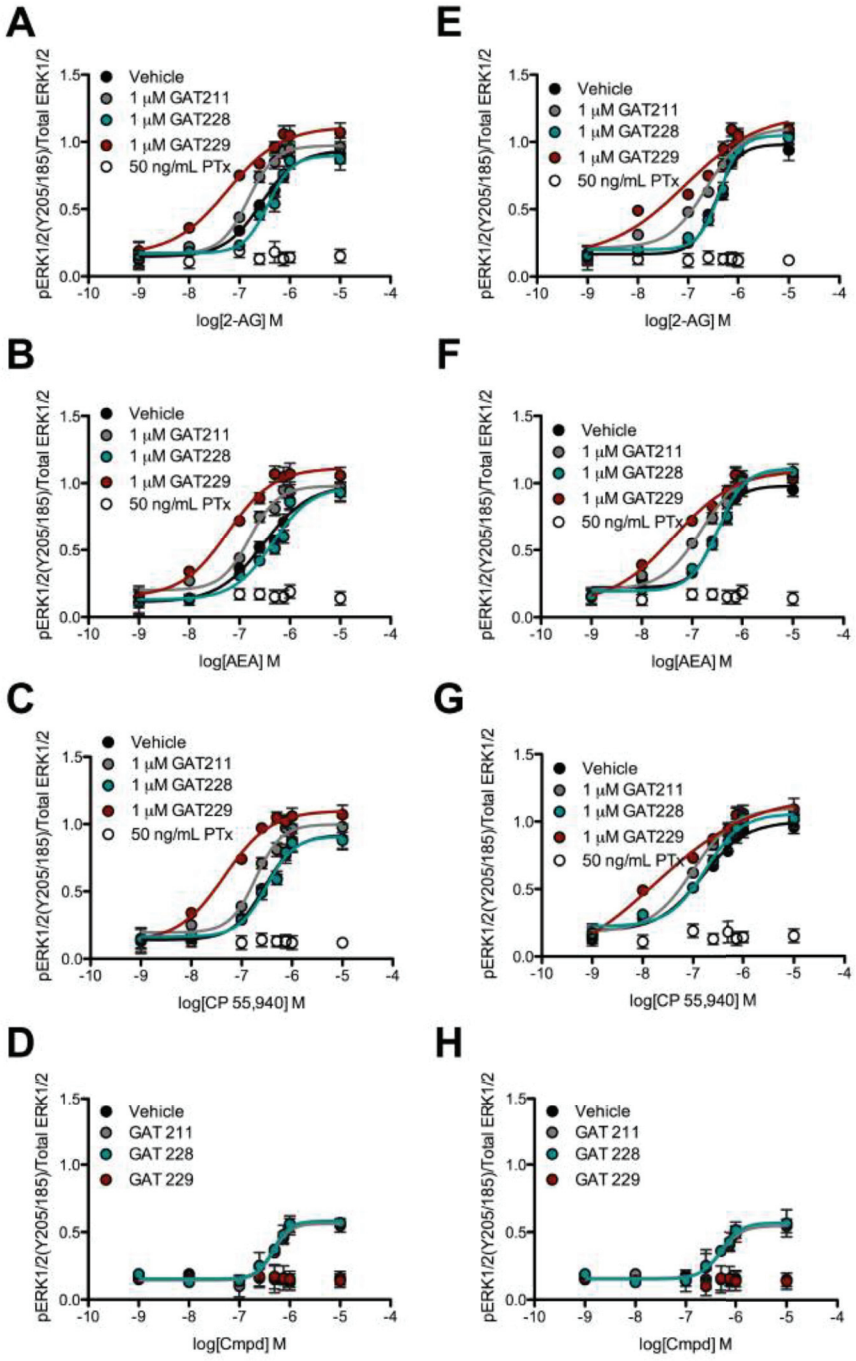

Figure 6-4. GAT211, GAT228, and GAT229 modulated cannabinoid- and CB_1-dependent ERK phosphorylation in HEK293A and Neuro2a cells. HEK293A cells transfected with CB_1-GFP[2]-containing plasmids **(A-D)** or Neuro2a cells endogenously expressing CB_1 **(E-H)** were treated for 10 min with 1 nM – 10 μM 2-AG, AEA, or CP ± 1 μM GAT211, GAT228, or GAT229 **(A-C,E-G)**, or 1 nM – 10 μM GAT211, GAT228, or GAT229 **(D,H)** and pERK(Y205/185)/Total ERK was measured *via* In-cell western. CRCs were fit using to a non-linear regression model with variable slope. Data are presented as the mean ± SEM. Further analysis of these data presented in tables 6-2 and 6-3. $N = 4$.

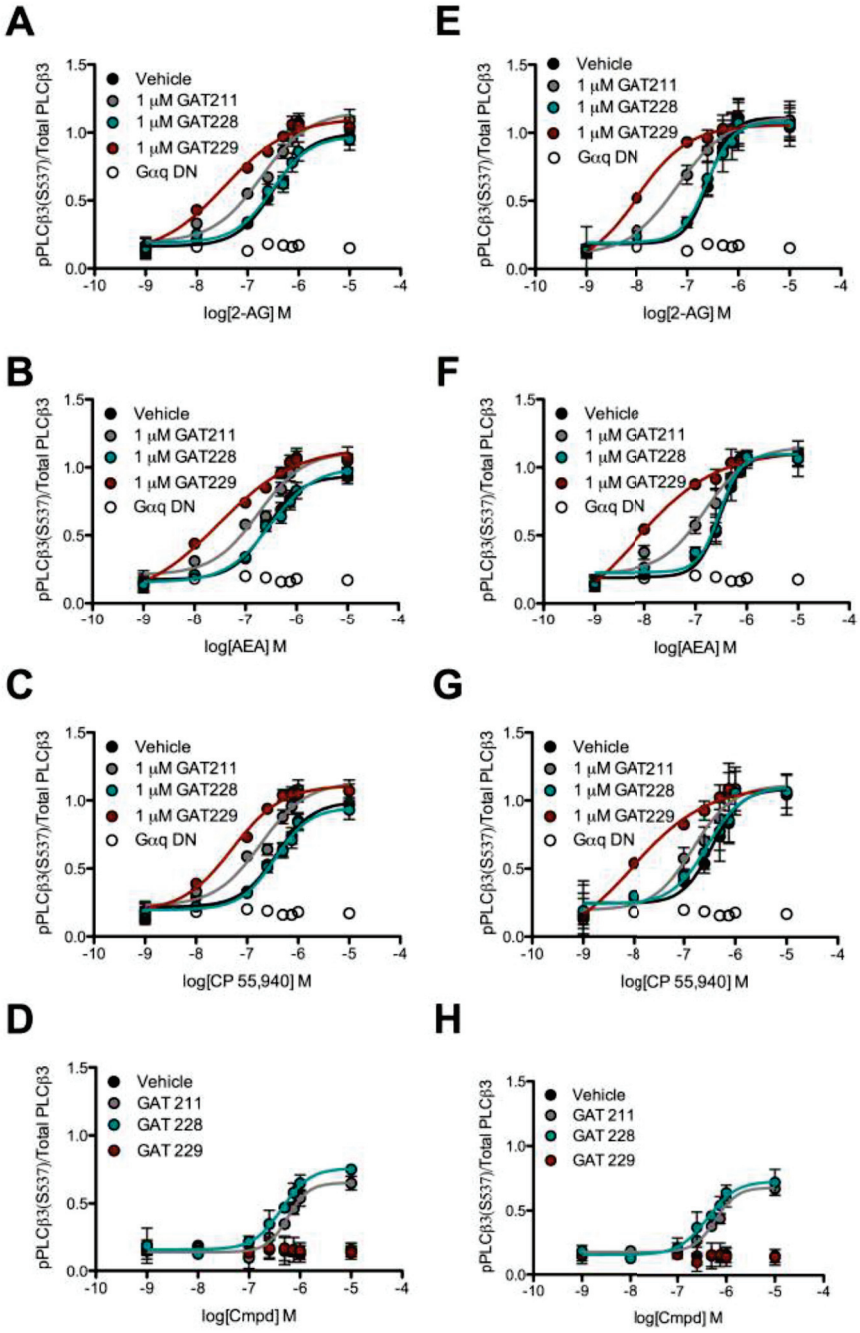

Figure 6-5. GAT211, GAT228, and GAT229 modulated cannabinoid- and CB_1-dependent PLCβ3 phosphorylation in HEK293A and Neuro2a cells. HEK293A cells transfected with CB_1-GFP^2-containing plasmids **(A-D)** or Neuro2a cells endogenously expressing CB_1 **(E-H)** were treated for 10 min with 1 nM – 10 μM 2-AG, AEA, or CP ± 1 μM GAT211, GAT228, or GAT229 **(A-C,E-G)**, or 1 nM – 10 μM GAT211, GAT228, or GAT229 **(D,H)** and pPLCβ3(S537)/Total PLCβ3 was measured *via* In-cell western. CRCs were fit using to a non-linear regression model with variable slope. Data are presented as the mean ± SEM. Further analysis of these data presented in tables 6-2 and 6-3. $N = 4$.

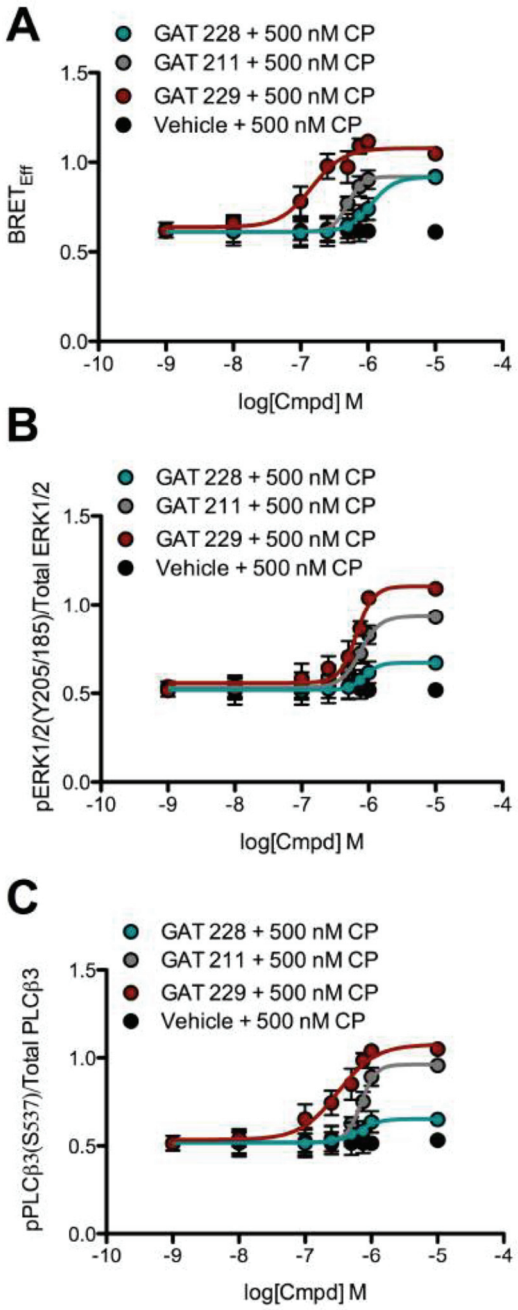

Figure 6-6. Determining the potency of GAT211, GAT228, and GAT229 at CB_1. HEK293A cells were transfected with arrestin2-Rluc- and CB_1-GFP^2-containing plasmids and $BRET^2$ was measured 30 min after treatment **(A)**, or with the CB_1-GFP^2-containing plasmid and ERK phosphorylation **(B)** or PLCβ3 phosphorylation **(C)** was measured 10 min after treatment with 1 nM – 10 μM GAT211, GAT228, or GAT229 ± 500 nM 2-AG, AEA, or CP. CRCs were fit using to a non-linear regression model with variable slope. Data are presented as the mean ± SEM. Further analysis of these data presented in tables 6-2 and 6-3. *N* = 4.

Table 6-2. Summary of data by assay for GAT211, GAT228, and GAT229.

	Arrestin2	
Compound	**pEC_{50} ± SEM**	**E_{max} (%) ± SEM**
GAT211	7.11 ± 0.12	129.54 ± 13.23
GAT228	7.08 ± 0.18	105.89 ± 4.85
GAT229	7.59 ± 0.16†*	126.98 ± 12.19*
	ERK ($G\alpha_{i/o}$)	
	pEC_{50} ± SEM	**E_{max} (%) ± SEM**
GAT211	7.19 ± 0.13	109.61 ± 16.11
GAT228	7.15 ± 0.15	96.85 ± 5.14
GAT229	7.49 ± 0.19*	100.45 ± 3.60^
	PLCβ3 ($G\alpha_q$)	
	pEC_{50} ± SEM	**E_{max} (%) ± SEM**
GAT211	7.26 ± 0.19	112.81 ± 14.21
GAT228	7.05 ± 0.13	96.30 ± 6.29
GAT229	7.48 ± 0.17*	118.55 ± 6.39*

pEC_{50} determined using non-linear regression analysis; E_{max} maximum (%) effect compared to orthosteric agonist alone, determined using non-linear regression analysis. Data are mean ± SEM. Data were calculated as the mean of data for each assay in HEK293A cells (pEC_{50}, Fig. 6-6) and HEK293A and Neuro2a cells treated with 2-AG, AEA or CP (E_{max}, Figs. 6-3, 6-4, 6-5). †$P < 0.01$ compared to GAT211, *$P < 0.01$ compared to GAT228, within assay; ^$P < 0.01$ compared to arrestin2 within compound, as determined by unpaired *t*-test.

Table 6-3. Summary of data by orthosteric probe for GAT211, GAT228, and GAT229.

	2-AG	
Compound	**pEC_{50} ± SEM**	**E_{max} (%) ± SEM**
GAT211	7.22 ± 0.08	121.94 ± 7.90
GAT228	7.08 ± 0.13	113.03 ± 9.22†
GAT229	7.57 ± 0.18†*	136.16 ± 4.66†*
	AEA	
	pEC_{50} ± SEM	**E_{max} (%) ± SEM**
GAT211	7.22 ± 0.17	124.79 ± 7.63
GAT228	7.15 ± 0.12	113.81 ± 9.69†
GAT229	7.55 ± 0.13†*	143.46 ± 4.37†*
	CP	
	pEC_{50} ± SEM	**E_{max} (%) ± SEM**
GAT211	7.18 ± 0.14	105.13 ± 1.74^
GAT228	7.12 ± 0.18	90.28 ± 1.11†^
GAT229	7.44 ± 0.16	132.99 ± 4.11†*

pEC_{50} determined using non-linear regression analysis; E_{max} maximum (%) effect compared to orthosteric agonist alone, determined using non-linear regression analysis. Data are mean ± SEM. Data were calculated as the mean of data for each assay in HEK293A cells (pEC_{50}, Fig. 6-6) and HEK293A and Neuro2a cells treated with 2-AG, AEA or CP (E_{max}, Figs. 6-3, 6-4, 6-5). †$P < 0.01$ compared to GAT211, *$P < 0.01$ compared to GAT228, within assay; ^$P < 0.01$ compared to 2-AG within compound, as determined by unpaired *t*-test.

than GAT228 (Table 6-2). No difference in potency between assays was observed for GAT211, GAT228, or GAT228 (Table 6-2). When data from assays were pooled and orthosteric ligands were compared, GAT229 was also a more potent (pEC_{50}) enhancer of 2-AG, AEA, and CP-mediated hCB_1 signaling than either GAT211 or GAT228 (Table 6-3). No difference in potency between the GAT compounds was observed when 2-AG, AEA, or CP was the orthosteric probe (*i.e.* no probe-dependent difference in potency) (Table 6-3).

The efficacy of GAT211, GAT228, and GAT229 were estimated from the data presented in figures 6-4 – 6-6 and calculated as % E_{max} relative to orthosteric ligand alone (Tables 6-2,-3). GAT229 was a more efficacious enhancer of arrestin2 recruitment and PLCβ3 phosphorylation than GAT228 in the presence of 500 nM CP (Table 6-2). GAT229 was a less efficacious enhancer of ERK phosphorylation than arrestin2 recruitment (Table 6-2). GAT229 was a more efficacious enhancer of 2-AG, AEA, and CP-mediated hCB_1 signaling than either GAT211 or GAT228 (Table 6-3). E_{max} was greater in the presence of 2-AG or AEA, compared to CP, for GAT211 and GAT228 (*i.e.* GAT211 and GAT228 displayed probe-dependence for 2-AG or AEA over CP) (Table 6-3). No probe-dependent difference in efficacy was observed for GAT229 (Table 6-3). These data are consistent with GAT229 acting as a CB_1 PAM.

6.4. DISCUSSION

6.4.1. GAT211 DISPLAYED ENANTIOMER-SPECIFIC ALLOSTERIC AGONIST AND PAM PROPERTIES

In this study, the racemic compound GAT211, and its enantiomers GAT228 (*R*) and GAT229 (*S*), were characterized as allosteric modulators of CB_1. Our collaborators, Drs. Roger Pertwee and Maria Cascio (University of Aberdeen) observed that GAT211 did not affect ligand binding to CB_2 at concentrations below 10 μM, suggesting this compound was CB_1-selective. Radioligand binding analysis demonstrated GAT211 reduced the rate of dissociation of [^{3}H]CP from hCB_1 in CHO cell membranes, and enhanced [^{3}H]CP binding in CHO cell membranes, consistent with a PAM of orthosteric ligand binding. When the enantiomers were investigated separately, GAT228 reduced [^{3}H]CP binding in CHO cell membranes, whereas GAT229

enhanced [^{3}H]CP binding in CHO cell membranes to a greater extent than either GAT211 or GAT228. These data lead us to conclude that while both GAT228 and GAT229 interacted with an allosteric site(s) at CB_1 distinct from CP, the majority of PAM activity was mediated by the *S*-(-)-enantiomer, GAT229. Further, we hypothesized that the partial allosteric agonist activity of GAT211 was attributed to the *R*-(-)-enantiomer, GAT228.

The hypotheses that GAT228 was an allosteric agonist and GAT229 was a PAM of CB_1 were tested CB_1 *via* arrestin2 recruitment ($BRET^2$), cAMP inhibition, ERK1/2 and PLCβ3 phosphorylation in HEK293A and Neuro2a cells. GAT228 reduced the potency and efficacy of CP-mediated arrestin2 recruitment and cAMP inhibition, as indicated by the calculated values α and β in the operational model of allosterism. GAT229 displayed almost no intrinsic efficacy alone and consistently displayed PAM activity in the low nanomolar range (~7.8 nM). GAT229 enhanced both the potency and efficacy of CP-dependent signaling, as indicated by the calculated values α and β in the operational model of allosterism. Together, these data are all consistent with our hypothesis that GAT229 was a potent PAM of CB_1 in multiple model systems and assays.

The three best-characterized allosteric modulators of CB_1 tested to date are Org27569, PSNCBAM-1, and lipoxin A_4 (Ahn *et al*., 2012, 2013; Baillie *et al*., 2013; Cawston *et al*., 2013; Horswill *et al*., 2007; Pamplona *et al*., 2012). Org27569 and PSNCBAM-1 paradoxically enhance orthosteric agonist binding to CB_1 and reduce orthosteric ligand-dependent signaling – they are PAMs of ligand binding, but NAMs of receptor signaling (Ahn *et al*., 2012, 2013; Horswill *et al*., 2007). Org27569 displays higher potency for CB_1 than GAT211 or its enantiomers, whereas PSNCBAM-1 displayed lower potency (pEC_{50} Org27569 ≈ 8.3, PSNCBAM-1 ≈ 6.1, GAT211 ≈ 7.2, GAT228 ≈ 7.1, GAT229 ≈ 7.5) (Ahn *et al*., 2012, 2013; Baillie *et al*., 2013; Cawston *et al*., 2013), but all display similar affinity for CB_1 [K_B (nM) Org27569 ≈ 7.6, PSNCBAM-1 ≈ 2.7 nM GAT211 ≈ 7.7, GAT228 ≈ 6.6, GAT229 ≈ 7.8] (Ahn *et al*., 2012, 2013; Baillie *et al*., 2013; Cawston *et al*., 2013). Lipoxin A_4 enhances both orthosteric ligand binding and CB_1 signaling (Pamplona *et al*., 2012). Lipoxin A_4 is more potent than GAT211 or its enantiomers (pEC_{50}

Lipoxin $A_4 \approx 8.2$), but has much lower affinity for CB_1 [K_B (nM) > 10,000] (Pamplona *et al*., 2012).

6.4.2. FUNCTIONAL SELECTIVITY

The activity of GAT211, GAT228, and GAT229 was characterized at several distinct pathways – arrestin2, cAMP inhibition and ERK1/2 ($G\alpha_{i/o}$), and PLCβ3 ($G\alpha_q$) – to determine whether these compounds were functionally selective. We have previously reported CP promotes arrestin2 recruitment to a greater extent than 2-AG or AEA (Laprairie *et al*., 2014a, 2015b). CP and 2-AG were also functionally selective for PLCβ3, being more efficacious activators of this pathway than AEA (Laprairie *et al*., 2014a, 2015b). In this study, GAT211 was functionally $G\alpha_{i/o}$-selective compared to arrestin2, as demonstrated by comparisons of α and β (Table 6-1). GAT228 was functionally arrestin2-selective in the absence of orthosteric ligand and did not enhance CP-dependent signaling (Table 6-1). GAT229 did not display functional selectivity (Table 6-1). Previous studies have observed that Org27569 is functionally selective against $G\alpha_{i/o}$ signaling relative to arrestin recruitment (Ahn *et al*., 2012, 2013; Baillie *et al*., 2013), suggesting Org27569 could limit $G\alpha_{i/o}$ signaling *in vivo* more effectively than other pathways. Our data demonstrate GAT211 and GAT229 could enhance $G\alpha_{i/o}$-dependent signaling *in vivo* more effectively than other pathways, which could enhance and maintain CB_1 activity (Cawston *et al*., 2013). Understanding the functional selectivity of allosteric CB_1 ligands may lead to the tailoring of ligands for different treatment strategies and outcomes.

6.4.3. PROBE-DEPENDENCE

Allosteric modulators are probe-dependent, that is, the efficacy of the allosteric modulator depends on the orthosteric probe being used (reviewed in Christopoulos and Kenakin, 2002). Previous studies have reported that Org27569 and PSNCBAM-1 both display probe-dependence because they are more potent modulators of CP binding and CB_1 activation than WIN 55,212-2 (Baillie *et al*., 2013). 2-AG, AEA, and CP were the orthosteric probes used in this study because 2-AG and AEA are the major endocannabinoids and CP is a standard high potency

reference compound routinely used for studying CB_1 activation (Sugiura *et al*., 1999). GAT211 displayed probe-dependence as more potent and efficacious enhancers of endocannabinoid (2-AG and AEA) signaling than CP binding and signaling. GAT229 did not display probe-dependence. These data indicate the PAM activity of GAT211 may be best-observed in the presence of endocannabinoids, and GAT229 remains highly active as a CB_1 PAM when endocannabinoids are the orthosteric agonist. One major reason allosteric modulators of CB_1 are attractive as potential therapeutics is that they would be less likely to promote psychotropic side-effects elicited by orthosteric CB_1 ligands (Christopoulos and Kenakin, 2002; Ross, 2007 Wootten *et al*., 2013). The observation that GAT211 and GAT229 are highly active when endocannabinoids are used as orthosteric agonists is promising because they may effectively enhance endogenous CB_1 signaling without the use of other CB_1 orthosteric agonists.

6.4.4. CONCLUSIONS

Positive allosteric modulation of CB_1 has the potential to effectively treat addiction, neurodegenerative diseases, pain and Huntington disease where direct agonists are limited by their side-effect profiles (Wootten *et al*., 2013). In this study the activity of the racemic compound GAT211, and its enantiomers GAT228 and GAT229, were characterized for the first time. GAT211 behaved as a moderate and selective PAM of CB_1 over CB_2 that enhanced both CP binding and agonist-mediated receptor signaling. GAT211 also displayed partial agonist activity. The PAM and partial agonist activity were attributed to each of the enantiomers of GAT211. GAT229 (*S*) was a potent CB_1 PAM and GAT228 (*R*) was an allosteric partial agonist at CB_1. To our knowledge, this study represents the first characterization of two enantiomers having unique allosteric effects at the same receptor. In conclusion, GAT211, GAT228, and GAT229 represent a series of novel allosteric modulators that may have therapeutic utility in a number of pathological states (Cairns *et al*., 2014; Slivicki *et al*., 2014).

CHAPTER 7

POSITIVE ALLOSTERIC MODULATION OF THE TYPE 1 CANNABINOID RECEPTOR REDUCES THE SIGNS AND SYMPTOMS OF HUNTINGTON DISEASE IN THE R6/2 MOUSE MODEL

Copyright statement

Portions of this chapter have been submitted for publication in: Laprairie RB, Zrein A, Bagher AM, Rourke JL, Cairns EA, Kelly MEM, Sinal CJ, Kulkarni PM, Thakur GA, Denovan-Wright EM (2016). Positive allosteric modulation of the type 1 cannabinoid receptor reduces the signs and symptoms of Huntington disease in the R6/2 mouse model. *Neurobiol dis.* **In preparation**. The manuscript has been modified to meet formatting requirements.

Contribution statement

The manuscript used as the basis for this chapter was written with guidance from Drs. Eileen Denovan-Wright, Melanie Kelly, and Ganesh Thakur. Data were collected by myself with assistance from Adel Zrein, Elizabeth Cairns, and Drs. Amina Bagher and Jillian Rourke. Critical equipment or reagents were provided by Pushkar Kulkarni and Drs. Christopher Sinal and Ganesh Thakur.

7.1. INTRODUCTION

Huntington disease (HD) is an inherited autosomal dominant disease in which patients suffer from depression, reduced cognition, behavioural changes, and uncontrollable choreiform movements over decades (reviewed in Shannon and Fraint, 2015). The causative agent of HD, the mutant huntingtin (mHtt) protein, affects the transcription of a subset of genes, reduces mitochondrial cellular respiration, and inhibits autophagic processes (Kumar *et al.*, 2014; Valor, 2015). mHtt-dependent transcriptional dysregulation occurs in multiple organ systems, but occurs earliest, and is most-pronounced, in the medium spiny projection neurons of the striatum (Francelle *et al.*, 2014; Kumar *et al*., 2014). One of the earliest transcriptional changes that occur in HD is the repression of the type 1 cannabinoid receptor (CB_1) in the striatum, leading to a reduction in CB_1 mRNA and protein (Denovan-Wright and Robertson, 2000; Glass *et al*., 2000). Lower levels of CB_1 have been observed in all models of HD studied to date and in patients suffering from HD (Allen *et al*., 2009; Dowie *et al*., 2009).

The decrease in CB_1 mRNA and protein observed in HD is strongly correlated with the progression and pathophysiology of HD (Mievis *et al*., 2011; Chiarlone *et al.*, 2014; Naydenov *et al*., 2014a). Transgenic R6/2 HD mice that are heterozygous for CB_1 (*i.e.* mHtt *x* $CB_1^{-/+}$) exhibit earlier HD-like symptom onset, more rapid disease progression, and greater neuronal cell death in the striatum than R6/2 HD mice with a full complement of CB_1 (Blázquez *et al.*, 2011; Mievis *et al*., 2011). Rescue of CB_1 *via* adeno-associated viral delivery in medium spiny projection neurons of R6/2 mice prevents loss of excitatory markers such a vGLUT-1, and a decrease in dendritic spine density, in the striatum, but does not change motor impairment (Chiarlone *et al.*, 2014; Naydenov *et al*., 2014a). Theses studies demonstrate that lower levels of CB_1, in the striatum and elsewhere, appear to contribute to HD pathogenesis, and increasing the abundance and/or activity of CB_1 may delay or reduce the severity of the signs and symptoms of HD.

Under non-pathological conditions CB_1 is the most-abundant G protein-coupled receptor in the central nervous system (Ross, 2007). Agonist-dependent activation of CB_1 can inhibit

neurotransmitter release from the pre-synaptic neuron, increase pro-survival signaling through pathways such as ERK and Akt, and/or lead to receptor internalization and downregulation, to varying degrees depending on the functional selectivity of the agonist (Pertwee, 2008; Piscitelli *et al*., 2012; Laprairie *et al*., 2014a). Because CB_1 limits neurotransmitter release and enhances pro-survival signaling pathways, its activation is considered neuroprotective (Piscitelli *et al*., 2012).

We recently reported that $G\alpha_{i/o}$-biased CB_1 agonists, such as anandamide (AEA) and 2-arachidonoylglycerol (2-AG), increase CB_1 mRNA and protein levels and improve cell viability in the ST*Hdh*$^{Q111/Q111}$ cell culture model of HD (Laprairie *et al*., 2015b). In contrast, administration of the arrestin-biased cannabinoid THC reduces CB_1 levels and cell viability in the ST*Hdh*$^{Q111/Q111}$ cell model of HD (Laprairie *et al*., 2015b). Moreover, THC increases seizure frequency in R6/1 HD mice (Dowie *et al*., 2010). These findings are significant because they suggest that enhancement of endocannabimimetic activity at CB_1 may be beneficial in HD, whereas THC-like activity may exacerbate cellular pathology in HD. The activity of endocannabinoids can be enhanced 1) directly through the direct administration of 2-AG and/or AEA, 2) *via* inhibition of catabolic enzymes such as FAAH, or 3) *via* positive allosteric modulators (PAM) of CB_1. Endocannabinoids are rapidly degraded when administered *in vivo* and are consequently of limited therapeutic potential (Pertwee, 2008). Increasing AEA levels *via* fatty acid amide hydrolase (FAAH) inhibition preserved CB_1 levels in R6/1 HD mice, but did not affect motor coordination (Dowie *et al*., 2010). Increasing 2-AG levels *via* abhydrolase domain-containing protein 6 (ABHD6) inhibition normalized brain-derived neurotrophic factor (BDNF) levels in R6/2 HD mice and reduced spontaneous seizure frequency, but did not alter the progressive decline in motor control (Naydenov *et al*., 2014b). Overall, we hypothesized that PAMs capable of increasing the potency and efficacy of endocannabinoids with respect to $G\alpha_{i/o}$-dependent CB_1 signaling may be the most-effective means of managing the signs and symptoms of HD while limiting adverse on-target effects associated with cannabinoids.

PAMs of CB_1 are candidates to treat the signs and symptoms of HD. CB_1 PAMs induce a conformational change in the receptor that enhances the receptor's affinity for, and efficacy of activation by, orthosteric ligands, such as AEA and 2-AG. Further, CB_1 PAMs lack intrinsic efficacy in the absence of an orthosteric ligand, and are therefore unlikely to produce the supraphysiological activation, desensitization, or downregulation of CB_1 associated with psychotropic side effects that may be induced by orthosteric CB_1 agonists (Ross, 2007; Wootten *et al*, 2013). The goal of the present study was to determine whether the recently characterized CB_1 allosteric modulators GAT211 (racemic, equimolar mixture of *R*- and *S*-enantiomers) (first described as 'compound A' Astra-Zeneca; Adam *et al.*, 2007), and its enantiomers GAT228 (*R*-enantiomer) and GAT229 (*S*-enantiomer) (Cairns *et al*., 2014; Slivicki *et al*., 2014; Laprairie *et al*., 2015c), affected the severity and progression of HD in cell culture and animal models of the disease. GAT229 is a CB_1 PAM that enhances orthosteric ligand binding to CB_1 in isolated CHO cell and mouse neuron membranes and increases the potency and efficacy of CB_1 orthosteric ligand-mediated signaling in HEK293A and Neuro2a cells with no intrinsic efficacy in the absence of orthosteric ligand (Laprairie *et al*., 2015c, 2016a). GAT228 is an allosteric partial agonist that binds to an allosteric site of CB_1 and increases CB_1-mediated signaling in HEK293A and Neuro2a cells independent of orthosteric ligand (Laprairie *et al*., 2015c, 2016a). The racemic compound, GAT211, has been shown to display intermediate effects between its two enantiomers in CB_1 ligand binding and CB_1-mediated cell signaling assays (Laprairie *et al*., 2015c, 2016a). The activity of GAT211, GAT228, and GAT229 was evaluated in ST*Hdh*$^{Q7/Q7}$ and ST*Hdh*$^{Q111/Q111}$ cells, and in the R6/2 mouse model of HD. The data presented in this study provide a first proof of principle for the use of CB_1 PAMs to treat the signs and symptoms of HD.

7.2. METHODS

7.2.1. DRUGS

GAT211, GAT228, and GAT229 were synthesized and provided by the laboratory of Dr. Ganesh A Thakur (Northeastern University). 2-arachidonoylglycerol (2-AG), anandamide (AEA),

and (-)-*cis*-3-[2-Hydroxy-4-(1,1-dimethylheptyl)phenyl]-*trans*-4-(3-hydroxypropyl)cyclohexanol (CP,55,940) were purchased from Tocris Bioscience (Bristol, UK). Cannabinoids were dissolved in DMSO (final concentration of 0.1% in assay media for all assays) and added directly to the media at the concentrations and times indicated. No effects of vehicle alone were observed compared to assay media alone.

7.2.2. CELL CULTURE

Conditionally immortalized wild-type (ST*Hdh*$^{Q7/Q7}$) or homozygous mutant (ST*Hdh*$^{Q111Q/111}$) mouse striatal progenitor cell lines expressing exon 1 from the human *huntingtin* allele in the mouse *huntingtin* locus were acquired from the Coriell Institute (Camden, NJ) (Trettel *et al*., 2000). Cells were propagated at 33°C, 5% CO_2 in DMEM supplemented with 10% FBS, 2 mM L-glutamine, 10^4 U/mL Pen/Strep, and 400 µg/mL geneticin. For all experiments, cells were serum-starved for 24 h.

7.2.3. PLASMIDS

Human CB_1-green fluorescent protein^2 (GFP^2) and arrestin2-*Renilla* luciferase (Rluc) (β-arrestin1) were cloned as fusion proteins at the C-terminus. hCB_1-GFP^2 was generated using the pGFP^2-N3 plasmid (PerkinElmer, Waltham, MA) as described previously (Bagher *et al*., 2013). arrestin2-Rluc was generated using the pcDNA3.1 plasmid (PerkinElmer, Waltham, MA) as described previously (Laprairie *et al*., 2015d). The GFP^2-Rluc fusion construct, and Rluc plasmids have also been described (Bagher *et al*., 2013).

7.2.4. BIOLUMINESCENCE RESONANCE ENERGY TRANSFER^2 (BRET^2)

Direct interactions between CB_1 and arrestin2 were quantified *via* BRET^2 (James *et al*., 2006). Cells were transfected with the indicated GFP^2 and Rluc constructs using Lipofectamine 2000, according to the manufacturer's instructions (Invitrogen) and treated as previously described (Laprairie *et al*., 2014a). Briefly, 48 h post-transfection cells were washed twice with cold 0.1 M PBS and suspended in BRET buffer [0.1 M PBS supplemented with glucose (1 mg/mL), benzamidine (10 mg/mL), leupeptin (5 mg/mL) and a trypsin inhibitor (5 mg/mL)].

Cells were treated with compounds as indicated (PerkinElmer) and coelenterazine 400a substrate (50 µM; Biotium, Hayward, CA) was added. Light emissions were measured at 460 nm (Rluc) and 510 nm (GFP^2) using a Luminoskan Ascent plate reader (Thermo Scientific, Waltham, MA), with an integration time of 10 s and a photomultiplier tube voltage of 1200 V. BRET efficiency ($BRET_{Eff}$) was determined using previously described methods (Bagher *et al*., 2013; Laprairie *et al*., 2014a).

7.2.5. IN-CELL™ WESTERNS

Cells were fixed for 10 min at room temperature with 4% paraformaldehyde and washed three times with 0.1 M PBS for 5 min each. Cells were incubated with blocking solution (0.1 M PBS, 20% Odyssey blocking buffer, and 0.1% TritonX-100) for 1 h at room temperature. Cells were incubated with primary antibody solutions directed against pERK1/2(Tyr205/185) (1:200) and ERK1/2 (1:200), (Santa Cruz Biotechnology) diluted in blocking solution overnight at 4°C. Cells were washed three times with 0.1 M PBS for 5 min each. Cells were incubated in $IR^{CW700dye}$ or $IR^{CW800dye}$ (1:500; Rockland Immunochemicals) and washed three times with 0.1 M PBS for 5 min each. Analyses were conducted using the Odyssey Imaging system and software (version 3.0; Li-Cor).

7.2.6. CELL VIABILITY ASSAYS

Viability assays (calcein-AM [Cal-AM], ethidium homodimer-1 [EthD-1]) were conducted according to the manufacturer's instructions (Live/Dead Cytotoxicity Assay, Life Technologies, Burlington, ON). Cal-AM fluorescence is an indicator of cellular esterase activity and mitochondrial respiration. Cal-Am fluorescence (460/510 nm) is reported as % esterase activity relative to vehicle-treated ST*Hdh*$^{Q7/Q7}$ cells (100%). EthD-1 fluorescence is an indicator of membrane permeability and cell death. EthD-1 fluorescence (530/620 nm) is reported as % membrane permeability relative to ST*Hdh*$^{Q7/Q7}$ cells treated with 70% methanol for 30 min (100%). Measurements of viability were made 18 h following cannabinoid treatment.

7.2.7. ANIMALS

Seven-week old, male, R6/2 HD mice [strain name B6CBA-Tg(HDexon1)62Gpb/3J bred on a C57BL/6J background] and age-matched, wild-type (C57BL/6J) mice (mean weight 20.3 ± 0.4 g) were purchased from The Jackson Laboratory (Bar Harbor, ME). Animals were group housed (3-5 per cage) with *ad libitum* access to food, water, and environmental enrichment and maintained on a 12 h light/dark cycle. Mice were randomly assigned to receive volume-matched, daily *i.p.* injections of vehicle (10% DMSO, 0.1% Tween-20 in saline) or 10 mg/kg GAT211, GAT228, or GAT229 for 21 days (n = 5 per group). Mice were weighed daily. All protocols were in accordance with the guidelines detailed by the Canadian Council on Animal Care (CCAC; Ottawa ON: Vol 1, 2nd Ed, 1993; Vol 2, 1984), approved by the Carleton Animal Care Committee at Dalhousie University. In keeping with the ARRIVE guidelines, power analyses were conducted to determine the minimum number of animals required for the study and animals were purchased – rather than bred – to limit animal waste. All assessments of animal behaviour were made by individuals blinded to treatment group (Kilkenny *et al*., 2010).

Genotype analysis was performed for R6/2 HD mice according to the protocol provided by The Jackson Laboratory to confirm the presence of the mutant *huntingtin* transgene and determine the number of CAG repeats (Mangiarini *et al*., 1996; Menalled *et al*., 2009). The mean number of CAG repeats observed in R6/2 mice was 127 ± 4 and was not different between treatment groups (data not shown). qRT-PCR was conducted to measure the amount of mHtt transcript in R6/2 mouse tissue according to the protocols of Mangiarini *et al*., 1996. mHtt transcript levels were not different between vehicle, GAT211, GAT228, or GAT229 treatment groups in striatum, cortex, adipose, or whole blood (data not shown).

7.2.8. BEHAVIOURAL ANALYSES

Internal body temperature was measured *via* rectal thermometer prior to the first injection and 24 h after injection every second day.

Analgesia was determined by assessing tail flick latency prior to the first injection and 24 h after injection every second day. Mice were restrained with the distal 1 cm of the tail placed into 55°C water and the time until the tail was removed was recorded as tail flick latency (sec). Observations were ended at 10 sec.

Locomotion was assessed in the open field test prior to the first injection and 24 h after injection every second day. Mice were placed in an open space 90 cm *x* 60 cm and total distance was recorded for 5 min. Data recorded included: total distance travelled over 5 min (m), number of vertical movements, % time spent in the central quadrant of the field, time spent grooming (sec), and time spent immobile (sec).

Health and disease progression were assessed during the open field test prior to the first injection and 24 h after injection every second day. Mice were monitored for nine signs of disease progression (Table 7-1) that were ranked on a scale of 0 (absent), 1 (mild form of behaviour detected), or 2 (pronounced form of behaviour detected) (Denovan-Wright *et al*., 2008). Individual scores from each sign were added to calculate the 'sum of behavioural change (/18)'.

An observer who was blinded to genotype and treatment group confirmed all behavioural assessments.

7.2.9. DEXA Scan

Upon completion of all drug treatments and behavioural analyses, mice were euthanized with an overdose (100 mg/kg) of pentobarbital sodium (*i.p.*) followed by exsanguination. Mice were placed in a prostrate position for whole body measurements, excluding the head, of total, fat, and lean masses by dual-energy X-ray absorptiometry using a Lunar Piximus2 bone densitometer (GE Medical Systems). All scans were subject to daily calibration and were performed by a single user who was blinded to genotype and treatment group.

7.2.10. Quantitative reverse transcriptase PCR (qRT-PCR)

RNA was harvested from the striatum, cortex, visceral adipose tissue, or whole blood of

Table 7-1. Phenotype assessment scoring scheme.

Clasping	0	1	2
Piloerection	0	1	2
Palpebral Closure	0	1	2
Uncoordinated Movements	0	1	2
Hunched Posture	0	1	2
Tail Dragging	0	1	2
Abnormal Back Leg Movement	0	1	2
Tentative Movement	0	1	2
Seizure	0	NA[a]	2
Tremor	0	1	2

0, no abnormal behavior observed; 1, mild form of behavior detected; 2, pronounced form of behavior detected.

[a]A seizure was rated as 2 if it occurred. There was no intermediate value for this behavior.

R6/2 mice and age-matched C57BL/6J littermates using the Trizol® (Invitrogen, Burlington, ON) extraction method according to the manufacturer's instruction. Reverse transcription reactions were carried out with SuperScript III® reverse transcriptase (+RT; Invitrogen), or without (-RT) as a negative control for use in subsequent PCR experiments according to the manufacturer's instructions. Two micrograms of RNA were used per RT reaction. qRT-PCR was conducted using the LightCycler® system and software (version 3.0; Roche, Laval, QC). Reactions were composed of a primer-specific concentration of $MgCl_2$ (Table 7-2), 0.5 µM each of forward and reverse primers (Table 7-2), 2 µL of LightCycler® FastStart Reaction Mix SYBR Green I, and 1 µL cDNA to a final volume of 20µL with dH_2O (Roche). The PCR program was: 95°C for 10 min, 50 cycles of 95°C 10 s, a primer-specific annealing temperature (Table 7-2) for 5 s, and 72°C for 10 s. Experiments always included sample-matched –RT controls, a no-sample dH_2O control, and a standard control containing product-specific cDNA of a known concentration. cDNA abundance was calculated by comparing the cycle number at which a sample entered the logarithmic phase of amplification (crossing point) to a standard curve generated by amplification of cDNA samples of known concentration (LightCycler Software version 4.1; Roche). Here, qRT-PCR data were normalized to the expression of β-actin (Blázquez *et al*., 2011).

7.2.11. STATISTICAL ANALYSES

Concentration-response curves (CRC) were fit using non-linear regression with variable slope (4 parameters) and used to calculate EC_{50} and E_{max} (GraphPad, Prism, v. 5.0). Statistical analyses were conducted by one- or two-way analysis of variance (ANOVA), as indicated in the figure legends, using GraphPad. *Post-hoc* analyses were performed using Tukey's (one-way ANOVA) or Bonferroni's (two-way ANOVA) tests. Homogeneity of variance was confirmed using Bartlett's test. All results are reported as the mean ± the standard error of the mean (SEM) or 95% confidence interval (CI), as indicated. *P* values < 0.01 were considered to be significant.

Table 7-2. Synthetic oligonucleotides used in this study.

Target	Oligonucleotide Sequence (5' - 3')	Anneal. Temp. (°C)	$MgCl_2$ (mM)	Product length (bp)
CB_1[a]	GGGCAAATTTCCTTGTAGCA GGCTAACGTGACTGAGAAA	58	1	129
CB_2	GGATGCCGGGAGACAGAAGTGA CCCATGAGCGGCAGGTAAGAAAT	57	2	506
NAPE-PLD	CTAGACTACGGCTCGGTCCT ACCAGTCCAGCTCAATCACG	59	5	127
DAGLα	TCTACACAGAACCCCGGGAC ACTGTGTGAGCCAGACGATG	55	3	108
FAAH	AAGGTGATTTCGTGGACCCC TTCCAGCCGAACGAGACTTC	58	4	150
MAGL	TTTCCGATGACAGCTTCGGG ACAAATCGCTAGAGGGGCTC	58	2	195
PGC1α[b]	TTGCTAGCGGTCCTCACAGA GGCTCTTCTGCCTCCTGA	60	2	161
BDNF-2[a]	AGTCTCCAGGACAAGGATGAAC AAGGATGGTCATCACTCTTCTCA	58	2	119
Leptin	TCCAGGATGACACCAAAACCC TGAAGTCCAAGCCAGTGACC	59	5	108
CCL5	GCTGTTTGCCTACCTCTG TCGAGTGACAAACACGACTGC	57	2	103
IL-1β	GAAATGCCACCTTTTGACAGTG CTGGATGCTCTCATCAGGACA	57	5	117
β-actin[a]	AAGGCCAACCGTGAAAAGAT GTGGTACGACCAGAGGCATAC	59	2	110
mHtt/Htt[c]	AAGCTAGCTGCAGTAACGCCATTT (mutant) ACCTGCATGTGAACCCAGTATTCTATC (wild-type) CTACAGCCCCTCTCCAAGGTTTATAG (common)	65	1.5	560 (mutant) 240 (wild-type)

[a]Blázquez *et al*., 2011; [b]Cui *et al*., 2006; [c]Menalled *et al*., 2009. All other primers self-designed using NCBI primer BLAST.

7.3. RESULTS

*7.3.1. ERK1/2 PHOSPHORYLATION AND ARRESTIN2 RECRUITMENT IN ST*HDH$^{Q7/Q7}$ AND *ST*HDH$^{Q111/Q111}$ *CELLS*

GAT229 (*S*-enantiomer) increased the pEC_{50} and E_{max} of 2-AG, AEA- and CP55,940-mediated CB_1- and $G\alpha_{i/o}$-dependent ERK1/2 phosphorylation in ST*Hdh*$^{Q7/Q7}$ and ST*Hdh*$^{Q111/Q111}$ cells (Fig. 7-1A-C and E-G, Table 7-3). The E_{max} of cannabinoid-dependent ERK1/2 phosphorylation is reduced by approximately 50% in ST*Hdh*$^{Q111/Q111}$ cells compared to ST*Hdh*$^{Q7/Q7}$ cells (Laprairie *et al*., 2015b). The pERK E_{max} was increased approximately 202% in GAT229-treated ST*Hdh*$^{Q111/Q111}$ cells compared to ST*Hdh*$^{Q111/Q111}$ cells treated with orthosteric agonist alone (Table 7-3), which was equivalent to a recovery of pERK levels to those observed in ST*Hdh*$^{Q7/Q7}$ cells (Fig. 7-1A-C and E-G). ΔpEC_{50} was not different between ST*Hdh*$^{Q7/Q7}$ and ST*Hdh*$^{Q111/Q111}$ cells following GAT229 treatment (Table 7-3). GAT229 displayed probe-dependence because the ΔpEC_{50}, but not E_{max}, was increased in the presence of CP55,940 more than in the presence of 2-AG or AEA (Table 1). GAT229 did not display intrinsic activity for the ERK assay in ST*Hdh*$^{Q7/Q7}$ or ST*Hdh*$^{Q111/Q111}$ cells (Fig. 7-1D,H, Table 7-3).

GAT228 (*R*-enantiomer) did not change the pEC_{50} or E_{max} of 2-AG, AEA- and CP55,940-mediated CB_1- and $G\alpha_{i/o}$-dependent ERK1/2 phosphorylation in ST*Hdh*$^{Q7/Q7}$ or ST*Hdh*$^{Q111/Q111}$ cells (Fig. 7-1A-C and E-G, Table 7-3). pEC_{50} and E_{max} were not different between ST*Hdh*$^{Q7/Q7}$ and ST*Hdh*$^{Q111/Q111}$ cells following GAT228 treatment (Table 7-3). In the pERK assay, GAT228 alone displayed high nanomolar potency that did not differ between cell types [202 (120 – 261) nM] and moderate efficacy (46.6 ± 5.5% compared to CP55,940 alone) that was greater for ST*Hdh*$^{Q7/Q7}$ cells than ST*Hdh*$^{Q111/Q111}$ cells (Fig. 7-1D,H, Table 7-3).

GAT211 (racemic mixture) displayed intermediate activity between its *S*- and *R*-enantiomers in the pERK assay. GAT211 increased the pEC_{50} and E_{max} of 2-AG, AEA- and CP55,940-mediated CB_1- and $G\alpha_{i/o}$-dependent ERK1/2 phosphorylation in ST*Hdh*$^{Q7/Q7}$ and

ST*Hdh*$^{Q111/Q111}$ cells, but less than GAT229 (Fig. 7-1A-C and E-G, Table 7-3). The pERK E_{max} was increased approximately 173% in GAT211-treated ST*Hdh*$^{Q111/Q111}$ cells compared to ST*Hdh*$^{Q111/Q111}$ cells treated with orthosteric agonist alone (Table 7-3), which, like GAT229 treatment, was equivalent to a recovery of pERK levels to those observed in ST*Hdh*$^{Q7/Q7}$ cells (Fig. 7-1A-C and E-G). ΔpEC_{50} was lower in ST*Hdh*$^{Q111/Q111}$ cells treated with 1 µM GAT211 + AEA compared to ST*Hdh*$^{Q7/Q7}$ exposed to the same treatment (Table 7-3). GAT211 displayed similar probe-dependence to GAT229 because the ΔpEC_{50}, but not E_{max}, was increased in the presence of CP55,940 more than in the presence of 2-AG or AEA (Table 7-3). Like GAT228, GAT211 alone displayed high nanomolar potency that did not differ between cell types [582 (494 – 643) nM] and moderate efficacy (37.3 ± 3.4% compared to CP55,940 alone) that was greater for ST*Hdh*$^{Q7/Q7}$ cells than ST*Hdh*$^{Q111/Q111}$ cells (Fig. 7-1D,H, Table 7-3).

GAT229 (*S*-enantiomer) increased the pEC_{50} and E_{max} of 2-AG, AEA- and CP55,940-mediated CB_1-dependent arrestin2 recruitment in ST*Hdh*$^{Q7/Q7}$ and ST*Hdh*$^{Q111/Q111}$ cells (Fig. 7-1I-K and M-O, Table 7-3). No differences in ΔpEC_{50} or *E*max were observed between ST*Hdh*$^{Q7/Q7}$ and ST*Hdh*$^{Q111/Q111}$cells (Table 7-3). GAT229 displayed probe-dependence because the ΔpEC_{50} was greater in the presence of CP55,940 than in the presence of 2-AG or AEA in ST*Hdh*$^{Q111/Q111}$cells, and the E_{max} was greater in the presence of AEA than CP55,940 or 2-AG in ST*Hdh*$^{Q111/Q111}$cells (Table 7-3). GAT229 did not display intrinsic activity for the arrestin2 assay in ST*Hdh*$^{Q7/Q7}$ or ST*Hdh*$^{Q111/Q111}$ cells (Fig. 7-1L,P, Table 7-3).

GAT228 (*R*-enantiomer) did not change the pEC_{50} or E_{max} of 2-AG, AEA- and CP55,940-mediated CB_1-dependent arrestin2 recruitment in ST*Hdh*$^{Q7/Q7}$ and ST*Hdh*$^{Q111/Q111}$ cells (Fig. 7-1I-K and M-O, Table 7-3). pEC_{50} and E_{max} were not different between ST*Hdh*$^{Q7/Q7}$ and ST*Hdh*$^{Q111/Q111}$ cells following GAT228 treatment (Table 7-3). In the arrestin2 assay, pEC_{50} and E_{max} did not differ between cell types treated with GAT228 [166 (112 – 206) nM; 39.24 ± 4.7% compared to CP55,940 alone) (Fig. 7-1L,P, Table 7-3).

GAT211 (racemic mixture) displayed intermediate activity between its *S*- and *R*-enantiomers in the arrestin2 assay. GAT211 increased the pEC_{50} and E_{max} of 2-AG, AEA- and CP55,940-mediated CB_1-dependent arrestin2 recruitment, but less than GAT229 (Fig. 7-1A-C and E-G, Table 7-3). ΔpEC_{50} was greater in ST*Hdh*$^{Q111/Q111}$ cells treated with 1 μM GAT211 + CP55,940 compared to ST*Hdh*$^{Q7/Q7}$ exposed to the same treatment (Table 7-3). GAT211 displayed similar probe-dependence to GAT229 because the ΔpEC_{50} was increased in the presence of CP55,940 more than in the presence of 2-AG or AEA in ST*Hdh*$^{Q111/Q111}$ cells, and the E_{max} was greater in the presence of AEA than CP55,940 or 2-AG in ST*Hdh*$^{Q111/Q111}$cells (Table 17-3). GAT211 displayed lower pEC_{50} and E_{max} than GAT228 that did not differ between cell types [292 (249 – 342) nM; 37.4 ± 2.1% compared to CP55,940 alone) (Fig. 7-1L,P, Table 7-3).

Regardless of the expression of mHtt, each GAT compound tested displayed signaling bias when pERK and arrestin2 assay data were compared. For GAT229, the ΔpEC_{50} was higher and the E_{max} was lower in the pERK assay compared to the arrestin2 assay in ST*Hdh*$^{Q7/Q7}$ cells treated with CP55,940 (Table 7-3). In ST*Hdh*$^{Q111/Q111}$ cells treated with GAT229, the ΔpEC_{50} was lower and the E_{max} was higher in the pERK assay compared to the arrestin2 assay when 2-AG or CP55,940 (E_{max} only) were the orthosteric ligands (Table 7-3). Unlike GAT229, GAT228 displayed agonist activity in the pERK and arrestin2 assays in the absence of orthosteric ligand. GAT228 alone, caused an increase in E_{max} that was higher in the pERK assay compared to the arrestin2 assay in ST*Hdh*$^{Q7/Q7}$ cells (Table 7-3). For GAT211, the ΔpEC_{50} was higher in the pERK assay compared to the arrestin2 assay in ST*Hdh*$^{Q7/Q7}$ cells treated with CP55,940, and the E_{max} was higher in the pERK assay compared to the arrestin2 assay in ST*Hdh*$^{Q111/Q111}$ cells treated with AEA (Table 7-3). Overall, GAT229 behaved as a PAM of 2-AG and AEA-mediated CB_1 signaling without having any inherent agonist activity. In contrast, GAT228 had agonist activity, but did not modulate orthosteric agonist activity. GAT211, an equimolar racemic mixture of GAT229 and GAT228, displayed an intermediate pattern of activity. Importantly, these compounds had the same relative activity in wild-type and mHtt-expressing cells.

Figure 7-1. Characterization of GAT211-, GAT228-, and GAT229-dependent effects on ERK1/2 phosphorylation and arrestin2 recruitment in ST*Hdh* cells. **A-H)** ST*Hdh*$^{Q7/Q7}$ and ST*Hdh*$^{Q111/Q111}$ cells were treated with 1 nM – 10 µM 2-AG, AEA, CP55,940, GAT211, GAT228, or GAT229 ± 1 µM GAT211, GAT228, or GAT229 for 10 min and ERK1/2 phosphorylation (Y185/204) compared to total ERK1/2 levels was determined *via* In-cell™ western. **I-P)** ST*Hdh*$^{Q7/Q7}$ and ST*Hdh*$^{Q111/Q111}$ cells were transfected with CB_1-GFP^2 and arrestin2-Rluc and treated with 1 nM – 10 µM 2-AG, AEA, CP55,940, GAT211, GAT228, or GAT229 ± 1 µM GAT211, GAT228, or GAT229 for 30 min and $BRET_{Eff}$ was determined. CRCs were fit using non-linear regression analysis with variable slope (4 parameter) using Prism (GraphPad v. 5.0). *N* = 6.

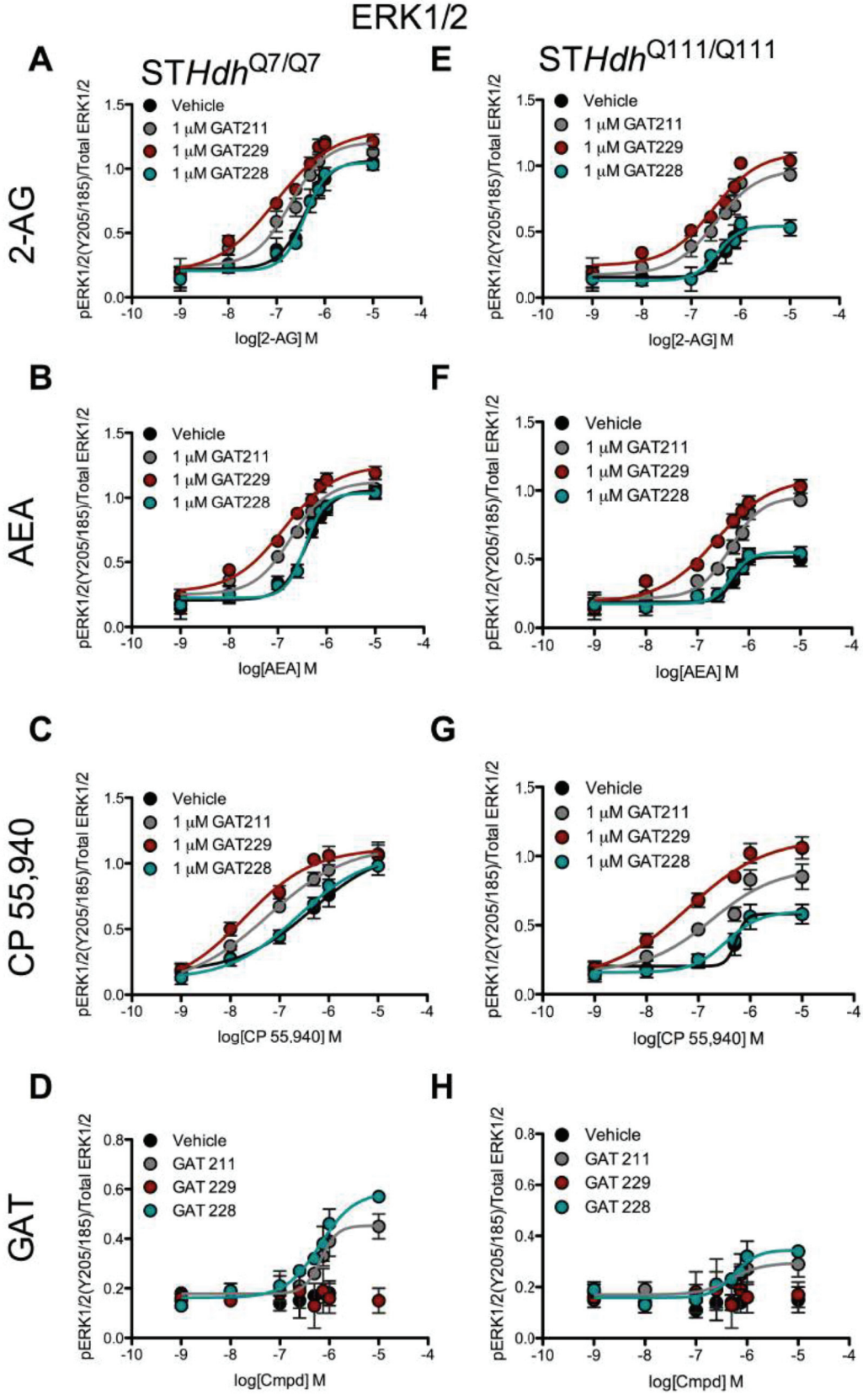
ERK1/2
A
STHdhQ7/Q7
E
STHdhQ111/Q111
2-AG
B
AEA
C
CP 55,940
D
GAT
F
G
H
Vehicle
1 μM GAT211
1 μM GAT229
1 μM GAT228
GAT 211
GAT 229
GAT 228
pERK1/2(Y205/185)/Total ERK1/2
log[2-AG] M
log[AEA] M
log[CP 55,940] M
log[Cmpd] M

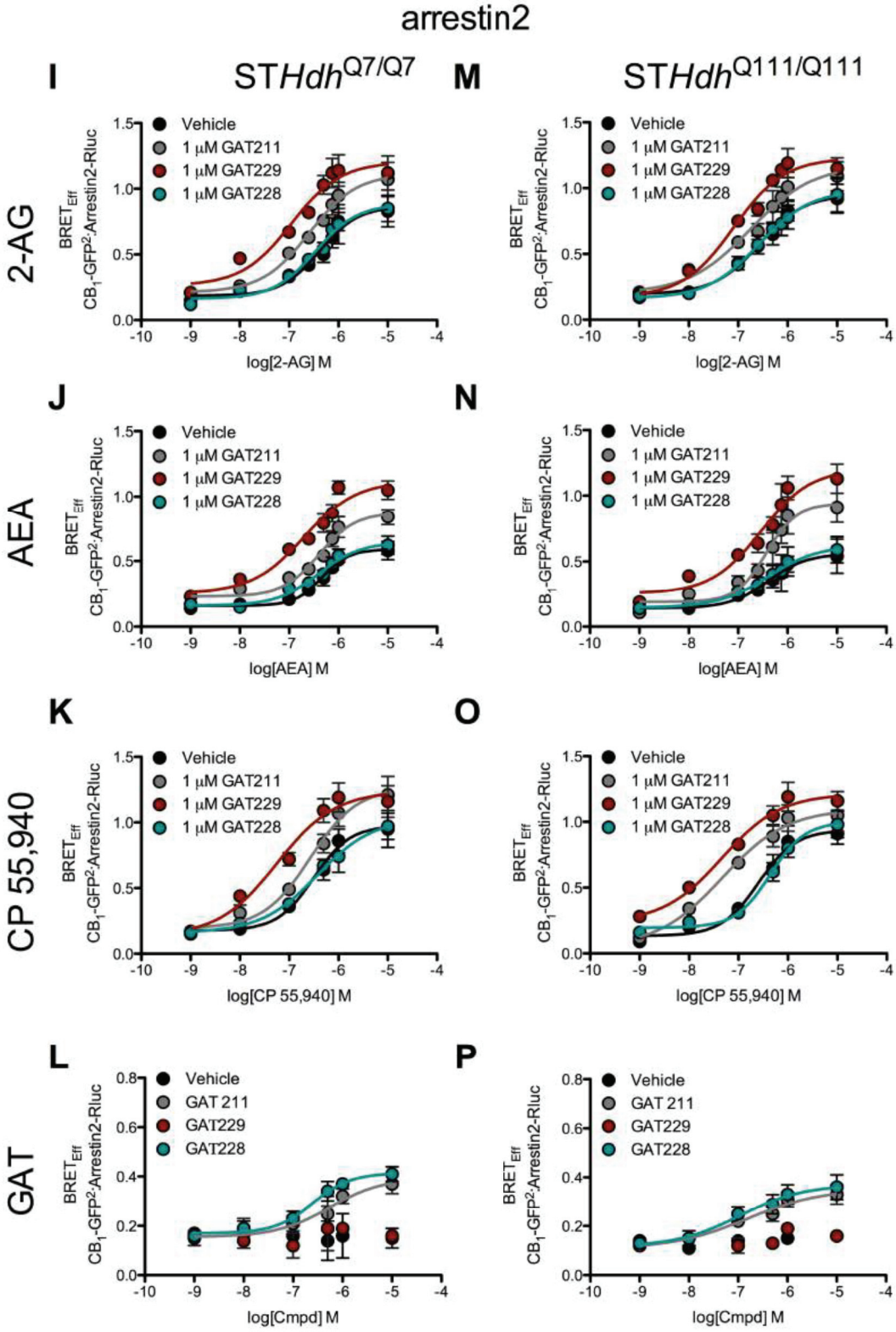
arrestin2
I
STHdhQ7/Q7
M
STHdhQ111/Q111
2-AG
AEA
CP 55,940
GAT
J
N
K
O
L
P
Vehicle
1 μM GAT211
1 μM GAT229
1 μM GAT228
GAT 211
GAT229
GAT228
BRETEff
CB1-GFP2:Arrestin2-Rluc
log[2-AG] M
log[AEA] M
log[CP 55,940] M
log[Cmpd] M

Table 7-3. Summary of data for GAT211, GAT228, and GAT229 in ST*Hdh*$^{Q7/Q7}$ and ST*Hdh*$^{Q111/Q111}$ cells.

	ERK1/2 ($G\alpha_{i/o}$)				arrestin2			
	ST*Hdh*$^{Q7/Q7}$		ST*Hdh*$^{Q111/Q111}$		ST*Hdh*$^{Q7/Q7}$		ST*Hdh*$^{Q111/Q111}$	
	ΔpEC_{50} ± SEM[a]	E_{max} ± SEM (%)[b]	ΔpEC_{50} ± SEM[a]	E_{max} ± SEM (%)[b]	ΔpEC_{50} ± SEM[a]	E_{max} ± SEM (%)[b]	ΔpEC_{50} ± SEM[a]	E_{max} ± SEM (%)[b]
1 μM GAT229	*N.C.*	*N.C.*	*N.C.*	*N.C.*	*N.C.*	*N.C.*	*N.C.*	*N.C.*
+ 2-AG	0.59 ± 0.18	122.37 ± 9.30	0.20 ± 0.15*^	202.91 ± 9.07*^	0.58 ± 0.20	139.08 ± 9.95	0.52 ± 0.15	129.21 ± 6.98
+ AEA	0.47 ± 0.12	117.94 ± 6.38	0.33 ± 0.10	211.27 ± 10.90*	0.36 ± 0.15	189.65 ± 8.61†	0.14 ± 0.19	179.83 ± 10.13†
+ CP 55,940	1.36 ± 0.19^†	100.45 ± 7.86^	0.95 ± 0.28†	194.63 ± 6.44*^	0.75 ± 0.26	126.98 ± 10.61	0.94 0.24†	129.34 ± 8.06
1 μM GAT228	*6.92 ± 0.12*	*58.78 ± 4.92^*	*6.47 ± 0.17*	*34.48 ± 3.93**	*6.60 ± 0.21*	*41.44 ± 3.22*	*6.96 ± 0.46*	*37.04 ± 5.51*
+ 2-AG	-0.01 ± 0.06	98.50 ± 5.01	0.12 ± 0.11	100.35 ± 4.65	0.08 ± 0.17	102.21 ± 9.39	0.01 ± 0.18	103.54 ± 10.13
+ AEA	0.03 ± 0.05	97.73 ± 4.84	0.04 ± 0.13	106.53 ± 4.69	0.07 ± 0.14	109.47 ± 5.54	-0.01 ± 0.27	111.79 ± 13.02
+ CP 55,940	0.27 ± 0.33	96.85 ± 11.23	0.20 ± 0.17	103.32 ± 5.33	-0.07 ± 0.22	105.89 ± 12.92	-0.24 ± 0.10	106.54 ± 6.19
1 μM GAT211	*6.17 ± 0.10*	*45.29 ± 4.17*	*6.30 ± 0.46*	*29.37 ± 5.69**	*6.26 ± 0.56*	*39.43 ± 9.82*	*6.81 ± 0.49*	*35.36 ± 6.46*
+ 2-AG	0.29 ± 0.12	113.63 ± 8.61	0.15 ± 0.14	179.17 ± 8.46*^	0.21 ± 0.14	128.80 ± 8.98	0.18 ± 0.23	123.63 ± 13.58
+ AEA	0.32 ± 0.11	106.23 ± 7.05	0.05 ± 0.09*	184.82 ± 6.02*	0.05 ± 0.11	147.65 ± 5.87	0.03 ± 0.14	168.21 ± 9.15†
+ CP 55,940	0.88 ± 0.30^†	102.52 ± 11.89	0.57 ± 0.29†	157.32 ± 12.07*	0.07 ± 0.17	129.54 ± 11.51	0.73 ± 0.27*†	117.09 ± 9.80

[a]pEC_{50} determined for GAT211, GAT228, or GAT229 alone; or determined as the change (Δ) in pEC_{50} compared to orthosteric agonist alone (1 nM - 10 μM) in the presence of 1 μM GAT211, GAT228, or GAT229. N.C., not converged.
[b]E_{max} (%) response compared to E_{max} for CP 55,940 alone determined for GAT211, GAT228, or GAT229 alone or at 1 μM GAT211, GAT228, or GAT229 in the presence of orthosteric agonist.

*$P < 0.01$ compared to ST*Hdh*$^{Q7/Q7}$ cells within assay; †$P < 0.01$ compared to other orthosteric agonists tested within GAT group; ^P < 0.01 compared to arrestin2 (BRETEff) within cell type, as determined *via* two-way ANOVA followed by Bonferroni's *post-hoc* analysis. $N = 6$.

7.3.2. CELL VIABILITY ASSAYS IN STHDH$^{Q7/Q7}$ AND STHDH$^{Q111/Q111}$ CELLS

ST*H*dh$^{Q7/Q7}$ and ST*Hdh*$^{Q111/Q111}$ cells were treated with 100 nM AEA ± 1 µM GAT211, GAT228, or GAT229 and mitochondrial respiration activity (% esterase activity relative to vehicle-treated ST*Hdh*$^{Q7/Q7}$ cells) and membrane permeability (% membrane permeability relative to 70% methanol-treated ST*Hdh*$^{Q111/Q111}$ cells) were quantified. Cell viability was lower in ST*Hdh*$^{Q111/Q111}$ cells compared to ST*Hdh*$^{Q7/Q7}$ cells and cell viability was increased following treatment with 100 nM AEA for 18 h (Fig. 7-2A,B). Treatment with 1 µM GAT211, GAT228, or GAT229 for 18 h did not change cell viability in ST*H*dh$^{Q7/Q7}$ or ST*Hdh*$^{Q111/Q111}$ cells (Fig. 7-2A,B). Treatment with 100 nM AEA + 1 µM GAT211 also increased cell viability in ST*Hdh*$^{Q111/Q111}$ cells compared to vehicle-treated ST*Hdh*$^{Q111/Q111}$ cells (Fig. 7-2A,B). Importantly, treatment with 100 nM AEA + 1 µM GAT229 increased cell viability in ST*Hdh*$^{Q111/Q111}$ cells compared to vehicle- and AEA-treated ST*Hdh*$^{Q111/Q111}$ cells. Therefore, GAT229 conferred a neuroprotective effect in the ST*Hdh*$^{Q111/Q111}$ cell culture model of HD that was greater than AEA alone, or GAT211 or GAT228.

7.3.3. ASSESSMENT OF LOCOMOTION, BEHAVIOUR, AND HD-LIKE SYMPTOM PROGRESSION IN R6/2 MICE

Internal temperature, analgesia, and anxiety were assessed in 7 week-old wild-type and R6/2 mice treated with 10 mg/kg/d *i.p.* GAT211, GAT228, or GAT229 for 21 d to determine how these compounds behaved *in vivo*. GAT211 GAT228 and GAT229 did not change body temperature in wild-type or R6/2 mice following the 21 d treatment period (Fig. 7-3A). GAT211, GAT228, and GAT229 did not produce an analgesic effect in the tail flick response assay in wild-type and R6/2 mice at the end of the 21 d treatment period (Fig. 7-3B). GAT211, GAT228, and to a lesser extent GAT229, each increased the % of time mice spent in the central quadrant of the open field – modelling an anxiolytic effect – consistent with enhanced CB_1 signaling in wild-type

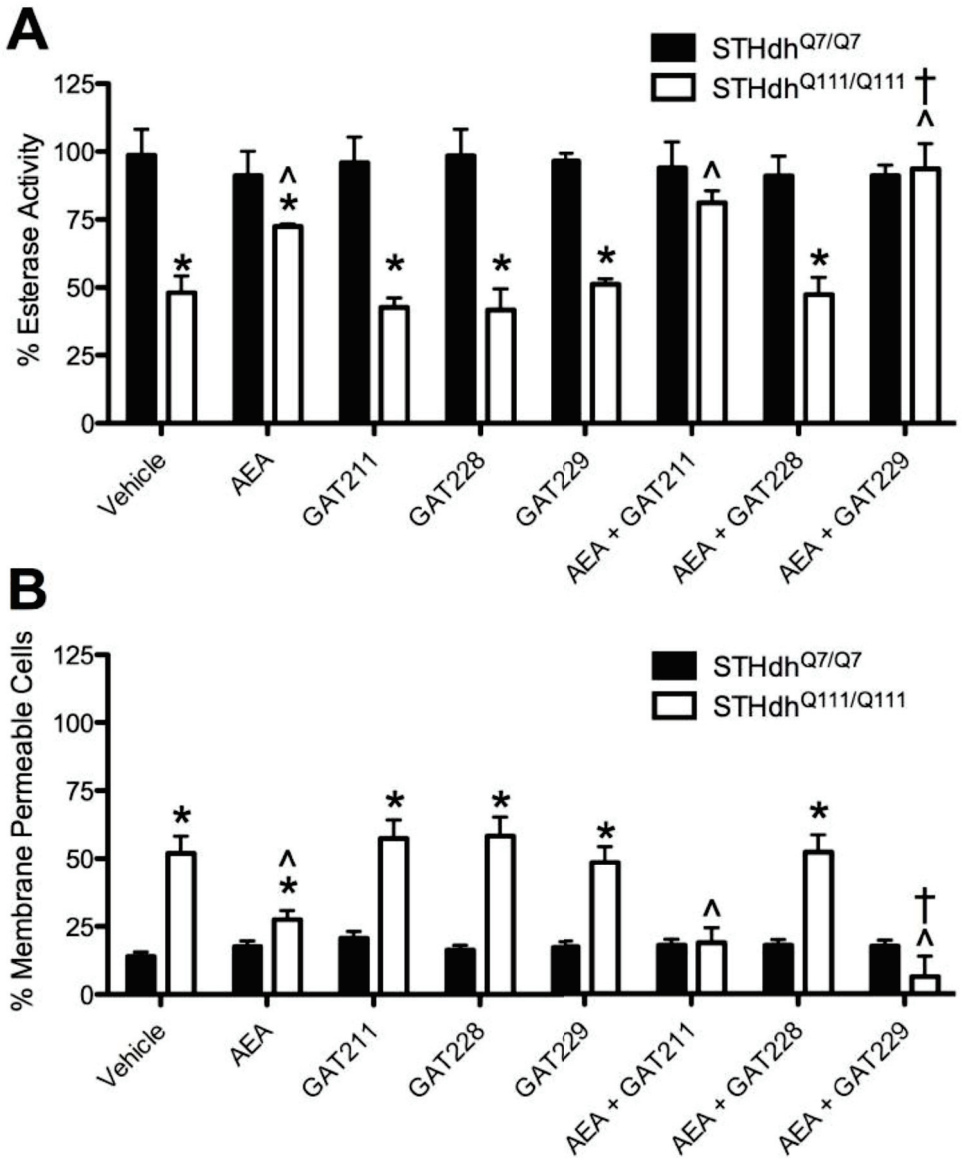

Figure 7-2. GAT211 and GAT229 enhanced the pro-survival effect of AEA in ST*Hdh*$^{Q111/Q111}$ cells. ST*Hdh*$^{Q7/Q7}$ and ST*Hdh*$^{Q111/Q111}$ cells were treated with vehicle (10% DMSO), 100 nM AEA, 1 µM GAT211, GAT228, or GAT229, or 100 nM AEA + 1 µM GAT211, GAT228, or GAT229 for 18 h and **A)** cellular esterase activity was quantified as a measure of cellular viability, or **B)** membrane permeability to the fluorescent dye EthD-1 was quantified as a measure of cell death, using the Live/Dead Cytotoxicity assay. *$P < 0.01$ compared to ST*Hdh*$^{Q7/Q7}$ cells within treatment, ^$P < 0.01$ compared to vehicle treatment within cell type, †$P < 0.01$ to AEA treatment within cell type, as determined *via* two-way ANOVA followed by Bonferroni's *post-hoc* analysis. $N = 6$.

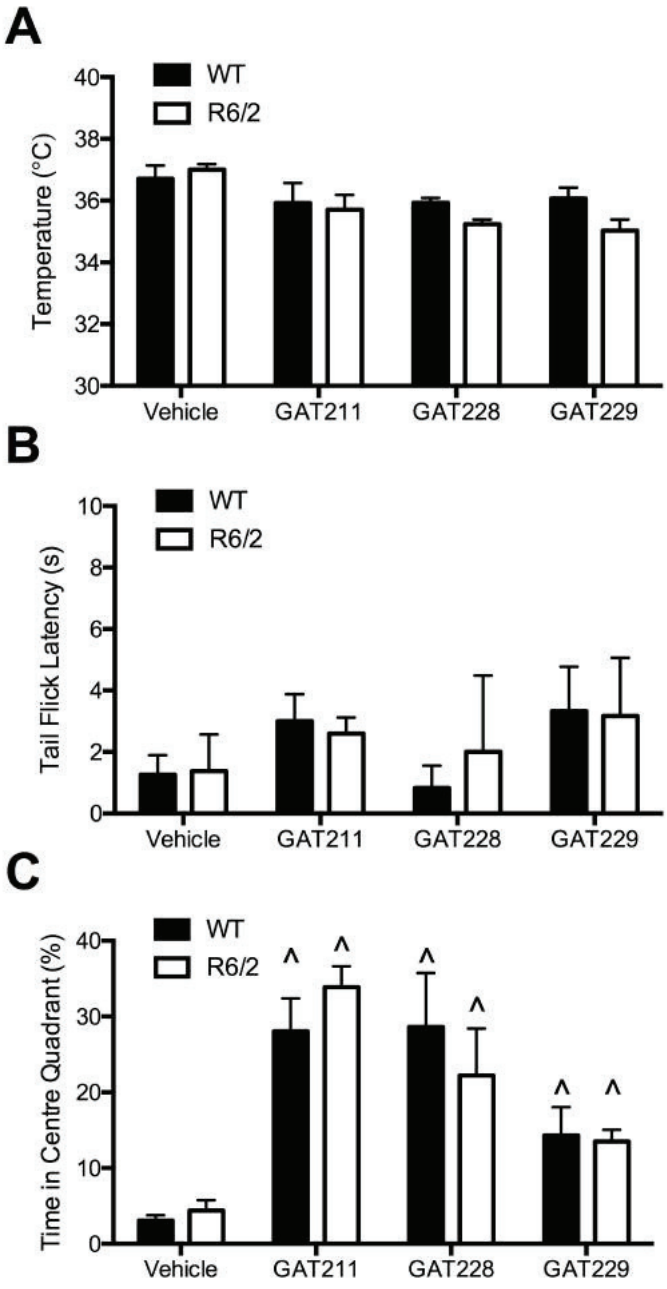

Figure 7-3. Assessment of tetrad effects in GAT211-, GAT228-, and GAT229-treated wild-type and R6/2 mice. Wild-type (C57BL/6J) and R6/2 mice were treated with vehicle or 10 mg/kg/d *i.p.* GAT211, GAT228, or GAT229 for 21 d. Measurements of body temperature, analgesia, and time in the centre quadrant of the open field shown here were made at the end of the treatment period (*i.e.* day 21). **A)** Body temperature was determined by rectal thermometer. **B)** Analgesia was determined by measuring the mouse's latency to remove their tail from a 55°C water bath (tail flick assay). **C)** Anxiety was modeled by measuring the percentage of time spent in the centre quadrant of the open field during 5 min open field assays. $^P < 0.01$ compared to vehicle within genotype as determined *via* two-way ANOVA followed by Bonferroni's *post-hoc* analysis. $N = 5$ per group.

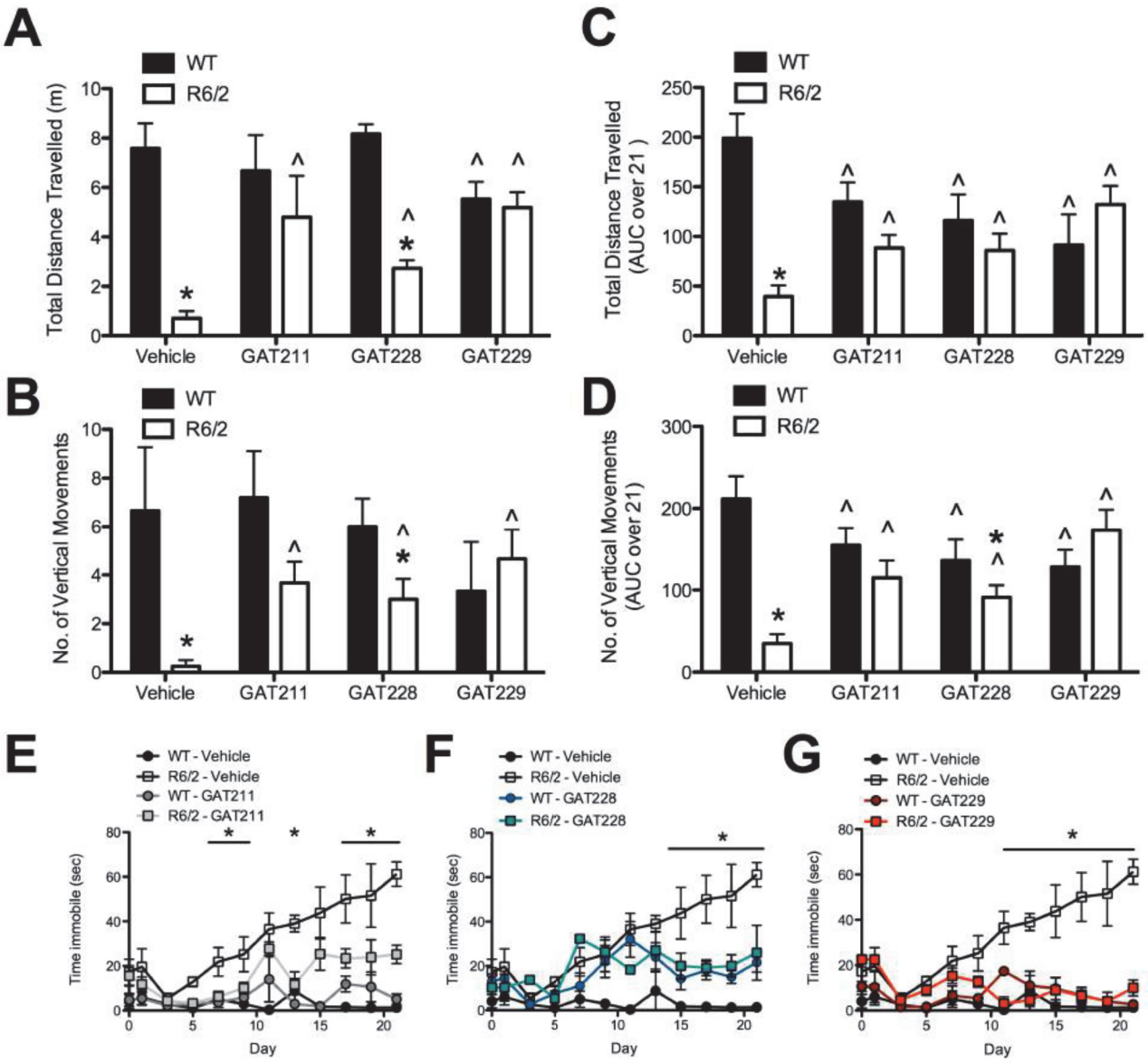

Figure 7-4. GAT211, GAT228, and GAT229 normalized locomotor activity in R6/2 mice. Wild-type (C57BL/6J) and R6/2 mice were treated with vehicle or 10 mg/kg/d *i.p.* GAT211, GAT228, or GAT229 for 21 d and measurements of total distance travelled (m), number of vertical movements, and time spent immobile (sec) in open field were made. **A**) Total distance travelled (m) in the open field test over 5 min at the end of the treatment period (*i.e.* day 21). **B**) Number of vertical movements in the open field test over 5 min at the end of the treatment period (*i.e.* day 21). **C**) Total area under the curve (AUC) for total distance travelled (m) in the open field test for the duration of the treatment period. **D**) Total AUC for the number of vertical movements in the open field test for the duration of the treatment period. *$P < 0.01$ compared to wild-type within treatment, ^$P < 0.01$ compared to vehicle within genotype. **E-G**) Time spent immobile (sec) in the open field test over 5 min. *$P < 0.01$ R6/2 treated with GAT compound *versus* R6/2 treated with vehicle within day. Statistical differences determined *via* two-way ANOVA followed by Bonferroni's *post-hoc* analysis. $N = 5$ per group.

and R6/2 mice at the end of the 21 d treatment period (Fig. 7-3C). No differences in change in body temperature, tail flick response, or time in centre quadrant were observed between wild-type and R6/2 mice (Fig. 7-3).

The R6/2 mouse model of HD begins to exhibit signs of motor impairment, including hypolocomotion in the open field, decreased duration on the rotarod, decreased performance on the accelerating rotarod, and increased time spent immobile, at approximately 7 weeks of age (Brooks and Dunnett, 2015). Total distance travelled, number of vertical movements, and time spent immobile in the open field were recorded in wild-type and R6/2 mice treated with vehicle or 10 mg/kg/d GAT211, GAT228, or GAT229 (*i.p.*) for 21 d beginning at 7 weeks of age. In wild-type mice, GAT211, GAT228, and GAT229 reduced the total distance travelled and the number of vertical movements at the end of the 21 d treatment period (Fig. 7-4A,B). Unlike GAT-treated wild-type mice, locomotor activity increased in GAT-treated R6/2 mice compared to vehicle-treated R6/2 mice (Fig. 7-4A,B). Treatment of R6/2 mice with GAT211, GAT228, and GAT229 was associated with increased distance travelled in the open field (Fig. 7-4A) and increased vertical movements (Fig. 7-4B) at the end of the 21 d treatment period. Total distance travelled and number of vertical movements remained lower in GAT228-treated R6/2 mice compared to GAT228-treated wild-type mice at the end of the 21 d treatment period (Fig. 7-4A,B). Area under the curve (AUC) was calculated for total distance travelled (m) and number of vertical movements for wild-type and R6/2 mice treated with vehicle or 10 mg/kg/d GAT211, GAT228, or GAT229 over the 21 d treatment period. Vehicle-treated R6/2 mice displayed low movement calculated as AUC compared to vehicle-treated wild-type mice (Fig. 7-4C,D). GAT211, GAT228, and GAT229 treatment was associated with reduced AUC for total distance travelled and the number of vertical movements in wild-type mice (Fig. 7-4C,D). Total locomotor activity (AUC) increased in GAT-treated R6/2 mice compared to vehicle-treated R6/2 mice (Fig. 7-4C,D). Number of vertical movements (AUC) remained significantly lower in GAT228-treated R6/2 mice compared to GAT228-treated wild-type mice (Fig. 7-4D). GAT211 and GAT229 did

not effect immobility time in wild-type mice (Fig. 7-4E,G). GAT228 increased immobility time in wild-type mice beginning at day 9 and continuing for the duration of the experiment (Fig. 7-4F). GAT211-treated R6/2 mice displayed reduced immobility time (days 7 – 9, 11, 17 – 21) compared to vehicle-treated R6/2 mice (Fig. 7-4E); GAT228-treated R6/2 mice displayed reduced immobility time (days 15 – 21) compared to vehicle-treated R6/2 mice (Fig. 7-4F); and GAT229-treated R6/2 mice displayed the greatest reduction in immobility time (days 11 – 21) compared to vehicle-treated R6/2 mice (Fig. 7-4G). While GAT211, GAT228, and GAT229 each normalized motor activity in R6/2 mice compared to vehicle treatment, GAT229 imparted the most benefit in reducing the motor impairment associated with HD in the R6/2 mouse model compared to vehicle, GAT211, or GAT228 treatment.

HD-like signs and symptoms were evaluated in R6/2 mice according to the measurements described in Table 7-1. Observations [scored as 0, 1, or 2 (Table 7-1)] were used to calculate a sum of behavioural changes (/18) for wild-type and R6/2 mice treated with vehicle or 10 mg/kg/d GAT211, GAT228, or GAT229 (*i.p.*) for 21 d beginning at 7 weeks of age (Fig. 4). Vehicle, GAT211, GAT228, and GAT229 did not affect any of the assessed measures in wild-type mice (Fig. 7-5). In vehicle-treated R6/2 mice, the sum of behavioural changes increased from an initial mean score of 4.5 ± 1.2 (day 0) to a final mean score of 15 ± 0.53 (day 21) (Fig. 7-5). The sum of behavioural changes was lower from days 11 – 17 in GAT211-treated R6/2 mice compared to vehicle-treated R6/2 mice (Fig. 7-5A), suggesting that symptom progression was delayed by treatment with 10 mg/kg GAT211. GAT228 treatment did not change the sum of behavioural changes in R6/2 mice compared to vehicle treatment (Fig. 7-5B). The sum of behavioural changes was lower from days 13 - 21 in GAT229-treated R6/2 mice compared to vehicle-treated R6/2 mice (Fig. 7-5C), indicating that symptom progression was delayed by treatment with 10 mg/kg GAT229 compared to vehicle and the racemic compound GAT211. As with modulation of

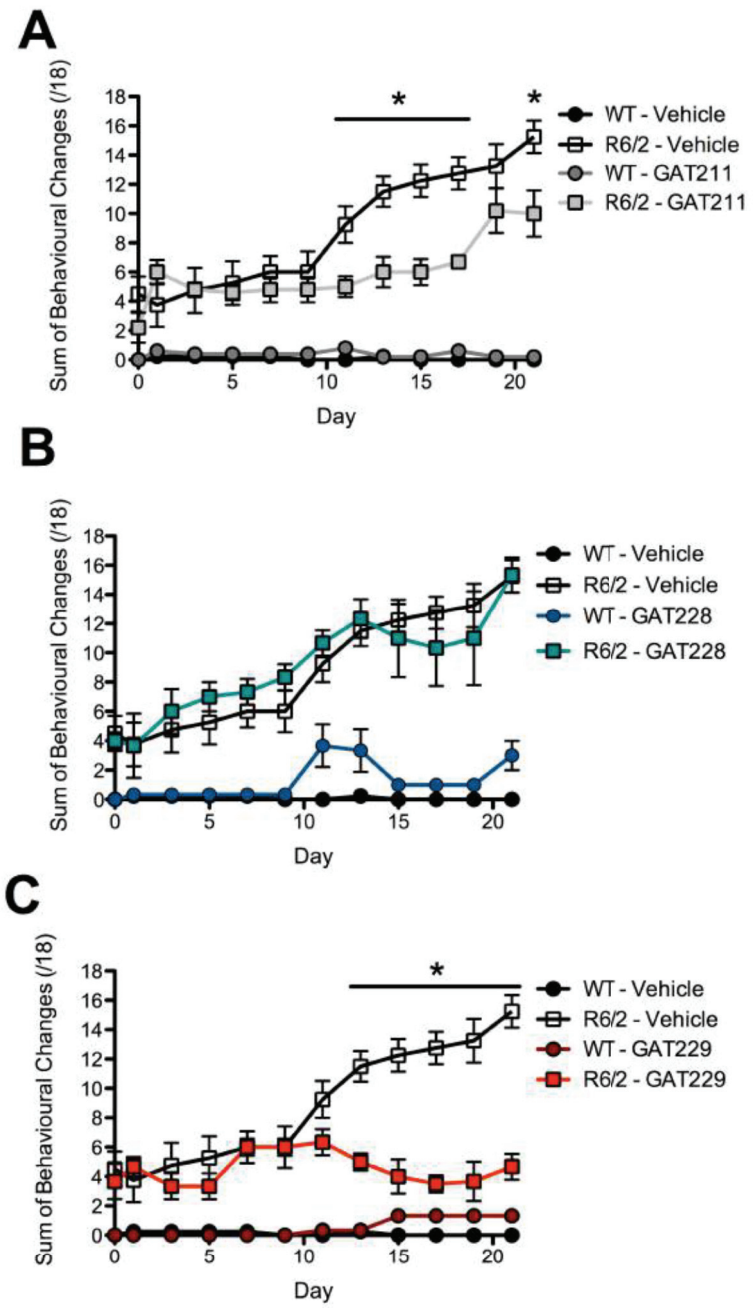

Figure 7-5. GAT211 and GAT229 delayed behavioural changes associated with HD in R6/2 mice. Wild-type (C57BL/6J) and R6/2 mice were treated with vehicle or 10 mg/kg/d *i.p.* GAT211 **(A)**, GAT228 **(B)**, or GAT229 **(C)** for 21 d and phenotype was assessed (see Table 7-1) 24 h after treatment every second day. **P* < 0.01 R6/2 treated with GAT compound *versus* R6/2 treated with vehicle within day as determined *via* two-way ANOVA followed by Bonferroni's *post-hoc* analysis. *N* = 5 per group.

locomotor activity (Fig. 7-4), GAT229 conferred the most benefit in delaying the signs and symptoms of HD, and normalizing animal behaviour, in the R6/2 mouse model of HD.

7.3.4. Body composition in R6/2 HD mice

R6/2 mice, and patients suffering from HD, experience a failure to gain weight and an increase in body fat content at the expense of lean tissue during the progression of HD (Fain *et al.*, 2001; Phan *et al*., 2009; Malejko *et al*., 2014). To determine whether GAT211, GAT228, or GAT229 altered weight gain and body composition, weight was measured in wild-type and R6/2 mice treated with vehicle or 10 mg/kg/d GAT211, GAT228, or GAT229 (*i.p.*) for 21 d beginning at 7 weeks of age and reported as % weight change compared to initial weight prior to treatment (Fig. 7-6A-D). Following euthanasia, DEXA scans were conducted to determine the % fat and % lean tissue in wild-type and R6/2 mice (Fig. 7-6E,F). Wild-type mice gained 27 ± 1.4% of their initial weight during the 21 d course of the experiment and weight gain did not differ between vehicle-, GAT211-, GAT228-, and GAT229-treated wild-type mice (Fig. 7-6A-D). As expected, vehicle-treated R6/2 mice lost 6.4 ± 0.59% of their initial body weight during the 21 d course of the experiment (Fig. 7-6A-D) (Fain *et al.*, 2001). GAT211-treated R6/2 mice gained 8.9 ± 5.1% of their initial body weight during the 21 d course of the experiment, showing improved weight gain compared to vehicle-treated R6/2 mice by day 15, but less weight gain compared to GAT211-treated wild-type mice (Fig. 7-6A,D). GAT228-treated R6/2 mice lost 4.7 ± 6.6% of their initial body weight during the 21 d course of the experiment, which was not different compared to vehicle-treated R6/2 mice (Fig. 7-6B,D). GAT229-treated R6/2 mice gained 11 ± 7.9% of their initial body weight during the 21 d course of the experiment, showing improved weight gain compared to vehicle-treated R6/2 mice by day 18 that was equivalent to the normal weight gain observed in GAT229-treated wild-type mice (Fig. 7-6C,D). R6/2 mice had a higher % fat, and a lower % lean tissue, compared to wild-type mice regardless of treatment, as determined *via post-mortem* DEXA scan (Fig. 7-6E,F). In addition, GAT228-treated R6/2 mice displayed a greater % fat, and a lower % lean tissue, than vehicle-treated R6/2

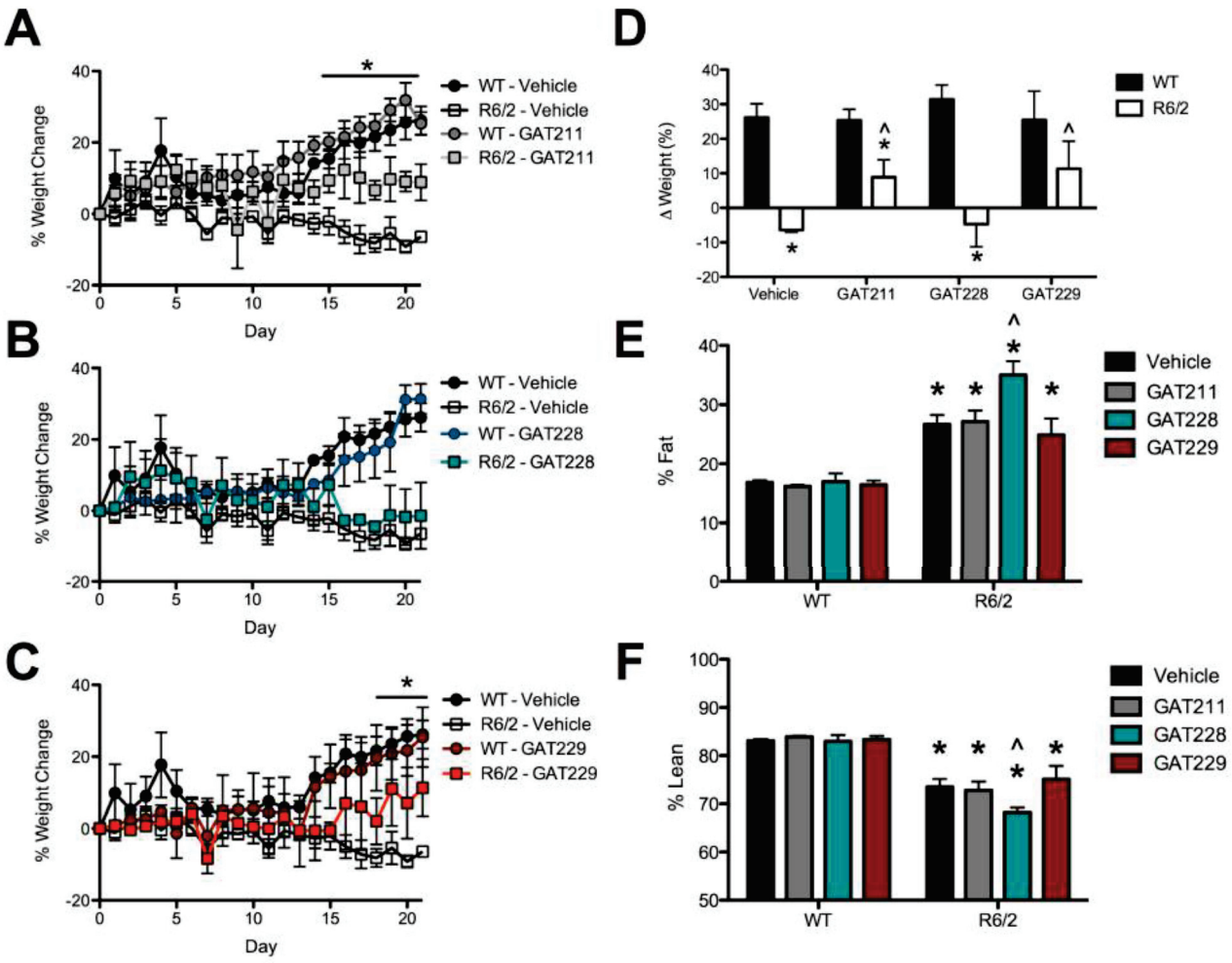

Figure 7-6. GAT211 and GAT229 improved weight gain in R6/2 mice. **A-D)** Wild-type (C57BL/6J) and R6/2 mice were treated with vehicle or 10 mg/kg/d *i.p.* GAT211 **(A)**, GAT228 **(B)**, or GAT229 **(C)** for 21 d and weight was measured 24 h after GAT treatment every day. **D)** Summary of total change in weight over 21 d duration of the experiment. *$P < 0.01$ R6/2 treated with GAT compound *versus* R6/2 treated with vehicle within day as determined *via* two-way ANOVA followed by Bonferroni's *post-hoc* analysis. $N = 5$ per group. **E,F**) DEXA scans of mice were conducted *post-mortem* to determine the % fat **(E)** tissue and % lean (**F)** tissue following the 21 d experiment. *$P < 0.01$ compared to wild-type within treatment, ^$P < 0.01$ compared to vehicle within genotype as determined *via* two-way ANOVA followed by Bonferroni's *post-hoc* analysis. $N = 5$ per group.

mice (Fig. 7-6E,F). Based on these data we concluded that the CB_1 PAM GAT229 promoted normal weight gain in R6/2 mice and was neutral with respect to changes in body composition that occur during HD pathogenesis. In contrast, the CB_1 allosteric agonist GAT228 was neutral with respect to weight gain in R6/2 mice and exacerbated the increase in body fat and loss of lean mass that occur during HD pathogenesis. As expected, the racemic compound GAT211 displayed effects intermediate effects between its two enantiomers.

7.3.5. GENE EXPRESSION IN THE BRAIN, ADIPOSE, AND BLOOD OF R6/2 HD MICE

$G\alpha_{i/o}/\beta\gamma$-biased CB_1 agonists, such as 2-AG and AEA, increase CB_1 mRNA and protein levels and decrease CB_2 mRNA and protein levels in ST*Hdh*$^{Q111/Q111}$ cells, normalizing the expression of these genes in the presence of mHtt (Laprairie *et al*., 2013, 2014a). We investigated whether treatment with GAT211, GAT228, or GAT229 altered CB_1 and CB_2 mRNA levels in the tissues of wild-type and R6/2 mice. CB_1 mRNA levels were lower in the striatum and cortex of vehicle-, GAT211-, and GAT228-treated R6/2 mice compared to treatment-matched wild-type mice (Fig. 7-7A,B). CB_1 mRNA levels were normalized to wild-type levels in the striatum and cortex of GAT229-treated R6/2 mice (Fig. 7-7A,B). CB_1 mRNA levels were higher in the visceral adipose of GAT228-treated R6/2 HD mice compared to vehicle-treated R6/2 mice and GAT228-treated wild-type mice (Fig. 7-7C). CB_1 mRNA levels were not different in the whole blood of wild-type and R6/2 mice (Fig. 7-7D). CB_2 mRNA levels were higher in the striatum, cortex, visceral adipose, and whole blood of vehicle-, GAT211-, and GAT228-treated R6/2 mice compared to treatment-matched wild-type mice (Fig. 7-7E-H). CB_2 mRNA levels were normalized to wild-type levels in the striatum, cortex, visceral adipose, and whole blood of GAT229-treated R6/2 mice (Fig. 7-7E-H). Additional analyses were conducted to determine if treatment with GAT211, GAT228, or GAT229 affected the expression of other components of the endocannabinoid system (Laprairie *et al*., 2014a,b). FAAH mRNA levels were elevated in the striatum, cortex, and visceral adipose of R6/2 mice compared to wild-type mice; this increase was exacerbated in GAT228-treated R6/2 mice in striatum and cortex and normalized in GAT229-

Figure 7-7. GAT2229 normalized gene expression in R6/2 mice. RNA was collected from the striatum, cortex, visceral adipose tissue, and whole blood of wild-type (C57BL/6J) and R6/2 mice treated with vehicle or 10 mg/kg/d *i.p.* GAT211, GAT228, or GAT229 for 21 d and converted to cDNA for qRT-PCR measurement of CB1 **(A-D)**, CB2 **(E-H)**, PGC1α **(I-K)**, leptin **(L)**, and BDNF-2 **(M,N)** relative to β-actin. **P* < 0.01 compared to wild-type within treatment, ^*P* < 0.01 compared to vehicle within genotype as determined *via* two-way ANOVA followed by Bonferroni's *post-hoc* analysis. *N* = 5 per group.

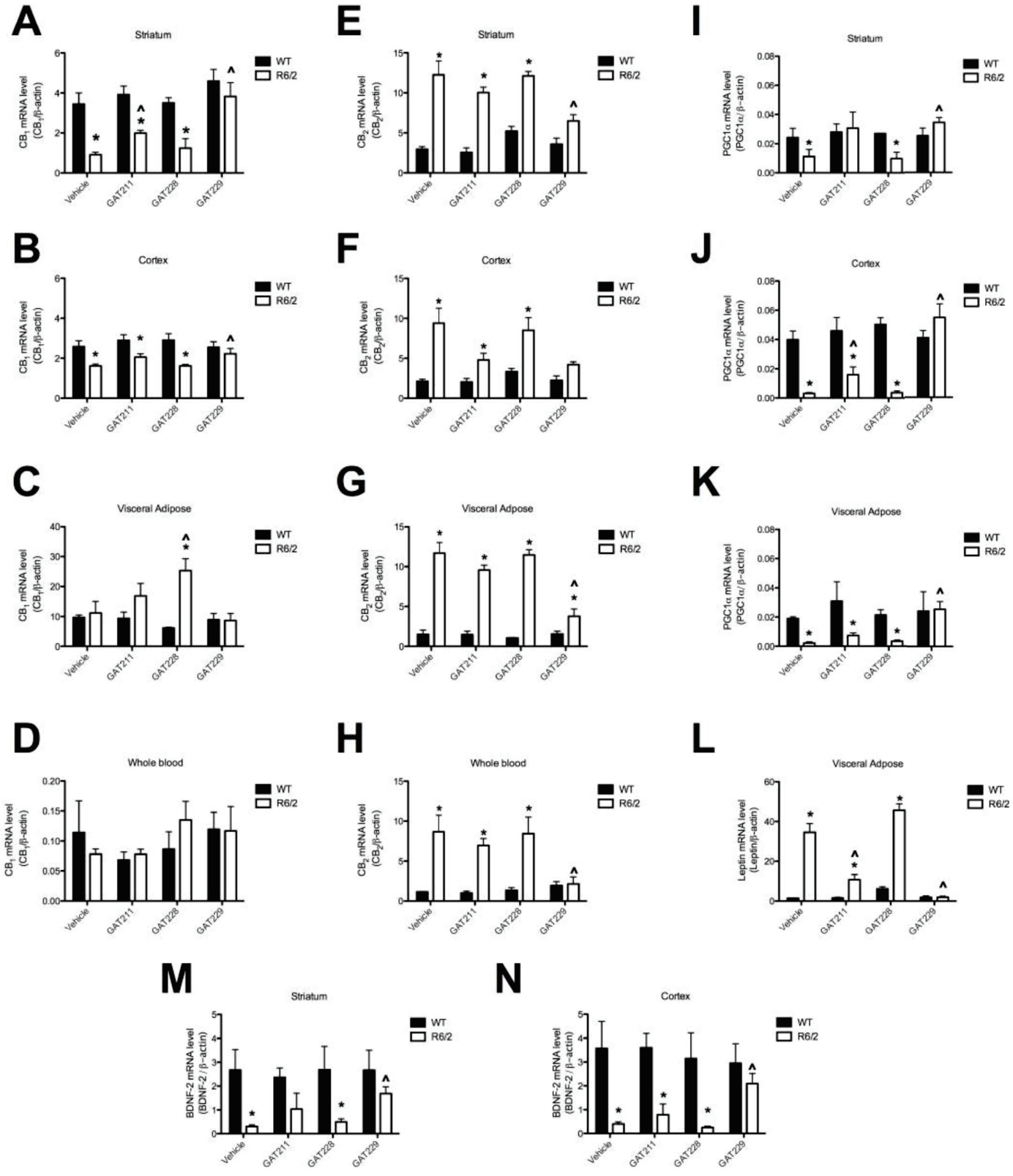
A
Striatum
CB1 mRNA level (CB1/β-actin)
WT
R6/2
Vehicle
GAT211
GAT228
GAT229
B
Cortex
C
Visceral Adipose
D
Whole blood
E
Striatum
CB2 mRNA level (CB2/β-actin)
F
Cortex
G
Visceral Adpose
H
Whole blood
I
Striatum
PGC1α mRNA level (PGC1α/β-actin)
J
Cortex
K
Visceral Adpose
L
Visceral Adpose
Leptin mRNA level (Leptin/β-actin)
M
Striatum
BDNF-2 mRNA level (BDNF-2 / β-actin)
N
Cortex

treated R6/2 mice in striatum (Table 7-4). MAGL mRNA levels were elevated in the cortex and visceral adipose of R6/2 mice compared to wild-type mice; this increase was normalized in GAT211- and GAT229-treated R6/2 mice in the cortex and visceral adipose (Table 7-4). NAPE-PLD mRNA levels were lower in the striatum and cortex of R6/2 mice compared to treatment-matched wild-type mice and not changed by GAT treatment (Table 7-4). DAGLα mRNA levels were not changed in any tissue by genotype or GAT treatment (Table 7-4).

mHtt-dependent transcriptional dysregulation of PGC1α, BDNF-2, leptin, IL-1β, and CCL5 in the brain, adipose, and blood may contribute to HD pathogenesis (Kumar *et al*., 2014). Activation of CB_1 has been shown to affect the expression of these genes *in vitro* (Fain *et al.,* 2001; Laprairie *et al.*, 2013, 2014a,b; Blázquez *et al*., 2015). Lower PGC1α levels contribute to lower mitochondrial respiration in the striatum and cortex and metabolic defects in the adipose (Fain *et al*., 2001). PGC1α mRNA levels were lower in the striatum, cortex, and visceral adipose of vehicle-, GAT211-, and GAT229-treated R6/2 mice compared to treatment-matched wild-type mice (Fig. 7-7I-K). PGC1α mRNA levels were normalized to wild-type levels in the striatum, cortex, and visceral adipose of GAT229-treated (and GAT211-treated in cortex) R6/2 mice (Fig. 7-7I-K). High leptin levels may contribute to elevated fat mass at the loss of lean tissue in HD patients (Phan *et al.*, 2009). Leptin mRNA levels were higher in the visceral adipose of vehicle-, GAT211-, and GAT229-treated R6/2 mice compared to treatment-matched wild-type mice (Fig. 7-7L). Leptin mRNA levels were normalized to wild-type levels in the visceral adipose of GAT229-treated R6/2 mice, and reduced in GAT211-treated R6/2 mice compared to vehicle-treated R6/2 (Fig. 7-7L). Loss of BDNF in the striatum is associated with neuronal atrophy and cell death (Blázquez *et al*., 2015). BDNF-2 mRNA levels were lower in the striatum and cortex of vehicle-, GAT211-, and GAT229-treated R6/2 mice compared to treatment-matched wild-type mice (Fig. 7-7M,N). BDNF-2 mRNA levels were normalized to wild-type levels in the striatum and cortex of GAT229-treated R6/2 mice (Fig. 7-7M,N). IL-1β and CCL5 mRNA levels were elevated in the striatum, cortex, and whole blood of R6/2 mice compared to wild-type mice; this

Table 7-4. Twenty-one day treatment with GAT211, GAT228, and GAT229 produced widespread changes in gene expression

	Striatum				*Cortex*				*Visceral Adipose*				*Whole blood*			
	WT		R6/2		WT		R6/2		WT		R6/2		WT		R6/2	
	FAAH															
Vehicle	0.030	± 0.001	0.145	± 0.013*	0.018	± 0.000	0.107	± 0.015*	0.030	± 0.009	0.188	± 0.044*	0.159	± 0.038	0.126	± 0.022
GAT211	0.067	± 0.011	0.163	± 0.041*	0.019	± 0.003	0.139	± 0.015*	0.030	± 0.007	0.259	± 0.075*	0.157	± 0.066	0.083	± 0.013
GAT228	0.054	± 0.012	0.257	± 0.053*^	0.012	± 0.001	0.235	± 0.046*^	0.027	± 0.008	0.252	± 0.060*	0.152	± 0.030	0.082	± 0.026
GAT229	0.057	± 0.031	0.104	± 0.018	0.018	± 0.002	0.089	± 0.018*	0.046	± 0.014	0.131	± 0.022*	0.185	± 0.056	0.105	± 0.025
	MAGL															
Vehicle	0.885	± 0.305	0.899	± 0.318	5.213	± 2.524	11.080	± 1.999*	2.490	± 0.424	7.813	± 1.888*	0.252	± 0.133	0.240	± 0.093
GAT211	1.216	± 0.436	0.938	± 0.317	4.050	± 0.504	10.842	± 3.869*	1.311	± 0.272	2.682	± 1.122^	0.197	± 0.038	0.241	± 0.078
GAT228	0.638	± 0.251	4.783	± 2.139*^	4.193	± 1.559	11.800	± 3.044*	1.091	± 0.214	7.547	± 1.960*	0.131	± 0.054	0.264	± 0.052
GAT229	1.007	± 0.326	0.631	± 0.188	6.820	± 2.211	4.690	± 1.357^	2.075	± 0.736	1.921	± 1.052^	0.317	± 0.224	0.220	± 0.023
	NAPE-PLD															
Vehicle	3.067	± 0.590	0.385	± 0.119*	3.023	± 0.390	0.387	± 0.106*	4.120	± 1.519	3.208	± 0.270	0.413	± 0.075	0.205	± 0.048
GAT211	3.280	± 0.241	0.670	± 0.247*	3.994	± 0.371	0.365	± 0.046*	5.746	± 1.511	5.110	± 1.005	0.293	± 0.069	0.189	± 0.030
GAT228	3.437	± 0.423	0.888	± 0.379*	3.280	± 0.344	0.305	± 0.020*	3.353	± 0.237	3.630	± 0.346	0.320	± 0.100	0.194	± 0.045
GAT229	3.473	± 1.114	0.363	± 0.094*	2.673	± 0.538	0.372	± 0.126*	3.087	± 0.492	6.103	± 2.374	0.302	± 0.091	0.228	± 0.104
	DAGLα															
Vehicle	0.026	± 0.014	0.028	± 0.011	0.013	± 0.005	0.022	± 0.006	0.003	± 0.000	0.002	± 0.000	0.015	± 0.005	0.016	± 0.002
GAT211	0.026	± 0.010	0.032	± 0.007	0.011	± 0.003	0.020	± 0.006	0.002	± 0.000	0.004	± 0.001	0.010	± 0.004	0.010	± 0.005
GAT228	0.041	± 0.012	0.031	± 0.009	0.025	± 0.005	0.024	± 0.003	0.002	± 0.001	0.003	± 0.000	0.010	± 0.005	0.016	± 0.006
GAT229	0.026	± 0.009	0.020	± 0.003	0.021	± 0.007	0.017	± 0.004	0.002	± 0.001	0.003	± 0.001	0.015	± 0.005	0.009	± 0.001

Data are expressed as mean ± SEM for relative cDNA abundance compared to β-actin. *$P < 0.01$ compared to WT within drug treatment; ^$P < 0.01$ compared to vehicle treatment within genotype, as determined *via* two-way ANOVA followed by Bonferroni's *post-hoc* analysis. $N = 5$.

Table 7-4 Continued. Twenty-one day treatment with GAT211, GAT228, and GAT229 produced widespread changes in gene expression

	Striatum		*Cortex*		*Whole blood*	
	WT	R6/2	WT	R6/2	WT	R6/2
	IL-1β					
Vehicle	1.343 ± 0.128	0.008 ± 0.003*	1.810 ± 0.178	0.009 ± 0.001*	0.048 ± 0.019	1.322 ± 0.313*
GAT211	1.088 ± 0.062	0.125 ± 0.052*	1.644 ± 0.104	0.420 ± 0.127*^	0.044 ± 0.015	0.279 ± 0.054
GAT228	0.842 ± 0.076	0.034 ± 0.018*	1.082 ± 0.284	0.012 ± 0.001*	0.028 ± 0.008	3.913 ± 1.124*^
GAT229	1.019 ± 0.056	0.812 ± 0.242^	1.169 ± 0.124	0.683 ± 0.236^	0.019 ± 0.003	0.112 ± 0.054
	CCL5					
Vehicle	0.029 ± 0.010	0.008 ± 0.003*	0.014 ± 0.005	0.002 ± 0.001*	7.763 ± 2.382	18.068 ± 2.627*
GAT211	0.061 ± 0.013	0.021 ± 0.005*	0.031 ± 0.006	0.014 ± 0.004^	7.382 ± 1.918	9.050 ± 2.268^
GAT228	0.052 ± 0.023	0.005 ± 0.003*	0.021 ± 0.010	0.001 ± 0.001*	8.443 ± 1.900	18.767 ± 1.947*
GAT229	0.051 ± 0.018	0.030 ± 0.009^	0.022 ± 0.009	0.013 ± 0.004^	8.093 ± 1.256	8.447 ± 3.518^

Data are expressed as mean ± SEM for relative cDNA abundance compared to β-actin. *$P < 0.01$ compared to WT within drug treatment; ^$P < 0.01$ compared to vehicle treatment within genotype, as determined *via* two-way ANOVA followed by Bonferroni's *post-hoc* analysis. $N = 5$.

increase normalized in GAT211-treated R6/2 mice in cortex and whole blood and in GAT229-treated R6/2 mice in striatum, cortex, and whole blood (Table 7-4).

Based on these data, we concluded that GAT229 treatment was associated with normalization of CB_1, CB_2, FAAH, MAGL, PGC1α, leptin, BDNF-2, IL-1β, and CCL5 mRNA levels in tissues where mHtt is known to affect transcription (Phan *et al.*, 2009; Kumar *et al.*, 2014), whereas GAT228 was either neutral or itself dysregulated gene expression (CB_1 in visceral adipose) and GAT211 displayed intermediated effects.

7.4. Discussion

7.4.1. The effects of GAT211, GAT228, and GAT229 in models of HD

In this study, the CB_1 allosteric modulators GAT211, GAT228, and GAT229 promoted cell viability in a cell culture model of medium spiny projection neurons expressing mHtt and in the R6/2 mouse model of HD. Our observations in ST*Hdh* cells confirm previous observations made in HEK293A and Neuro2a cells, where GAT229 produced effects consistent with a pure CB_1 PAM, GAT228 acted as a CB_1 allosteric partial agonist, and GAT211 displayed intermediate effects (see Ch. 6). Importantly, GAT229 enhanced pERK1/2 in ST$Hdh^{Q111/Q111}$ cells to wild-type levels in the presence of the endocannabinoids 2-AG and AEA, and improved cellular viability in ST$Hdh^{Q111/Q111}$ cells. The pharmacological activity of GAT211, GAT228, and GAT229 at CB_1 was not affected by the expression of mHtt. These data support the hypothesis that positive allosteric modulation of endocannabinoid-mediated CB_1 signaling enhances cellular viability through cell-intrinsic processes (Laprairie *et al*., 2015b).

Whereas a CB_1 orthosteric agonist would elicit immediate, acute cannabimimetic effects *in vivo* (Bosier *et al.*, 2010), the allosteric modulators GAT211, GAT228, and GAT229 each elicited cannabimimetic effects only after repeated exposures in wild-type and R6/2 mice. Because GAT228 is a partial allosteric agonist (Laprairie *et al*., 2015c), the cannabimimetic effects observed in GAT228-treated mice may have resulted from direct CB_1 activation and not PAM activity. This idea is supported by the observations that GAT228-dependent effects were

transient – due to receptor desensitization – and GAT228-treated mice were unique among wild-type mice in their immobility (*i.e.* catalepsy) in the open field test. GAT229-dependent cannabimimetic effects may have been the result of: 1) gradual and sustained enhancement of endocannabinoid-mediated CB_1 signaling; 2) accumulation of GAT229; or 3) accumulation of a metabolite of GAT229 that in turn affected the endocannabinoid system (Bosier *et al*., 2010; Long *et al*., 2009; Ignatowska-Jankowska *et al*., 2015). The racemic compound GAT211 consistently elicited *in vivo* effects that were intermediate between its enantiomers. A single dose and treatment paradigm was chosen to test each of the GAT compounds used in this study. Additional studies are required to determine the pharmacodynamic and pharmacokinetic properties of GAT211, GAT228, and GAT229 (Pamplona *et al*., 2012; Ignatowska-Jankowska *et al*., 2015). Importantly for the purposes of this study, the chosen dose and treatment paradigm affected the progression of HD-like symptoms in the R6/2 mouse model of HD.

7.4.2. Managing the signs and symptoms of HD via positive allosteric modulation of CB_1

Multiple lines of evidence from cell culture models of HD (Blázquez *et al*., 2011, 2015; Laprairie *et al*., 2013), mouse models of HD that lack CB_1 (mHtt *x* $CB_1^{-/-}$) (Blázquez *et al*., 2011; Mievis *et al*., 2011), and mouse models of HD where CB_1 expression is rescued by adeno-associated viral delivery (Chiarlone *et al.*, 2014; Naydenov *et al*., 2014a) support the hypothesis that enhancing CB_1-dependent signaling and/or the available pool of CB_1 in the striatum reduces the signs and symptoms of HD. Unfortunately, past attempts to enhance CB_1-dependent signaling *in vivo* with various CB_1 agonists have met with varied results: HU210 treatment reduces mHtt aggregation but increases seizure frequency in R6/1 mice (Dowie *et al*., 2010), inhibition of FAAH reduces striatal atrophy but does not affect motor coordination (Dowie *et al*., 2010), and THC treatment exacerbates deteriorating performance in the accelerating rotarod and decreases CB_1 binding in the striatum (Dowie *et al*., 2010; Valdeolivas *et al*., 2012). Based on our understanding of CB_1 agonist bias (Laprairie *et al*. 2014a, 2015b; Khajehali *et al*., 2015), enhancement of endocannabinoid-dependent signaling would be expected to produce the greatest

benefit, while arrestin-biased agonists – such as THC – would be expected to promote receptor internalization and reduced CB_1 binding as observed by Dowie *et al*. (2009).

Here, treatment with the CB_1 PAM GAT229 – and the racemic compound GAT211 – improved and sustained locomotor activity and delayed the progression of HD-like symptoms in R6/2 mice, as expected for a compound that enhances the potency and efficacy of 2-AG- and AEA-dependent signaling through CB_1. That GAT228 also improved locomotor activity is not unexpected as it also activated CB_1, although not necessarily as a PAM. In contrast to R6/2 mice, treatment with the GAT compounds reduced locomotor activity in wild-type mice. We hypothesize that this may be the result of different distribution of CB_1 in wild-type *versus* R6/2 mice: activation of the high density of striatal CB_1 receptors in wild-type mice results in overall reduced locomotor activity, whereas the relative density of CB_1 receptors is shifted away from the striatum to the cortex and substantia nigra in HD mice resulting in increased motor control from cortical neurons projecting to the striatum (Chiodi *et al*., 2012; Horne *et al*., 2013). Our observation that GAT treatment brought locomotor activity in wild-type and R6/2 mice to approximately the same level supports this hypothesis.

Failure to gain weight and altered body composition are observed in mouse models of HD and human patients suffering from HD (Phan *et al*., 2009; Süssmuth *et al*., 2015). Because CB_1 activation is known to promote weight gain (Cardinal *et al*., 2012) and enhance adipogenesis (reviewed in Cluny *et al*., 2012), compounds that target CB_1 for the treatment of HD must be either neutral or beneficial with respect to metabolic effects. Treatment with GAT229, and the racemic compound GAT211, was associated with weight gain in R6/2 mice and did not affect body composition. GAT228, however, exacerbated an increase in % body fat at the expense of lean tissue in R6/2 mice, suggesting this compound was detrimental in the R6/2 model of HD with respect to metabolism.

We have previously reported that AEA-dependent CB_1 signaling increases the expression of several genes whose transcription is repressed in the presence of mHtt including CB_1, PGC1α,

BDNF-2, IL-1β, and CCL5 (Laprairie *et al*., 2013, 2014b), and decreases the expression of several genes whose transcription is increased in HD, such as CB_2, (Laprairie *et al*., 2014b). In keeping with those observations, we found that treatment of R6/2 mice with GAT229 normalized the expression of CB_1, CB_2, PGC1α, BDNF-2, IL-1β, and CCL5 in the striatum, cortex, visceral adipose, and whole blood. Moreover, we found that leptin mRNA levels were normalized in R6/2 mice treated with GAT229. These data support our earlier hypothesis (Laprairie *et al*., 2013) that enhancement of endocannabinoid-mediated, CB_1-dependent, signaling normalizes the expression of genes regulated by the endocannabinoid system and critical to neuroprotection (*e.g.* BDNF-2, PGC1α), inflammation (*e.g.* CB_2, IL-1β) and energy homeostasis (*e.g.* PGC1α, leptin) that are dysregulated in HD and may contribute to disease pathophysiology (Cui *et* al., 2006; Blázquez *et al.*, 2011, 2015; Cluny *et al*., 2012; Laprairie *et al*., 2013, 2014a,b).

7.4.3. CONCLUSIONS

Additional characterization of the pharmacodynamic and pharmacokinetic properties of CB_1 PAMs *in vivo* is required to optimize their use (Ross, 2007; Gamage *et al*., 2014) and analyses of these compounds in more protracted models of HD is required (Menalled *et al*., 2014; Brooks and Dunnett, 2015; Menalled and Brunner, 2015). Here, positive allosteric modulation of CB_1 enhanced cell viability in the ST*Hdh*$^{Q111/Q111}$ cell culture model; increased locomotor activity, delayed HD-like symptom progression, improved weight gain, and normalized gene expression in the R6/2 mouse model of HD. In conclusion, positive allosteric modulation of CB_1 may be a legitimate means of reducing and delaying the progression of HD.

CHAPTER 8

DISCUSSION

8.1. OBJECTIVES OF THIS RESEARCH

The overall objective of my research was to study the signaling properties of the type 1 cannabinoid receptor (CB_1) and apply my findings to the modulation of CB_1 activity in the presence of the mutant huntingtin protein (mHtt). My hypothesis was that $G\alpha_{i/o}$-biased signaling *via* CB_1 would increase CB_1 activity and abundance, while arrestin-biased signaling would exacerbate the overall loss of CB_1 function in Huntington disease (HD) models and consequently exacerbate the signs of HD in those models.

8.2. SUMMARY OF RESEARCH

8.2.1. DYSREGULATION OF THE CYTOKINE AND ENDOCANNABINOID SYSTEMS IN HUNTINGTON DISEASE

Transcriptional dysregulation is a major pathological feature of HD. Reduced CB_1 mRNA and protein levels are well-documented in HD (Denovan-Wright and Robertson, 2000; Glass *et al*., 2000), but changes in other components of the endocannabinoid system (ECS) during HD progression were less well-characterized prior to the initiation of my graduate work. I observed that CB_1 mRNA expression was under the control of p65/RelA and activation of CB_1 increased CB_1 mRNA through a $G\alpha_{i/o}$/$G\beta\gamma$- and p65/RelA-dependent mechanism (Laprairie *et al*., 2013). p65/RelA regulates the expression of multiple genes. Given that p65/RelA levels were lower in human HD tissue and R6/2 HD mice compared to healthy controls, I wanted to determine whether the levels of components of the ECS and cytokine system that might be under the regulatory control of p65/RelA were dysregulated in HD. The promoters of the CB_1, interleukin 1β (IL-1β), IL-8, chemokine C-C motif ligand 5 (CCL5), granulocyte-macrophage colony-stimulating factor (GM-CSF), macrophage inflammatory protein 1β (MIP-1β), and tumor necrosis factor α (TNFα) genes all contain p65/RelA regulatory elements. Levels of CB_1, IL-1β, IL-8, CCL5, GM-CSF, MIP-1β, and TNFα were lower in human HD tissue and R6/2 HD mice compared to normal human or wild-type mouse tissue. Activation of p65/RelA *via* the CB_1 agonist arachidonoyl-2'-chloroethylamine (ACEA) normalized CB_1 and CCL5 expression in the

ST*Hdh*$^{Q111/Q111}$ cell model of HD. Therefore, CB_1- and $G\alpha_{i/o}/G\beta\gamma$-dependent p65/RelA activation may normalize the expression of down-regulated genes in HD.

Type 2 cannabinoid receptor (CB_2) and fatty acid amide hydrolase (FAAH) gene promoters do not contain p65/RelA regulatory elements. CB_2 and FAAH levels were higher in human HD tissue compared to control tissue and R6/2 HD mice compared to wild-type mice. Changes in CB_2 and FAAH expression occur late in HD progression whereas changes in CB_1 expression occur early (Luthi-Carter *et al*., 2002). Thus, changes in CB_2 and FAAH levels may represent compensatory changes during disease progression rather than early effects attributed directly to mHtt (Laprairie *et al*., 2015a). Activation of CB_1 and p65/RelA normalized CB_2 and FAAH mRNA levels in the ST*Hdh*$^{Q111/Q111}$ cell model of HD.

This work is presented in chapter 2 and published as "The cytokine and endocannabinoid systems are co-regulated by NF-κB p65/RelA in cell culture and transgenic mouse models of Huntington disease and in striatal tissue from Huntington disease patients" (Laprairie *et al*., 2014b; *J Neuroimmunol*). From these data I conclude that activation of CB_1- $G\alpha_{i/o}/G\beta\gamma$-, p65/RelA-dependent signaling may normalize the mRNA levels of multiple transcripts and improve cell functionality in the presence of mHtt.

8.2.2. CB_1 LIGAND BIAS IN HUNTINGTON DISEASE: CANNABINOID CHOICE MATTERS

Biased CB_1 agonism is observable in living systems (Nguyen *et al*., 2012). Δ^9-tetrahydrocannabinol (THC) administration does not produce an anti-nociceptive effect, but does produce anxiolytic and hypothermic responses, in arrestin1 knockout mice (Nguyen *et al*., 2012), demonstrating that arrestin-biased ligands, like THC, facilitate the anti-nociceptive effect associated with CB_1 activation *in vivo*. Prior to my graduate research, the bias of common, widely-used CB_1 agonists, such as 2-arachidonoylglycerol (2-AG), anandamide (AEA), THC, cannabidiol (CBD), CP55,940, and WIN55,212-2, had not been directly compared and quantified using accepted methods for the analysis of ligand bias (Bosier *et al*., 2010; Kenakin and

Christopoulos, 2013). I sought to understand the bias of CB_1 agonists and then apply this information of agonist bias to the pathophysiology of HD.

I began my investigation of CB_1 agonist bias in the ST*Hdh*$^{Q7/Q7}$ cell culture model of medium spiny projection neurons (MSN). In this system, THC and CP55,940 were arrestin2-biased agonists compared to other cannabinoids tested and these compounds promoted CB_1 internalization and decreased CB_1 protein levels. 2-AG, AEA, and WIN55,212-2, displayed $G\alpha_{i/o}$ and $G\beta\gamma$ bias. 2-AG, AEA, THC, and WIN55,212-2 also activated $G\alpha_q$-dependent pathways. CP55,940 and cannabidiol (CBD) both signaled through $G\alpha_s$, but only CP55,940 activated $G\alpha_s$ *via* CB_1. Only treatment with 2-AG and AEA, the cannabinoids that were the most-efficacious activators of $G\alpha_{i/o}$ and $G\beta\gamma$-dependent signaling, produced an increase in CB_1 mRNA and protein abundance. These data demonstrate that cannabinoids with different signaling bias can produce functionally opposite effects, reduced CB_1 (arrestin bias) *versus* increased CB_1 ($G\alpha_{i/o}$ bias), despite activating the same receptor. This work is presented in chapter 3 and published as "Type 1 Cannabinoid Receptor Ligands Display Functional Selectivity in a Cell Culture Model of Striatal Medium Spiny Projection Neurons" (Laprairie *et al*., 2014a; *J Biol Chem*). Based on these data, I hypothesized that *only* $G\alpha_{i/o}$ and $G\beta\gamma$-biased CB_1 agonists would improve cell viability in cell culture models of HD because of their ability to increase CB_1 mRNA and protein abundance.

I tested the hypothesis that *only* $G\alpha_{i/o}$ and $G\beta\gamma$-biased CB_1 agonists would improve cell viability in cell culture models of HD because of their ability to increase CB_1 mRNA and protein abundance in the ST*Hdh*$^{Q111/Q111}$ cell culture model of MSNs expressing mHtt. I applied the operational model of ligand bias (Ehlert *et al*., 2011) to concentration-response data for arrestin2-, $G\alpha_{i/o}$-, $G\alpha_q$-, $G\alpha_s$-, and $G\beta\gamma$-dependent signaling obtained using ST*Hdh*$^{Q7/Q7}$ and ST*Hdh*$^{Q111/Q111}$ cells treated with WIN55,212-2, CP55,940, 2-AG, AEA, THC, CBD or an equimolar mixture of THC and CBD. Using this approach, I was able to complete statistical comparisons of biased agonism between cannabinoids and and between ST*Hdh*$^{Q7/Q7}$ and ST*Hdh*$^{Q111/Q111}$ cell types.

Although the E_{max} of $G\alpha_{i/o}$-dependent ERK phosphorylation was 50% lower in ST*Hdh*$^{Q111/Q111}$ cells compared to ST*Hdh*$^{Q7/Q7}$, $G\alpha_{i/o}$ bias was observed for 2-AG, AEA, and THC+CBD in ST*Hdh*$^{Q111/Q111}$ cells. 2-AG, AEA, and the mixture of THC and CBD, displayed the greatest $G\alpha_{i/o}$ bias compared to arrestin, $G\alpha_q$, and $G\alpha_s$ bias. 2-AG and AEA did not display bias between $G\alpha_{i/o}$ and $G\beta\gamma$. THC+CBD was less potent and efficacious than 2-AG and AEA at improving cell viability in ST*Hdh*$^{Q111/Q111}$ cells. The conclusion of this study was that $G\alpha_{i/o}$/$G\beta\gamma$ bias was correlated with improved cell viability (mitochondrial respiration, membrane permeability) and functionality (GABA release, CB_1 levels), whereas arrestin bias was correlated with reduced cell viability in ST*Hdh*$^{Q111/Q111}$ cells. Therefore, 2-AG and AEA were the best-suited cannabinoids, among those tested, at reducing the detrimental, cell intrinsic, effects of mHtt in a cell culture model. This work is presented in chapter 4 and has been accepted for publication as "Biased Type 1 cannabinoid receptor signaling influences neuronal viability in a cell culture model of Huntington disease." (Laprairie *et al*., 2015b; *Mol Pharmacol*).

My studies of CB_1 signaling bias *in vitro* support the previous findings that THC exacerbates some signs and symptoms of HD in R6/1 HD mice whereas enhanced endocannabinoid levels *via* FAAH or ABHD6 inhibition reduces some signs and symptoms of HD in R6/1 and R6/2 HD mice (Dowie *et al*., 2010; Naydenov *et al*., 2014b). WIN55,212-2 prevents motor deficits and the loss of MSNs in R6/1 HD mice when administered for 8 weeks (Pietropaolo *et al*., 2015). In my studies, WIN55,212-2 displayed $G\alpha_{i/o}$/$G\beta\gamma$ bias in ST*Hdh*$^{Q111/Q111}$ cells, but was a more potent and efficacious agonist of arrestin recruitment than 2-AG and AEA in ST*Hdh*$^{Q111/Q111}$ cells (Laprairie *et al*., 2015b). Chronic, direct activation of CB_1 *via* WIN55,212-2, or other synthetic agonists, may result in supraphysiological activation, desensitization, and arrestin-dependent receptor downregulation (Ross, 2007). Therefore, enhancement of highly $G\alpha_{i/o}$/$G\beta\gamma$-biased endocannabinoid-dependent signaling at CB_1 is the most likely means of reducing HD signs and symptoms if CB_1 is targeted.

Clinical data support the hypothesis that arrestin-biased cannabinoids, such as THC, are likely to exacerbate the signs and symptoms of HD (Müller-Vahl *et al*., 1999). THC and the THC derivative nabilone are either ineffective or exacerbate choreiform movement in HD patients (Müller-Vahl *et al.*, 1999; Miesel and Friedman, 2012; Koppel *et al.*, 2014). CBD is a NAM of CB_1 in cell culture (Laprairie *et al*., 2015d). CBD displays a multiplicity of actions *in vivo* (McPartland *et al.*, 2014) and when administered alone does not alter HD progression in patients (Consroe *et al*., 1991). My data suggests that THC+CBD enhances $G\alpha_{i/o}/G\beta\gamma$-dependent signaling in ST*Hdh*$^{Q111/Q111}$ cells compared to THC (Laprairie *et al*., 2015b). Equimolar THC with CBD is currently available as the oromucosal spray Sativex®, and is used to manage spasticity in multiple sclerosis and neuropathic pain (Koppel *et al*., 2014). However, a recent phase II clinical trial that assessed changes in motor, cognitive, psychiatric, and functional symptoms in HD patients receiving 1 – 12 sprays of Sativex® per day for 8 months found no toxic or beneficial effects of Sativex® in HD (García-Caldenty *et al.*, 2015). Beyond clinical trials of cannabinoids in HD, HD patients may use marijuana either recreationally or in a personal attempt to control the symptoms of their disease (Koppel *et al*., 2014). Most seized and medically available marijuana contains a high percentage of THC relative to CBD (Koppel *et al.*, 2014). Marijuana also contains many more cannabinoids whose pharmacological activity is unknown and have not been tested in the context of HD (McPartland *et al*., 2014). I conclude that modern, high-THC strains of marijuana would at minimum be ineffective at reducing chorea in HD (Koppel *et al*., 2014) and may exacerbate the signs and symptoms of HD.

8.2.3. The therapeutic potential of CB_1 allosteric modulators

The endocannabinoids 2-AG and AEA are likely to provide the most benefit in managing the signs and symptoms of HD, relative to other cannabinoids, because of their signaling bias. 2-AG and AEA, however, are highly labile compounds that are rapidly degraded when administered *in vivo* and this property limits the therapeutic utility of exogenously administered 2-AG and AEA (Pertwee, 2008).

I began examining CB_1 allosteric modulators when I found that CBD reduced both the potency and efficacy of 2-AG- and THC-dependent signaling through CB_1 in HEK293A and ST*Hdh*$^{Q7/Q7}$ cells. Analysis of these data using the operational model of allosterism (Keov *et al*., 2011) demonstrated that CBD behaved as a negative allosteric modulator (NAM) of CB_1-dependent signaling at concentrations lower than its reporter affinity for the CB_1 orthosteric site (McPartland *et al*., 2015). These data help to explain why CBD elicited no CB_1-dependent effect alone, but limited the deleterious effects of THC when THC and CBD were co-administered in ST*Hdh*$^{Q111/Q111}$ cells expressing mHtt (Laprairie *et al*., 2015b). This work is presented in chapter 5 and published as "Cannabidiol is a negative allosteric modulator of the type 1 cannabinoid receptor" (Laprairie *et al*., 2015d; *Br J Pharmacol*). From this work I was able to gain insight into the molecular pharmacology of allosteric modulators and provide rationale for the use of *positive allosteric modulators* (*PAM)* in enhancing the signaling and/or abundance of CB_1 in HD.

The pharmacological activity of GAT228 (*R*-enantiomer), GAT229 (*S*-enantiomer), and the racemic compound GAT211 (equimolar concentrations of the *R*- and *S*-enantiomers) was evaluated *in vitro* in HEK293A and Neuro2a cells using the operational model of allosterism (Adam *et al.*, 2007; Keov *et al*., 2011). GAT228 (*R*-enantiomer) was an allosteric agonist, while GAT229 (*S*-enantiomer) was a potent PAM. GAT211 displayed properties consistent with both positive allosteric modulation of CB_1 and partial agonist activity of CB_1 *via* an allosteric site (*i.e.* ago-PAM). Importantly, GAT211 and GAT229 enhanced the potency and efficacy of 2-AG- and AEA-dependent $G\alpha_{i/o}$ intracellular signaling *via* CB_1 in both HEK293A cells heterologously expressing CB_1 and Neuro2a cells that endogenously express CB_1. This work is presented in chapter 6 and is in prepration for submission as "Characterization of the novel positive allosteric modulator of the type 1 cannabinoid receptor GAT211, and its enantiomers GAT228 and GAT229" (Laprairie *et al*., 2016a; *J Biol Chem* – in preparation). Therefore, GAT211, GAT228, and GAT229 represent novel CB_1 PAMs that display enantiomer-specific activity and represent a

possible means of enhancing the $G\alpha_{i/o}$-biased signaling of the endocannabinoids 2-AG and AEA *in vivo*.

In order to test the hypothesis that positive allosteric modulation of endocannabinoid-mediated CB_1 signaling reduces the signs and symptoms of HD, the activity of GAT211, GAT228, and GAT229 was evaluated in ST*Hdh*$^{Q111/Q111}$ cells expressing mHtt and then in the R6/2 mouse model of HD. GAT211 and GAT229 both enhanced the neuroprotective effect of AEA in ST*Hdh*$^{Q111/Q111}$ cells, indicating that these compounds ameliorated some deleterious, cell-intrinsic, effects of mHtt. Treatment with GAT211, GAT228, or GAT229 at 10 mg/kg/d for 21 d (*i.p.*) was associated with improved locomotor activity in R6/2 mice, with the PAM GAT229 being the most-efficacious among these compounds. GAT229, and to a lesser extent GAT211, delayed symptom progression in R6/2 mice, whereas GAT228 did not alter symptom progression. GAT229 and GAT211 normalized levels of CB_1, CB_2, PGC1α, BDNF-2, and IL-1β mRNA in R6/2 HD mice to wild-type levels. Given that GAT229 normalized CB_1 transcript levels, these data support the correlation between CB_1 abundance and HD pathogenesis observed elsewhere (Blázquez *et al*., 2011; Mievis *et al*., 2011; Chiarlone *et al*., 2014; Naydenov *et al*., 2014a). Others and myself have previously demonstrated the regulatory link between $G\alpha_{i/o}$-dependent CB_1 signaling and levels of CB_1, CB_2, PGC1α, BDNF-2, and IL-1β (Dowie *et al.,* 2009; Laprairie *et al*., 2013, 2014b; Blázquez *et al*., 2015).

Metabolic defects, including failure to gain weight and loss of lean tissue, represent unmet clinical concerns for HD patients (Ravinet-Trillou *et al.*, 2004). In addition to changes in behavioural and locomotor function, GAT229 and GAT211 normalized metabolic defects in R6/2 HD mice (Laprairie *et al*., 2015c, 2016b – in preparation). GAT229, and to a lesser extent GAT211, treatment was associated with weight gain and normalization of leptin transcript levels in R6/2 mice with no change in body composition compared to vehicle-treated R6/2 mice (Laprairie *et al*., 2016b – in preparation). CB_1 abundance and activation in the hypothalamus and adipose are positively correlated with weight gain (Ravinet-Trillou *et al*., 2004) and negatively

correlated with leptin levels (Iannotti *et al*., 2014). Leptin levels are positively correlated with increasing free-fat mass in patients with HD (Süssmuth *et al.*, 2015). GAT229-dependent enhancement of hypothalamic CB_1 may have normalized leptin expression and promoted weight gain in R6/2 mice. CB_1 PAMs may, therefore, address the metabolic symptoms of HD, in addition to cognitive, behavioural, and motor symptoms of HD. This research is presented in chapter 7 and is in preparation for publication as "Positive allosteric modulation of the type 1 cannabinoid receptor reduces the signs and symptoms of Huntington disease in the R6/2 mouse model" (Laprairie *et al*., 2016b; *Neurobiol Dis* – in preparation).

8.3. CONSIDERATIONS AND FUTURE WORK

The important research that I have conducted to date has laid the foundations for understanding the general mechanisms of CB_1 ligand bias and allostery and applied this knowledge to the specific case of HD. In this research I have utilized a cell culture model of HD whose cellular deficits are the result of mHtt expression (Trettel *et al.*, 2000) and an animal model of HD that displays early disease onset and rapid disease progression (Menalled *et al*., 2014). These models are highly useful in understanding the molecular biology of HD and screening drug compounds. Future research into CB_1-targetted therapeutics to manage HD should build on this foundational research by 1) studying pharmacotherapeutic modulation of CB_1 in HD models that re-capitulate the progressive, protracted course within of HD, such as zQ175 knock-in mice (Menalled *et al*., 2014), and 2) gain insight into how cannabinoid-based drugs, including marijuana, effect the progression of HD. The following questions and discussion of future work are based on these two aims.

As discussed above, given that HD patients are likely to expose themselves to cannabinoids, how might cannabinoids affect the signs and symptoms of HD? The first case report of a cannabinoid producing a beneficial effect in HD described a reduction in chorea following oral administration of cannabidiol (CBD) (600 mg/day) for 2 weeks in 3 HD patients (aged 30 – 56) that had exhibited HD symptoms for 7 – 12 years and were not taking other

medications to control their HD symptoms (Sandyk *et al*., 1986). Mild improvements in choreiform movement (5 – 15%) were observed using the chorea severity evaluation scale in the first week, and further improvements (20 – 40%) were observed in the second week in all 3 patients receiving CBD (Sandyk *et al*., 1986). Choreic movements returned to a pre-CBD state 48 h after withdrawal from CBD (Sandyk *et al*., 1986). A small follow-up study of this work reported a reduction in dystonia following oral administration of CBD (100 - 600 mg/day for 6 weeks) in 5 HD patients that had exhibited symptoms for 8 – 12 years (Consroe *et al*., 1986). Side-effects included hypotension, dry mouth, lightheadedness, sedation, and exacerbation of Parkinsonian hypokinesia in 2 patients receiving > 300 mg/day CBD (Consroe *et al*., 1986). Since this case report, 2 additional case reports have found no beneficial or toxic effects of oral CBD in HD patients (Lastres-Becker *et al.*, 2002; Zhornitsky and Patvin, 2012). Use of other medications was not reported in these reports of CBD use (Consroe *et al*., 1986; Lastres-Becker *et al.*, 2002; Zhornitsky and Patvin, 2012). Nabilone, a synthetic Δ^9-tetrahydrocannabinol (THC) derivative, at a single dose of 1.5 mg, exacerbated chorea (chorea severity evaluation scale) and motor impairment for 2 days in a 58 year-old male HD patient that had exhibited chorea for 6 years and not receiving other medications (Müller-Vahl *et al*., 1999). However, a second case report found that 1 mg/day nabilone for 2 weeks reduced chorea for several hours following oral administration in a male patient that had been diagnosed with HD 7 years prior to the report (Consroe *et al*., 1991; Kluger *et al*., 2015). The case reports do not describe any effects of CBD or nabilone on cognition, behavior, or metabolism (Koppel *et al*., 2014). No case reports of THC, Sativex®, synthetic or endogenous cannabinoid exist in the literature (Koppel *et al*., 2014). No case reports of oral, oromucosal, or smoked cannabinoids for the treatment of HD, or used by HD patients for recreational purposes, exist in the literature (Koppel *et al*., 2014).

As of December 2015, 3 double-blind, placebo-controlled, cross-over clinical trials of cannabinoids for use in managing the signs and symptoms of HD have been completed. The first of these clinical trials was to determine the safety and efficacy of oral CBD [10 mg/kg/day (in

capsules) for 6 weeks] in 15 neuroleptic-free patients with HD (Consroe *et al*., 1991). Patients were assessed once weekly for chorea severity (chorea severity evaluation scale), *Cannabis* side effect inventory, and plasma CBD levels (Consroe *et al*., 1991). The study concluded that no positive or adverse clinical differences were observed between CBD and placebo treatment in neuroleptic-free patients with HD receiving an average daily dose of 700 mg/day (Consroe *et al*., 1991). A second pilot study was conducted to assess the safety and efficacy of nabilone (1 or 2 mg/day for 5 weeks) at reducing Unified Huntington's disease Rating Scale (UHDRS) symptom severity in 44 patients displaying HD motor symptoms for 1 – 7 years (Curtis *et al*., 2009). In this trial, the UHDRS treatment effect with either dose of nabilone was small (Curtis *et al*., 2009). The UHDRS treatment effect was reported as mean improvement from baseline with 95% confidence interval [motor score 0.86 (-1.8 – 3.52), chorea 1.68 (0.44 – 2.92), cognition 3.57 (-3.41 – 10.55), behavior 4.01 (-0.11 – 8.13), neuropsychiatric index (NPI) 6.43 (0.2 – 12.66)] (Curtis *et al*., 2009). Nabilone was safe, well-tolerated, and did not exacerbate chorea (Curtis *et al*., 2009). In addition, no psychotic episodes were reported (Curtis *et al*., 2009). The authors of this study concluded that larger and longer randomized control trials of nabilone were warranted, but no follow-up studies are currently being conducted (Curtis *et al*., 2009). The most-recent clinical trial assessed the safety and efficacy of Sativex® (2.7 mg THC + 2.6 mg CBD oromucosal spray, 1 – 12 self-administered sprays/day for 12 weeks). In this trial, 25 patients with HD were assessed for UHDRS severity score and levels of cerebrospinal BDNF (García-Caldenty *et al.*, 2015; Fernández-Ruiz *et al*., 2015). Although the primary results of this study have not yet been published, the clinical trial demonstrated Sativex® was safe and well-tolerated, but did not alter HD symptoms or progression (Sagredo *et al*., 2012; García-Caldenty *et al.*, 2015; García-Yébenes *et al*., 2015; Fernández-Ruiz *et al*., 2015). Based on these clinical trials, 2 recently published systematic reviews independently concluded that the available data does not demonstrate that cannabinoid-based medicines are beneficial in HD (Koppel *et al*., 2014; Arjmand *et al*., 2015). However, the authors of these systematic reviews state that the completed

trials were underpowered to detect differences and did not consider disease state (Koppel *et al*., 2014; Arjmand *et al*., 2015). Therefore, conclusions about the effects of cannabinoids in HD may be premature (Koppel *et al*., 2014; Arjmand *et al*., 2015).

HD patients are prescribed typical and atypical antipsychotics, antidepressants and tetrabenazine to control specific symptoms. CBD, THC, nabilone, and many other cannabinoids are metabolized by CYP2C9 and CYP3A4 (Watanabe *et al*., 2007). Patients who display poor CYP2C9 activity (CYP2C9*3/*3 homozygotes) have been shown to have plasma THC concentrations that are 3-fold higher than those of normal CYP2C9 metabolizers (CYP2C9*1/*1 homozygote) (Sachse-Seeboth *et al*., 2009). The selective serotonin reuptake inhibitors fluoxetine and fluvoxamine, and tetrabenazine, are known CYP2C9 inhibitors and the co-administration of these compounds would result in higher plasma cannabinoid concentrations (Heneryck *et al.*, 1999). Smoked marijuana has also been shown to induce CYP1A2 activity (Jusko *et al.*, 1979). Chlorpromazine, and other typical antipsychotics, are metabolized by CYP1A2. Smoked marijuana has been shown to increase the metabolism of chlorpromazine, resulting in a 50% reduction in chlorpromazine plasma concentrations (Jusko *et al.*, 1979; Chetty *et al*., 1994). THC has also been shown to enhance the CNS depressant effects of amitriptyline, clozapine, olanzapine, and quetiapine (Drugbank.ca, downloaded 10/12/15) Given that CB_1 is known to effect dopaminergic and serotonergic signaling, interactions between cannabinoids and these drugs are likely (Glass and Felder, 1997; Przybyla and Watts, 2010). Attention should be paid to side effects which are more likely to potentiated due to the co-administration of cannabinoids, antipsychotics, antidepressants and tetrabenazine including, excessive sedation, dizziness and drowsiness.

The observations made to date indicate that strains of marijuana with high absolute levels of THC or high levels of THC relative to CBD would either be neutral or would aggravate the signs and symptoms of HD (Koppel *et al.*, 2014). Within this question, the timing of exposure to marijuana is an important consideration. CB_1 levels fluctuate in the limbic system and prefrontal

cortex as part of the normal developmental process (reviewed in Laprairie *et al*., 2012). As a result, marijuana exposure during adolescence, when CB_1 levels are high in the prefrontal cortex and limbic system, has been associated with an increased risk of developing schizophrenia compared to marijuana exposure later in life (Radhakrishnan *et al.*, 2014; van Winkel and Kuepper., 2014). Because CB_1 activity is known to diminish prior to the onset of overt psychiatric or motor symptoms in HD (van Laere *et al*., 2010), early exposure to marijuana may accelerate disease onset and progression, further reducing quality of life for HD patients. I propose that the long-term effects of THC (and other cannabinoids) on HD progression need to be studied in a genetically-accurate, slowly progressing, animal model of HD, such as the zQ175 mouse (Menalled *et al*., 2014) as well as in observational studies of HD patients using marijuana according to their age, use patterns, strains of marijuana, and symptom profiles (Koppel *et al*., 2014).

Patients seeking *Cannabis* or cannabinoid-based medicines for the treatment of HD should be made aware that "cannabinoid-based therapies are of unknown efficacy for HD" and the existing evidence does not support the use of *Cannabis* for the treatment of their disease [The American Academy of Neurology (AAN), Kluger *et al*., 2015]. Future clinical studies of cannabinoids in HD should assess the effect of these agents at different HD disease stages, the effect of cannabinoids used in combination with other drugs, and thoroughly assess important changes in cognition, behavior, depression, irritability, appetite, and metabolic dysfunction in addition to motor symptoms (Koppel *et al*., 2014; Arjmand *et al*., 2015). Pre-clinical data suggests that some, select cannabinoids used over extended periods of time may, in fact, help to normalize the HD-dependent ECS dysfunction (Laprairie *et al*., 2015a). This warrants the investigation of biased cannabinoids, allosteric modulators, and inhibitors of cannabinoid metabolism (Arjmand *et al*., 2015; Laprairie *et al*., 2015a).

Are CB_1 PAMs a favourable treatment strategy for HD compared to biased orthosteric cannabinoids? Although I observed that $G\alpha_{i/o}$-biased orthosteric CB_1 agonists improved cell

viability in ST*Hdh*$^{Q111/Q111}$ cells (Laprairie *et al*., 2015c, 2016a), current evidence leads me to conclude that direct activation of CB_1 with synthetic cannabinoids results in supra-physiological receptor activation and desensitization, which may be deleterious in HD (Sim-Selley and Martin, 2002; Dowie *et al*., 2010; Nguyen *et al.*, 2012). Future studies of CB_1 signaling should determine the structure-activity relationship of both orthosteric and allosteric CB_1 ligands. That is, the specific amino acid residues of the orthosteric and allosteric sites that mediate signal bias and inhibition and potentiation of signaling in order to design highly selective biased compounds with as few on-target side effects as possible (Christopoulos and Kenakin, 2002). I would characterize the structure-activity relationship of CB_1 ligand-directed signaling using a series of covalent probes that bind specific amino acids within CB_1 and relate the structure of these compounds to their biased signaling *in vitro* and *in vivo*. From these data, I would be able to characterize the residue-specific CB_1 ligand-interaction landscape and the molecular pharmacology of biased orthosteric and allosteric CB_1 ligands. Obtaining the crystal structure of CB_1 will advance our understanding of ligand-directed signaling through CB_1 significantly.

Can CB_1 PAMs be developed that are better drug compounds than the probe PAMs tested here? In my studies GAT211, GAT228, and GAT229 are referred to as probe compounds because they were designed to be highly specific to the allosteric site of CB_1 (Adam *et al*., 2007). Their demonstrated specificity and affinity for CB_1 does not mean, however, that they are good drug candidates *per se*. GAT228 and GAT229 contain a highly reactive nitro group (see Fig. 6-1). Nitro groups are known to broadly inhibit CYP450 enzymes, and many nitroaromatic compounds (*e.g.* metronidazole) are known to be mutagenic and carcinogenic when used chronically (Strauss, 1997). While the presence of a nitro group does not completely negate a compound from being developed into a drug, it represents one concern among many unknowns for such CB_1 PAMs. Because HD is an inherited autosomal dominant disease that can be diagnosed through genetic testing, when is the best time to begin treatment with CB_1-targetted PAMs? How long should treatment continue in order to maximize quality and duration of life for patients suffering from

HD? This question is connected with the previous question of marijuana exposure because the long-term negative and positive effects of targeting CB_1 must be known in order to make decisions regarding safety and efficacy.

GAT211, GAT228, and GAT229 are new chemicals and therefore the pharmacokinetic and pharmacodynamic properties of these chemicals have not been examined. In my studies, only one treatment paradigm was studied (10 mg/kg/d for 21 d) and we did not determine how GAT211, GAT228, and GAT229 were distributed, metabolized, or excreted, or whether whether CB_1 binding was affected. Org27569 is the most-studied allosteric modulator of CB_1 signaling *in vitro* and in cell culture, yet it displays no CB_1 activity *in vivo* (Gamage *et al*., 2014). The endogenous CB_1 PAM lipoxin A_4 appears to act *via* CB_1 *in vivo*, but its effects are transient (Pamplona *et al*., 2012). The synthetic CB_1 PAM ZCZ011 does not evoke tetrad responses in healthy C56BL/6J mice when administered acutely, but is analgesic in the chronic constriction nerve injury model of neuropathic pain and carrageenan model of inflammatory pain (Ignatowska-Jankowska *et al*., 2015). GAT228 and GAT229 elicited some tetrad responses when administered chronically *in vivo*, which is expected for orthosteric agonists acting through CB_1, but not allosteric modulators. The tetrad responses observed for GAT228 are logical given that GAT228 is an allosteric agonist (Laprairie *et al*., 2016b). GAT229 did not display tetrad effects when administered acutely, which is consistent with a CB_1 PAM (Ross, 2007). However, GAT229 did evoke tetrad responses when administered over 21 d. GAT229-dependent tetrad responses may have been the result of 1) sustained enhancement of 2-AG- and AEA-mediated CB_1 activation; 2) accumulation of GAT229; or 3) accumulation of a metabolite of GAT229 that in turn affected CB_1 (Bosier *et al*., 2010; Long *et al*., 2009; Ignatowska-Jankowska *et al*., 2015). In order to confirm that the effects of GAT228 and GAT229 occur *via* CB_1, I would conduct additional experiments with CB_1 antagonists and CB_1 knockout mice. I would also conduct studies with different doses and treatment paradigms to assess the metabolism, potency and

efficacy of GAT211, GAT228, and GAT229 *in vivo* in control mice and in the zQ175 genetically accurate, progressive mouse model of HD (Menalled *et al*., 2014).

Beyond HD, CB_1 allosteric modulators may be used in the treatment of other pathological conditions. CB_1 PAMs may be useful as anxiolytics, treatments of post-traumatic stress disorder, and both centrally- and peripherally-mediated pain because they enhance the inhibitory effects of pre-synaptic CB_1 (Slivicki *et al.*, 2014; Cairns *et al.*, 2014; Ignatowska-Jankowska *et al*., 2015; Laprairie *et al*., 2015c). CB_1 NAMs may be useful an antiepileptics, and treatments of addiction and obesity that are able to limit CB_1-dependent signaling with limited adverse psychotropic effects compared to previously tested orthosteric inverse agonists (Pertwee, 2005; Laprairie *et al*., 2015d). As our understanding of CB_1 allosteric modulators continues to advance the questions outlined here will be important questions to answer for multiple pathological conditions, including HD.

8.4. CONCLUSIONS

The culmination of my work to-date supports the hypothesis that the locomotor, cognitive, behavioural, metabolic, and cell-intrinsic molecular signs of HD can be managed *via* targeting of CB_1 so long as $G\alpha_{i/o}$-dependent signaling downstream is selectively enhanced without supraphysiological activation, desensitization, or receptor downregulation. To this end, CB_1 PAMs represent the ideal pharmacological means of enhancing CB_1 levels and abundance. The delay of symptom onset observed in R6/2 HD mice treated with the probe compounds GAT211, GAT228, and GAT229 provides a first proof-of-concept for positive allosteric modulators as therapeutics in HD.

REFERENCES

Adam L, Salois D, Rihakova L, Lapointe S, St-Onge S, Labrecque J, Payza K (2007). Positive allosteric modulators of CB1 receptors. Symposium on the Cannabinoids. Saint-Saveur, QC, CAN. International Cannabinoid Research Society, p. 86.

Adams P, Falek A, Arnold J (1988). Huntington disease in Georgia: age at onset. *Am J Hum Genet* **43**: 695 – 704.

Ahn KH, Mahmoud MM, Kendall DA (2012). Allosteric modulator ORG27569 induces CB1 cannabinoid receptor high affinity agonist binding state, receptor internalization, and Gi protein-independent ERK1/2 kinase activation. *J Biol Chem* **287**: 12070 – 12082.

Ahn KH, Mahmoud MM, Shim JY, Kendall DA (2013). Distinct roles of β-arrestin 1 and β-arrestin 2 in ORG27569-induced biased signaling and internalization of the cannabinoid receptor 1 (CB1). *J Biol Chem* **288**: 9790 – 9800.

Allen KL, Waldvogel HJ, Glass M, Faull RL (2009). Cannabinoid (CB(1)), GABA(A) and GABA(B) receptor subunit changes in the globus pallidus in Huntington's disease. *J Chem Neuroanat* **37**: 266 – 281.

Anavi-Goffer S, Fleischer D, Hurst DP, Lynch DL, Barnett-Norris J, Shi S, Lewis DL, Mukhopadhyay S, Howlett AC, Reggio PH, Abood ME (2007). Helix 8 Leu in the CB1 cannabinoid receptor contributes to selective signal transduction mechanisms. *J Biol Chem* **282**: 25100 – 25113.

Anderson RL, Randall MD, Chan SL (2013). The complex effects of cannabinoids on insulin secretion from rat isolated islets of Langerhans. *Eur J Pharmacol* **706**: 56 – 62.

Arjmand S, Vaziri Z, Behzadi M, Abbassian H, Stephens GJ, Shabani M (2015). Cannabinoids and Tremor Induced by Motor-related Disorders: Friend or Foe? *Neurotherapeutics* **12**: 778 – 787.

Armstrong R, Tuan QL, Frost EE, Broke RC, Vana AC (2002). Absence of fibroblast growth factor 2 promotes oligodendroglial repopulation of demyelinated white matter. *J Neurosci* **22**: 8574 – 8585.

Arnett HA, Mason J, Marino M, Suzuki K, Matsushima GK, Ting JP (2001). TNFα promotes proliferation of oligodendrocyte progenitors and remyelination. *Nat Neurosci* **4**: 1116 – 1122.

Arning L, Saft C, Wieczorek S, Andrich J, Kraus PH, Epplen JT (2007). NR2A and NR2B receptor gene variations modify age at onset in Huntington disease in a sex-specific manner. *Hum Genet* **122**: 175 – 182.

Atwal RS, Xia J, Pinchev D, Taylor J, Epand RM, Truant R (2007). Huntingtin has a membrane association signal that can modulate huntingtin aggregation, nuclear entry and toxicity. *Hum Mol Genet* **16**: 2600 – 2615.

Atwood BK, Mackie K (2010). CB2: a cannabinoid receptor with an identity crisis. *Br J Pharmacol* **160**: 467 – 479.

Bagher AM, Laprairie RB, Kelly ME, Denovan-Wright EM (2013). Co-expression of the human cannabinoid receptor coding region splice variants (hCB_1) affects the function of hCB_1 receptor complexes. *Eur J Pharmacol* **721**: 341 – 354**.**

Baillie GL, Horswill JG, Anavi-Goffer S, Reggio PH, Bolognini D, Abood ME, McAllister S, Strange PG, Stephens GJ, Pertwee RG, Ross RA (2013). CB(1) receptor allosteric modulators display both agonist and signaling pathway specificity. *Mol Pharmacol* **83**: 322 – 38.

Bakshi K, Mercier RW, Pavlopoulos S (2007). Interaction of a fragment of the cannabinoid CB1 receptor C-terminus with arrestin-2. *FEBS Letters* **581**: 5009 – 5016.

Ballard DW, Dixon EP, Peffer NJ, Bogerd H, Doerre S, Stein B, Greene WC (1992). The 65-kDa subunit of human NF-kappa B functions as a potent transcriptional activator and a target for v-Rel-mediated repression. *Proc. Natl Acad Sci USA* **89**: 1875 – 1879.

Bari M, Battista N, Valenza M, Mastrangelo N, Malaponti M, Catanzaro G, Centonze D, Finazzi-Agrò A, Cattaneo E, Maccarrone M (2013). In vitro and in vivo models of Huntington's disease show alterations in the endocannabinoid system. *FEBS J* **280**: 3376 – 3388.

Barnett-Norris J, Hurst DP, Lynch DL, Guarnieri F, Makriyannis A, Reggio PH (2002). Conformational memories and the endocannabinoid binding site at the cannabinoid CB1 receptor. *ACS Med Chem Lett* **45**:3649 – 3659.

Becanovic K, Pouladi MA, Lim RS, Kuhn A, Pavlidis P, Luthi-Carter R, Hayden MR, Leavitt BR (2010). Transcriptional changes in Huntington disease identified using genome-wide expression profiling and cross-platform analysis. *Hum Mol Genet* **19**: 1438 – 1452.

Bekkers JM, Stevens CF (1991). Excitatory and inhibitory autaptic currents in isolated hippocampal neurons maintained in cell culture. *Proc Natl Acad Sci USA* **88**: 7834 – 7838.

Beglinger LJ, Adams WH, Langbehn D, Fiedorowicz JG, Jorge R, Biglan K, Caviness J, Olson B, Robinson RG, Kieburtz K, Paulsen JS (2014). Results of the citalopram to enhance cognition in Huntington disease trial. *Mov Disord* **29**: 401 – 405.

Benn CL, Slow EJ, Farrell LA, Graham R, Deng Y, Hayden MR, Cha JH (2007) Glutamate receptor abnormalities in the YAC128 transgenic mouse model of Huntington's disease. *Neuroscience* **147**: 354 – 372.

Bisogno T, Hanus L, De Petrocellis L, Tchilibon S, Ponde DE, Brandi I, Moriello AS, Davis JB, Mechoulam R, Di Marzo V (2001). Molecular targets for cannabidiol and its synthetic analogues: effect on vanilloid VR1 receptors and on the cellular uptake and enzymatic hydrolysis of anandamide. *Br J Pharmacol* **134**: 845 – 52.

Björqvist M, Wild EJ, Thiele J, Silvestroni A, Andre R, Lahiri N, Raibon E, Lee RV, Benn CL, Soulet D, Magnusson A, Woodman B, Landles C, Pouladi MA, Hayden MR, Khalili-Shirazi A, Lowdell MW, Brundin P, Bates GP, Leavitt BR, Möller T, Tabrizi SJ (2008). A novel pathogenic pathway of immune activation detectable before clinical onset in Huntington's disease. *J Med Exp* **205**: 1869 – 1877.

Black JW, Leff P (1983). Operational models of pharmacological agonism. *Proc Roy Soc London B* **220**: 141 – 162.

Blair RE, Deshpande LS, Sombati S, Elphick MR, Martin BR, DeLorenzo RJ (2009). Prolonged exposure to WIN55,212-2 causes downregulation of the CB1 receptor and the development of tolerance to its anticonvulsant effects in the hippocampal neuronal culture model of acquired epilepsy. *Neuropharmacology* **57**: 208 – 218.

Blázquez C, Chiarlone A, Sagredo O, Aguado T, Pazos MR, Resel E, Palazuelos J, Julien B, Salazar M, Borner C, Benito C, Carrasco C, Diez-Zaera M, Paoletti P, Diaz-Hernandez M, Ruiz C, Sendter M, Lucas JJ, de Yebenes JG, Marsicano G, Monory K, Lutz B, Romero J, Alberch J, Gines S, Kraus K, Fernandez-Ruiz J, Galve-Roperh I, and Guzman M (2011) Loss of striatal type 1 cannabinoid receptors is a key pathogenic factor in Huntington's disease. *Brain* **134**: 119 – 36.

Blázquez C, Chiarlone A, Bellocchio L, Resel E, Pruunsild P, García-Rincón D, Sendtner M, Timmusk T, Lutz B, Galve-Roperh I, Guzmán M (2015). The CB1 cannabinoid receptor signals striatal neuroprotection via a PI3K/Akt/mTORC1/BDNF pathway. *Cell Death Differ* **22:** 1618 – 1629**.**

Bolognini D, Cascio MG, Parolaro D, Pertwee RG (2012). AM630 behaves as a protean ligand at the human cannabinoid CB2 receptor. *Br J Pharmacol* **165**: 2561 – 2574.

Bonelli RM, Wenning GK, Kapfhammer HP (2004). Huntington's disease: present treatments and future therapeutic modalities. *Int Clin Psychopharmacol* **19**: 51 – 62.

Bonhaus DW, Chang LK, Kwan J, Martin GR (1998). Dual activation and inhibition of adenylyl cyclase by cannabinoid receptor agonists: evidence for agonist-specific trafficking of intracellular responses. *J Pharmacol Exp Ther* **287**: 884 – 888.

Börner C, Hollt V, Sebald W, Kraus J (2007). Transcriptional regulation of the cannabinoid receptor type 1 gene in T cells by cannabinoids. *J Leukoc Biol* **81**: 336 – 343.

Borovecki F, Lovrecic L, Zhou J, Jeong H, Then F, Rosas HD, Hersch SM, Hogarth P, Bouzou B, Jensen RV, Krainc D (2002). Genome-wide expression profiling of human blood reveals biomarkers for Huntington's disease. *Proc Natl Acad Sci USA* **102**: 11023 – 11028.

Bosier B, Tilleux S, Najimi M, Lambert DM, Hermans E (2007). Agonist selective modulation of tyrosine hydroxylase expression by cannabinoid ligands in a murine neuroblastoma cell line. *J Neurochem* **102**: 1996 – 2007.

Bosier B, Hermans E, Lambert DM (2008a). Differential modulation of AP-1- and CRE-driven transcription by cannabinoid agonists emphasizes functional selectivity at the CB1 receptor. *Br J Pharmacol* **155**: 24 – 33.

Bosier B, Lambert DM, Hermans E (2008b) Reciprocal influences of CB1 cannabinoid receptor agonists on ERK and JNK signalling in N1E-115 cells. *FEBS Lett* **582**: 3861 – 3867.

Bosier B, Muccioli GG, Hermans E, Lambert DM (2010). Functionally selective cannabinoid receptor signalling: therapeutic implications and opportunities. *Biochem Pharmacol* **80**, 1 – 12.

Botelho EP, Wang E, Chen JY, Holley S, Andre V, Cepeda C, Levine MS (2014). Differential Synaptic and Extrasynaptic Glutamate-Receptor Alterations in Striatal Medium-Sized Spiny Neurons of Aged YAC128 Huntington's Disease Mice. *PLoS Curr* **6**: doi 10.1371.

Bouchard J, Truong J, Bouchard K, Dunkelberger D, Desrayaud S, Moussaoui S, Tabrizi SJ, Stella N, Muchowski PJ (2012). Cannabinoid receptor 2 signaling in peripheral immune cells modulates disease onset and severity in mouse models of Huntington's disease. *J Neurosci* **32**: 18259 – 18268.

Breivogel CS, Selley DE, Childers SR (1998). Cannabinoid receptor agonist efficacy for stimulating [35S]GTPgammaS binding to rat cerebellar membranes correlates with aongist-induced decreases in GDP affinity. *J Biol Chem* **273**: 16865 – 16873.

Brooks SP, Dunnett SP (2015). Mouse models of Huntington's disease. *Curr Top Behav Neurosci* **22**: 101 – 133.

Cairns EA, Archibald ML, Straiker A, Kulkarni PM, Thakur GA, Baldridge WH, Kelly MEM (2014). Modifying CB1 receptor signaling to reduce intraocular pressure in a mouse model of ocular hyptertenstion. International Cannabinoids Research Symposium, Baveno, IT. International Cannabinoid Research Society, p. 1-19.

Cardinal P, Bellocchio L, Clark S, Cannich A, Klugmann M, Lutz B, Marsicano G, Cota D (2012). Hypothalamic CB1 cannabinoid receptors regulate energy balance in mice. *Endocrinology* **153**: 4136 – 4143.

Carroll JB, Bates GP, Steffan J, Saft C, Tabrizi SJ (2015). Treating the whole body in Huntington's disease. *Lancet Neurol* **14**: 1135 – 1142.

Campos AC, Moreira FA, Gomes FV, Del Bel EA, Guimarães FS (2012). Multiple mechanisms involved in the large-spectrurm therapeutic potential of cannabidiol in psychiatric disorders. *Philos Trans R Soc Lond B Biol Sci* **367**: 3364 – 3378.

Canals M, Milligan G (2008). Constitutive activity of the cannabinoid CB1 receptor regulates the function of co-expressed Mu opioid receptors. *J Biol Chem* **283**: 11424 – 11434.

Cao C, Temel Y, Blokland A (2006). Progression deterioration of reaction time performance and choreiform symptoms in a new Huntington's disease transgenic rat model. *Behav Brain Res* **170**: 257 – 261.

Cascio MG, Bolognini D, Pertwee RG, Palazzo E, Corelli F, Pasquini S, Di Marzo V, Miaone S (2010). In vitro and in vivo pharmacological characterization of two novel selective cannabinoid CB(2) receptor inverse agonists. *Pharmacol Res* **61**: 349 – 354.

Cawston EE, Redmond WJ, Breen CM, Grimsey NL, Connor M, Glass M (2013). Real-time characterization of cannabinoid receptor 1 (CB1) allosteric modulators reveals novel mechanism of action. *Br J Pharmacol* **170**: 893 – 907.

Cha JH, Kosinski CM, Kerner JA, Alsdorf SA, Mangiarini L, Davies SW, Penney JB, Bates GP, Young AB (1998). Altered brain neurotransmitter receptors in treasgenic mice expressing a portion of an abnormal human Huntington disease gene. *Proc Natl Acad Sci USA* **95**: 6480 – 6485.

Cha JH (2000). Transciptional dysregulation in Huntington's disease. *Trends Neurosci* **23**: 387 – 392.

Chetty M, Miller R, Moodley SV (1994). Smoking and body weight influence the clearance of chlorpromazine. *Eur J Clin Pharmacol* **46**: 523 – 526.

Chiarlone A, Bellocchio L, Blázquez C, Resel E, Soria-Gómez E, Cannich A, Ferrero JJ, Sagredo O, Benito C, Romero J, Sánchez-Prieto J, Lutz B, Fernández-Ruiz J, Galve-Roperh I, Guzmán M (2014). A restricted population of CB1 cannabinoid receptors with neuroprotective activity. *Proc Natl Acad Sci U S A* **111**: 8257 – 8262.

Chiodi V, Uchigashima M, Beggiato S, Ferrante A, Armida M, Martire A, Potenza RL, Ferraro L, Tanganelli S, Watanabe M, Domenici MR, Popoli P (2012). Unbalance of CB1 receptors expressed in GABAergic and glutamatergic neurons in a transgenic mouse model of Huntington's disease. *Neurobiol Dis* **45**: 983 – 991.

Chou SY, Weng JY, Lai HL, Liao F, Sun SH, Tu PH, Dickson DW, Chern Y (2008). Expanded-polyglutamine huntingtin protein suppresses the secretion and production of a chemokine (CCL5/RANTES) by astrocytes. *J Neurosci* **28**: 3277 – 3290.

Christopoulos A, Kenakin T (2002). G protein-coupled receptor allosterism and complexing. *Pharmacol Rev* **54**: 323 – 74.

Christopoulos A (2014). Advances in G protein-coupled receptor allostery: from function to structure. *Mol Pharmacol* **86**: 463 – 478.

Cluny NL, Reimer RA, Sharkey KA (2012). Cannabinoid signalling regulates inflammation and energy balance: the importance of the brain-gut axis. *Brain Behav Immun* **26**: 691- 698.

Consroe P, Sandyk R, Snider SR (1986). Open label evaluation of cannabidiol in dystonic movement disorders. *Int J Neurosci* **30**: 277 – 282.

Consroe P, Laguna J, Allender J, Snider S, Stern L, Sandyk R, Kennedy K, Schram K (1991). Controlled clinical trial of cannabidiol in Huntington's disease. *Pharmacol Biochem Behav* **40**: 701 – 708.

Costa B, Trovato AE, Comelli F, Giagnoni G, Colleoni M (2007). The non-psychoactive cannabis constituent cannabidiol is an orally effective therapeutic agent in rat chronic inflammatory and neuropathic pain. *Eur J Pharmacol* **556**: 75 – 83.

Cota D, Marsicano G, Lutz B, Vicennati V, Stalla GK, Pasquali R, Pagotto U (2003). Endogenous cannabinoid system as a modulator of food intake. *Int J Obes* **27**: 289 – 301.

Coutts AA, Anavi-Goffer S, Ross RA, MacEwan DJ, Mackie K, Pertwee RG, Irving AJ (2001). Agonist-induced internalization and trafficking of cannabinoid CB1 recceptors in hippocampal neurons. *J Neurosci* **21**: 2425 – 2433.

Cui L, Jeong H, Borovecki F, Parkhurst CN, Tanese N, Krainc D (2006). Transcriptional repression of PGC-1alpha by mutant huntingtin leads to mitochondrial dysfunction and neurodegeneration. *Cell* **127**: 59 – 69.

Cupini LM, Costa C, Sarchielli P, Bari M, Battista N, Eusebi P, Calabresi P, Maccarrone M (2008). Degradation of endocannabinoids in chronic migraine and medication overuse headache. *Neurobiol Dis* **30**: 186 – 189.

Curtis A, Mitchell I, Patel S, Ives N, Rickards H (2009). A pilot study using nabilone for symptomatic treatment in Huntington's disease. M*ov Disord* **24**: 2254 – 2259.

Daigle TL, Kearn CS, Mackie K (2008). Rapid CB1 cannabinoid receptor desensitization defines the time course of ERK1/2 MAP kinase signaling. *Neuropharmacol* **54**: 36 – 44.

Dalrymple, A, Wild EJ, Joubert R, Sathasivam K, Björkqvist M, Petersén A, Jackson GS, Isaacs JD, Kristiansen M, Bates GP, Leavitt BR, Keir G, Ward M, Tabrizi SJ (2007). Proteomic profiling of plasma in Huntington's disease reveals neuroinflammatory activation and biomarker candidates. *J Proteome Res* **6**: 2833 – 2840.

Dalton GD, Howlett AC (2012). Cannabinoid CB1 receptors transactivate multiple receptor tyrosine kinases and regulate serine/threonine kinases to activate ERK in neuronal cells. *Br J Pharmacol* **165**: 2497 – 2511.

De Backer B, Maebe K, Verstraete AG, Charlier C (2012). Evolution of the content of THC and other major cannabinoids in drug-type cannabis cuttings and seedlings during growth of plants. *J Forensic Sci* **57**: 918 – 922.

Delorme C, Rogers A, Lau B, Francisque H, Welter ML, Vidal SF, Yelnik J, Durr A, Grabli D, Karachi C (2015). Deep brain stimulation of the internal pallidum in Huntington's disease patients: clinical outcome and neuronal firing patterns. *J Neurol* **263**: 290 – 298.

Denovan-Wright EM, Newton RA, Armstrong JN, Babity JM, Robertson HA (1998). Acute administration of cocaine, but not amphetamine, increases the level of synaptotagmin IV mRNA in the dorsal striatum of rat. *Brain Res Mol Brain Res* **55**: 350 – 354.

Denovan-Wright EM, Robertson HA (2000). Cannabinoid receptor messenger RNA levels decrease in a subset of neurons of the lateral striatum, cortex and hippocampus of transgenic Huntington's disease mice. *Neuroscience* **98**: 705 – 713.

Denovan-Wright EM, Attis M, Rodriguez-Lebron E, Mendel RJ (2008). Sustained striatal ciliary neurotrophic factor expression negatively affects behavior and gene expression in normal and R6/1 mice. *J Neurosci Res* **86**: 1748 – 1757.

Desplats PA, Kass KE, Gilmartin T, Stanwood GD, Woodward EL, Head SR, Sutcliffe JG, Thomas EA (2006). Selective deficits in the expression of striatal-enriched mRNAs in Huntington's disease. *J Neurochem* **96**: 743 – 757.

Devane WA, Hanus L, Breuer A, Pertwee RG, Stevenson LA, Griffin G, Gibson D, Mandelbaum A, Etinger A, Mechoulam R (1992). Isolation and structure of a brain constituent that binds to the cannabinoid receptor. *Science* **258**: 1946 – 1949.

Devinsky O, Cilio MR, Cross H, Fernandez-Ruiz J, French J, Hill C, Katz R, Di Marzo V, Jutras-Aswad D, Notcutt WG, Martinez-Orgado J, Robson PJ, Rohrback BG, Thiele E, Whalley B, Friedman D (2014). Cannabidiol: Pharmacology and potential therapeutic role in epilepsy and other neuropsychiatric disorders. *Epilepsia* **55:** 791 – 802.

Di Marzo V, Stella N, Zimmer A (2015). Endocannabinoid signalling and the deteriorating brain. *Nat Rev Neurosci* **16**: 30 – 42.

Dowie MJ, Bradshaw HB, Howard ML (2009). Altered CB1 receptor and endocannabinoid levels precede motor symptom onset in a transgenic mouse model of Huntington's disease. *Neuroscience* **163**: 456 – 65.

Dowie MJ, Howard ML, Nicholson LF, Faull RL, Hannan AJ, Glass M (2010). Behavioural and molecular consequences of chronic cannabinoid treatment in Huntington's disease transgenic mice. *Neuroscience* **170**: 324 – 336.

DrugBank v. 4.3. Dronnabinol (syn: (-)-delta9-trans-Tetrahydrocannabinol). In: DrugBank.ca [Internet]. Ottawa (ON): Canadian Institutes of Health Research (CAN). 10/12/2015. Available from: http://www.drugbank.ca/drugs/DB00470#interactions.

Dupré DJ, Thompson C, Chen Z, Rollin S, Larrivée JF, Le Gouill C, Rola-Pleszczynski M, Stanková J (2007). Inverse agonist-induced signaling and down-regulation of the platelet-activating factor receptor. *Cell Signal* **19**: 2068 – 2079.

Edlinger M, Seppi K, Fleischhacker W, Hofer A (2013). Treatment of psychotic and behavioral symptoms with clozapine, aripiprazole, and reboxetine in a patient with Huntington's disease. *Int J Clin Psychopharmacol* **28**: 214 – 216.

Ehlert FJ, Suga H, Griffin MT (2011). Quantifying agonist activity at G protein-coupled receptors. *J Vis Exp* **58**: e3179.

Ehlert RJ (2015). Functional studies cast light on receptor states. *Trends Pharmacol Sci* **36**: 596 – 604.

Ellrichmann G, Reick C, Saft C, Linker RA (2013). The role of the immune system in Huntington's disease. *Clin Dev Immunol* **2013**: 541259.

Fain JN, Del Mar NA, Meade CA, Reiner A, Goldowitz D (2001). Abnormalities in the functioning of adipocytes from R6/2 mice that are transgenic for the Huntington's disease mutation. *Hum Mol Genet* **10**: 145 – 152.

Falenski KW, Thorpe AJ, Schlosburg JE, Cravatt BF, Abdullah RA, Smith TH, Selley DE, Lichtman AH, Sim-Selley LJ (2010). FAAH-/- mice display differential tolerance, dependence, and cannabinoid receptor adaptation after delta 9-tetrahydrocannabinol and anandamide administration. *Neuropsychopharmacol* **35**: 1775 – 1787.

Fay JF, Farrens DL (2013). The membrane proximal region of the cannabinoid receptor CB1 N-terminus can allosterically modulate ligand affinity. *Biochemistry* **52**: 8286 – 8294.

Fernández-Ruiz J, Gomez M, Hernandez M, de Miguel R, Ramos JA (2004). Cannabinoids and gene expression during development. *Neurotox Res* **6**: 389 – 401.

Fernández-Ruiz J (2009). The endocannabinoid system as a target for the treatment of motor dysfunction. *Br J Pharmacol* **156**: 1029 – 1040.

Fernández-Ruiz J, Romero J, Ramos JA *(*2015). Endocannabinoids and Neurodegenerative Disorders: Parkinson's Disease, Huntington's Chorea, Alzheimer's Disease, and Others. *Handb Exp Pharmacol* **231**: 233 – 259.

Ferreira SG, Teixeira FM, Garção P, Agostinho P, Ledent C, Cortes L, Mackie K, Köfalvi A (2012). Presynaptic CB(1) cannabinoid receptors control frontocortical serotonin and glutamate release--species differences. *Neurochem Int* **61**: 219 – 226.

Foroud T, Gray J, Ivashina J, Conneally PM (1999). Differences in duration of Huntington's disease based on age at onset. *J Neurol Neurosurg Psychiatry* **66**: 52 – 56.

Francelle L, Galvan L, Brouillet E (2014). Possible involvement of self-defense mechanisms in the preferential vulnerability of the striatum in Huntington's disease. *Front Cell Neurosci* **8**: 295.

Franciosi S, Ryu JK, Shim Y, Hill A, Connolly C, Hayden MR, McLarnon JG, Leavitt BR (2012). Age-dependent neurovascular abnormalities and altered microglial morphology in the YAC128 mouse model of Huntington disease. *Neurobiol Dis* **45**: 438 – 449.

Furshpan EJ, MacLeish PR, O'Lague PH, Potter DD (1976). Chemical transmission between rat sympathetic neurons and cardiac myocytes developing in microcultures: evidence for cholinergic, adrenergic, and dual-function neurons. *Proc Natl Acad Sci USA* **73**:4225 – 4229.

Gadavarthi SK, Narender D, Mishra A, Goswami A, Rao SN, Nukina N, Jana NR (2009). Induction of chemokines, MCP-1, and KC in the mutant huntingtin expressing neuronal cells because of proteasomal dysfunction. *J Neurochem* **108**: 787 – 795.

Gamage TF, Ignatowska-Jankowska BM, Wiley JL, Abdelrahman M, Trembleau L, Greig IR, Thakur GA, Tichkule R, Poklis J, Ross RA, Pertwee RG, Lichtman AH (2014). In-vivo pharmacological evaluation of the CB1-receptor allosteric modulator Org-27569. *Behav Pharmacol* **25**: 182 – 185.

Garcıa-Caldentey J, Trillo P, Ruiz C et al. (2015). A double-blind, cross-over, placebo-controlled, phase II trial with Sativex in Huntington's disease. **Submitted.**

Garcia de Yébenes J. Neuroprotection by Cannabinoids in Huntington's Disease. In: ClinicalTrials.gov [Internet]. Bethesda (MD): National Library of Medicine (US). 10/12/2015. Available from: https://clinicaltrials.gov/ct2/show/NCT01502046?term=Huntington%27s+disease+AND+cannabinoid&rank=1 NLM Identifier: NCT01502046.

Gatley SJ, Lan R, Pyatt B, Gifford AN, Volkow ND, Markiyannis A (1997) Binding of the non-classical cannabinoid CP55,940 and the diarylpyrazole AM251 to rodent brain cannabinoid receptors. *Life Sci* **61**: 191 – 197.

Gerdeman GL, Fernandez-Ruiz J. The endocannabinoid system in the physiology and pathology in the basal ganglia. In: Kofalvi A, editor. *Cannabinoids and the brain*. Springer Verlag; 2008.

Georgieva T, Devanathan S, Stropova D, Park CK, Salamon Z, Tollin G, Hruby VJ, Roeske WR, Yamamura HI, Varga E (2008). Unique agonist-bound cannabinoid CB1 receptor conformations indicate agonist specificity in signalling. *Eur J Pharmacol* **581**: 19 – 29.

Ghose J, Sinha M, Das E, Jana NR, Bhattacharyya NP (2011). Regulation of miR-146a by RelA/NFkB and p53 in STHdh(Q111)/Hdh(Q111) cells, a cell model of Huntington's disease. *PLoS One* **6**: e23837.

Gil Polo C, Cubo Delgado E, Mateos Cachorro A, Rivadeneyra Posadas J, Mariscal Pérez N, Armesto Formoso D (2015). Energy balance in Huntington's disease. *Ann Nutr Metab* **67**: 267 – 273.

Giuffrida A, Beltramo M, Piomelli D (2001). Mechanisms of endocannabinoid inactivation: biochemistry and pharmacology. *J Pharmacol Exp Ther* **298**: 7 – 14.

Glass M, Faull RL, Dragunow M (1993). Loss of cannabinoid receptors in the substantia nigra in Huntington's disease. *Neuroscience* **56**: 523 – 527.

Glass M, Felder CC (1997). Concurrent stimulation of cannabinoid CB1 and dopamine D2 receptors augments cAMP accumulation in striatal neurons: evidence for a Gs linkage to the CB1 receptor. *J Neurosci* 17: 5327 – 5333.

Glass M, Northrup JK (1999). Agonist selective regulation of G proteins by cannabinoid CB(1) and CB(2) receptors. *Mol Pharmacol* **56**: 1362 – 1369.

Glass M, Dragunow M, Faull RL (2000). The pattern of neurodegeneration in Huntington's disease: a comparative study of cannabinoid, dopamine, adenosine and GABA(A) receptor alterations in the human basal ganglia in Huntington's disease. *Neuroscience*. **97**: 505 – 519.

Griffin MT, Figueroa KW, Liller S, Ehlert FJ (2007). Estimation of agonist activity a G protein-coupled receptors: analysis of M2 muscarinic receptor signaling through Gi/o, Gs, and G15. *J Pharmacol Exp Ther* **321**: 1193 – 1207.

Gu G, Rojo AA, Zee MC, Yu J, Simerly RB (1996). Hormonal regulation of CREB phosphorylation anteroventral periventricular nucleus. *J Neurosci* **16**: 3035 – 3044.

Halliday GM, McRitchie DA, Macdonald V, Double KL, Trent RJ, McCusker E (1998). Regional specificity of brain atrophy in Huntington's disease. *Experimental neurology* **154**: 663 – 672.

Hayakawa K, Mishima K, Irie K, Hazekawa M, Mishima S, Fujioka M, Orito K, Egashira N, Katsurabayashi S, Takasaki K, Iwasaki K, Fujiwara M (2008). Cannabidiol prevents a post-ischemic injury progressively induced by cerebral ischemia via a high-mobility group box1-inhibiting mechanism. *Neuropharmacol* **55**: 1280 – 1286.

Hebb AL, Robertson HA, Denovan-Wright EM (2004). Striatal phosphodiesterase mRNA and protein levels are reduced in Huntington's disease transgenic mice prior to the onset of motor symptoms. *Neuroscience* **123**: 967 – 981.

Heneryck A, De Vriendt C, Belpaire FM (1999). Inhibition of CYP2C9 by selective serotonin reuptake inhibitors: in vitro studies with tolbutamide and (S)-warfarin using human liver microsomes. *Eur J Clin Pharmacol* **54**: 947 – 951.

Heng MY, Detloff PJ, Wang PL, Tsien JZ, Albin RL (2009). In vivo evidence for NMDA receptor-mediated excitotoxicity in a murine genetic model of Huntington disease. *J Neurosci* **29**: 3200 – 3205.

Higuchi S, Irie K, Mishima S, Araki M, Ohji M, Shirakawa A, Akitake Y, Matsuyama K, Mishima K, Mishima K, Iwasaki K, Fujiwara M (2010). The cannabinoid 1-receptor silent antagonist O-2050 attenuates preference for high-fat diet and activated astrocytes in mice. *J Pharmacol Sci* **112**: 369 – 372.

Hodges A, Andrew DS, Aragaki AK, Kuhm A, Sengtag T, Hughes G, Elliston LA, Hartog C, Goldstein DR, Thu D, Hollingsworth ZR, Collin F, Synek B, Holmans PA, Young AB, Wexler NS, Delorenzi M, Kooperberg C, Augood SJ, Faull RL, Olson JM, Jones L, Luthi-Carter R (2006). Regional and cellular gene expression changes in human Huntington's disease brain. *Hum Mol Genet* **15**: 965 – 977.

Hogel M, Laprairie RB, Denovan-Wright EM (2012). Promoters Are Differentially Sensitive to N-Terminal Mutant Huntingtin-Mediated Transcriptional Repression. *PLoS One* **7**: e41152.

Hooft RW, Straver LH, Spek AL (2008). Determination of absolute structure using Bayesian statistics on Bijvoet differences. *J Appl Crystallogr* **41**: 96 – 103.

Horne EA, Coy J, Swinney K, Fung S, Cherry AE, Marrs WR (2013). Downregulation of cannabinoid receptor 1 from neuropeptide Y interneurons in the basal ganglia of patients with Huntington's disease and mouse models. *Eur J Neurosci* **37**: 429 – 440.

Horswill JG, Bali U, Shaaban S, Keily JF, Jeevaratnam P, Babbs AJ, Reynet C, Wong Kai In P (2007). PSNCBAM-1, a novel allosteric antagonist at cannabinoid CB1 receptors with hypophagic effects in rats. *Br J Pharmacol* **152**: 805 – 814.

Howlett AC, Barth F, Bonner TI, Cabral G, Casellas P, Devane WA, Felder CC, Herkenham M, Mackie K, Martin BR, Mechoulam R, Pertwee RG (2002). International Union of Pharmacology. XXVII. Classification of Cannabinoid Receptors. *Pharmacol Rev* **54**: 161 – 202.

Hudson BD, Hebert TE, Kelly ME (2010). Physical and functional interaction between CB1 cannabinoid receptors and beta2-adrenoceptors. *Br J Pharmacol* **160**: 627 – 642.

Hudson BD, Christiansen E, Murdoch H, Jenkins L, Hansen AH, Madsen O, Ulven T, Milligan G (2014). Complex pharmacology of novel allosteric free fatty acid 3 receptor ligands. *Mol Pharmacol* **86**: 200 – 210.

Huntington's disease collaborative research group (HDCRG) (1993). A novel gene containing a trinucleotide repeat that is expanded and unstable on Huntington's disease chromosomes. The Huntington's Disease Collaborative Research Group. *Cell* **72**: 971 – 983.

Iannotti FA, Hill CL, Leo A, Alhusaini A, Soubrane C, Mazzarella E, Russo E, Whalley BJ, Di Marzo V, Stephens GJ (2014). Nonpsychotropic plant cannabinoids, cannabidivarin (CBDV) and cannabidiol (CBD), activate and desensitize transient receptor potential vanilloid 1 (TRPV1) channels in vitro: potential for the treatment of neuronal hyperexcitability. *ACS Chem Neurosci* **5**: 1131 – 1141.

Ignatowska-Jankowska BM, Baillie GL, Kinsey S, Crowe M, Ghosh S, Owens RA, Damaj IM, Poklis J, Wiley JL, Zanda M, Zanato C, Greig IR, Lichtman AH, Ross RA (2015). A Cannabinoid CB1 Receptor-Positive Allosteric Modulator Reduces Neuropathic Pain in the Mouse with No Psychoactive Effects. *Neuropsychopharmacol* **40**: 2948 – 2959.

James JR, Oliveira MI, Carmo AM, Iaboni A, Davis SJ (2006). A rigorous experimental framework for detecting protein oligomerization using bioluminescence resonance energy transfer. *Nat Methods* **3**: 1001 – 1006.

Jin W, Brown S, Roche JP, Hsieh CP, Celver JP, Kovoor A, Chavkin C, Mackie K (1999). Distinct domains of the CB1 cannabinoid receptor mediate desensitization and internalization. *J Neurosci* **19**: 3773 – 3780.

Jones NA, Hill AJ, Smith I, Bevan SA, Williams CM, Whalley BJ, Stephens GJ (2010). Cannabidiol displays antiepileptiform and antiseizure properties in vitro and in vivo. *J Pharmacol Exp Ther* **332**: 569 – 577.

Jusko WJ, Gardner MJ, Mangione A, Schentag JJ, Koup JR, Vance JW (1979). Factors affecting theophylline clearances: age, tobacco, marijuana, cirrhosis, congestive heart failure, obesity, oral contraceptives, benzodiazepines, barbiturates, and ethanol. *J Pharm Sci* **68**: 1358 – 1366.

Kathmann M, Flau K, Redmer A, Tränkle C, Schlicker E (2006). Cannabidiol is an allosteric modulator at mu- and delta-opioid receptors. *Naunyn Schmiedebergs Arch Pharmacol* **372**: 354 – 361.

Kearn CS, Greenberg MJ, DiCamelli R, Kurzawa K, Hillard CJ (1999). Relationships between ligand affinities for the cerebellar cannabinoid receptor CB1 and the induction of GDP/GTP exchange. *J Neurochem* **72**: 2379 – 2387.

Kenakin T, Watson C, Muniz-Medina V, Christopoulos A, Novick S (2011). A simple method for quantifying functional selectivity and agonist bias. *ACS Chem Neurosci* **3**: 193 – 203.

Kenakin T, Christopoulos A (2013). Measurements of ligand bias and functional selectivity. *Nat Rev Drug Discov* **12**: 483.

Keov P, Sexton PM, Christopoulos A (2011). Allosteric modulator of G protein-coupled receptors: A pharmacological perspective. *Neuropharmacol* **60**: 24 – 35.

Khajehali E, Malone DT, Glass M, Sexton PM, Christopoulos A, Leach K (2015). Biased agonism and biased allosteric modulation at the CB1 cannabinoid receptor. *Mol Pharmacol* **88**: 368 – 379.

Kilkenny C, Browne WJ, Cuthill IC, Emerson M, Altman DG (2010). Improving bioscience research reporting: The ARRIVE guidelines for reporting animal research. *PLoS Biol* **8**: e1000412

Kinsey SG, Naidu PS, Cravatt BF, Dudley DT, Lichtman AH (2011). Fatty acid amide hydrolase blockade attenuates the development of collagen-induced arthritis and related thermal hyperalgeisa in mice. *Pharmacol Biochem Behav* **99**: 718 – 725.

Klöppel S, Gregory S, Scheller E, Minkova L, Razi A, Durr A, Roos RA, Leavitt BR, Papoutsi M, Landwehrmeyer GB, Reilmann R, Borowsky B, Johnson H, Mills JA, Owen G, Stout J, Scahill RI, Long JD, Rees G, Tabrizi SJ; Track-On investigators (2015). Compensation in Preclinical Huntington's Disease: Evidence From the Track-On HD Study. *EBioMedicine* **4**: 1420 – 1429.

Kloster E, Saft C, Epplen JT, Arning L (2013). CNR1 variation is associated with the age at onset in Huntington disease. *Eur J Med Genet* **56**: 416 – 419.

Kluger B, Triolo P, Jones W, Jankovic J (2015). The therapeutic potential of cannabinoids for movement disorders. *Mov Disord* **30**: 313 – 327.

Knowles RB, Chin J, Ruff CT, Hyman BT (1999). Demonstration by fluorescence resonance energy transfer of a close association between activated MAP kinase and neurofibrilary tangles: implications for MAP kinase activation in Alzheimer's disease. *J Neuropathol Exp Neurol* **58**: 1090 – 1098.

Kondo S, Kondo H, Nakane S, Kodaka T, Tokumura A, Waku K, Sugiura T (1998). 2-arachidonylglycerol, an endogenous cannabinoid recpetor agonist: identification as one of the major species of monoacylglycerols in various rat tissues, and evidence for its generation through Ca^{2+}-dependent and –independent mechanisms. *FEBS Letters* **429**: 152 – 156.

Koppel BS, Brust JC, Fife T, Bronstein J, Youssof S, Gronseth G, Gloss D (2014). Systematic review: efficacy and safety of medical marijuana in selected neurologic disorders: report of the Guideline Development Subcommittee of the American Academy of Neurology. *Neurology* **82**: 1556 – 1563.

Kreitzer AC, Regher WG (2001). Retrograde inhibition of presynaptic calcium influx by endogenous cannabinoinds at excitatory synapses onto purkinje cells. *Neuron* **29**: 717 – 721.

Kumar A, Vaish M, Ratan RR (2014). Transcriptional dysregulation in Huntington's disease: a failure of adaptive transcriptional homeostasis. *Drug Discov Today* **19**: 956 – 962.

Kumar A, Kumar Singh S, Kumar V, Kumar D, Agarwal S, Rana MK (2015). Huntington's disease: an update of therapeutic strategies. *Gene* **556**: 91 – 97.

Laprairie RB, Kelly ME, Denovan-Wright EM (2012). The dynamic nature of type 1 cannabinoid receptor (CB_1) gene transcription. *Br J Pharmacol* **167**: 1583 – 1595.

Laprairie RB, Kelly MEM, Denovan-Wright EM (2013). Cannabinoids increase type 1 cannabinoid receptor expression in a cell culture model of striatal neurons: Implications for Huntington's disease. *Neuropharmacol* **72**: 47 – 57.

Laprairie RB, Bagher AM, Kelly ME, Dupré DJ, Denovan-Wright EM (2014a) Type 1 Cannabinoid Receptor Ligands Display Functional Selectivity in a Cell Culture Model of Striatal Medium Spiny Projection Neurons. *J Biol Chem* **289**: 24845 – 24862.

Laprairie RB, Warford JR, Hutchings S, Robertson GS, Kelly MEM, Denovan-Wright EM (2014b). The cytokine and endocannabinoid systems are co-regulated by NF-κB p65/RelA in cell culture and transgenic mouse models of Huntington's disease and in striatal tissue from Huntington's disease patients. *J Neuroimmunol* **267**: 61 – 72.

Laprairie RB, Bagher AM, Precious SV, Denovan-Wright EM (2015a). Components of the endocannabinoid and dopamine systems are dysregulated in Huntington's disease: analysis of publicly available microarray datasets. *Pharmacol Res Persp* **3**: e00104.

Laprairie RB, Bagher AM, Kelly ME, Denovan-Wright EM (2015b) Cannabinoid functional selectivity influences neuronal viability in a cell culture model of Huntington's disease. *Mol Pharmacol* **89**: 364 – 375.

Laprairie RB, Zrein A, Bagher AM, Kulkarni PM, Thakur GA, Kelly MEM, Denovan-Wright EM (2015c). Enantiomer-specific positive allosteric modulation of the type 1 cannabinoid receptor for the treatment of Huntington's disease. International Cannabinoids Research Symposium. Wolfville, NS, p. 58.

Laprairie RB, Bagher AM, Kelly ME, Denovan-Wright EM (2015d). Cannabidiol is a negative allosteric modulator of the type 1 cannabinoid receptor. *Br J Pharmcol* **172**: 4790 – 4805.

Laprairie RB, Kulkarni PM, Kelly MEM, Pertwee RG, Straiker A, Denovan-Wright EM, Thakur GA (2016a). Characterization of the novel positive allosteric modulator of the type 1 cannabinoid receptor GAT211, and its enantiomers GAT228 and GAT229. *J Biol* Chem. **In preparation.**

Laprairie RB, Zrein A, Bagher AM, Rourke JL, Cairns EA, Kelly MEM, Sinal CJ, Kulkarni PM, Thakur GA, Denovan-Wright EM (2016b). Positive allosteric modulation of the type 1 cannabinoid receptor reduces the signs and symptoms of Huntington disease in the R6/2 mouse model. *Neurobiol dis.* **In preparation**.

Lastres-Becker I, de Miguel R, De Petrocellis L, Makriyannis A, Di Marzo V, Fernández-Ruiz J (2003). Compounds acting at the endocannabinoid and/or endovanilloid systems reduce hyperkinesia in a rat model of Huntington's disease. *J Neurochem* **84**: 1097 – 1109.

Lauckner JE, Hille B, Mackie K (2005). The cannabinoid agonist WIN55,212-2 increases intracellular calcium via CB1 receptor coupling to Gq/11 G proteins. *Proc Natl Acad Sci USA* **102**: 19144 – 19149.

Lavoie C, Mercier JF, Salahpour A, Umapathy D, Breit A, Villeneuve LR, Zhu WZ, Xiao RP, Lakatta EG, Bouvier M, Hébert TE (2002). Beta 1/beta 2-adrenergic receptor heterodimerization regulates beta 2-adrenergic receptor internalization and ERK signaling efficacy. *J Biol Chem* **277**: 35402 – 35410.

Lazenka MF, Selley DE, Sim-Selley LJ (2013). Brain regional differences in CB1 receptor adaptation and regulation of transcription. *Life Sci* **92**: 446 – 452.

Lee JM, Ivanova EV, Seong IS, Cashorali T, Kohane I, Gusella JF, MacDonald ME (2007). Unbiased gene expression analysis implicates the huntingtin polyglutamine tract in extra-mitochondrial energy metabolism. *PLoS Genet* **3**: e135.

Levison SW, McCarthy KD (1991). Characterization and partial purification of AIM: a plasma protein that induces rat cerebral type 2 astroglia from bipotential glial progenitors. *J Neurochem* **57**: 782 – 794.

Li SH, Cheng AL, Zhou H, Lam S, Rao M, Li H, Li XJ (2002). Interaction of Huntington disease protein with transcriptional activator Sp1. *Mol Cell Biol* **22**: 1277 – 1287.

Long JZ, Li W, Booker L, Burston JJ, Kinsey SG, Schlosburg JE, Pavon FJ, Serrano AM, Selley DE, Parsons LH, Lichtman AH, Cravatt BF (2009). Selective blockade of 2-arachidonylglycerol hydrolysis produces cannabinoid behavioral effects. *Nat Chem Biol* **5**: 37 – 44.

Lopez-Rodriguez AB, Siopi E, Finn DP, Marchand-Leroux C, Garcia-Seguera LM, Jafarian-Tehrani M, Viveros MP (2013). CB1 and CB2 cannabinoid receptor antagonists prevent minocycline-induced neuroprotection following traumatic brain injury in mice. *Cereb Cortex* **25**: 35 – 45.

Lovrecic L, Kastrin A, Kobal J, Pirtosek Z, Krainc D, Peterlin B (2009). Gene expression changes in blood as a putative biomarker for Huntington's disease. *Mov Disord* **24**: 2277 – 2281.

Luthi-Carter R, Strand AD, Hanson SA, Kooperberg C, Schilling G, La Spada AR, Merry DE, Young AB, Ross CA, Borchelt DR, Olson JM (2002). Polyglutamine and transcription: gene expression changes shared by DRPLA and Huntington's disease mouse models reveal context-independent effects. *Hum Mol Genet* **15**: 1927 – 1937.

Luttrell LM, Maudsley S2, Bohn LM (2015). Fulfilling the Promise of "Biased" G Protein-Coupled Receptor Agonism. *Mol Pharmacol* **88**: 579 – 588.

MacCoubrey IC, Moore PL, Haugland RP (1990). Quantitative fluorescence measurements of cell viability (cytotoxicity) with a multi-well plate scanner. *J Cell Biol* **111**: 303.

Magen I, Avraham Y, Ackerman Z, Vorobiev L, Mechoulam R, Berry EM (2009). Cannabidiol ameliorates cognitive and motor impairments in mice with bile duct ligation. *J Hepatol* **51**: 528 – 534.

Mailleux P, Vanderhaeghen JJ (1992). Distribution of neuronal cannabinoid receptor in the adult rat brain: A comparative receptor binding radioautography and in situ hybridization histochemistry. *Neuroscience* **48**: 655 – 688.

Malejko K, Weydt P, Süßmuth SD, Grön G, Landwehrmeyer BG, Abler B (2014). Prodromal Huntington disease as a model for functional compensation of early neurodegeneration. *PLoS One* **9**: e114569.

Mangiarini Sathasivam K, Seller M, Cozens B, Harper A, Hetherington C, Lawton M, Trottier Y, Lehrach H, Davies SW, Bates GP (1996). Exon 1 of the HD gene with an expanded CAG repeat is sufficient to cause a progressive neurological phenotype in transgenic mice. *Cell* **87**: 493 – 506.

Marcora E, Kennedy MB (2010). The Huntington's disease mutation impairs Huntingtin's role in the transport of NF-κB from the synapse to the nucleus. *Hum Mol Genet* **19**: 4373 – 4384.

Martin B, Mechoulam R, Razdan RK (1999). Discovery and characterization of endogenous cannabinoids. *Life Sci* **65**: 573 – 595.

Martin DD, Ladha S, Ehrnhoefer DE, Hayden MR (2015). Autophagy in Huntington disease and huntingtin in autophagy. *Trends Neurosci* **38**: 26 – 35.

Mason SL, Barker RA (2015). Advancing pharmacotherapy for treating Huntington's disease: a review of the existing literature. *Exp Opin Pharmacother* **4**: 1 – 12.

McBride JL, Clark RL (2016). Stereotaxic Surgical Targeting of the Nonhuman Primate Caudate and Putamen: Gene Therapy for Huntington's Disease. *Methods Mol Biol* **1382**: 409 – 428.

McCaw EA, Hu H, Gomez GT, Hebb AL, Kelly ME, Denovan-Wright EM (2004). Structure, expression and regulation of the cannabinoid receptor gene (CB1) in Huntington's disease transgenic mice. *Eur J Biochem* **271**: 4909 – 4920.

McIntosh BT, Hudson B, Yegorova S, Jollimore CA, Kelly ME (2007). Agonist-dependent cannabinoid receptor signaling in human trabecular meshwork cells. *Br J Pharmacol* **152**: 1111 – 1120.

McKenzie FR, Milligan G (1991). Cholera toxin impairment of opioid-mediated inhibitionof adenylate cyclase in neuroblastoma x glioma hybrid cells is due to a toxin-induced decrease in opioid receptor levels. *Biochem J* **275:** 175 – 181.

McPartland JM, Duncan M, Di Marzo V, Pertwee RG (2015). Are cannabidiol and Δ(9) - tetrahydrocannabivarin negative modulators of the endocannabinoid system? A systematic review. *Br J Pharmacol* **172**: 737 – 763.

Mechoulam R, Peters M, Murillo-Rodriguez E, Hanuš LO (2007). Cannabidiol – Recent Advances. *Chem Biodivers* **4**: 1678 – 1692.

Meisel K, Friedman JH (2012). Medical marijuana in Huntington's disease: report of two cases. *Med Health RI* **95**: 178 – 179.

Menalled El-Khodor BF, Patry M, Suárez-Fariñas M, Orenstein SJ, Zahasky B, Leahy C, Wheeler V, Yang XW, MacDonald M, Morton AJ, Bates G, Leeds J, Park L, Howland D, Signer E, Tobin A, Brunner D (2009). Systematic behavioral evaluation of Huntington's disease transgenic and knock-in mouse models. *Neurobiol Dis* **35**: 319 – 336.

Menalled Kudwa AE, Oakeshott S, Farrar A, Paterson N, Filippov I, Miller S, Kwan M, Olsen M, Beltran J, Torello J, Fitzpatrick J, Mushlin R, Cox K, McConnell K, Mazzella M, He D, Osborne GF, Al-Nackkash R, Bates GP, Tuunanen P, Lehtimaki K, Brunner D, Ghavami A, Ramboz S, Park L, Macdonald D, Munoz-Sanjuan I, Howland D (2014). Genetic deletion of transglutaminase 2 does not rescue the phenotypic deficits observed in R6/2 and zQ175 mouse models of Huntington's disease. *PLoS One* **9**: e99520.

Mievis S, Blum D, Ledent C (2011). Worsening of Huntington disease phenotype in CB1 receptor knockout mice. *Neurobiol Dis* **42**: 524 – 529.

Milligan G, Unson CG, Wakelam MJ (1989). Cholera toxin treatment produces down-regulationof the alpha-subunit of the stimulatory guanine-nucleotide-binding protein (Gs). *Biochem J* **262**: 643 – 649.

Miller LK, Devi LA (2011). The highs and lows of cannabinoid receptor expression in disease: mechanisms and their therapeutic implications. *Pharmacol Rev* **63**: 461 – 470.

Mukhopadhyay S, Howlett AC (2005). Chemically distinct ligands promote differential CB1 cannabinoid receptor-Gi protein interactions. *Mol Pharmacol* **67**: 2016 – 2024.

Mukhopadhyay B, Liu J, Osei-Hyiaman D, Godlewski G, Mukhopadhyay P, Wang L, Jeong WI, Gao B, Duester G, Mackie K, Kojima S, Kunos G (2010). Transcriptional regulation of cannabinoid receptor-1 expression in the liver by retinoic acid acting via retinoic acid receptor-gamma. *J Biol Chem* **285**: 19002 – 19011.

Müller-Vahl KR, Schneider U, Emrich HM (1999). Nabilone increases choreatic movements in Huntington's disease. *Mov Disord* **14**: 1038 – 1040.

Naydenov AV, Sepers MD, Swinney K, Raymond LA, Palmiter RD, Stella N (2014a). Genetic rescue of CB1 receptors on medium spiny neurons prevents loss of excitatory striatal synapses but not motor impairment in HD mice. *Neurobiol Dis* **71**: 140 – 150.

Naydenov AV, Horne EA, Cheah CS, Swinney K, Hsu KL, Cao JK, Marrs WR, Blankman JL, Tu S, Cherry AE, Fung S, Wen A, Li W, Saporito MS, Selley DE, Cravatt BF, Oakley JC, Stella N (2014b). ABHD6 blockade exerts antiepileptic activity in PTZ-induced seizures and in spontaneous seizures in R6/2 mice. *Neuron* **83**: 361 – 371.

Nestler EJ, Barrot M, Self DW (2001). DeltaFosB: a sustained molecular switch for addiction. *Proc Natl Acad Sci USA* **98**: 11042 – 11046.

Newcombe RG (1981). A life table for onset of Huntington's chorea. *Ann Hum Genet* **45**: 375 – 385.

Nguyen HP, Björqvist M, Bode FJ, Stephan M, von Hörsten S (2010). Serum levels of a subset of cytokines show high interindividual variability and are not altered in rats transgenic for Huntington´s disease. *PLoS Curr* **2**: RRN1190.

Nguyen PT, Schmid CL, Raehal KM, Selley DE, Bohn LM, Sim-Selley LJ (2012). β-arrestin2 regulates cannabinoid CB1 receptor signaling and adaptation in a central nervous system region-dependent manner. *Biol Psychiatry* **71**: 714 – 724.

Obara Y, Okano Y, Ono S, Yamauchi A, Hoshino T, Kurose H, Nakahata N (2008). Betagamma subunits of G(i/o) suppress EGF-induced ERK5 phosphorylation, whereas ERK1/2 phosphorylation is enhanced. *Cell Signal* **20**: 1275 – 1283.

Pamplona FA, Ferreira J, Menezes de Lima O Jr, Duarte FS, Bento AF, Forner S, Villarinho JG, Bellocchio L, Wotjak CT, Lerner R, Monory K, Lutz B, Canetti C, Matias I, Calixto JB, Marsicano G, Guimarães MZ, Takahashi RN (2012). Anti-inflammatory lipoxin A4 is an endogenous allosteric enhancer of CB1 cannabinoid receptor. *Proc Natl Acad Sci U S A* **109**: 21134 – 21139.

Paoletti P, Vila I, Rifé M, Lizcano JM, Alberch J, Ginés S (2008). Dopaminergic and Glutamatergic Signaling Crosstalk in Huntington's Disease Neurodegeneration: The Role of p25/Cyclin-Dependent Kinase 5. *Neurobiol Dis* **28**: 10090 – 10101.

Park MH, Lee YK, Lee YH, Kim YB, Yun YW, Nam SY, Hwang SJ, Han SB, Kim SU, Hong JT (2009). Chemokines released from astrocytes promote chemokine receptor 5-mediated neuronal cell differentiation. *Exp Cell Res* **315**: 2715 – 2726.

Pazos MR, Sagredo O, Fernandez-Ruiz J (2008). The endocannabinoid system in Hungtington's disease. *Curr Pharm Des* **14**: 2317 – 2325.

Pazos MR, Mohammed N, Lafuente H, Santos M, Martínez-Pinilla E, Moreno E, Valdizan E, Romero J, Pazos A, Franco R, Hillard CJ, Alvarez FJ, Martínez-Orgado J (2013). Mechanisms of

cannabidiol neuroprotection in hypoxic-ischemic newborn pigs: role of 5HT(1A) and CB2 receptors. *Neuropharmacology* **71**: 282 – 291.

Pertwee RG, Ross RA, Craib SJ, Thomas A (2002). (-)-Cannabidiol antagonizes cannabinoid receptor agonists and noradrenaline in the mouse vas deferens. *Eur J Pharmacol* **456**: 99 – 106.

Pertwee RG (2005). Inverse agonism and neutral antagonism at cannabinoind CB_1 receptors. *Life Sci* **76**: 1307 – 1324.

Pertwee RG (2008). Ligands that target cannabinoid receptors in the brain: from THC to anandamide and beyond. *Addict Biol* **13**: 147 – 159.

Pertwee RG, Howlett AC, Abood ME, Alexander SP, Di Marzo V, Elphick MR, Greasley PJ, Hansen HS, Kunos G, Mackie K, Mechoulam R, Ross RA (2010). International Union of Basic and Clinical Pharmacology. LXXIX. Cannabinoid receptors and their ligands: beyond CB1 and CB2. *Pharmacol Rev* **62**: 588 – 631.

Phan J, Hickey MA, Zhang P, Chesselet MF, Reue K (2009). Adipose tissue dysfunction tracks disease progression in two Huntington's disease mouse models. *Hum Mol Genet* **18**: 1006 – 1016.

Pietropaolo S, Bellocchio L, Ruiz-Calvo A, Cabanas M, Du Z, Guzmán M, Garret M, Cho YH (2015). Chronic cannabinoid receptor stimulation selectively prevents motor impairments in a mouse model of Huntington's disease. *Neuropharmacol* **89**: 368 – 374.

Piscitelli F, Ligresti A, La Regina G, Coluccia A, Morera L, Allarà M, Novellino E, Di Marzo V, Silvestri R (2012). Indole-2-carboxamides as allosteric modulators of the cannabinoid CB1 receptor. *J Med Chem* **55**: 5627 – 5631.

Prasad KN, Bondy SC (2015). Inhibition of Early Biochemical Defects in Prodromal Huntington's disease by Simultaneous Activation of Nrf2 and Elevation of Multiple Micronutrients. *Curr Aging Sci* **9**: 61 – 70.

Price MR, Baillie GL, Thomas A, Stevenson LA, Easson M, Goodwin R, McLean A, McIntosh L, Goodwin G, Walker G, Westwood P, Marrs J, Thomson F, Cowley P, Christopoulos A, Pertwee RG, Ross RA (2005). Allosteric modulation of the cannabinoid CB1 receptor. *Mol Pharmacol* **68**: 1484 – 1495.

Proto MC, Gazzerro, P, Di Croce L, Santoro A, Malfitano AM, Pisanti S, Laezza C, Bifulco M (2011). Interaction of endocannabinoid system and steroid hormones in the control of colon cancer cell growth. *J Cell Physiol* **227**: 250 – 258.

Przybyla JA, Watts VJ (2010). Ligand-induced regulation and localization of cannabinoid CB1 and dopamine DRL receptor heterodimers. *J Pharmacol Exp Ther* **332**: 710 – 719.

Radhakrishnan R, Wilkinson ST, D'Souza DC (2014). Gone to pot – a review of the association between cannabis and psychosis. *Front Psychiatry* **5**: 54.

Rajesh M, Mukhopadhyay P, Hasko G (2008). CB2 cannabinoid receptor agonists attenuate TNF-alpha-induced human vascular smooth muscle cell proliferation and migration. *Br J Pharmacol* **153**: 347 – 357.

Ramsay D, Kellett E, McVey M, Rees S, Milligan G (2002). Homo- and hetero-oligomeric interactions between G-protein-coupled receptors in living cells monitored by two variants of bioluminescence resonance energy transfer (BRET): hetero-oligomers between receptor subtypes form more efficiently than between less closely related sequences. *Biochem J* **365**: 429 – 440.

Ramsingh AI, Manley K, Rong Y, Reilly A, Messer A (2015). Transcriptional dysregulation of inflammatory/immune pathways after active vaccination against Huntington's disease. *Hum Mol Genet* **24**: 6186 – 6197.

Ravache M, Weber C, Merienne K, Trottier Y (2010). Transcriptional activation of REST by Sp1 in Huntington's disease models. *PLoS One* 5: e14311.

Ravinet Trillou C, Delgorge C, Menet C, Arnone M, Soubrié P (2004). CB1 cannabinoid receptor knockout in mice leads to leanness, resistance to diet-induced obesity and enhanced leptin sensitivity. *Int J Obes Relat Metab Disord* **28**: 640 – 648.

Roos RA, Hermans J, Vegter-van der Vlis M, van Ommen GJ, Bruyn GW (1993). Duration of illness in Huntington's disease is not related to age at onset. *J Neurol Neurosurg Psychiatry* **56**: 98 – 100.

Ross RA (2007). Allosterism and cannabinoind CB(1) receptors: the shape of things to come. *Trends Pharmacol Sci* **28**: 567 – 572.

Ross CA, Aylward EH, Wild EJ, Langbehn DR, Long JD, Warner JH, Scahill RI, Leavitt BR, Stout JC, Paulsen JS, Reilmann R, Unschuld PG, Wexler A, Margolis RL, Tabrizi SJ (2014). Huntington disease: natural history, biomarkers and prospects for therapeutics. *Nat Rev Neurol* **10**: 204 – 216.

Rubino T, Vigano D, Premoli F, Castiglioni C, Bianchessi S, Zippel R, Parolaro D (2006). Changes in expression of G protein-coupled receptor kinases and β-arrestins in mouse brain during cannabinoid tolerance. *Mol Neurobiol* **33**: 199 – 213.

Runne Kuhn A, Wild EJ, Pratyaksha W, Kristiansen M, Isaacs JD, Régulier E, Delorenzi M, Tabrizi SJ, Luthi-Carter R (2007). Analysis of potential transcriptomic biomarkers for Huntington's disease in peripheral blood. *Proc Natl Acad Sci U S A* **104**: 14424 – 14429.

Russo EB, Burnett A, Hall B, Parker KK (2005). Agonistic properties of cannabidiol at 5-HT1a receptors. *Neurochem Res* **30**: 1037 – 1043.

Ryan W, Singer M, Razdan RK, Compton DR, Martin BR (1995). A novel class of potent tetrahydrocannabinols (THCS): 2'-yne-delta 8- and delta 9- THCS. *Life Sci* **56**: 2013 – 2020.

Ryan D, Drysdale AJ, Pertwee RG, Platt B (2007). Interactions of cannabidiol with endocannabinoid signalling in hippocampal tissue. *Eur J Neurosci* **25**: 2093 – 2102.

Ryberg E, Larsson N, Sjögren S, Hjorth S, Hermansson NO, Leonova J, Elebring T, Nilsson K, Drmota T, Greasley PJ (2007). The orphan receptor GPR55 is a novel cannabinoid receptor. *Br J Pharmacol* **152**: 1092 – 1101.

Sachse-Seeboth C, Pfeil J, Sehrt D, Meineke I, Tzvetkov M, Bruns E, Poser W, Vormfelde SV, Brockmöller J (2009). Interindividual variation in the pharmacokinetics of delta9-

tetrahydrocannabinol as related to genetic polymorphisms in CYP2C9. *Clin Pharmacol Ther* **85**: 273 – 276.

Sadri-Vakili G, Menon AS, Farrell LA, Keller-McGandy CE, Cantuti-Castelvetri I, Standaert DG, Augood SJ, Yohrling GJ, Cha JH (2006). Huntingtin inclusions do not down-regulate specific genes in the R6/2 Huntington's disease mouse. *Eur J Neurosci* **23**: 3171 – 3175.

Sagredo O, Ramos JA, Decio A, Mechoulam R, Fernández-Ruiz J (2007). Cannabidiol reduced the striatal atrophy caused 3-nitropropionic acid in vivo by mechanisms independent of the activation of cannabinoid, vanilloid TRPV1 and adenosine A2A receptors. *Eur J Neurosci* **26**: 843 – 851.

Sagredo O, González S, Aroyo I, Pazos MR, Benito C, Lastres-Becker I, Romero JP, Tolón RM, Mechoulam R, Brouillet E, Romero J, Fernández-Ruiz J (2009). Cannabinoid CB2 receptor agonists protect the striatum against malonate toxicity: relevance for Huntington's disease. *Glia* **57**: 1154 – 1167.

Sagredo O, Pazos MR, Satta V, Ramos JA, Pertwee RG, Fernández-Ruiz J (2011). Neuroprotective effects of phytocannabinoid-based medicines in experimental models of Huntington's disease. *J Neurosci Res* 89: 1509 – 1518.

Sagredo O, Pazos MR, Valdeolivas S, Fernandez-Ruiz J (2012). Cannabinoids: novel medicines for the treatment of Huntington's disease. *Recent Pat CNS Drug Discov* **7**: 41 – 48.

Sandyk R, Consroe P, Stern LZ (1986). Effects of cannabidiol in Huntington's disease. *Neurology* **36**: 342.

Schlosburg JE, Blankman JL, Long JZ, Nomura DK, Pan B, Kinsey SG, Nguyen PT, Ramesh D, Booker L, Burston JJ, Thomas EA, Selley DE, Sim-Selley LJ, Liu QS, Lichtman AH, Cravatt BF (2010). Chronic monoacylglycerol lipase blockade causes functional antagonism of the endocannabinoid system. *Nat Neurosci* **13**: 1113 – 1119.

Schiffer D, Caldera V, Mellai M, Conforti P, Cattaneo E, Zuccato C (2014). Repressor element-1 silencing transcription factor (REST) is present in human control and Huntington's disease neurones. *Neuropathol Apply Neurobiol* **40**: 899 – 910.

Scotter EL, Goodfellow CE, Graham ES, Dragunow M, Glass M (2010). Neuroprotective potential of CB1 receptor agonists in an in vitro model of Huntington's disease. *Br J Pharmacol* **160**: 747 – 761.

Shannon KM, Fraint A (2015). Therapeutic advances in Huntington's disease. *Mov Disord* **30**: 1539 – 1546.

Sharma S, Taliyan R (2015). Transcriptional dysregulation in Huntington's disease: The role of histone deacetylases. *Pharmacol Res* **100**: 157 – 169.

Shenoy SK, Drake MT, Nelson CD, Houtz DA, Xiao K, Madabushi S, Reiter E, Premont RT, Lichtarge O, Lefkowitz RJ (2006). beta-arrestin-dependent, G-protein-independent ERK1/2 activation by the beta2 adrenergic receptor. *J Biol Chem* **281**: 1261 – 1273.

Silvestroni A, Faull RL, Strand AD, Möller T (2009). Distinct neuroinflammatory profile in post-mortem human Huntington's disease. *Neuroreport* **20**: 1098 – 1103.

Sim-Selley LJ, Martin BR (2002). Effect of chronic administration of R-(+)-[2,3-Dihydro-5-methyl-3-[(morpholinyl)methyl]pyrrolo[1,2,3-de]-1,4-benzoxazinyl]-(1-naphthalenyl)methanone mesylate (WIN55,212-2) or delta(9)-tetrahydrocannabinol on cannabinoid receptor adaptation in mice. *J Pharmacol Exp Ther* **303**: 36 – 44.

Sim-Selley LJ, Schechter NS, Rorrer WK, Dalton GD, Hernandez J, Martin BR, Selley DE (2006). Prolonged recovery rate of CB1 receptor adaptation after cessation of long-term cannabinoid administration. *Mol Pharmacol* **70**: 986 – 996.

Simpson JN, McGinty JF (1995). Forskolin induces preproenkephalin and preprodynorphin mRNA in rat striatum as demonstrated by in situ histochemistry. *Synapse* **19**: 151 – 159.

Singh SN, Bakshi K, Mercier RW, Makriyannis A, Pavlopoulos S (2011). Binding between a distal C-terminus fragment of cannabinoid receptor 1 and arrestin-2. *Biochemistry* **50**: 2223 – 2234.

Smith PB, Compton DR, Welch SP, Razdan RK, Mechoulam R, Martin BR (1994). The pharmacological activity of anandamide, a putative endogenous cannabinoid, in mice. *J Pharmacol Exp Ther* **270**: 219 – 227.

Smith NJ, Ward RJ, Stoddart LA, Hudson BD, Kostenis E, Ulven T, Morris JC, Tränkle C, Tikhonova IG, Adams DR, Milligan G (2011). Extracellular loop 2 of the free fatty acid receptor 2 mediates allosterism of phenylacetamide ago-allosteric modulator. *Mol Pharmacol* **80**: 163 – 173.

Soldati C, Bithell A, Conforti P, Cattaneo E, Buckley NJ (2011). Rescue of gene expression by modified REST decoy oligonucleotides in a cellular model of Huntington's disease. *J Neurochem* **116**: 415 – 425.

Spek AL (2009). Structure validation in chemical crystallography. *Act Crystallogr D Biol Crystallogr* **65**: 148 – 55.

Straiker A, Mackie K (2005). Depolarization-induced suppression of excitation in murine autaptic hippocampal neurones. *J Physiol* **569**: 501 – 517.

Straiker A, Wager-Miller J, Hutchens J, Mackie K (2012). Differential signaling in human cannabinoid CB(1) receptors and their splice variants in autaptic hippocampal neurons. *Br J Pharmacol* **165**: 2660 – 2671.

Slivicki RA, Deng L, Kulkarnia PM, Cascio M, Pertwee RG, Thakur GA, Hohmann AG (2014). Positive allosteric modulation of CB1 with GAT211 supresses paclitaxel-induced neuropathic pain while bypassing unwanted side effects of CB1 receptor activation. International Cannabinoids Research Symposium, Baveno, IT. International Cannabinoid Research Society, p. 13.

Strauss MJ (1997). The nitroaromatic group in drug design. Pharmacology and toxicology (for nonpharmacologists). *Ind Eng Chem Prod Res Dev* **18**: 158 – 166.

Sugiura T, Kodaka T, Nakane S, Miyashita T, Kondo S, Suhara Y, Takayama H, Waku K, Seki C, Baba N, Ishima N (1999). Evidence that the cannabinoid CB1 receptor is a 2-arachidonylglycerol receptor. Structure-activity relationship of 2-arachidonylglycerol, ether-linked analogues, and related compounds. *J Biol Chem* **274**: 2794 – 2801.

Süssmuth SD, Müller VM, Geitner C, Landwehrmeyer GB, Iff S, Gemperli A, Orth M (2015). Fat-free mass and its predictors in Huntington's disease. *J Neurol* **262**: 1533 – 1540.

Thomas A, Baillie GL, Phillips AM, Razdan RK, Ross RA, Pertwee RG (2007). Cannabidiol displays unexpectedly high potency as an antagonist of CB1 and CB2 receptor agonists in vitro. *Br J Pharmacol* **150**: 613 – 623.

Tedroff J, Waters S, Barker RA, Roos R, Squitieri F (2015). Antidopaminergic Medication is Associated with More Rapidly Progressive Huntington's Disease. *J Huntingtons Dis* **4**: 131 – 140.

Tooyama I, Kremer HP, Hayden MR, Kimura H, McGeer EG, McGeer PL (1993). Acidic and basic fibroblast growth factor-like immunoreactivity in the striatum and midbrain in Huntington's disease. *Brain Res* **610**: 1 – 7.

Trettel F, Rigamonti D, Hilditch-Maguire P, Wheeler VC, Sharp AH, Persichetti F, Cattaneo E, MacDonald ME (2000). Dominant phenotypes produced by the HD mutation in STHdh(Q111) striatal cells. *Hum Mol Genet* **9**: 2799 – 2809.

Valdeolivas S, Satta V, Pertwee RG, Fernández-Ruiz J, Sagredo O (2012). Sativex-like combination of phytocannabinoids is neuroprotective in malonate-lesioned rats, an inflammatory model of Huntington's disease: role of CB1 and CB2 receptors. *ACS Chem Neurosci* 3: 400 – 406.

Vallée M, Vitiello S, Bellocchio L, Hébert-Chatelain E, Monlezun S, Martin-Garcia E, Kasanetz F, Baillie GL, Panin F, Cathala A, Roullot-Lacarrière V, Fabre S, Hurst DP, Lynch DL, Shore DM, Deroche-Gamonet V, Spampinato U, Revest JM, Maldonado R, Reggio PH, Ross RA, Marsicano G, Piazza PV (2014). Pregnenolone can protect the brain from cannabis intoxication. *Science* **343**: 94 – 98.

Valor LM (2015). Transcription, epigenetics and ameliorative strategies in Huntington's Disease: a genome-wide perspective. *Mol Neurobiol* **51**: 406 – 423.

van der Lee MMC, Blomenrohr M, van der Doelen AA, Wat, JWY, Smits N, Hanson BJ, van Koppen CJ, Zaman GJR (2009). Pharmacological characterization of receptor redistribution and β-arrestin recruitment assays for the cannabinoid receptor 1. *J Biomol Screen* **14**: 811 – 823.

van Laere K, Casteels C, Dhollander I, Goffin K, Grachev I, Bormans G, Vandenberghe W (2010). Widespread decrease of type 1 cannabinoid receptor availability in Huntington disease in vivo. *J Nucl Med* **51**: 1413 – 1417.

van Winkel R, Kuepper R (2014). Epidemiological, Neurobiological, and Genetic Clues to the Mechanisms Linking Cannabis Use to Risk for Nonaffective Psychosis. *Ann Rev Clin Psych* **10**: 767 – 791.

Varga EV, Georgiva T, Tumati S, Alves I, Salamon Z, Tollin G, Yamamura HI, Roeske WR (2008). Functional selectivity in cannabinoid signalling. *Curr Mol Pharmacol* **1**: 273 – 284.

Vonsattel JP, Myers RH, Stevens TJ, Ferrante RJ, Bird ED, Richardson EP Jr (1985). Neuropathological classification of Huntington's disease. *J Neuropathol Exp Neurol* **44**: 559 – 577.

Vrecl M, Norregaard PK, Almholt DLC, Elster L, Pogacnik A, Heding A (2009). β-arrestin-based $BRET^2$ screening assay for the "non"-β-arrestin binding CB1 receptor. *J Biomol Screen* **14**: 371 – 380.

Wang X, Horswill JG, Whalley BJ, Stephens GJ (2011). Effects of the allosteric antagonist 1-(4-chlorophenyl)-3-[3-(6-pyrrolidin-1-ylpyridin-2-yl)phenyl]urea (PSNCBAM-1) on CB1 receptor modulation in the cerebellum. *Mol Pharmacol* **79**: 758 – 67.

Warby SC, Graham RK, Hayden MR (2014). Huntington disease. *Gene Reviews*. **Eds**. Pagon RA, Adam MP, Ardinger HH, et al. Seattle (WA): University of Washington, Seattle; 1993-2015. Available from: http://www.ncbi.nlm.nih.gov/books/NBK1305/

Watanabe K, Yamaori S, Funahashi T, Kimura T, Yamamoto I (2007). Cytochrome P450 enzymes involved in the metabolism of tetrahydrocannabinols and cannabinol by human hepatic microsomes. *Life Sci* **80**: 1415 – 1419.

Welch SP, Eads M (1999). Synergistic interactions of endogenous opioids and cannabinoid systems. *Brain Res* **848**: 183 – 190.

Wild E, Magnusson A, Lahiri N, Krus U, Orth M, Tabrizi SJ, Björkqvist M (2011). Abnormal peripheral chemokine profile in Huntington's disease. *PLoS Curr* **3**: RRN1231.

Wiley JL, Compton DR, Dai D, Lainton JA, Phillips M, Huffman JW (1998). Structure-activity relationships of indole- and pyrrole-derived cannabinoids. *J Pharmacol Exp Ther* **295**: 995 – 1004.

Wiley JL, Breivogel CS, Mahadevan A, Pertwee RG, Cascio MG, Bolognini D, Huffman JW, Walentiny DM, Vann RE, Razdan RK, Martin BR (2011). Structural and pharmacological analysis of O-2050, a putative neutral cannabinoid CB(1) receptor antagonist. *Eur J Pharmacol* **651**: 96 – 105.

Wiley JL, Marusich JA, Zhang Y, Fulp A, Maitra R, Thomas BF, Mahadevan A (2012). Structural analogs of pyrazole and sulfonamide cannabinoids: effects on acute food intake in mice. *Eur J Pharmacol* **695**: 62 – 70.

Wootten D, Christopoulos A, Sexton PM (2013). Emerging paradigms in GPCR allostery: implications for drug discovery. *Nat Rev Drug Discov* **12**: 630 – 644.

Wu DF, Yang LQ, Goschke A, Stumm R, Brandenburg LO, Liang YJ, Höllt V, Koch T (2008). Role of receptor internalization in the agonist-induced desensitization of cannabinoid type 1 receptors. *J Neurochem* **104**: 1132 – 1143.

Wu H-Y, Hudry E, Hashimoto T, Uemura K, Fan Z-Y, Berezovska O, Grosskreutz CL, Bacskai BJ, Hyman BT (2012). Distinct dendritic spine and nuclear phases of calcineurin activation after exposure to Amyloid β revealed by novel FRET assay. *J Neurosci* **32**: 5298 – 5309.

Young D (2016). Gene Therapy-Based Modeling of Neurodegenerative Disorders: Huntington's Disease. *Methods Mol Biol* **1382**: 383 – 395.

Zhai W, Jeong H, Cui L, Krainc D, Tjian R (2005). In vitro analysis of huntingtin-mediated transcriptional repression reveals multiple transcription factor targets. *Cell* **123**: 1241 – 1253.

Zhornitsky S, Potvin S (2012). Cannabidiol in humans-the quest for therapeutic targets. *Pharmaceuticals (Basel)* **5**: 529 – 552.

Zuccato C, Belyaev N, Conforti P, Ooi L, Tartari M, Papadimou E, MacDonald M, Fossale E, Zeitlin S, Buckley N, Cattaneo E (2007). Widespread disruption of repressor element-1 silencing transcription factor/neuron-restrictive silencer factor occupancy at its target genes in Huntington's disease. *J Neurosci* **27**: 6972 – 6983.

Zuccato C, Cattaneo E (2014). Huntington’s disease. *Handb Exp Pharmacol* **220**: 357 – 409.

APPENDIX A COPYRIGHT PERMISSIONS

Chapter 1: Introduction. Laprairie RB, Bagher AM, Precious SV, Denovan-Wright EM (2015). Components of the endocannabinoid and dopamine systems are dysregulated in Huntington's disease: analysis of publicly available microarray datasets. *Pharmacol Res Perspect* **3**: e00104.

WILEY

Title: Components of the endocannabinoid and dopamine systems are dysregulated in Huntington\'s disease: analysis of publicly available microarray datasets

Author: Robert B. Laprairie,Amina M. Bagher,Sophie V. Precious,Eileen M. Denovan-Wright

Publication: Pharmacology Research & Perspectives

Publisher: John Wiley and Sons

Date: Jan 5, 2015

Logged in as:
Robert Laprairie
Account #:
3000983897
LOGOUT

Open Access Article

This article is available under the terms of the Creative Commons Attribution Non-Commercial No Derivatives License CC BY-NC-ND (which may be updated from time to time) and permits **non-commercial** use, distribution, and reproduction in any medium, without alteration, provided the original work is properly cited and it is reproduced verbatim.

For an understanding of what is meant by the terms of the Creative Commons License, please refer to Wiley's Open Access Terms and Conditions.

Permission is not required for **non-commercial** reuse. For **commercial** reuse, please hit the "back" button and select the most appropriate **commercial** requestor type before completing your order.

If you wish to adapt, alter, translate or create any other derivative work from this article, permission must be sought from the Publisher. Please email your requirements to RightsLink@wiley.com.

BACK CLOSE WINDOW

Chapter 2: The cytokine and endocannabinoid systems are co-regulated by NF-κB p65/RelA in cell culture and transgenic mouse models of Huntington disease and in striatal tissue from Huntington disease patients. Laprairie RB, Warford JR, Hutchings S, Robertson GS, Kelly MEM, Denovan-Wright EM (2014). The cytokine and endocannabinoid systems are co-regulated by NF-κB p65/RelA in cell culture and transgenic mouse models of Huntington's disease and in striatal tissue from Huntington's disease patients. *J Neuroimmunol* **267**: 61 – 72.

Format	both print and electronic
Are you the author of this Elsevier article?	Yes
Will you be translating?	No
Title of your thesis/dissertation	Biased agonists and allosteric modulators of the type 1 cannabinoid receptor: potential treatments for Huntington disease
Expected completion date	Feb 2016
Estimated size (number of pages)	31
Elsevier VAT number	GB 494 6272 12
Permissions price	0.00 CAD
VAT/Local Sales Tax	0.00 CAD / 0.00 GBP
Total	0.00 CAD
Terms and Conditions	

INTRODUCTION

1. The publisher for this copyrighted material is Elsevier. By clicking "accept" in connection with completing this licensing transaction, you agree that the following terms and conditions apply to this transaction (along with the Billing and Payment terms and conditions established by Copyright Clearance Center, Inc. ("CCC"), at the time that you opened your Rightslink account and that are available at any time at http://myaccount.copyright.com).

GENERAL TERMS

2. Elsevier hereby grants you permission to reproduce the aforementioned material subject to the terms and conditions indicated.
3. Acknowledgement: If any part of the material to be used (for example, figures) has appeared in our publication with credit or acknowledgement to another source, permission must also be sought from that source. If such permission is not obtained then that material may not be included in your publication/copies. Suitable acknowledgement to the source must be made, either as a footnote or in a reference list at the end of your publication, as follows:
"Reprinted from Publication title, Vol /edition number, Author(s), Title of article / title of chapter, Pages No., Copyright (Year), with permission from Elsevier [OR APPLICABLE SOCIETY COPYRIGHT OWNER]." Also Lancet special credit - "Reprinted from The Lancet, Vol. number, Author(s), Title of article, Pages No., Copyright (Year), with permission from Elsevier."
4. Reproduction of this material is confined to the purpose and/or media for which permission is hereby given.
5. Altering/Modifying Material: Not Permitted. However figures and illustrations may be altered/adapted minimally to serve your work. Any other abbreviations, additions, deletions and/or any other alterations shall be made only with prior written authorization of Elsevier Ltd. (Please contact Elsevier at permissions@elsevier.com)
6. If the permission fee for the requested use of our material is waived in this instance, please be advised that your future requests for Elsevier materials may attract a fee.
7. Reservation of Rights: Publisher reserves all rights not specifically granted in the

combination of (i) the license details provided by you and accepted in the course of this licensing transaction, (ii) these terms and conditions and (iii) CCC's Billing and Payment terms and conditions.
8. License Contingent Upon Payment: While you may exercise the rights licensed immediately upon issuance of the license at the end of the licensing process for the transaction, provided that you have disclosed complete and accurate details of your proposed use, no license is finally effective unless and until full payment is received from you (either by publisher or by CCC) as provided in CCC's Billing and Payment terms and conditions. If full payment is not received on a timely basis, then any license preliminarily granted shall be deemed automatically revoked and shall be void as if never granted. Further, in the event that you breach any of these terms and conditions or any of CCC's Billing and Payment terms and conditions, the license is automatically revoked and shall be void as if never granted. Use of materials as described in a revoked license, as well as any use of the materials beyond the scope of an unrevoked license, may constitute copyright infringement and publisher reserves the right to take any and all action to protect its copyright in the materials.
9. Warranties: Publisher makes no representations or warranties with respect to the licensed material.
10. Indemnity: You hereby indemnify and agree to hold harmless publisher and CCC, and their respective officers, directors, employees and agents, from and against any and all claims arising out of your use of the licensed material other than as specifically authorized pursuant to this license.
11. No Transfer of License: This license is personal to you and may not be sublicensed, assigned, or transferred by you to any other person without publisher's written permission.
12. No Amendment Except in Writing: This license may not be amended except in a writing signed by both parties (or, in the case of publisher, by CCC on publisher's behalf).
13. Objection to Contrary Terms: Publisher hereby objects to any terms contained in any purchase order, acknowledgment, check endorsement or other writing prepared by you, which terms are inconsistent with these terms and conditions or CCC's Billing and Payment terms and conditions. These terms and conditions, together with CCC's Billing and Payment terms and conditions (which are incorporated herein), comprise the entire agreement between you and publisher (and CCC) concerning this licensing transaction. In the event of any conflict between your obligations established by these terms and conditions and those established by CCC's Billing and Payment terms and conditions, these terms and conditions shall control.
14. Revocation: Elsevier or Copyright Clearance Center may deny the permissions described in this License at their sole discretion, for any reason or no reason, with a full refund payable to you. Notice of such denial will be made using the contact information provided by you. Failure to receive such notice will not alter or invalidate the denial. In no event will Elsevier or Copyright Clearance Center be responsible or liable for any costs, expenses or damage incurred by you as a result of a denial of your permission request, other than a refund of the amount(s) paid by you to Elsevier and/or Copyright Clearance Center for denied permissions.

LIMITED LICENSE

The following terms and conditions apply only to specific license types:
15. **Translation**: This permission is granted for non-exclusive world **English** rights only unless your license was granted for translation rights. If you licensed translation rights you

may only translate this content into the languages you requested. A professional translator must perform all translations and reproduce the content word for word preserving the integrity of the article.
16. **Posting licensed content on any Website**: The following terms and conditions apply as follows: Licensing material from an Elsevier journal: All content posted to the web site must maintain the copyright information line on the bottom of each image; A hyper-text must be included to the Homepage of the journal from which you are licensing at http://www.sciencedirect.com/science/journal/xxxxx or the Elsevier homepage for books at http://www.elsevier.com; Central Storage: This license does not include permission for a scanned version of the material to be stored in a central repository such as that provided by Heron/XanEdu.
Licensing material from an Elsevier book: A hyper-text link must be included to the Elsevier homepage at http://www.elsevier.com . All content posted to the web site must maintain the copyright information line on the bottom of each image.

Posting licensed content on Electronic reserve: In addition to the above the following clauses are applicable: The web site must be password-protected and made available only to bona fide students registered on a relevant course. This permission is granted for 1 year only. You may obtain a new license for future website posting.
17. **For journal authors:** the following clauses are applicable in addition to the above:
Preprints:
A preprint is an author's own write-up of research results and analysis, it has not been peer-reviewed, nor has it had any other value added to it by a publisher (such as formatting, copyright, technical enhancement etc.).
Authors can share their preprints anywhere at any time. Preprints should not be added to or enhanced in any way in order to appear more like, or to substitute for, the final versions of articles however authors can update their preprints on arXiv or RePEc with their Accepted Author Manuscript (see below).
If accepted for publication, we encourage authors to link from the preprint to their formal publication via its DOI. Millions of researchers have access to the formal publications on ScienceDirect, and so links will help users to find, access, cite and use the best available version. Please note that Cell Press, The Lancet and some society-owned have different preprint policies. Information on these policies is available on the journal homepage.
Accepted Author Manuscripts: An accepted author manuscript is the manuscript of an article that has been accepted for publication and which typically includes author-incorporated changes suggested during submission, peer review and editor-author communications.
Authors can share their accepted author manuscript:

- immediately
    - via their non-commercial person homepage or blog
    - by updating a preprint in arXiv or RePEc with the accepted manuscript
    - via their research institute or institutional repository for internal institutional uses or as part of an invitation-only research collaboration work-group
    - directly by providing copies to their students or to research collaborators for their personal use
    - for private scholarly sharing as part of an invitation-only work group on

commercial sites with which Elsevier has an agreement
- after the embargo period
  - via non-commercial hosting platforms such as their institutional repository
  - via commercial sites with which Elsevier has an agreement

In all cases accepted manuscripts should:

- link to the formal publication via its DOI
- bear a CC-BY-NC-ND license - this is easy to do
- if aggregated with other manuscripts, for example in a repository or other site, be shared in alignment with our hosting policy not be added to or enhanced in any way to appear more like, or to substitute for, the published journal article.

Published journal article (JPA): A published journal article (PJA) is the definitive final record of published research that appears or will appear in the journal and embodies all value-adding publishing activities including peer review co-ordination, copy-editing, formatting, (if relevant) pagination and online enrichment.
Policies for sharing publishing journal articles differ for subscription and gold open access articles:
Subscription Articles: If you are an author, please share a link to your article rather than the full-text. Millions of researchers have access to the formal publications on ScienceDirect, and so links will help your users to find, access, cite, and use the best available version.
Theses and dissertations which contain embedded PJAs as part of the formal submission can be posted publicly by the awarding institution with DOI links back to the formal publications on ScienceDirect.
If you are affiliated with a library that subscribes to ScienceDirect you have additional private sharing rights for others' research accessed under that agreement. This includes use for classroom teaching and internal training at the institution (including use in course packs and courseware programs), and inclusion of the article for grant funding purposes.
Gold Open Access Articles: May be shared according to the author-selected end-user license and should contain a CrossMark logo, the end user license, and a DOI link to the formal publication on ScienceDirect.
Please refer to Elsevier's posting policy for further information.
18. **For book authors** the following clauses are applicable in addition to the above:
Authors are permitted to place a brief summary of their work online only. You are not allowed to download and post the published electronic version of your chapter, nor may you scan the printed edition to create an electronic version. **Posting to a repository:** Authors are permitted to post a summary of their chapter only in their institution's repository.
19. **Thesis/Dissertation**: If your license is for use in a thesis/dissertation your thesis may be submitted to your institution in either print or electronic form. Should your thesis be published commercially, please reapply for permission. These requirements include permission for the Library and Archives of Canada to supply single copies, on demand, of the complete thesis and include permission for Proquest/UMI to supply single copies, on demand, of the complete thesis. Should your thesis be published commercially, please reapply for permission. Theses and dissertations which contain embedded PJAs as part of the formal submission can be posted publicly by the awarding institution with DOI links back to the formal publications on ScienceDirect.

20. **Other Conditions**:

v1.8

Questions? customercare@copyright.com or +1-855-239-3415 (toll free in the US) or +1-978-646-2777.

Chapter 3: Type 1 cannabinoid receptor ligands display functional selectivity in a cell culture model of striatal medium spiny projection neurons. Laprairie RB, Bagher AM, Kelly MEM, Dupré DJ, Denovan-Wright EM (2014). Type 1 Cannabinoid Receptor Ligands Display Functional Selectivity in a Cell Culture Model of Striatal Medium Spiny Projection Neurons. *J Biol Chem* **289**: 24845 – 24862.

11200 Rockville Pike
Suite 302
Rockville, Maryland 20852

August 19, 2011

American Society for Biochemistry and Molecular Biology

To whom it may concern,

It is the policy of the American Society for Biochemistry and Molecular Biology to allow reuse of any material published in its journals (the Journal of Biological Chemistry, Molecular & Cellular Proteomics and the Journal of Lipid Research) in a thesis or dissertation at no cost and with no explicit permission needed. Please see our copyright permissions page on the journal site for more information.

Best wishes,

Sarah Crespi

American Society for Biochemistry and Molecular Biology
11200 Rockville Pike, Rockville, MD
Suite 302
240-283-6616
JBC | MCP | JLR

Chapter 4: Type 1 cannabinoid receptor ligand bias influences neuronal viability in a cell culture model of Huntington disease. Laprairie RB, Bagher AM, Kelly MEM, Denovan-Wright EM (2016). Biased type 1 cannabinoid receptor signaling influences neuronal viability in a cell culture model of Huntington disease. *Mol Pharmacol* **89**: 364 – 375.

January 4, 2016

Robert Brad Laprairie
Department of Pharmacology
Dalhousie University
Rm 6E, 5850 College St.
Halifax, Nova Scotia B3H 4R2
Canada

Email: robert.laprairie@gmail.com

Dear Robert Laprairie:

This is to grant you permission to include the following article in your thesis entitled "BIASED AGONISTS AND ALLOSTERIC MODULATORS OF THE TYPE 1 CANNABINOID RECEPTOR: POTENTIAL TREATMENTS FOR HUNTINGTON DISEASE" for Dalhousie University:

> Robert B Laprairie, Amina M Bagher, Melanie E M Kelly, and Eileen M Denovan-Wright, Biased Type 1 Cannabinoid Receptor Signalling Influences Neuronal Viability in a Cell Culture Model of Huntington Disease, *Mol Pharmacol* published ahead of print December 23, 2015, doi:10.1124/mol.115.101980

On the first page of each copy of this article, please add the following:

> Reprinted with permission of the American Society for Pharmacology and Experimental Therapeutics. All rights reserved.

In addition, the original copyright line published with the paper must be shown on the copies included with your thesis.

Sincerely yours,

Richard Dodenhoff
Journals Director

9650 Rockville Pike | Bethesda | MD | 20814-3995
P: (301) 634-7060 | F: (301) 634-7061 | E: info@aspet.org | www.aspet.org

Chapter 5: Cannabidiol is a negative allosteric modulator of the type 1 cannabinoid receptor.
Laprairie RB, Bagher AM, Kelly MEM, Denovan-Wright EM (2015). Cannabidiol is a negative allosteric modulator of the type 1 cannabinoid receptor. *Br J Pharmacol* **172**: 4790 – 4805.

JOHN WILEY AND SONS LICENSE TERMS AND CONDITIONS

Dec 17, 2015

This Agreement between Robert B Laprairie ("You") and John Wiley and Sons ("John Wiley and Sons") consists of your license details and the terms and conditions provided by John Wiley and Sons and Copyright Clearance Center.

License Number	3771430552703
License date	Dec 17, 2015
Licensed Content Publisher	John Wiley and Sons
Licensed Content Publication	British Journal of Pharmacology
Licensed Content Title	Cannabidiol is a negative allosteric modulator of the cannabinoid CB1 receptor
Licensed Content Author	R B Laprairie,A M Bagher,M E M Kelly,E M Denovan-Wright
Licensed Content Date	Oct 13, 2015
Pages	16
Type of use	Dissertation/Thesis
Requestor type	Author of this Wiley article
Format	Print and electronic
Portion	Full article
Will you be translating?	No
Title of your thesis / dissertation	Biased agonists and allosteric modulators of the type 1 cannabinoid receptor: potential treatments for Huntington disease
Expected completion date	Feb 2016
Expected size (number of pages)	31
Requestor Location	Robert B Laprairie Rm 6E 5850 College St. Halifax, NS B3H4R2 Canada Attn: Robert B Laprairie
Billing Type	Invoice
Billing Address	Robert B Laprairie Rm 6E 5850 College St. Halifax, NS B3H4R2 Canada Attn: Robert B Laprairie

Total 0.00 CAD

Terms and Conditions

TERMS AND CONDITIONS

This copyrighted material is owned by or exclusively licensed to John Wiley & Sons, Inc. or one of its group companies (each a"Wiley Company") or handled on behalf of a society with which a Wiley Company has exclusive publishing rights in relation to a particular work (collectively "WILEY"). By clicking "accept" in connection with completing this licensing transaction, you agree that the following terms and conditions apply to this transaction (along with the billing and payment terms and conditions established by the Copyright Clearance Center Inc., ("CCC's Billing and Payment terms and conditions"), at the time that you opened your RightsLink account (these are available at any time at http://myaccount.copyright.com).

Terms and Conditions

- The materials you have requested permission to reproduce or reuse (the "Wiley Materials") are protected by copyright.

- You are hereby granted a personal, non-exclusive, non-sub licensable (on a stand-alone basis), non-transferable, worldwide, limited license to reproduce the Wiley Materials for the purpose specified in the licensing process. This license, **and any CONTENT (PDF or image file) purchased as part of your order,** is for a one-time use only and limited to any maximum distribution number specified in the license. The first instance of republication or reuse granted by this license must be completed within two years of the date of the grant of this license (although copies prepared before the end date may be distributed thereafter). The Wiley Materials shall not be used in any other manner or for any other purpose, beyond what is granted in the license. Permission is granted subject to an appropriate acknowledgement given to the author, title of the material/book/journal and the publisher. You shall also duplicate the copyright notice that appears in the Wiley publication in your use of the Wiley Material. Permission is also granted on the understanding that nowhere in the text is a previously published source acknowledged for all or part of this Wiley Material. Any third party content is expressly excluded from this permission.

- With respect to the Wiley Materials, all rights are reserved. Except as expressly granted by the terms of the license, no part of the Wiley Materials may be copied, modified, adapted (except for minor reformatting required by the new Publication), translated, reproduced, transferred or distributed, in any form or by any means, and no derivative works may be made based on the Wiley Materials without the prior permission of the respective copyright owner.**For STM Signatory Publishers clearing permission under the terms of the STM Permissions Guidelines only, the terms of the license are extended to include subsequent editions and for editions in other languages, provided such editions are for the work as a whole in situ and does not involve the separate exploitation of the permitted figures or extracts,** You may not alter, remove or suppress in any manner any copyright, trademark or other notices displayed by the Wiley Materials. You may not license, rent, sell, loan,

lease, pledge, offer as security, transfer or assign the Wiley Materials on a stand-alone basis, or any of the rights granted to you hereunder to any other person.

- The Wiley Materials and all of the intellectual property rights therein shall at all times remain the exclusive property of John Wiley & Sons Inc, the Wiley Companies, or their respective licensors, and your interest therein is only that of having possession of and the right to reproduce the Wiley Materials pursuant to Section 2 herein during the continuance of this Agreement. You agree that you own no right, title or interest in or to the Wiley Materials or any of the intellectual property rights therein. You shall have no rights hereunder other than the license as provided for above in Section 2. No right, license or interest to any trademark, trade name, service mark or other branding ("Marks") of WILEY or its licensors is granted hereunder, and you agree that you shall not assert any such right, license or interest with respect thereto

- NEITHER WILEY NOR ITS LICENSORS MAKES ANY WARRANTY OR REPRESENTATION OF ANY KIND TO YOU OR ANY THIRD PARTY, EXPRESS, IMPLIED OR STATUTORY, WITH RESPECT TO THE MATERIALS OR THE ACCURACY OF ANY INFORMATION CONTAINED IN THE MATERIALS, INCLUDING, WITHOUT LIMITATION, ANY IMPLIED WARRANTY OF MERCHANTABILITY, ACCURACY, SATISFACTORY QUALITY, FITNESS FOR A PARTICULAR PURPOSE, USABILITY, INTEGRATION OR NON-INFRINGEMENT AND ALL SUCH WARRANTIES ARE HEREBY EXCLUDED BY WILEY AND ITS LICENSORS AND WAIVED BY YOU.

- WILEY shall have the right to terminate this Agreement immediately upon breach of this Agreement by you.

- You shall indemnify, defend and hold harmless WILEY, its Licensors and their respective directors, officers, agents and employees, from and against any actual or threatened claims, demands, causes of action or proceedings arising from any breach of this Agreement by you.

- IN NO EVENT SHALL WILEY OR ITS LICENSORS BE LIABLE TO YOU OR ANY OTHER PARTY OR ANY OTHER PERSON OR ENTITY FOR ANY SPECIAL, CONSEQUENTIAL, INCIDENTAL, INDIRECT, EXEMPLARY OR PUNITIVE DAMAGES, HOWEVER CAUSED, ARISING OUT OF OR IN CONNECTION WITH THE DOWNLOADING, PROVISIONING, VIEWING OR USE OF THE MATERIALS REGARDLESS OF THE FORM OF ACTION, WHETHER FOR BREACH OF CONTRACT, BREACH OF WARRANTY, TORT, NEGLIGENCE, INFRINGEMENT OR OTHERWISE (INCLUDING, WITHOUT LIMITATION, DAMAGES BASED ON LOSS OF PROFITS, DATA, FILES, USE, BUSINESS OPPORTUNITY OR CLAIMS OF THIRD PARTIES), AND WHETHER OR NOT THE PARTY HAS BEEN ADVISED OF THE POSSIBILITY OF SUCH DAMAGES. THIS LIMITATION SHALL APPLY NOTWITHSTANDING ANY FAILURE OF ESSENTIAL PURPOSE OF ANY LIMITED REMEDY PROVIDED HEREIN.

- Should any provision of this Agreement be held by a court of competent jurisdiction to be illegal, invalid, or unenforceable, that provision shall be deemed amended to achieve as nearly as possible the same economic effect as the original provision, and the legality, validity and enforceability of the remaining provisions of this Agreement shall not be affected or impaired thereby.

- The failure of either party to enforce any term or condition of this Agreement shall not constitute a waiver of either party's right to enforce each and every term and condition of this Agreement. No breach under this agreement shall be deemed waived or excused by either party unless such waiver or consent is in writing signed by the party granting such waiver or consent. The waiver by or consent of a party to a breach of any provision of this Agreement shall not operate or be construed as a waiver of or consent to any other or subsequent breach by such other party.

- This Agreement may not be assigned (including by operation of law or otherwise) by you without WILEY's prior written consent.

- Any fee required for this permission shall be non-refundable after thirty (30) days from receipt by the CCC.

- These terms and conditions together with CCC's Billing and Payment terms and conditions (which are incorporated herein) form the entire agreement between you and WILEY concerning this licensing transaction and (in the absence of fraud) supersedes all prior agreements and representations of the parties, oral or written. This Agreement may not be amended except in writing signed by both parties. This Agreement shall be binding upon and inure to the benefit of the parties' successors, legal representatives, and authorized assigns.

- In the event of any conflict between your obligations established by these terms and conditions and those established by CCC's Billing and Payment terms and conditions, these terms and conditions shall prevail.

- WILEY expressly reserves all rights not specifically granted in the combination of (i) the license details provided by you and accepted in the course of this licensing transaction, (ii) these terms and conditions and (iii) CCC's Billing and Payment terms and conditions.

- This Agreement will be void if the Type of Use, Format, Circulation, or Requestor Type was misrepresented during the licensing process.

- This Agreement shall be governed by and construed in accordance with the laws of the State of New York, USA, without regards to such state's conflict of law rules. Any legal action, suit or proceeding arising out of or relating to these Terms and Conditions or the breach thereof shall be instituted in a court of competent jurisdiction in New York County in the State of New York in the United States of America and each party hereby consents and submits to the personal jurisdiction of such court, waives any

objection to venue in such court and consents to service of process by registered or certified mail, return receipt requested, at the last known address of such party.

WILEY OPEN ACCESS TERMS AND CONDITIONS

Wiley Publishes Open Access Articles in fully Open Access Journals and in Subscription journals offering Online Open. Although most of the fully Open Access journals publish open access articles under the terms of the Creative Commons Attribution (CC BY) License only, the subscription journals and a few of the Open Access Journals offer a choice of Creative Commons Licenses. The license type is clearly identified on the article.

The Creative Commons Attribution License

The Creative Commons Attribution License (CC-BY) allows users to copy, distribute and transmit an article, adapt the article and make commercial use of the article. The CC-BY license permits commercial and non-

Creative Commons Attribution Non-Commercial License

The Creative Commons Attribution Non-Commercial (CC-BY-NC)License permits use, distribution and reproduction in any medium, provided the original work is properly cited and is not used for commercial purposes.(see below)

Creative Commons Attribution-Non-Commercial-NoDerivs License

The Creative Commons Attribution Non-Commercial-NoDerivs License (CC-BY-NC-ND) permits use, distribution and reproduction in any medium, provided the original work is properly cited, is not used for commercial purposes and no modifications or adaptations are made. (see below)

Use by commercial "for-profit" organizations

Use of Wiley Open Access articles for commercial, promotional, or marketing purposes requires further explicit permission from Wiley and will be subject to a fee.

Further details can be found on Wiley Online Library

http://olabout.wiley.com/WileyCDA/Section/id-410895.html

Other Terms and Conditions:

v1.10 Last updated September 2015

Questions? customercare@copyright.com or +1-855-239-3415 (toll free in the US) or +1-978-646-2777.